

Potential of Polymers of Intrinsic Microporosity (PIM) in Membrane Technologies for a Water- Focused Sustainable Future

Dissertation

Esra Çalışkan

Hamburg, 2025

University of Hamburg

Faculty of Mathematics, Informatics, and Natural Sciences

Department of Chemistry

Dissertation with the aim of achieving a doctoral degree (Dr. rer. nat.)

Supervisor: Prof. Dr. Volker Abetz

Co-supervisor: Dr. Volkan Filiz

1st Referee: Prof. Dr. Volker Abetz

2nd Referee: Prof. Dr. Tobias Beck

Date of oral examination: June 20, 2025

This work has been carried out between November 2018 and February 2022 under the supervision of Prof. Dr. Volker Abetz at the Institute of Membrane Research, Helmholtz Zentrum Hereon (Geesthacht, Germany) and the Institute of Physical Chemistry, University of Hamburg (Department of Chemistry, Faculty of Mathematics, Informatics, and Natural Sciences). The dissertation has been submitted as a cumulative thesis.

List of Publications

Caliskan, E.; Shishatskiy, S.; Neumann, S.; Abetz, V.; Filiz, V. Investigation of the Side Chain Effect on Gas and Water Vapor Transport Properties of Anthracene-Maleimide Based Polymers of Intrinsic Microporosity. *Polymers* (Basel), 2021, 14(1).
<https://doi.org/10.3390/polym14010119>

Caliskan, E.; Shishatskiy, S.; Abetz, V.; Filiz, V. Pioneering the preparation of porous PIM-1 membranes for enhanced water vapor flow. *RSC Adv.* 2024, 14, 9631–9645.
<https://doi.org/10.1039/D3RA08398E>

Caliskan, E.; Shishatskiy, S.; Filiz, V. Comparative Study of Polymer of Intrinsic Microporosity-Derivative Polymers in Pervaporation and Water Vapor Permeance Applications. *Polymers*. 2024; 16(20):2932. <https://doi.org/10.3390/polym16202932>

Table of Contents

| | |
|--|------|
| List of Publications | iv |
| Table of Contents | v |
| Figures | viii |
| Tables | ix |
| Abbreviations | x |
| Constants and Variables | xiv |
| 1. Abstract | 1 |
| 2. Zusammenfassung | 5 |
| 3. Theoretical background | 9 |
| 3.1. Introduction to membranes | 9 |
| 3.2. Classification of membranes | 11 |
| 3.2.1. Natural membranes | 11 |
| 3.2.2. Synthetic membranes | 11 |
| 3.2.2.1. Symmetric (isotropic) membranes | 13 |
| 3.2.2.2. Asymmetric (anisotropic) membranes | 14 |
| 3.3. Membrane applications | 14 |
| 3.3.1. Gas separation | 14 |
| 3.3.1.1. Gas transport mechanism | 15 |
| 3.3.1.2. Classification of polymers for gas separation | 17 |
| 3.3.1.3. Trade-off between permeability and selectivity | 19 |
| 3.3.2. Pervaporation | 22 |
| 3.3.2.1. Basics of pervaporation | 23 |
| 3.3.2.2. Current applications of pervaporation | 24 |
| 3.3.2.3. Pervaporation membrane materials | 25 |
| 3.3.2.4. Challenges of pervaporation | 28 |
| 3.3.3. Membrane distillation | 28 |
| 3.3.3.1. Membrane distillation configurations and application area | 30 |
| 3.3.3.2. Membrane distillation characteristics | 31 |
| 3.3.3.3. Materials used in membrane distillation | 32 |
| 3.3.3.4. Limitations of membrane distillation | 34 |

| | |
|---|-----|
| 3.4. Membrane fabrication techniques..... | 35 |
| 3.4.1. Phase inversion | 35 |
| 3.4.2. Interfacial polymerization..... | 36 |
| 3.4.3. Solution casting..... | 37 |
| 3.5. Step growth polymerization..... | 37 |
| 3.6. Polymers of intrinsic microporosity (PIM)..... | 40 |
| 3.6.1. Synthesis of PIM-1 | 40 |
| 3.6.2. Synthesis of PIM-7 | 42 |
| 3.6.3. Applications of PIM-1 | 43 |
| 3.6.3.1. Gas separation..... | 43 |
| 3.6.3.2. Pervaporation | 44 |
| 3.6.3.3. Nanofiltration..... | 45 |
| 3.6.4. Fractional free volume theory..... | 45 |
| 3.6.5. Physical aging | 47 |
| 3.6.6. Further studies on PIM-1 | 48 |
| 4. Objective of this work..... | 50 |
| 5. Cumulative part..... | 52 |
| 5.1. Article 1: Investigation of the side chain effect on gas and water vapor transport properties of anthracene-maleimide based polymers of intrinsic microporosity..... | 52 |
| 5.1.1. Author contributions | 53 |
| 5.1.2. Funding and acknowledgements..... | 53 |
| 5.1.3. Publication | 53 |
| 5.2. Article 2: Pioneering the preparation of porous PIM-1 membranes for enhanced water vapor flow | 80 |
| 5.2.1. Author contributions | 81 |
| 5.2.2. Funding and acknowledgements..... | 81 |
| 5.2.3. Publication | 81 |
| 5.3. Article 3: Comparative study of polymer of intrinsic microporosity-derivative polymers in pervaporation and water vapor permeance applications..... | 97 |
| 5.3.1. Author contributions | 98 |
| 5.3.2. Funding and acknowledgements..... | 98 |
| 5.3.3. Publication | 98 |
| 6. Discussion..... | 117 |

| | |
|--|-----|
| 6.1. Summary of findings-Article 1 | 117 |
| 6.2. Summary of findings-Article 2 | 118 |
| 6.3. Summary of findings-Article 3 | 119 |
| 7. References | 120 |
| 8. Appendix | 132 |
| 8.1. Article 1: Investigation of the side chain effect on gas and water vapor transport properties of anthracene-maleimide based polymers of intrinsic microporosity | 132 |
| 8.1.1. Graphical abstract | 132 |
| 8.1.2. Supporting information | 132 |
| 8.2. Article 2: Pioneering the preparation of porous PIM-1 membranes for enhanced water vapor flow | 142 |
| 8.2.1. Graphical abstract | 142 |
| 8.2.2. Supporting information | 142 |
| 8.3. Article 3: Comparative study of polymer of intrinsic microporosity-derivative polymers in pervaporation and water vapor permeance applications | 153 |
| 8.3.1. Graphical abstract | 153 |
| 8.3.2. Supporting information | 153 |
| 8.4. Safety hazards | 156 |
| 8.5. Copyright permissions | 159 |
| 8.5.1. Figure 2 | 159 |
| 8.5.2. Figure 4 | 160 |
| 8.5.3. Figure 6 | 167 |
| 8.5.4. Figure 8 | 175 |
| 9. Acknowledgements | 181 |
| 10. Declaration of oath | 184 |

Figures

| | |
|---|-----|
| Figure 1: Schematic representation of typical membrane structure. Reprinted with permission from Mahenthiran, A.V. and Z.A. Jawad, 2021, Membranes [15]. | 13 |
| Figure 2: Gas transport mechanisms: (a) Knudsen diffusion, (b) Molecular sieving, (c) Solution-diffusion model [18]. | 15 |
| Figure 3: Robeson upper bound: Permeability-selectivity trade-off. Reprinted with permission from Panapitiya, N., et al., 2016, Materials [31]. | 20 |
| Figure 4: Comparison of upper bound for glassy polymer and rubbery polymer based on O ₂ permeability over O ₂ /N ₂ selectivity data [33]. | 21 |
| Figure 5: Schematic representation of pervaporation process. Reprinted with permission from Pulyalina, A., et al., 2020, Symmetry [37]. | 22 |
| Figure 6: Illustration of various pervaporation membranes [39]. | 25 |
| Figure 7: Principle of membrane distillation through the hydrophobic membrane. Reprinted with permission from Karanasiou, A. et al., 2018, Water [50]. | 29 |
| Figure 8: Schematic representation of membrane distillation configurations: (a) direct contact membrane distillation, (b) air gap membrane distillation, (c) sweep gas membrane distillation, (d) vacuum membrane distillation. | 31 |
| Figure 9: Example of degree of polymerization over conversion. Reprinted with permission from Abdelghafour, M.M., et al., 2021, Polymers [85]. | 39 |
| Figure 10: Synthesis of PIM-1. Reagents and conditions: (i) K ₂ CO ₃ , DMF, 60 °C, 72 hours. | 41 |
| Figure 11: 3D molecular model of PIM-1 rendering contortion and ladder like structure. Reprinted with permission from McKeown, N.B. and P.M. Budd, 2006, Chem. Soc. Rev. [92]. | 42 |
| Figure 12: Synthesis of PIM-7. Reagents and conditions: (i) 18-crown-6, K ₂ CO ₃ , DMF, 150 °C [88]. | 43 |
| Figure 13: Representation of glass transition from rubbery to glassy state. | 46 |
| Figure 14: Graphical abstract of article 1. | 132 |
| Figure 15: Graphical abstract of article 2. | 142 |
| Figure 16: Graphical abstract of article 3. | 153 |

Tables

| | |
|--|-----|
| Table 1: List of Abbreviations | x |
| Table 2: Constants and variables | xiv |
| Table 3: Membrane process classification according to driving forces [3] | 10 |
| Table 4: Common polymers used in membrane applications | 12 |
| Table 5: Gas permeability coefficient of industrial polymeric membranes..... | 15 |
| Table 6: Common polymers used for gas separation membranes | 21 |
| Table 7: Types of polymeric membranes used in pervaporation..... | 26 |
| Table 8: Hansen solubility parameters of some solvents [46] | 27 |
| Table 9: Commercial membrane distillation membranes and their permeate flux in various feed compositions [61]..... | 33 |
| Table 10: Gas transport data* of PIM-1 [90]..... | 44 |
| Table 11: List publication: Publication-1 | 53 |
| Table 12: List of contribution: Publication-2..... | 81 |
| Table 13: List of contribution: Publication-3..... | 98 |

Abbreviations

Table 1: List of Abbreviations

| | |
|-------------------|--------------------------------------|
| $^1\text{H-NMR}$ | Hydrogen-nuclear magnetic resonance |
| AGMD | Air gap membrane distillation |
| BBr_3 | Boron tribromide |
| CA | Cellulose acetate |
| CDCl_3 | Deuterated chloroform |
| CHCl_3 | Chloroform |
| CLD | Chain length distribution |
| CNT | Carbon nanotube |
| CS | Chitosan |
| DCB | Dichlorobenzene |
| DCM | Dichloromethane |
| DCMD | Direct contact membrane distillation |
| DEB | Diethyl benzene |
| DMAc | Dimethylacetamide |
| DMF | Dimethylformamide |
| DMSO-d_6 | Deuterated dimethyl sulfoxide |
| DSC | Differential scanning calorimetry |
| EtOH | Ethanol |
| FFV | Fractional free volume |

| | |
|--------------------------------|---|
| FTIR | Fourier-Transform-Infrared spectroscopy |
| GPC | Gel permeation chromatography |
| H ₂ SO ₄ | Sulfuric acid |
| IP | Interfacial polymerization |
| K ₂ CO ₃ | Potassium carbonate |
| LEP | Liquid entry pressure |
| MD | Membrane distillation |
| MOFs | Metal-organic frameworks |
| NaCl | Sodium chloride |
| NaOH | Sodium hydroxide |
| NF | Nanofiltration |
| NIPS | Nonsolvent phase separation |
| NMP | N-Methyl-2-pyrrolidone |
| PA | Polyamide |
| PAN | Polyacrylonitrile |
| PC | Polycarbonate |
| PDMS | Polydimethylsiloxane |
| PE | Polyethylene |
| PEBA | Poly (ether-block-amide) |
| PEC | Polyelectrolyte complex |
| PEI | Polyetherimide |
| PI | Polyimide |

| | |
|---------|---|
| PIM | Polymers of intrinsic microporosity |
| POSS | Polyhedral oligomeric silsesquioxane |
| PP | Polypropylene |
| PPO | Poly(phenylene oxide) |
| PS | Polysulfone |
| PTFE | Polytetrafluoroethylene |
| PTMSP | Poly(1-trimethylsilyl-1-propyne) |
| PVA | Poly(vinyl alcohol) |
| PVDF | Poly(vinylidene fluoride) |
| RO | Reverse osmosis |
| SEC | Size-exclusion chromatography |
| SEIPS | Solvent evaporation-induced phase separation |
| SEM | Scanning electron microscopy |
| SGMD | Sweep gas membrane distillation |
| TFC | Thin film composite |
| TFCM | Thin film composite membrane |
| TFTPN | 2,3,5,6-Tetrafluoro-terephthalonitrile |
| TGA | Thermal gravimetric analysis |
| TG-FTIR | Thermogravimetric analysis coupled FTIR spectroscopy |
| THF | Tetrahydrofuran |
| TIPS | Thermal induce phase separation |
| TTSBI | 5,5',6,6'-Tetrahydroxy-3,3',3',3'-tetramethyl-1,1'-spirobisindane |

| | |
|------|--------------------------------|
| UF | Ultrafiltration |
| VIPS | Vapor-induced phase separation |
| VLE | Vapor-liquid equilibrium |
| VMD | Vacuum membrane distillation |
| VOCs | Volatile organic compounds |

Constants and Variables

Table 2: Constants and variables

| | |
|------------------|--|
| \overline{M}_n | Number average molecular weight |
| \overline{M}_o | Average molar mass of the repeating unit |
| \overline{M}_w | Weight average molecular weight |
| \overline{X}_n | Number average degree of polymerization |
| A | Membrane area |
| b | Langmuir affinity parameter |
| B | Pore geometry coefficient |
| C | Concentration of a gas |
| C'_H | Langmuir sorption capacity |
| C_H | Concentration of the penetrant in the free volume |
| D | Diffusivity of a gas |
| \bar{D} | Polymer dispersity, polydispersity (or more recently dispersity without the poly, as per IUPAC recommendation) |
| dc/dx | Concentration gradient |
| d_{max} | Maximum pore radius |
| E' | Tensile strength modulus |
| f | Maximum number of functional groups take place in the polymerization per monomer |
| J | Constant flux |
| k_D | Henry's law constant |

| | |
|---------------|---|
| K_n | Knudsen diffusion |
| l | Membrane thickness |
| p | Fractional conversion of fractional groups |
| p | Partial pressure of a gas |
| P | Permeability of a gas |
| r | Stoichiometry |
| S | Solubility of a gas |
| t | Time |
| T_g | Glass transition temperature |
| V_f | Free volume of the polymer |
| V_{oc} | Occupied free volume of the polymer |
| V_{sp} | Specific volume of the polymer |
| V_w | van der Waals volume of the repeating unit of the polymer |
| W | Weight of the permeate |
| y_w, x_w | Mass fractions of components |
| α | Separation factor |
| β | Weight of the sample in displaced liquid |
| γ_L | Surface tension of liquid |
| $\Delta\mu_i$ | Chemical potential of a component |
| δ_d | Energy of dispersion forces between molecules |
| Δf_i | Fugacity of a component |
| δ_h | Energy of hydrogen bonds between molecules |

| | |
|---------------|---|
| δ_p | Energy of polar intramolecular forces between molecules |
| Δp | Hydrostatic pressure |
| Δp_i | Partial pressure of a component |
| ΔT | Temperature potential |
| $\Delta \phi$ | Electrical potential |
| θ | Contact angle |
| χ | Weight of the sample in air |
| ρ_l | Density of air |
| ρ_o | Density of fluorinated liquid |

1. Abstract

Water is the most important substance of life, supporting ecosystems, economies, and human health. Nevertheless, today there is an undeniable problem of water scarcity. Due to population growth, climate change and pollution, one of the most critical challenges of the 21st century is now access to clean water. Global estimates suggest that billions of people lack access to safe drinking water, and demand for clean water is projected to grow exponentially in the coming decades. Technological innovations are essential to tackle this challenge. Membrane processes have attracted a great deal of attention due to their ability to desalinate and recover water in an energy-efficient and cost-effective way, making them a small carbon footprint technology. Membrane-based systems offer a versatile platform to address various challenges related to water treatment, including desalination, contaminant removal, and recovery of valuable resources, and ensuring sustainable water cycles.

Membrane technologies utilize selective separation processes using seawater, wastewater, and industrial effluents as sources for clean water. Basic membrane applications include gas and water vapor separation, reverse osmosis, nanofiltration, pervaporation and membrane distillation. Among these, reverse osmosis is the pressure driven process of separating of water from the saline solutions across the membrane. In nanofiltration, another pressure-driven system, ionic components are separated from wastewater to produce clean water. Membrane distillation is a thermally driven process and a promising technology that uses hydrophobic membranes to separate solutions from salt and concentrate them. Another water treatment process is pervaporation that removes water from organic mixtures or volatile compounds. In addition, gas and water vapor separation technologies support water treatment processes by the separation of water vapor from humidified air or drying systems, which are also very important processes for energy efficiency.

Polymers are attractive materials for membrane applications due to their good processability and low scale-up costs. Polymers of intrinsic microporosity (PIM) have been developed in recent years as a promising material for membrane applications due to their unique properties. One of the main properties of the first synthesized PIM (PIM-1) that makes it attractive for membrane applications is its high free volume. The rigid and contorted molecular structure allows rapid diffusion of

penetrant through this free volume cavitation in transport events and makes PIM-1 an important candidate for selective separations. Another property is the hydrophobic nature of PIM-1, which is very important in membrane applications where water transport without allowing liquid penetration is critical. In addition, PIM-1 is an excellent polymer that is readily soluble in a wide range of solvents, making it easy to process and modify. For this reason, PIM-1 can be modified and functionalized according to its intended use in many studies. Given these properties, PIM-1 has been a promising polymer for many membrane applications and is a highly adaptable material that offers the potential to develop innovative solutions for water-related challenges.

To date, PIM-1 has been tested in various membrane applications and has shown promising results. Among the major applications is gas separation. PIM-1 has been the focus of many studies due to its high selectivity and selectivity compared to conventional gas separation membranes. Other PIM-1 studies, which have focused on functionalization or post-modifications-, have aimed to improve penetrant selectivity, or increase free volume. Pervaporation has been studied as another application to hydrophilize PIM-1 by altering its function. Although significant progress has been made, there remains a paucity in fully exploiting the potential of PIM-1 in integrated water-related processes, particularly in combining water vapor separation, membrane distillation and pervaporation. For this purpose, this work comprises three different sub-studies. PIM-1 transport properties were investigated in three different water transport processes, all using PIM-1 and its derivatives in common.

Firstly, the high free volume of PIM-1 was exploited to evaluate the gas and water vapor separation performance. Modifications have been made to the PIM-1 skeleton to further increase the fractional free volume. Specifically, an anthracene maleimide based component was synthesized and comonomers were obtained by introducing different aliphatic and aromatic side groups by Diels-Alder reaction. Subsequently, a series of homopolymers and copolymers were synthesized with the monomers constituting PIM-1 following thick films preparation with each of the homopolymer and copolymer to investigate their transport properties. It was observed that the introduction of bulky groups increased the fractional free volume, thereby increasing the penetrant diffusion and hence the permeability. In the homopolymer in which aromatic groups were added, water affinity increased, and water solubility elevated, which had a positive effect on water vapor permeability. The effects of these modifications on the selectivity and permeability of PIM-1 and

PIM-based homopolymers and copolymers on gas and water vapor separation performance were investigated.

In the second study, the hydrophobic nature of PIM-1 was exploited to explore its potential in membrane distillation applications. The aim was to prepare PIM-1 membranes with a porous structure as a requirement for membrane distillation, going beyond the traditional method of PIM-1 preparation. Nonsolvent induced phase separation process was used to prepare porous membranes. The challenge was to create the appropriate solvent / nonsolvent combination for PIM-1. After several try-outs, the optimum concentration of THF/NMP/PIM-1 (solvent/nonsolvent/polymer) was determined, and casting of a porous membrane was executed. In addition, PIM-1 thin film composite membrane was prepared to see the effect of membrane porous structure on water flux. Water flux measurements conducted with the prepared membranes revealed that large pores increased the water flux abruptly, while in relatively smaller pores, water flux was almost non-existent. However, when the porous membrane is compared with the thin film composite membrane, the water vapor permeation is much higher in the porous membrane. Accordingly, the findings of our study indicate that the development of a porous hydrophobic PIM-1 membrane which allows the transport of water in vapor form but does not allow liquid flow is promising in membrane distillation applications.

Considering the information obtained up to here, in our last study, it is aimed to improve water vapor transport by preparing thin film composite membrane with more functional PIM based polymers which represent the homopolymer series we obtained in the first study. Utilizing the thin film composite membranes prepared by PIM-1 and homopolymers, water flux measurements were carried out in the pervaporation setup. Additionally, an in-house instrument employing the 'pressure increase' method was used to measure the water vapor permeability. When the water permeabilities obtained from the two different methods are compared, the values obtained from the pervaporation experiment are much higher for homopolymers with aromatic and bulky groups owing to their water affinity and higher free volume. The conclusion is that these PIM based homopolymers are good candidates for pervaporation applications.

This PhD work provides a comprehensive evaluation of the findings from abovementioned studies. The performance of the developed membranes was evaluated in gas and water vapor separation, membrane distillation and pervaporation applications considering permeability, selectivity, and

structural stability parameters. These evaluations aim to identify the most suitable PIM-1 membrane design and modifications for each specific application. The overall goal of this work is to provide a better understanding of the material properties of PIM-1 and their impact on practical membrane applications. By systematically modifying and optimizing PIM-1 and its derivatives, this work contributes to the advancement of membrane technology for industrial and environmental applications.

2. Zusammenfassung

Wasser stellt die wichtigste Grundlage des Lebens dar und spielt eine zentrale Rolle für die Stabilität von Ökosystemen, die Funktionsfähigkeit von Volkswirtschaften sowie die menschliche Gesundheit. Dennoch ist die globale Wasserknappheit ein dringliches und unbestreitbares Problem. Bedingt durch das Bevölkerungswachstum, den Klimawandel und die zunehmende Umweltverschmutzung zählt der Zugang zu sauberem Wasser zu den größten Herausforderungen des 21. Jahrhunderts. Schätzungen zufolge haben weltweit Milliarden von Menschen keinen Zugang zu sicherem Trinkwasser. Gleichzeitig wird erwartet, dass die Nachfrage nach sauberem Wasser in den kommenden Jahrzehnten exponentiell ansteigen wird.

Technologische Innovationen sind essenziell, um diese Problematik zu adressieren. Insbesondere Membranverfahren haben sich aufgrund ihrer Effizienz bei der energie- und kostengünstigen Entsalzung und Rückgewinnung von Wasser als vielversprechende Technologie etabliert. Sie zeichnen sich durch einen geringen CO₂-Fußabdruck aus und bieten eine vielseitige Plattform zur Bewältigung zahlreicher Herausforderungen in der Wasseraufbereitung. Dazu zählen unter anderem die Entsalzung, die Entfernung von Schadstoffen, die Rückgewinnung wertvoller Ressourcen und die Förderung nachhaltiger Wasserkreisläufe.

Membrantechnologien nutzen selektive Trennverfahren, bei denen Meerwasser, Abwasser und industrielle Abwässer als Quellen für sauberes Wasser dienen. Zu den grundlegenden Membrananwendungen gehören die Trennung von Gas und Wasserdampf, die Umkehrosmose, die Nanofiltration, die Pervaporation und die Membrandestillation. Bei der Umkehrosmose werden Schadstoffe und auch Salze unter hohem Druck aus Salzwasser abgetrennt. Bei der Nanofiltration, einem weiteren druckbetriebenen System, werden ionische Bestandteile aus dem Abwasser abgetrennt, um sauberes Wasser zu erzeugen. Die Membrandestillation ist ein thermisch angetriebener Prozess und eine vielversprechende Technologie, bei der hydrophobe Membranen verwendet werden, um Lösungen von Salz zu trennen und zu konzentrieren. Ein weiteres Wasseraufbereitungsverfahren ist die Pervaporation, bei der Wasser aus organischen Gemischen oder flüchtigen Verbindungen entfernt wird. Darüber hinaus unterstützen Gas- und Wasserdampftrenntechnologien Wasseraufbereitungsprozesse durch die Abscheidung von

Wasserdampf aus befeuchteter Luft oder Trocknungssystemen, die ebenfalls sehr wichtige Prozesse für die Energieeffizienz sind.

Polymere sind aufgrund ihrer guten Verarbeitbarkeit und geringen Scale-up-Kosten attraktive Materialien für Membrananwendungen. Polymere mit intrinsischer Mikroporosität (PIM-1) wurden in den letzten Jahren aufgrund ihrer einzigartigen Eigenschaften als vielversprechendes Material für Membrananwendungen entwickelt. Eine der Haupteigenschaften von PIM-1, die es für Membrananwendungen attraktiv macht, ist sein hohes freies Volumen. Die starre und verdrehte Molekülstruktur ermöglicht eine schnelle Diffusion des Penetrationsmittels durch diese Hohlräume mit freiem Volumen bei Transportvorgängen und macht PIM-1 zu einem wichtigen Kandidaten für selektive Trennungen. Eine weitere Eigenschaft ist die hydrophobe Natur von PIM-1, die bei Membrananwendungen, bei denen der Wassertransport ohne Eindringen von Flüssigkeit entscheidend ist, sehr wichtig ist. Darüber hinaus ist PIM-1 ein ausgezeichnetes Polymer, das in einer Vielzahl von Lösungsmitteln leicht löslich ist, wodurch es sich leicht verarbeiten und modifizieren lässt. Aus diesem Grund kann PIM-1 in vielen Studien je nach Verwendungszweck modifiziert und funktionalisiert werden. Aufgrund dieser Eigenschaften ist PIM-1 ein vielversprechendes Polymer für viele Membrananwendungen und ein äußerst anpassungsfähiges Material, das das Potenzial bietet, innovative Lösungen für wasserbezogene Herausforderungen zu entwickeln. Bisher wurde PIM-1 in verschiedenen Membrananwendungen erforscht und hat insbesondere bei der Gastrennung vielversprechende Ergebnisse gezeigt.

PIM-1 stand im Fokus zahlreicher Studien, insbesondere aufgrund seiner hohen Selektivität im Vergleich zu herkömmlichen Gastrennmembranen. Weitere Untersuchungen konzentrierten sich auf die chemische Modifikation von PIM-1, um die Selektivität für spezifische Penetranten zu verbessern oder das freie Volumen des Polymers zu erhöhen.

Ein weiteres Anwendungsfeld von PIM-1 ist die Pervaporation. Hierbei wurde das Polymer durch funktionelle Modifikationen hydrophilisiert, um seine Leistungsfähigkeit in diesem Bereich zu optimieren. Obwohl bereits bedeutende Fortschritte erzielt wurden, bleibt das Potenzial von PIM-1 in integrierten, wasserbezogenen Prozessen bislang weitgehend ungenutzt. Dies gilt insbesondere für die Kombination verschiedener Technologien wie der Wasserdampftrennung, Membrandestillation und Pervaporation.

Im Rahmen dieser Arbeit werden drei verschiedene Teilstudien durchgeführt, um die Transporteigenschaften von PIM-1 in wasserbezogenen Anwendungen systematisch zu untersuchen. Alle drei Studien verwenden PIM-1 und seine funktionalisierten Derivate, um das Verhalten des Polymers in unterschiedlichen Wassertransportprozessen zu analysieren.

Zunächst wurde das hohe freie Volumen von PIM-1 genutzt, um die Gas- und Wasserdampf-Trennleistung zu bewerten. Am PIM-1-Gerüst wurden Modifikationen vorgenommen, um das fraktionierte freie Volumen weiter zu erhöhen. Insbesondere wurde eine auf Anthracenmaleimid basierende Komponente synthetisiert und durch Einführung verschiedener aliphatischer und aromatischer Seitengruppen durch Diels-Alder-Reaktion wurden Comonomere erhalten. Anschließend wurde eine Reihe von Homopolymeren und Copolymeren mit den Monomeren, aus denen PIM-1 besteht, synthetisiert, nachdem mit jedem der Homopolymere und Copolymere dicke Filme hergestellt worden waren, um ihre Transporteigenschaften zu untersuchen. Es wurde beobachtet, dass die Einführung von voluminösen Gruppen das fraktionierte freie Volumen erhöhte, wodurch die Diffusion des Penetrants und damit die Permeabilität erhöht wurde. Bei dem Homopolymer, dem aromatische Gruppen hinzugefügt wurden, stieg die Wasseraffinität und die Wasserlöslichkeit, was sich positiv auf die Wasserdampfdurchlässigkeit auswirkte. Die Auswirkungen dieser Modifikationen auf die Selektivität und Permeabilität von PIM-1 und PIM-basierten Homopolymeren und Copolymeren auf die Gas- und Wasserdampf-Trennleistung wurden untersucht.

In der zweiten Studie wurde die hydrophobe Natur von PIM-1 genutzt, um sein Potenzial für Anwendungen in der Membrandestillation zu erforschen. Das Ziel bestand darin, PIM-1-Membranen mit einer porösen Struktur als Voraussetzung für die Membrandestillation herzustellen, die über die traditionelle Methode der PIM-1-Herstellung hinausgeht. Zur Herstellung poröser Membranen wurde ein nicht lösungsmittelinduzierter Phasentrennungsprozess verwendet. Die Herausforderung bestand darin, die geeignete Lösungsmittel/Nichtlösungsmittel-Kombination für PIM-1 zu finden. Nach mehreren Versuchen wurde die optimale Konzentration der THF/NMP/PIM-1-Kombination (Lösungsmittel/Nichtlösungsmittel/Polymer) bestimmt und das Gießen der porösen Membran durchgeführt. Darüber hinaus wurde eine PIM-1-Dünnschicht-Verbundmembran hergestellt, um die Auswirkungen der porösen Membranstruktur auf den Wasserfluss zu untersuchen. Die mit den

hergestellten Membranen durchgeführten Wasserflussmessungen ergaben, dass große Poren den Wasserfluss abrupt erhöhten, während bei relativ kleinen Poren der Wasserfluss fast nicht vorhanden war. Vergleicht man jedoch die poröse Membran mit der Dünnschicht-Verbundmembran, so ist die Wasserdampfpermeation in der porösen Membran viel höher. Dementsprechend wird die Entwicklung eines porösen hydrophoben PIM-1, das den Transport von Wasser in Dampfform, aber keinen Flüssigkeitsstrom zulässt, aufgrund der Ergebnisse unserer Studie als vielversprechend für Anwendungen in der Membrandestillation angesehen.

Unter Berücksichtigung der bisher gewonnenen Informationen zielt unsere letzte Studie darauf ab, den Wasserdampftransport durch die Herstellung einer Dünnschicht-Verbundmembran mit funktionelleren PIM-basierten Polymeren zu verbessern, die die Homopolymerserie darstellen, die wir in der ersten Studie erhalten haben. Unter Verwendung der aus PIM-1 und Homopolymeren hergestellten Dünnschicht-Verbundmembranen wurden Wasserflussmessungen im Pervaporationsaufbau durchgeführt. Zusätzlich wurde ein hausinternes Instrument, das die „Druckanstiegsmethode“ anwendet, zur Messung der Wasserdampfdurchlässigkeit verwendet. Beim Vergleich der mit den beiden unterschiedlichen Methoden ermittelten Wasserdurchlässigkeiten sind die Werte aus dem Pervaporationsversuch für Homopolymere mit aromatischen und sperrigen Gruppen aufgrund ihrer Wasseraffinität und ihres höheren freien Volumens viel höher. Daraus lässt sich schließen, dass diese PIM-basierten Homopolymere gute Kandidaten für Pervaporationsanwendungen sind.

Diese Doktorarbeit bietet eine umfassende Auswertung der Ergebnisse der oben genannten Studien. Die Leistung der entwickelten Membranen wurde in Gas- und Wasserdampftrennung, Membrandestillation und Pervaporation unter Berücksichtigung von Permeabilität, Selektivität und strukturellen Stabilitätsparametern bewertet. Diese Bewertungen zielen darauf ab, das am besten geeignete PIM-1-Membrandesign und die am besten geeigneten Modifikationen für jede spezifische Anwendung zu ermitteln. Das übergeordnete Ziel dieser Arbeit besteht darin, ein besseres Verständnis der Materialeigenschaften von PIM-1 und ihrer Auswirkungen auf praktische Membrananwendungen zu vermitteln. Durch die systematische Modifizierung und Optimierung von PIM-1 und seinen Derivaten trägt diese Arbeit zur Weiterentwicklung der Membrantechnologie für industrielle und umwelttechnische Anwendungen bei.

3. Theoretical background

3.1. Introduction to membranes

A membrane is a sheet of material that acts as a barrier or separator between two substances. It allows the transport of certain substances selectively based on the factors such as size, solubility or charge. Membranes play a pivotal role in our daily life including filtration, separation, biochemistry and energy transformation while performing purification and selective transport functions, which are vital for separation mechanism. Membranes have become integral to chemical industry, owing to the ability to regulate the permeation rate of chemical species across the membrane. To exemplify, in separation processes, the objective is to enable the permeation of specific components in a mixture while impeding the transport of others. In drug delivery applications, membranes are employed to moderate the release of drugs from a reservoir into the body [1]. Membrane separation offers numerous advantages in both industrial and environmental applications, making it a preferred choice. It is a clean technology that helps conserve energy and can replace traditional processes like filtration, distillation, ion exchange, and chemical treatment systems. Membrane technology facilitates continuous separation processes to be conducted under mild conditions, requiring relatively low energy consumption and eliminating the need for additives. Additionally, this technology can be integrated with other separation processes, allowing for the development of hybrid processes that combine the strengths of multiple techniques [2]. Membrane separation processes can be divided into two categories as physical and chemical processes. The diverse range of membrane separation processes can be further categorized based on the driving force applied, the type and configuration of the membrane, or the removal capabilities and mechanisms involved. By applying a driving force such as a gradient of pressure, temperature, concentration, or electrical potential across the membrane, the transport of specific substances can be accomplished.

Membrane processes can be categorized into distinct groups depending on the specific driving force employed as seen in **Table 3**. Pressure-driven processes comprise reverse osmosis, ultrafiltration, microfiltration, and gas separation. Concentration gradient-driven processes

encompass dialysis, while partial pressure-driven processes include pervaporation. Membrane distillation is thermally driven process that uses the vapor pressure difference between the sides of the membrane. Lastly, electrical potential-driven processes involve electrolysis and electro dialysis. Each of these categories promotes different driving forces to facilitate the transport of substances through membranes [3, 4].

Table 3: Membrane process classification according to driving forces [3]

| Membrane process | Driving force |
|-----------------------|--|
| Microfiltration | Hydrostatic pressure (Δp) |
| Ultrafiltration | Hydrostatic pressure (Δp) |
| Reverse osmosis | Hydrostatic pressure (Δp), chemical potential ($\Delta \mu_i$) |
| Gas separation | Hydrostatic pressure (Δp), fugacity (Δf_i) |
| Pervaporation | Partial pressure (Δp_i), fugacity (Δf_i) |
| Membrane distillation | Temperature potential (ΔT) |
| Electro dialysis | Electrical potential ($\Delta \phi$) |

Apart from the driving force, the membrane itself has an importance to actuate both selectivity and flux. The structure and material of the membrane specify its properties, correspondingly the type of applications which membrane can be used for. Microfiltration exploits open structure (porous) membranes which retains the particles with a diameter larger than 10 nm. The open structures show low hydrodynamic resistance, therefore, high flux with relatively low hydrostatic pressure can be achieved. On the other hand, ultrafiltration employs denser membrane structure since higher applied pressure is needed to separate macromolecules with high molecular weight from aqueous solution. In certain cases, it is feasible to separate low molecular weight components of similar sizes from each other. To achieve this, a highly dense (asymmetric) membrane is used, leading to a significant increase in hydrodynamic resistance. This process is referred to as reverse osmosis. As one progresses from microfiltration to ultrafiltration, nanofiltration, and ultimately reverse osmosis, the hydrodynamic resistance intensifies, necessitating higher driving forces. Gas separation processes can utilize two types of membrane morphology depending on the application

either a dense membrane which facilitates the transport via diffusion, or a porous membrane enables Knudsen flow. Additionally, pervaporation and vapor permeation rely on a dense separating layer as membrane structure while membrane distillation involves porous membrane structure where the vapor transport occurs through the hot and cold side of the membrane [5]. In the subsequent sections of this dissertation, gas separation, pervaporation and membrane distillation will be discussed in more details.

3.2. Classification of membranes

Based on their origin, membranes can be categorized into two categories: natural and synthetic membranes.

3.2.1. Natural membranes

Generally, biological membranes are referred to natural membranes which serve as selectively permeable barriers within living organisms. These membranes vary between different organisms. For example, plants and bacteria have chemically different membranes than animals, and there are multiple membrane structures such as chloroplasts, mitochondria and the nucleus within the cells. Furthermore, the cell membrane not only acts as a selectively permeable barrier, but also separates the intracellular environment from the extracellular matrix. Membranes in animals are composed of a phospholipid bilayer. Numerous biological processes utilize membrane which are essential components for both physical and chemical functions. These functions include fundamental processes like metabolism, as well as the accumulation and utilization of energy within biological systems [6].

3.2.2. Synthetic membranes

Synthetic membranes can be fabricated by a diverse range of materials, including organic substances such as polymers and liquids, as well as inorganic materials like carbons and zeolites. Nevertheless, polymer-based membranes dominate the membrane industry due to their cost-effectiveness and wide range of applications [7]. The main aspect of polymeric membranes is the affinity of polymer material towards specific components. The characteristic that makes polymeric membranes attractive is the ability to control the pore size during membrane formation. The choice of a suitable polymer depends on the specific task at hand. Examples of common polymeric

membranes include cellulose acetate (CA), polyacrylonitrile (PAN), polyimide, polycarbonate (PC), polyethylene (PE), polypropylene (PP), polytetrafluoroethylene (PTFE) , and poly(vinylidene fluoride) (PVDF) [8]. The examples of polymers used in main membrane application can be seen in **Table 4**.

Table 4: Common polymers used in membrane applications.

| Application | Polymer |
|-----------------------|--|
| Microfiltration | Poly(vinylidene fluoride), polyethersulfone, cellulose acetate, polypropylene, polyamide [9] |
| Ultrafiltration | Poly(vinylidene fluoride), polysulfone, polyethersulfone, polyacrylonitrile, cellulose acetate [10] |
| Reverse osmosis | Cellulose acetate, polyamide, polysulfone [11] |
| Gas separation | Cellulose acetate, poly(dimethylsiloxane), polycarbonate, polyimide, polysulfone, poly(phenylene oxide) [12] |
| Pervaporation | Polyvinyl alcohol, polyimide, poly(lactic acid), cellulose acetate [13] |
| Membrane distillation | Polyethylene, polypropylene, polytetrafluoroethylene, polyvinylidene fluoride, cellulose acetate, poly(dimethylsiloxane), polyether sulfone [14] |

Synthetic membranes are categorized based on their cross-sectional morphology as either symmetric (isotropic) or asymmetric (anisotropic). This classification is shown in **Figure 1**.

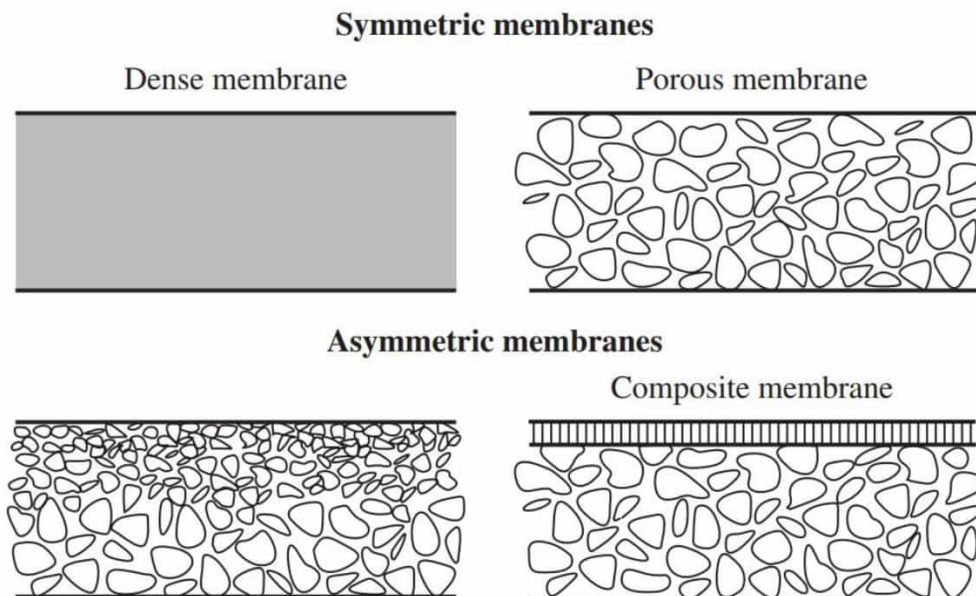


Figure 1: Schematic representation of typical membrane structure. Reprinted with permission from Mahenthiran, A.V. and Z.A. Jawad, 2021, Membranes [15].

3.2.2.1. Symmetric (isotropic) membranes

Symmetric membranes can be also subdivided into two groups such as porous and non-porous (dense) membranes. Porous membranes are generally utilized in microfiltration, ultrafiltration and nanofiltration that each of them is categorized based on the pore size. Microfiltration membranes basically possesses a rigid, highly porous structure with interconnected pores distributed randomly, typically ranging from 0.01 to 10 μm in diameter. Ultrafiltration membranes have smaller pore size ranging from 2-100 nm, while nanofiltration membranes have pore size between 0.1-2 nm [5]. In principle, particles in the range of between largest and smallest pore size of the membrane are selectively rejected, depending on the distribution of pore sizes. However, particles that are significantly smaller than the smallest pores pass through the membrane. Therefore, the separation of solutes using porous membranes primarily depends on the molecular size and pore size distribution. The other symmetric type of membrane which is non-porous (dense) membrane comprises a dense film that facilitates the transport of the permeants through the membrane by diffusion driven by pressure, temperature or concentration gradients. Since the separation of different components in a mixture depends on their diffusivity and solubility in the membrane material, dense membranes can effectively separate permeants of similar size if their solubility in the membrane material exhibits significant variation. The main applications of dense membranes

are gas separation, pervaporation, and reverse osmosis, often featuring an anisotropic structure to optimize the flux [1].

3.2.2.2. Asymmetric (anisotropic) membranes

In membrane separation processes, high transport rate is preferred for economic efficiency which leads to a necessity of membranes as thin as possible, since there is an inverse relation between thickness of the membrane and the transport rate of the species through the membrane. However, conventional film fabrication methods typically restrict the production of mechanically robust and defect-free films to a thickness limit of approximately 20 μm . Therefore, a different type of membranes was developed which are asymmetric membranes. These membranes are composed of a thin, dense top layer that has the thickness lower than 0.5 μm , supported by a porous sublayer. The transport rate is primarily governed by the skin layer. Mostly, asymmetric membranes perform significantly higher permeation rates compared to symmetric membranes of similar thickness because there is an inverse relationship between transport rate and membrane thickness [16].

3.3. Membrane applications

3.3.1. Gas separation

In the last twenty years, membrane technology has emerged as an attractive option for gas separation. Membrane-based gas separation offers many advantages such as low energy costs and low capital investments. Additionally, membrane separation units have a relatively small carbon footprint, which is important in environments like offshore gas processing platforms. Consequently, due to the central role of gases in the chemical feedstock industry, membrane separation has gained significant importance from an economic standpoint. However, to make a membrane beneficial for carbon capture, there is still a need for significant improvements in membrane material selection and performance, system design, and membrane module development [12]. Polymeric membranes play a significant role in the industrial gas separation market, offering a strong combination of performance and cost-effectiveness. Numerous polymers have been investigated for membrane applications, including polysulfone, polyimide, and cellulose acetate. However, only a few of them have found practical use in industrial membrane gas separation. **Table 5** exhibits the gas permeability of common industrial polymers.

Table 5: Gas permeability coefficient of industrial polymeric membranes

| | Permeability coefficient @ 30 °C (Barrer) | | | | |
|-----------------------------|---|----------------|----------------|-----------------|-----------------|
| Polymer | H ₂ | O ₂ | N ₂ | CO ₂ | CH ₄ |
| Polyimide | 28.1 | 2.13 | 0.32 | 10.7 | 0.25 |
| Polysulfone | 14 | 1.4 | 0.25 | 5.6 | 0.25 |
| Cellulose acetate | 2.63 | 0.59 | 0.21 | 6.3 | 0.21 |
| Polydimethylsiloxane (PDMS) | 550 | 500 | 250 | 2700 | 800 |
| Polyphenyleneoxide | 113 | 16.8 | 3.81 | 76 | 11 |

3.3.1.1. Gas transport mechanism

Gas separation processes are primarily determined by the permeability and selectivity of the membrane. Additionally, the structural characteristic of the membrane has a great influence on the gas transport. Gas separation membranes can be divided into two groups: porous and non-porous membranes, based on their flux density and selectivity. Porous membranes are characterized by pore flow model, while solution diffusion models are used to describe gas transport mechanism of non-porous membranes as illustrated in **Figure 2** [17].

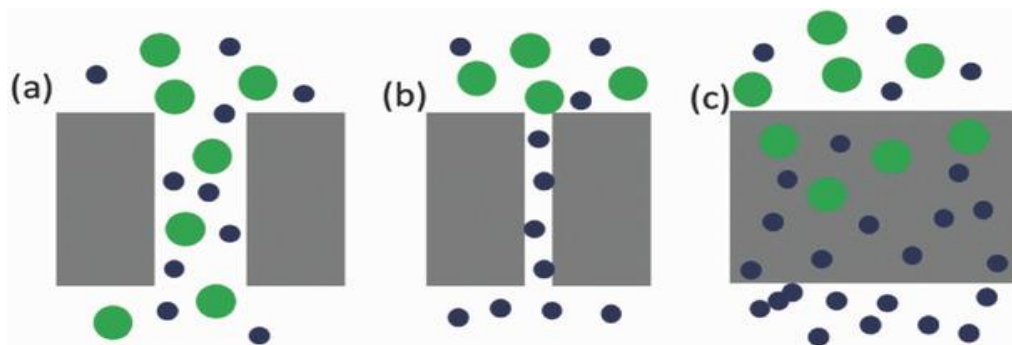


Figure 2: Gas transport mechanisms: (a) Knudsen diffusion, (b) Molecular sieving, (c) Solution-diffusion model [18].

Pore flow model

The pore flow model considers uniform concentrations of solvent and solute within the membrane and represents the chemical potential gradient across the membrane solely as a pressure gradient [19]. In this model, the flow hinges on the pore size of a porous membrane and the mean free path

of molecules. The primary mechanisms in the porous media are Knudsen diffusion, viscous flow and molecular sieving. Gas transport is governed by Knudsen diffusion, if the pore size is smaller than 0.1 μm (equal to or smaller than the mean free path of gas molecules) [20]. In Knudsen diffusion (K_n), collisions occur primarily between gas molecules and the pore wall when $K_n > 10$. The driving force for Knudsen diffusion is equivalent to the partial pressure gradient, which is proportional to the total pressure gradient in a single-gas system [21]. On the other hand, the interaction between gas molecules themselves prevails the interaction between gas molecules and pore walls, when $K_n < 0.1$. This type of transport is called viscous flow (Poiseuille flow) [22]. The other transport mechanism, molecular sieving, occurs when the pore size is between 5 Å and 20 Å. When the pore size of the membrane falls into the range of the gas molecule size, gas molecules can easily pass through the pores, resulting in a high separation factor.

Solution-diffusion model

In this transport model, a uniform pressure is assumed across the membrane and the chemical potential gradient within the membrane is predicated only as a concentration gradient. In other words, since pressure is constant, the transport of the gas molecules is driven by diffusion due to concentration gradients [19]. Solution-diffusion transport eventuates in dense (non-porous) membranes. Gas separation is based on the mechanism of the sorption of the permeant into the membrane, the permeation by diffusion through the membrane following the desorption at the low pressure side of the membrane [12]. Dense polymers do not acquire fixed pores, nonetheless, the polymer chains do not pack efficiently leading to formation of free volume where the molecule transport occurs through this free volume. **Equation 1** describes the solution-diffusion model as the permeability (P), which is proportional to the solute flux of the certain concentration difference across the membrane, is the product of the kinetic diffusivity (D) and the thermodynamic solubility (S) [23].

$$P = D \cdot S \quad (1)$$

The term of permeability is an intrinsic property of the material which is determined by the product of the number of molecules dissolved and their rate of migration through the membrane matrix. Permeability unit is usually expressed by Barrer, where 1 Barrer = $1 \times 10^{-10} \text{ cm}^3 \text{ (STP) cm}/(\text{cm}^2 \text{ s cmHg})$. In membrane science, another term 'permeance' is also a commonly used parameter which is related to permeability which is defined as the ratio of permeability to the thickness of the

membrane. Gas permeance is often expressed as GPU, where $1 \text{ GPU} = 1 \times 10^{-6} \text{ cm}^3 \text{ (STP)/(cm}^2 \text{ s cmHg)}$. A very important aspect focused on membrane applications is the membrane selectivity or so-called separation factor ($\alpha_{a/b}$) which is the ratio of permeability of two gases (a and b) as seen in the **Equation 2**. The selectivity is bigger than one that also means there is no separation when it is equal to 1.

$$\alpha_{a/b} = \frac{P_a}{P_b} \quad (2)$$

The concentration gradient or diffusion coefficient describes how easily a penetrant can diffuse across the membrane. The constant flux, in this case, is described by Fick's law (**Equation 3**).

$$J = -D \frac{dc}{dx} \quad (3)$$

where D is the diffusion coefficient and dc/dx is the concentration gradient across the membrane. The diffusion coefficient of a penetrant is a kinetic parameter and is a function of the properties of both the penetrant and the polymer that builds up the membrane. On the other hand, the solubility coefficient (S) defines how much of a penetrant can be retained by the membrane in a single instance. The equation used to calculate the solubility coefficient is given in **Equation 4**.

$$S_i = \frac{C_i}{p_i} \quad (4)$$

where, S_i represents the solubility coefficient, C_i is the concentration within the membrane, and p_i is the partial pressure of component i in the feed flow [24].

3.3.1.2. Classification of polymers for gas separation

Most of the polymers used in gas separation can be divided into two groups, which are either rubbery or glassy polymers. Rubbery polymers are prone to be soft and flexible while glassy polymers are rigid and usually brittle. The diffusion rate of large molecules is hindered due to molecular motion is limited. The differentiating factor between the rubbery and glassy states is the glass transition temperature (T_g) of the polymer. Around T_g , properties such as specific heat capacity, dielectric constant, density, conductivity or charge mobility, and rates of gas/liquid diffusion throughout the polymer vary.

Rubbery polymers

Rubbery polymers are assumed to be in a thermodynamic equilibrium state, and gas solubility in these polymers follows Henry's law where the sorption of gases resembles the sorption of gases in low molecular weight liquids (**Equation 5**):

$$C = k_D \cdot p \quad (5)$$

where C is gas concentration, k_D is the Henry's law constant and p is the pressure. Diffusion of gases in rubber typically follows the Fick's law when rubber does not undergo structural rearrangement (i.e. crystallization) in a gaseous environment. At low penetrant concentrations, the diffusion coefficient is generally independent of gas concentration [25]. The mobility of polymer chains is the most important characteristic for rubbery polymers. Gas permeability through rubbery polymers is typically higher than in glassy polymers. The reason is that rubbery polymers have more backbone mobility, since the loss of restrictions on rotations due to bulky side groups or due to interactions among chains. Even though this feature supports the increase of permeability, it causes to reduce in selectivity due to size dependent separation is hindered. In such modifications, it is seen that the increase in the size of the side groups leads to less chain flexibility follows an increase in T_g but reduction in permeability. However, adjustment on the chain flexibility whereas the side groups are intact is possible to moderate the permeability. The presence of Si-O bonds either in the backbone or in the side chain assist to increase the chain mobility, consequently the escalation on permeability [26].

Glassy polymers

The chemical structure of glassy polymers has a much more significant effect on gas permeation compared to rubbery polymers. Glassy polymers are typically considered to be in a non-equilibrium state, and this condition arises from the non-equilibrium excess free volume. The excess volume enables a new sorption site for penetrants which is not available in rubbery polymers. Consequently, an additional sorption mechanism which is called 'Langmuir isotherm' occurs in this free volume (**Equation 6**).

$$C_H = \frac{C'_H b p}{1 + b p} \quad (6)$$

where C_H is the concentration of the penetrant in the free volume, C'_H is the Langmuir sorption capacity, b is the Langmuir affinity parameter, and p is the pressure [27]. The molecules absorbed

by this mechanism have less diffusional mobility compared to those absorbed by the Henry's law mode. Due to that, the analysis of transient permeability experiments is more complex for glassy polymers than for rubbery polymers. In order to describe gas transport in glassy polymers, the three-parameter dual-mode sorption isotherm model is used (**Equation 7**).

$$C = k_D p + \frac{C'_H b p}{1 + b p} \quad (7)$$

In the light of these facts, the dual-mode sorption model indicates that the equilibrium concentration of a gas differs between glassy and rubbery polymers. In the case of rubbery polymers, the concentration shows a direct proportionality to the applied pressure. However, in glassy polymers, the equilibrium concentration is usually non-linear with the applied pressure and approaches an asymptotic value as the pressure increases. This can be attributed to the saturation of free volumes, which prevents further accommodation of penetrants [28].

3.3.1.3. Trade-off between permeability and selectivity

Gas separation membranes are aimed to use the polymers that show both high permeability and selectivity. Higher permeability leads to reduction in the membrane area required to purify a certain amount of gas, consequently lowering the capital cost of membrane units. Over the years, the gas separation properties of numerous polymers have been measured, and significant research effort has been spent for the development of polymers that are both more permeable and more selective than first-generation materials [29]. A trade-off relation has been plotted by Robeson between permeability and selectivity, which is based on the fact that the selectivity decreases while permeability increases. Robeson introduced a double logarithmic plot which is shown in **Figure 3** that depicts the relationship between selectivity and permeability. This plot is useful tool for the evaluation of the polymeric materials performance on gas separation and is used for establishing an "upper bound" which is drawn by the literature data [30]. One of the goals in gas separation membrane research is to develop the membranes which goes beyond the upper bound with separation performance in the desired region.

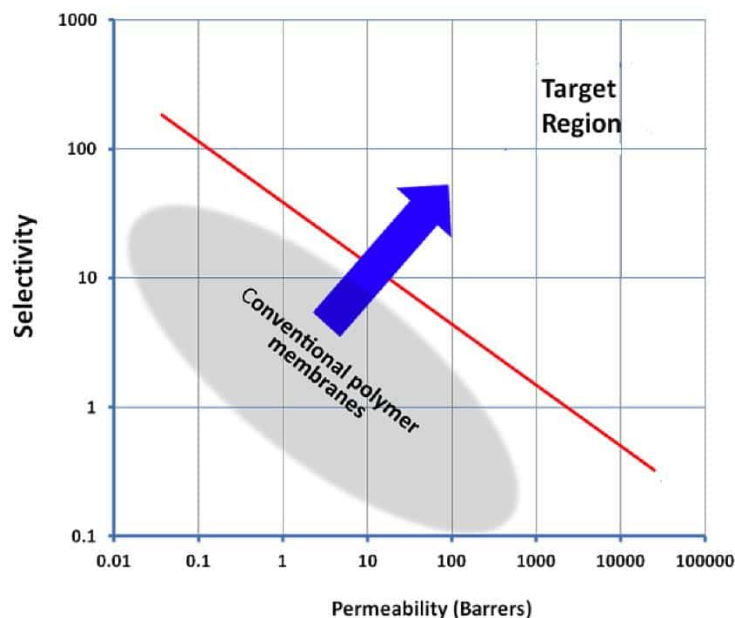


Figure 3: Robeson upper bound: Permeability-selectivity trade-off. Reprinted with permission from Panapitiya, N., et al., 2016, Materials [31].

The significant research conducted in this field has led to the discovery of polymeric membranes that surpass the original upper bound, therefore, Robeson revised the existing data and introduced the “2008 upper bound” plot [32]. One of the corresponding representations of the revisited upper bound is shown in **Figure 4**. As it is also explained in the section 3.3.1.2., it can be seen that rubbery polymers have lower permeability than glassy polymers.

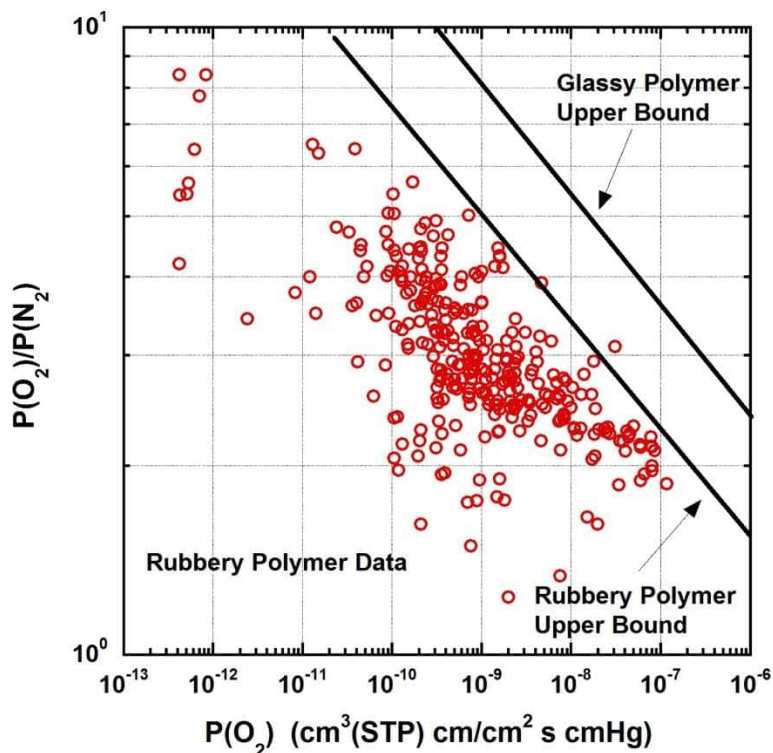


Figure 4: Comparison of upper bound for glassy polymer and rubbery polymer based on O₂ permeability over O₂/N₂ selectivity data [33].

Despite the fact that many polymers have been synthesized over the years and surpassed the Robeson's upper bound reaching the high permeability and selectivity zone, the other polymer properties such as mechanical stability, aging and the cost of the material were affected adversely. Therefore, it hinders the utilization of the newly developed polymers in a large scale of membrane fabrications.

Table 6: Common polymers used for gas separation membranes.

| | |
|-----------------------------|--|
| Polyimide (PI) | Polycarbonate (PC) |
| Polyetherimide (PEI) | Poly(vinylidene fluoride) (PVDF) |
| Polysulfone (PS) | Cellulose acetate (CA) |
| Poly(phenylene oxide) (PPO) | Polyamide (PA) |
| Polydimethylsiloxane (PDMS) | Poly(1-trimethylsilyl-1-propyne) (PTMSP) |

3.3.2. Pervaporation

The term "pervaporation," derived from the combination of "permeation" and "evaporation," was first proposed by Kober to describe the selective permeation of water through a cellulose nitrate film from aqueous albumin and toluene solution. Since then, numerous studies have been conducted to further develop this technology. [34]. Pervaporation is a separation technique, which utilizes a semi-permeable membrane, where a liquid comes into contact with the membrane on the feed side. The driving force for the vapor transport arises from a chemical potential difference created by using a vacuum or using a sweep gas causing the vapor which is collected on the permeate side of the membrane (**Figure 5**). This allows for the selective separation of components in the liquid phase [35]. Principally, the separation capability of the pervaporation process relies on the preferential sorption and diffusion of components within the membrane. As a result, pervaporation can overcome the thermodynamic vapor-liquid equilibrium (VLE) limitations and requires less energy compared to traditional distillation technology, as it only requires the latent heat of vaporization[36].

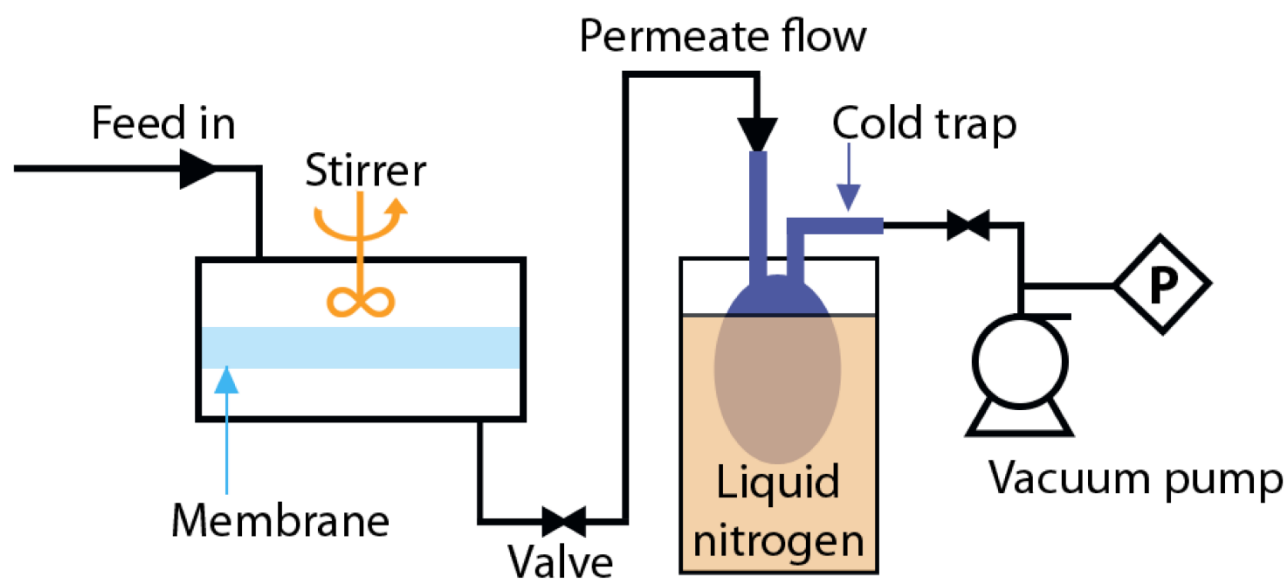


Figure 5: Schematic representation of pervaporation process. Reprinted with permission from Pulyalina, A., et al., 2020, Symmetry [37].

Furthermore, pervaporation technology is also suitable for the purification of thermally sensitive organics, such as aromatic compounds, in the food industry. Pervaporation is suitable for the

separation of liquid mixtures containing small molecules such as water, organic solvents, isomer and azeotrope. Pervaporation, vapor permeation and gas permeation are closely related processes. In all techniques, the driving force is the chemical potential gradient which is originated by the partial vapor pressure gradient of the components. The separation occurs by the physical-chemical affinity between the membrane material and the components to be transported, which is based on sorption and solubility phenomena [38].

3.3.2.1. Basics of pervaporation

The transport mechanism of pervaporation membranes generally follows the solution-diffusion model, as in the case for gas separation membranes. In general, the penetrants are adsorbed from the feed liquid into the membrane, then diffused through the active layer of the membrane which follows the desorption of the penetrant to the vapor phase on the permeate side [35]. Permeability and selectivity represent the intrinsic transport properties of pervaporation membranes, as in the case of gas separation membranes. The separation efficiency can be enhanced by improving the solubility selectivity and diffusion selectivity of the penetrants, which can be achieved by tailoring the chemical property and morphology of pervaporation membrane. Both the intrinsic properties and the fabrication technique of the membrane material play a significant role to determine the separation performance. The efficiency of pervaporation membrane material is typically expressed as in the **Equation 8**.

$$J = \frac{W}{At} \quad (8)$$

where J is total flux, W is weight of the permeate, A is membrane area and t is time. The relation between permeation flux and the transport parameters is given in **Equation 9**.

$$J_i = \frac{P_i \Delta p_i}{l} \quad (9)$$

where J_i is permeate flux of the component, P_i is permeability, Δp_i is partial pressure difference across the membrane, l is membrane thickness. The other parameter which determines the membrane performance is the separation factor (α) and it can be defined in the following equation (**Equation 10**).

$$\alpha = \frac{y_{wi}/y_{wj}}{x_{wi}/x_{wj}} \quad (10)$$

where y_w and x_w are the mass fractions of the components i and j in the permeate and feed side, respectively [39].

3.3.2.2. Current applications of pervaporation

Pervaporation is an ecofriendly and cost-effective technology for the separation of liquids in various industrial processes. Due to its versatility, pervaporation can be used for the purification of a wide range of mixtures with different chemical and physical properties by adjusting membrane characteristics that address different issues. Pervaporation can be categorized based on the composition of the feed solution, as follows: dehydration of organic solvents, removal of organic compounds from aqueous solutions, and separation of organic mixtures.

Organic solvent dehydration has a great importance in the separation industry. Organics such as low molecular weight alcohols, ethers, and ketones easily form azeotropes and mix with water at any proportion [40]. Conventional separation technologies are often considered not cost-effective since they require high energy inputs. However, pervaporation can tackle with these challenges as it is not limited by the vapor-liquid equilibrium, therefore, it allows to decompose the azeotropes. The most exploited applications to remove water from alcohol solution are to purify ethanol or isopropanol which share a high demand in chemical industry [41].

The removal of organic compounds from aqueous solutions is another important issue, especially from an environmental point of view. This application includes wastewater treatment, recycling of valuable organics and pollution control. In this regard, pervaporation is a competitive technique in wastewater treatment and is useful for the removal of volatile organic compounds (VOCs) [42]. Because of these reasons, the recovery of alcohols from water has become an important research area due to the growing interest in bioalcohol production as an alternative to fossil fuels in recent years [43].

The separation of organic mixtures has become of great importance due to the industrial need for efficient methods to separate mixtures such as benzene/cyclohexane, benzene/hexane, toluene/heptane, ethylbenzene/xylene, p-xylene/o-xylene, etc. Since the components in these pairs have similar physicochemical properties, the effective separation of these mixtures according to the solubility parameter theory is the challenge of this application [40, 44]. In general, the

separation of organic mixtures is based on differences in steric effects, polarity and affinity of different organic molecules to membrane materials.

The main limitation for the wide field of application is the lack of suitable membranes and modules with good long-term stability in organic solvents [45].

3.3.2.3. Pervaporation membrane materials

In the selection of pervaporation membrane material, affinity and size sieving are two important parameters. Size sieving function can improve the diffusion selectivity of the components in case of solvent dehydration. To date, several membrane materials have been used to serve pervaporation application including polymeric membranes, inorganic membrane, mixed-matrix membranes and 2D material membranes. The schematic representation of pervaporation membranes is shown in **Figure 6**.

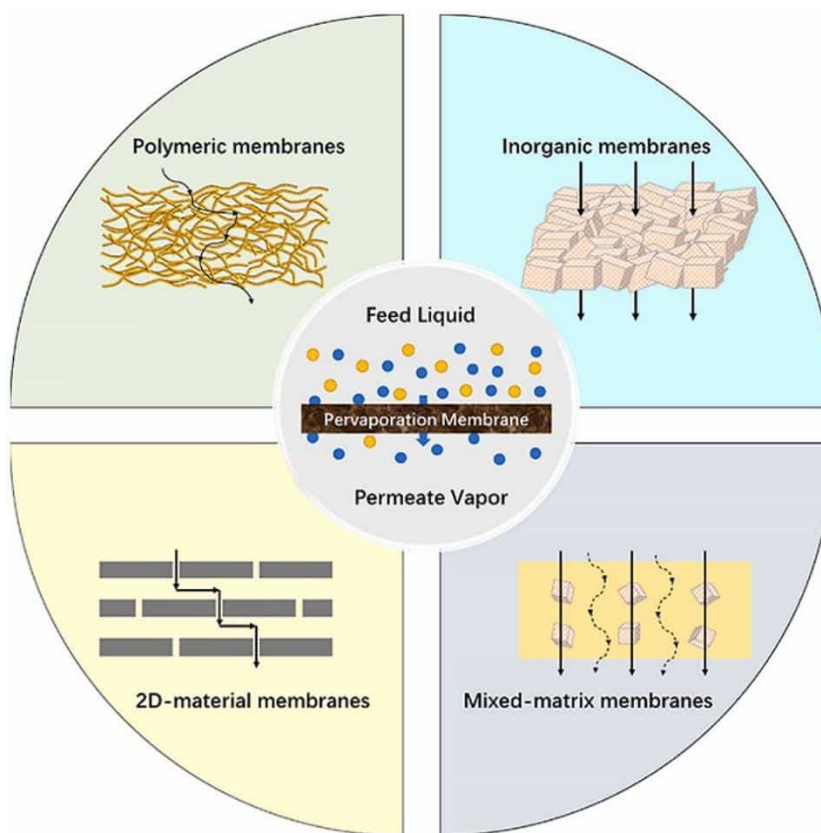


Figure 6: Illustration of various pervaporation membranes [39].

Among them, polymeric membranes are favorable since their ease of fabrication and modification. Polymeric membranes used in pervaporation can be classified such as hydrophilic and hydrophobic membranes. **Table 7** shows the common polymeric membranes used in pervaporation.

Table 7: Types of polymeric membranes used in pervaporation.

| Hydrophilic membranes | Hydrophobic membranes |
|-------------------------------|--|
| Poly(vinyl alcohol) (PVA) | Polydimethylsiloxane (PDMS) |
| Polyamide (PA) | Poly (ether-block-amide) (PEBA) |
| Polyimide (PI) | Poly (1-(trimethylsilyl)- 1-propyne) (PMTSP) |
| Polyelectrolyte complex (PEC) | Polytetrafluoroethylene (PTFE) |

Hydrophilic membranes

Such kind of membranes are used for exclusion of water form organic solvents and solvent mixtures, focusing on azeotropic mixtures. Hydrophilic membranes can interact with water molecules via hydrogen bonding, ion-dipole interactions or dipole-dipole interactions. Generally, glassy polymers, which exhibit limited chain mobility and low free volume that allows the separative permeation on the molecular size level, are utilized for hydrophilic water selective membranes [40]. The common hydrophilic pervaporation membranes primarily used in the dehydration of organic solvents are poly(vinyl alcohol) (PVA), chitosan (CS), polysulfone (PS), polyimide (PI), polyamide (PA), and polyaniline. Nevertheless, these hydrophilic membranes suffer from swelling in water, thus, decreasing stability. As a result of this, an increase of permeation flux occurs whereas separation factor reduces. Therefore, a membrane material should acquire an optimum hydrophilicity-hydrophobicity balance. The research has been focused on the development of pervaporation materials with good chemical and thermal stability for dehydration of solvents at high operation temperatures. To serve this, the polymers which contain rigid chains have been developed [46]. In comparison to water filtration and gas separation processes, pervaporation has distinguished aspects regarding operating conditions. From a process point of

view, pervaporation does not require high feed pressure. Instead, a high operation temperature is needed to enhance efficiency, since the feed contains liquid and the permeate is vapor [35].

Hydrophobic membranes

Hydrophobic pervaporation membranes are usually organophilic and are employed in solvent recovery application. These membranes allow the selective permeation of the solvent from solvent-water mixtures. Hydrophobic pervaporation membranes have a great potential to efficiently remove low concentrations of organic compounds from wastewater as a green approach [42]. Unlike the hydrophilic membranes used for solvent dehydration, the hydrophobic pervaporation mechanism depends only on the sorption selectivity and are inconvenient for diffusion selectivity aiming to selective permeability of organics from water. The reason of that is the diffusivity of organic compounds is lower than that of water in regard to molecule size. In this point, the thermodynamic sorption of components in the membrane which can be related to the solubility parameter, is significant for the design of hydrophobic membranes. To simplify, if the solubility parameter of a component is close to the membrane material, then the component has a strong affinity towards membrane resulting high sorption performance. The solubility parameters of small molecules can be calculated based on the Hansen solubility parameter theory, taking into account contributions from hydrogen bonding, polar, and dispersive forces [39]. The difference in solubility parameter between penetrants and their individual differences with the membrane can enhance the selectivity.

Table 8: Hansen solubility parameters of some solvents [46]

| Liquids | Hansen solubility parameters (MPa ^{0.5}) | | |
|-------------|--|-------------------------------|-------------------------------|
| | δ_p : polar component | δ_h : Hydrogen bonding | δ_d : dispersive force |
| Water | 17.0 | 43.3 | 15.0 |
| Methanol | 22.3 | 12.3 | 15.1 |
| Benzene | 0 | 2.0 | 18.4 |
| Cyclohexane | 0 | 0.2 | 16.8 |

3.3.2.4. Challenges of pervaporation

The lack of membranes with high efficiency, selectivity and stability for pervaporation applications is one of the main barriers to development. Polymeric membranes are preferred due to their compact structure, ease of fabrication and scale-up, and low material costs. However, the necessity to balance between permeability and selectivity of these membranes limits their performance. The development of membrane materials is critical for pervaporation to compete with other separation techniques. Desirable membrane materials should offer exceptional productivity and separation efficiency [39, 45].

Inorganic materials generally show higher separation performance than polymeric membranes due to their superior thermal and solvent stability. However, their fragility, complex manufacturing processes and high cost limit their use. Researchers are working on the integration of organic and inorganic components that can offer superior separation performance and combined advantages. In this process, the compatibility of polymeric and inorganic components should be considered as an important aspect [47].

The physicochemical properties a good membrane must possess include mechanical stability, thermal durability and chemical resistance. These properties are vital to maintain long-term stability in harsh environmental conditions and minimize solvent-induced swelling. It is also a common challenge that a membrane material may exhibit high separation performance for a particular solvent mixture, but not for other mixtures. In other words, it is understood that different mixtures require different types of membranes. Therefore, the selection and testing of membrane materials should be specific to various mixture pairs [46, 48].

Besides the development of new materials and advanced manufacturing techniques, successful membrane development requires a thorough understanding of the mass transport dynamics across the membrane. Such groundwork is the basis for the structural design of the membrane as well as for process optimization and performance evaluations, and this information can directly determine the effectiveness of separation technologies.

3.3.3. Membrane distillation

Membrane distillation (MD) is a thermally driven membrane process, which relies on the vapor pressure difference between the hot and cold sides of a porous hydrophobic membrane to facilitate

the selective transport of water vapor across the membrane. As a result, water vapor condenses on the cold side of the membrane, resulting in the production of high-quality distilled water [49, 50].

Figure 7 shows the mechanism of membrane distillation.

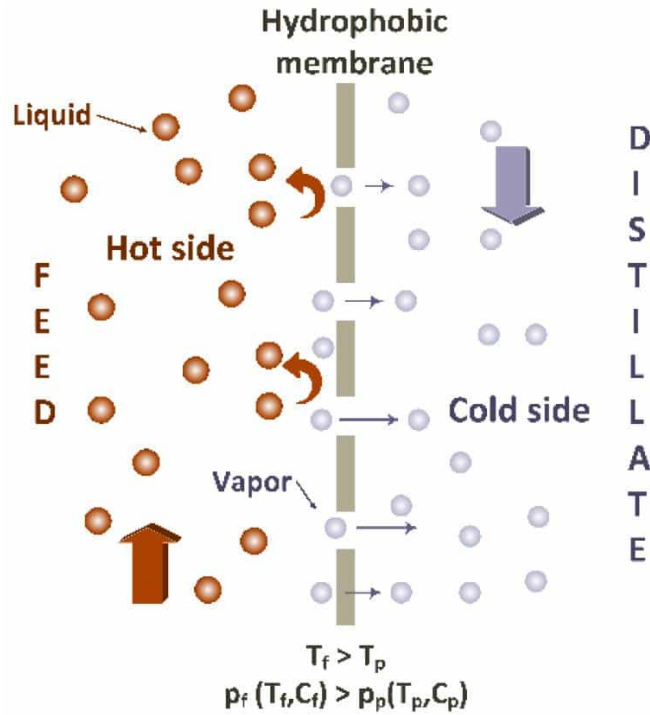


Figure 7: Principle of membrane distillation through the hydrophobic membrane. Reprinted with permission from Karanasiou, A. et al., 2018, Water [50].

MD offers many attractive features and one of them is low operating costs. Unlike traditional processes, it does not require heating the solution (mainly water) up to its boiling point, resulting in lower temperatures required for operation. Additionally, the hydrostatic pressure required in MD is lower compared to pressure-driven membrane processes such as reverse osmosis (RO). Hence, MD is considered a cost-effective process that can utilize inexpensive materials such as plastics, which have less demanding membrane properties but alleviate corrosion issues. Another feature which makes MD favorable is the membrane pore size required for MD as it is relatively larger than in other membrane separation processes such as reverse osmosis. As a result, MD process is less affected by fouling. Moreover, MD process can be operated using low-grade heat sources such as waste heat, solar energy and geothermal energy. Such capabilities have increased the interest in MD and research has focused on improving the characteristics of MD technology.

Considering that water scarcity is one of the biggest challenges today and the demand for fresh water has been increasing over the last two decades, MD becomes a promising technology for desalination of high saline waters in this context [51-53].

3.3.3.1. Membrane distillation configurations and application area

Generally, there are four types of MD configuration system to impose the mechanism of MD which relies on vapor pressure difference between the feed and permeate sides of the membrane. **Figure 8** presents the schematic representations of these configurations.

- a) Direct contact membrane distillation (DCMD): In DCMD, which is the most basic MD configuration, the hot feed solution is in direct contact with the hot surface of the membrane. Evaporation starts at the feed surface of the membrane and vapor transport takes place due to the pressure difference across the membrane followed by the condensation within the membrane module. Since the membrane is hydrophobic, only vapor phase is present in the membrane pores and feed solution does not penetrate through the membrane. A disadvantage of this configuration is heat lost by conduction. [52, 54].
- b) Air gap membrane distillation (AGMD): In this design, the feed solution is in direct contact with the hot side of the membrane as described in DCMD. However, there is stagnant air between the cold side of the membrane and condenser. Therefore, vapor passes through the membrane by crossing this air gap and condenses over the cold side of the membrane. Owing to this air gap, heat loss is lowered and wetting on the permeate is prevented. However, the main drawback is that the air gap creates an additional resistance to vapor transport [52, 55].
- c) Sweep gas membrane distillation (SGMD): Similar to AGMD, mobile inert gas is introduced on the permeate side of the membrane. The vapor is swept and then condensed outside of the membrane. The benefit of this configuration is that mass transfer is promoted by virtue of inert gas which is not stationary unlike in AGMD. Yet, the design introduces the complexity in terms of installation of additional equipment and the heat recovery is difficult [52, 55].
- d) Vacuum membrane distillation (VMD): In this configuration, a pump is used to generate the vacuum at the permeate side and the condensation of the vapor occurs outside of the

membrane module. In comparison to AGMD, heat loss is negligible but there is higher probability of pore wetting [52, 56].

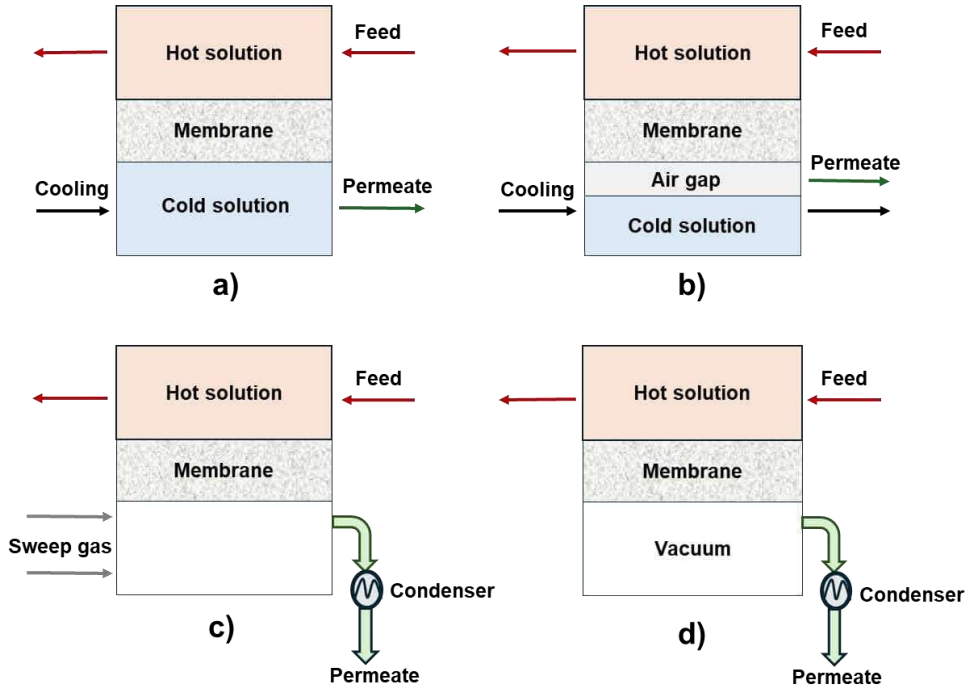


Figure 8: Schematic representation of membrane distillation configurations: (a) direct contact membrane distillation, (b) air gap membrane distillation, (c) sweep gas membrane distillation, (d) vacuum membrane distillation.

DCMD and AGMD are generally used for desalination, water treatment, and concentration of aqueous solutions in food industries. SGMD and VMD are usually used to remove volatile organic or dissolved gas from an aqueous solution [57].

3.3.3.2. Membrane distillation characteristics

MD performance is greatly influenced by several parameters. In general, MD material must be porous, hydrophobic, thermally stable and chemically resistant to the feed solution. Principally, membrane materials are identified by following characteristics.

- **Liquid entry pressure (LEP):** It can be defined as the minimum hydrostatic pressure introduced to the feed solution before it surmounts the hydrophobic forces of the membrane and penetrates into the membrane pores. LEP is a key parameter, which determines the membrane wetting and should be as high as possible, which can be achieved by narrow

pore size and high contact angle [58]. Typical LEP value of commercial MD membranes are between 1-4 bar. LEP can be calculated by Young-Laplace equation as follows (**Equation 11**).

$$LEP = \frac{-4 B \gamma_L \cos \theta}{d_{max}} \quad (11)$$

where B is the pore geometry coefficient, γ_L is the surface tension of liquid, θ is the contact angle, d_{max} is the maximum pore radius.

- Permeate flux: Another critical parameter is the permeate flux, which can be affected by the pore characteristics of the membrane. For instance, permeate flux increases as the pore size and porosity of the membrane increase. On the other hand, there is an inverse relation between permeate flux and the membrane thickness, therefore, the membrane thickness should be as thin as possible [59].
- Thermal stability: Membrane material should exhibit high thermal stability and resist towards high temperature. Depending on membrane nature (amorphous or crystalline), membrane properties may inversely change beyond the transition temperatures [59].
- Chemical stability: Membrane material should not chemically interact with any substance in the feed solution, otherwise the membrane matrix may deteriorate. For this reason, the membrane material requires to be chemically stable to the substances in the solution [59].

3.3.3.3. Materials used in membrane distillation

Hydrophobicity is the key element for the membrane material used in MD. Therefore, the membrane material must be inherently hydrophobic, or the membrane surface must be modified to be hydrophobic. The most commonly used porous hydrophobic membranes are made of different polymers such as poly(vinylidene fluoride) (PVDF), polytetrafluoroethylene (PTFE) and polypropylene (PP). **Table 9** shows some examples of commercial membranes for MD application. Among them, PTFE is the most preferential polymer since it has advantageous features such as high hydrophobicity, low surface energy, low intramolecular forces, high chemical stability and high crystallinity. On the other hand, PTFE is hard to process due to its insolubility in any solvents. Therefore, the most common technique to fabricate PTFE membranes are sintering-extrusion or melt-extrusion processes [60].

Table 9: Commercial membrane distillation membranes and their permeate flux in various feed compositions [61]

| Membrane, Manufacturer | Feed solution composition | Permeate flux (kg/m ² h) |
|------------------------------|---------------------------|-------------------------------------|
| PVDF, Millipore [®] | Distilled water | 67 |
| PVDF, Millipore [®] | 14-25 wt% NaCl | 59-40 |
| PTFE, Gelman [®] | Distilled water | 67.3 |
| PTFE, Gelman [®] | 30 g/l NaCl | 51.1 |
| PTFE, Osmonics [®] | 0.6 g/l NaCl | 80 |
| PP, Accurel [®] | Tap water | 33.3 |
| PP, Accurel [®] | 1.0 wt% NaCl | 41.4 |

Besides PTFE, PP is another polymer used in MD applications which has good thermal and mechanical properties. In comparison to PTFE and PVDF, PP possesses lower surface tension, resulting low contact angle, thus low hydrophobicity which makes it disadvantageous for MD application. The fabrication techniques to obtain porous PP are the melt-extrusion stretching and thermally induced phase separation [62]. PVDF, on the other hand, is a semi-crystalline polymer with good chemical stability, which is widely exploited in MD applications. Unlike PTFE, PVDF is soluble in many solvents at room temperature, making it easy to prepare porous PVDF membranes by phase separation. For this reason, PVDF is extensively studied for MD [61]. In addition to these commercial membranes, extensive research is being carried out on the use of new materials in MD. New commercial fluoropolymers such as HALAR[®] and Hyflon AD[®] have recently drawn the attention to utilize in MD. Apart from polymeric membranes, ceramic and mixed matrix membranes prepared by graphene or carbon nanotubes have also been studied for use in MD applications and showed promising results [63]. The development of MD materials is still a subject of ongoing research to efficiently exploit the advantages of the process.

3.3.3.4. Limitations of membrane distillation

Over the years, numerous innovations have been made to alleviate the major problems used in MD, such as membrane wetting and fouling and the resulting low flux rate [64]. Membrane fouling occurs when unwanted substances accumulate on the surface or in the pores of the membrane and adversely affects the overall performance of the MD. If not managed properly, it can lead to membrane damage, premature membrane replacement and shutdown of operation. As with other membrane separation processes, the fouling problem of MD has not yet been solved. Fouling remains key challenge in MD and differs from pressure-driven membrane processes due to differences in membrane structure and operating conditions [65]. Despite promising performance, MD has yet to reach the widespread industrial adoption, primarily due to stability and long-term desalination performance concerns. Stable flow and high desalination performance in long-term operations are key factors to be addressed for the industrialization of MD. However, in continuous MD processes, a reduction in flow rate is often observed due to fouling and membrane wetting. Membrane wetting severely affects MD performance as membranes become increasingly less hydrophobic and feed leaks through the pores, leading to deterioration of product water quality, especially in long-term operations. In water treatment applications of MD, membrane wetting becomes a bigger problem, especially when the effluent contains low surface tension substances such as organic compounds or surfactants, and this is seen as one of the main reasons for the lack of industrial adoption of MD [66]. The most common theme addressed by researchers for MD development is membrane wetting on MD performance. In this context, membrane wetting prevention strategies are gaining importance. These methods include modification of hydrophobic, hydrophilic, oleophobic and omniphobic properties of membranes. Such modifications aim to provide higher performance and durability in MD processes by preventing the adhesion of water and other liquids to membrane surfaces. Hydrophobic and oleophobic modifications are particularly effective in preventing wetting by increasing the water and oil repellency of the membrane surface. Omniphobic modifications provide resistance to both water and oil-based fluids, making them ideal for a wide range of applications. Hydrophilic modifications can be useful in specific applications, often by increasing the membrane's ability to attract liquids. Each of these techniques is the subject of current research to improve the efficiency and long-term functionality of MD systems [67, 68].

3.4. Membrane fabrication techniques

Various methods for polymer membrane production have been developed over the years. The selection of the appropriate technique depends on the choice of polymer and the desired structure of the membrane. The most widely used techniques for the preparation of polymeric membranes involve phase inversion, interfacial polymerization and solution casting.

3.4.1. Phase inversion

Most commercial membranes are obtained by the phase inversion method due to its easy processability, low cost and flexible production scales. In general, phase inversion is divided into four groups, namely nonsolvent induced phase separation (NIPS), thermal induced phase separation (TIPS), vapor-induced phase separation (VIPS) and solvent evaporation-induced phase separation (SEIPS).

- Nonsolvent induced phase separation (NIPS): Most commercially available membranes are prepared by this method. In this process, a polymer solution (containing polymer and solvent) is poured onto a suitable support and then immersed in a coagulation bath containing a nonsolvent liquid. During this process, the exchange between the solvent and the nonsolvent causes precipitation. The viscosity of the polymer solution plays a critical role in this process, as it affects the diffusive exchange rate during phase inversion, thereby influencing pore size and macrovoid formation. These structural characteristics ultimately determine the mechanical properties, flux, and separation performance of the membrane [16, 71].
- Thermally induced phase separation (TIPS): In creating a microporous polymer membrane by this technique, a polymer is first mixed with a high-boiling, low molecular weight liquid to form a homogeneous solution at high temperatures. This mixture is then rapidly cooled to induce phase separation. Finally, the solution undergoes solvent extraction and drying to remove all solvent, resulting in a structured microporous membrane [72].
- Vapor-induced phase separation (VIPS): In this membrane formation process, a film containing a polymer and solvent is exposed to a vapor atmosphere saturated with a non-solvent but also containing the solvent. This high concentration of solvent in the vapor prevents the solvent in the cast film from evaporating. The membrane is formed as the non-

solvent diffuses into the cast film, leading to a porous structure without a top dense layer. Additionally, in some processes like hollow fiber membrane production or when the solvent is miscible with water, an evaporation step is sometimes added before the immersion precipitation to initiate precipitation from the vapor phase, which aids in the membrane's formation [70].

- Solvent evaporation-induced phase separation (SEIPS): In this method, the polymer is dissolved in a mixture of solvent and non-solvent, where the solvent is more volatile than the non-solvent. As the solvent evaporates, the composition shifts towards a higher concentration of the nonsolvent and polymer. This shift eventually leads to the precipitation of the polymer, resulting in the formation of a membrane with a skin structure [73].

3.4.2. Interfacial polymerization

Interfacial polymerization (IP) is a common method for fabricating composite membranes used for applications such as nanofiltration, reverse osmosis and gas separation. Interfacial polymerization which is a method used in microcapsule coating of polymeric products, comprises two complementary monomers dissolved in separate phases: organic phase and aqueous phase. Polymerization occurs at the interface of these two immiscible phases during the microencapsulation process, leading to the formation of a thin polymer shell around the encapsulated core. Interfacial polymerization processes are facilitated by the addition of different surfactants, positively or negatively charged, as well as hydrophilic surfactants in the aqueous phase. [76, 77]. IP has several advantages over other membrane preparation methods. IP membranes form an ultra-thin, less than 50 nm thick selective layer by preventing continuous diffusion and monomer reaction which makes IP a self-limiting process. On the other hand, IP proceeds at the interface of two phases and has no special requirement for high purity of reactants. Moreover, IP process is easy to scale up and implement in industrial production [78].

In recent years, the membranes prepared by interfacial polymerization have made significant progress and are widely used industrially in applications such as thin film composite membranes (TFCM) for water treatment. Interfacial polymerization is a promising method for various membrane applications, offering advantages such as tunable porosity, alternative surface chemistry and easy doping [79].

3.4.3. Solution casting

Solution casting is a simple and effective method used to produce composite membranes. In this process, the polymer solution is poured onto a porous support using a coating applicator. The wet coating thickness and polymer concentration are carefully adjusted to effectively control the thickness of the coating layer. With this method, the thickness of the selective layer can usually range from less than 1 micrometer to several few dozen micrometers. However, since it is difficult to achieve a selective layer thinner than 1 micrometer, there are limitations to the thickness controlled by the coating applicator. This process is particularly favored for its advantages of thickness control and fast production [80].

3.5. Step growth polymerization

The majority of polymers made by step-growth polymerization are polyesters, polyamides and polyurethanes. Step-growth polymerization involves gradual bonding reactions between bifunctional or multifunctional components by releasing of small molecules such as water and alcohol. The reaction of bifunctional or multifunctional monomers forms dimers, trimers, oligomers. At the end, high molecular weight polymers or branched polymers or networks are comprised [81, 82]. In presence of bifunctional moieties, linear step-growth polymerization occurs while in case of multifunctional monomers react, network step-growth polymerization takes place. The characteristics to understand the step-growth polymerization are chain length distribution (CLD), which refers to the number of mass fraction of macro species with a given number of monomers incorporated, and its related averages such as the number/mass average chain length. Main factors are functionality degree of the monomers (f) which stands for the maximum number of functional groups that attend in the polymerization per monomer, and the stoichiometry (r) which represents for the relative presence of certain functional groups at the beginning [83]. Linear polymerization can be achieved when the functionality equals to two, when this is not the case, branching or crosslinking occurs. To estimate the molar mass of the polymers prepared by step-growth polymerization, Carother's theory is used [84]. According to that, the number average degree of polymerization (\overline{X}_n) can be calculated by **Equation 12**.

$$\overline{X}_n = \frac{1}{(1-p)} \quad (12)$$

where p represents for the fractional conversion of functional groups, which can be derived from **Equation 13**.

$$p = \frac{f_r}{f_o} \quad (13)$$

where f_r is the number of functional groups that have reacted and f_o is the number of functional groups that are initially present.

Equation 12 applies when AB type monomers or stoichiometrically equal AA and BB monomers are used in the reaction. For non-stoichiometric reaction, **Equation 14** is used.

$$\overline{X}_n = \frac{1+r}{(1+r-2rp)} \quad (14)$$

where r represents for stoichiometric ratio of functional groups as seen in **Equation 15**.

$$r = \frac{N_{AA}}{N_{BB}} \quad (15)$$

N_{AA} and N_{BB} are initial number of functional groups of AA and BB monomers, respectively.

Basically, if $r=1$, it means that there is a stoichiometric balance, while, if $r \neq 1$ indicates that excess amount of one of the monomers in the reaction is utilized, which leads to the earlier termination of the polymerization due to the completion of the excess monomer usage, thus, lower molecular weight polymer.

According to Carother's theory, the degree of polymerization across the conversion of the reaction show such graph as seen in **Figure 9**.

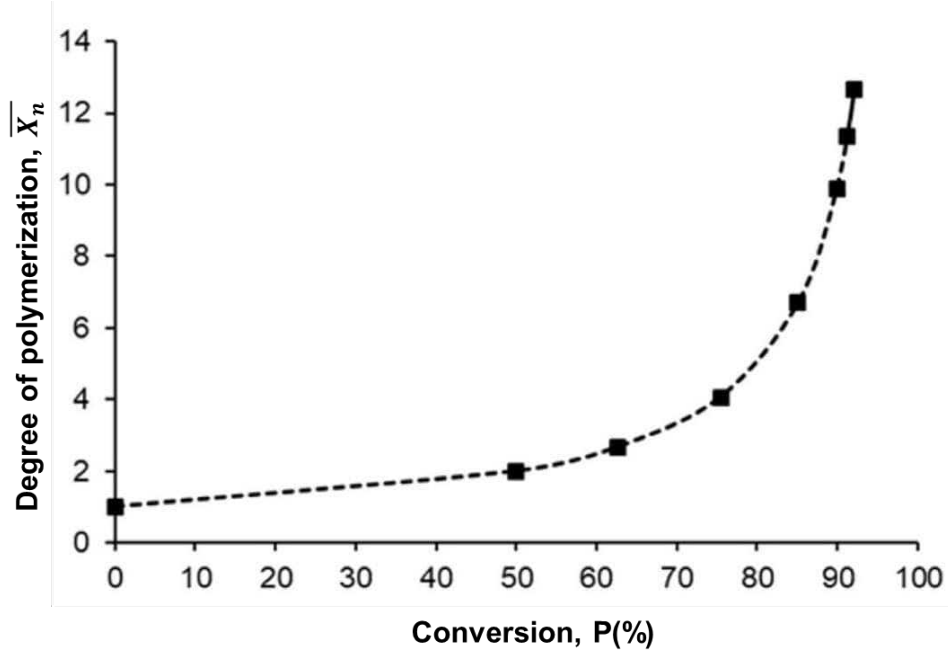


Figure 9: Example of degree of polymerization over conversion. Reprinted with permission from Abdelghafour, M.M., et al., 2021, Polymers [85].

The number average molecular weight, (\overline{M}_n) can be used as a measure of reaction success, \overline{M}_0 represents the average molar mass of the repeating unit (**Equation 16**).

$$\overline{M}_n = \overline{M}_0 \overline{X}_n \quad (16)$$

According to the equation 16, the weight average molecular weight (\overline{M}_w), can also be used for the identification of the polymerization success as follows (**Equation 17** and **Equation 18**):

$$\text{In case of } r = 1 \quad \overline{M}_w = \overline{M}_0 \frac{(1+p)}{(1-p)} \quad (17)$$

$$\text{In case of } r \neq 1 \quad \overline{M}_w = \overline{M}_0 \frac{(1+r)(1+p)}{(1+r-2rp)} \quad (18)$$

Another significant parameter of step-growth polymerization is dispersity, \mathcal{D} , which describes the degree of polymerization (**Equation 19** and **Equation 20**).

$$\text{In case of } r = 1 \quad \mathcal{D} = \frac{\overline{M}_w}{\overline{M}_n} = 1 + p \quad (19)$$

$$\text{In case of } r \neq 1 \quad \mathcal{D} = \frac{(1+r)(1+p)}{(1+r-2rp)} \quad (20)$$

3.6. Polymers of intrinsic microporosity (PIM)

Nanoporous materials have an important place in adsorption, separation and heterogeneous catalysis applications due to their large and accessible surface areas. The term 'microporous' refers to material pore size lower than 2 nm while 'mesoporous' stands for pore size is between 2-50 nm. Since the last decades, there has been a focus on the development of microporous polymers by the introduction of rigid ladder-like components connected to units that allow the backbone structure to bend or rotate. As a result of that, polymer chains cannot pack efficiently in the solid state following to formation of microporous structure. From this point of view, McKeown and Budd introduced the term and polymer family of 'polymers of intrinsic microporosity (PIM)' in 2004 [86]. Intrinsic microporosity can be described as a continuous network of interconnected intermolecular voids, which forms as a direct consequence of the shape and rigidity of the macromolecules. PIMs are a class of linear or crosslinked polymers which exhibit intrinsic microporosity and they are categorized as glassy polymers [87]. Unlike conventional microporous materials, PIMs are soluble in common solvents (tetrahydrofuran, chloroform, dichloromethane etc.) and can be easily processed by solvent-based techniques. They are thermally stable materials that show high apparent surface area (more than 700 m²g⁻¹, BET method) with microporous morphology [88]. By incorporation of spirocyclic or triptycene units (non-linear sites of contortion), PIMs acquire a rigid and contorted backbone which leads to a polymer that cannot fill the voids efficiently. Owing to these unique features, PIMs became favorable for adsorbent or catalysis applications in comparison to traditional microporous materials i.e. zeolites or activated carbons. Generally, PIMs are obtained by polycondensation of a tetrafunctional hydroxylated aromatic monomer and an activated tetrafluorinated aromatic monomer. Among PIMs, PIM-1 and PIM-7 are the most commonly used polymers. Their common features are acquisition of contorted structure, thermal stability and the range of apparent surface area (>700 m²g⁻¹). Their distinguishing characteristics are solubility and the synthesis scheme.

3.6.1. Synthesis of PIM-1

One of the most important polymers of the PIM family is PIM-1. There are different approaches for PIM-1 synthesis in the literature while the most traditional one is low-temperature method [89]. This method follows the step-growth polymerization of equimolar quantities of bis-catechol

(5,5',6,6' tetrahydroxy 3,3,3',3' tetramethyl 1,1' spirobisindane) and tetrafluoroterephthalonitrile (TFTPN) in as solution of anhydrous dimethylformamide (DMF) by using two-fold excess amount of dry powdered potassium carbonate (K_2CO_3) at 60 °C under N_2 atmosphere for 24-72 hours. The reaction scheme is depicted in **Figure 10**. However, there are alternative approaches to prepare PIM-1, which are the so-called high temperature method that follows a faster synthetic route, which involves high-speed stirring of the reaction mixture in dimethylacetamide (DMAc) at 150 °C under N_2 environment for 8-10 minutes. The addition of toluene or diethyl benzene (DEB) towards the end of the reaction to maintain the stirrability is the key feature of this method [90]. Despite the both methods enable the sufficient molar mass to further obtain mechanically stable films of PIM-1, the low temperature method is easier to control the reaction, however, the high temperature method allows to obtain higher average molecular weight.

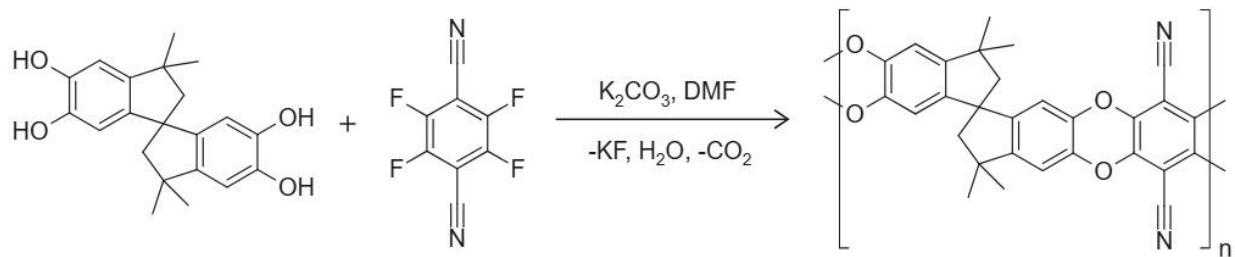


Figure 10: Synthesis of PIM-1, conditions: 60 °C, 72 hours.

Figure 11 renders a 3D molecular model of PIM-1 showing its randomly contorted macromolecular shape in virtue of the spiro center, and the connected to ring ladder chain which prevents the efficient filling of the space resulting in microporosity. PIM-1 is easily soluble in most of organic solvents such as tetrahydrofuran, *o*-dichlorobenzene and chloroform, and can be cast from solution to form a robust membrane for further application. Dynamic mechanical analysis of a cast film of PIM-1 depicts a tensile strength modulus (E') is about 1 GPa, which hardly decreases as the temperature is increased up to 350 °C in air [91, 92]. However, as molecular weight of PIM-1 decreases, the chain entanglements become less effective. This weakens intermolecular interactions and reduces mechanical stability, consequently, the tensile modulus decreases. The glass transition temperature (T_g) of PIM-1 is not detectable before the thermal decomposition by using the conventional methods like differential scanning calorimetry (DSC), however, there has been effort to improve the techniques to detect T_g of PIM-1 [93].

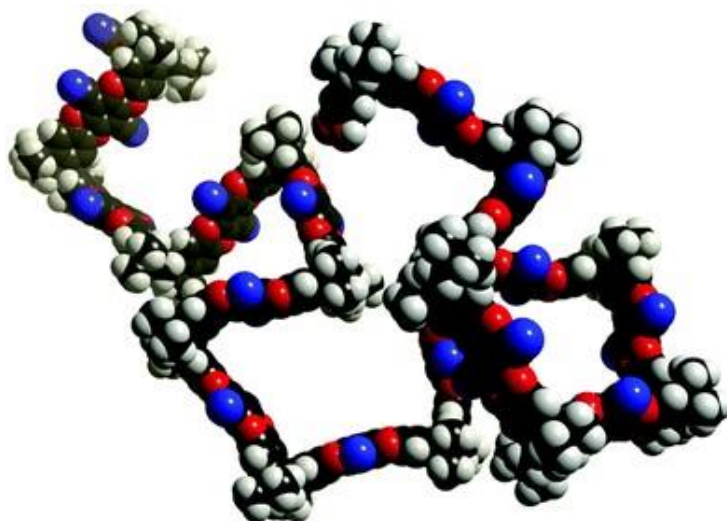


Figure 11: 3D molecular model of PIM-1 rendering contortion and ladder like structure.

Reprinted with permission from McKeown, N.B. and P.M. Budd, 2006, Chem. Soc. Rev. [92].

3.6.2. Synthesis of PIM-7

PIM-7 differentiates from PIM-1 in terms of the monomer used in the polycondensation reaction to obtain the polymer. PIM-7 employs 7,7',8,8'-tetrachloro-phenazyl-3,3,3',3'-tetramethyl-1,1'-spirobisindane as shown in **Figure 12**. Therefore, this leads to the structure differences of the resulting polymer repeat units. The phenazyl unit acts a ligand for the coordination of metal ions and its membrane is easily cross-linked with Pd(II) salts. PIM-7 is soluble in chloroform, *o*-dichlorobenzene and *m*-cresol [88, 94]

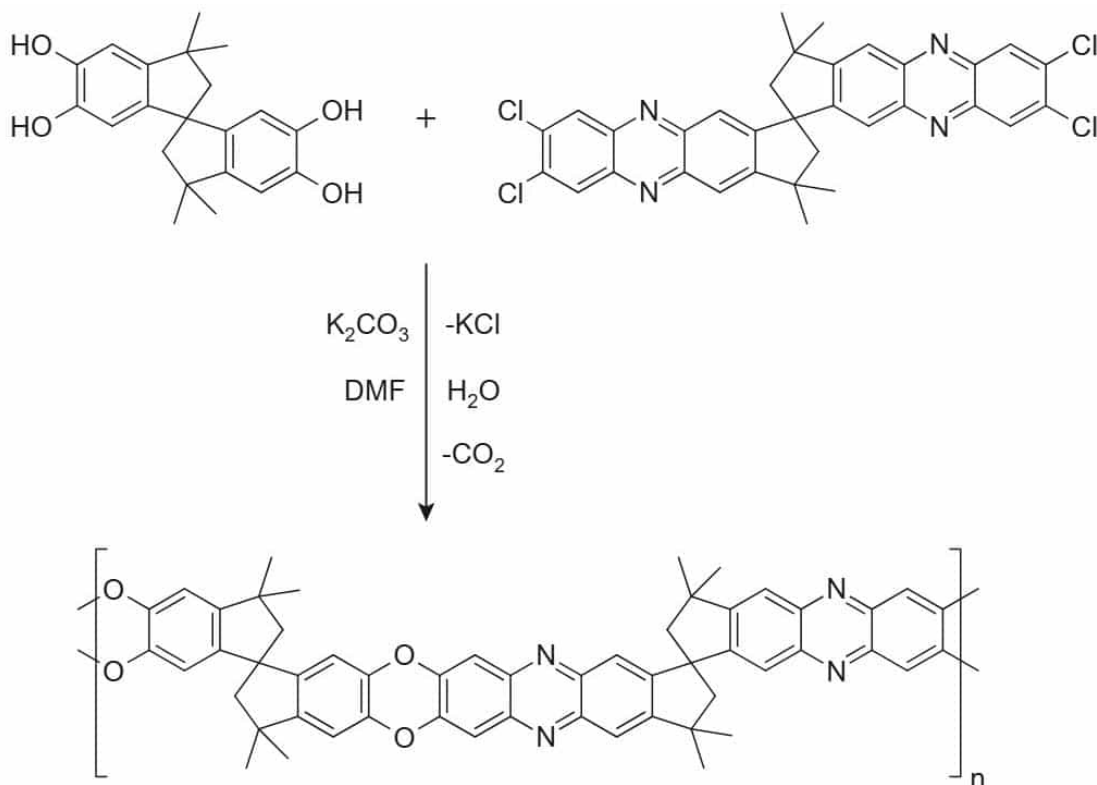


Figure 12: Synthesis of PIM-7, condition: 150 °C [88].

3.6.3. Applications of PIM-1

3.6.3.1. Gas separation

Since their discovery, PIMs have drawn a great attention as gas separation membranes due to their attractive properties towards gas transport. Particularly, numerous studies can be found in the literature regarding gas transport properties of PIM-1 [95-100]. PIM-1 exhibits relatively high permeability and good permselectivity allowing it to be escalated beyond to Robeson's upper bound [32]. **Table 10** gives an insight of gas transport properties of PIM-1 after casting (no aging). It can be seen that PIM-1 shows good permeability against gas pairs as well as high solubility towards CO_2 . The reason is for that might be attributed to the nitrile groups in PIM-1 structure which are polar groups and enforces the intermolecular interactions between [94].

Table 10: Gas transport data* of PIM-1 [94]

| | P (Barrer) | D ($10^{-8}\text{cm}^2\text{s}^{-1}$) | S ($10^{-3}\text{cm}^3\text{cm}^{-3}\text{cmHg}^{-1}$) | α (x/N ₂) |
|-----------------|------------|---|--|------------------------------|
| O ₂ | 370 | 81 | 46 | 4.0 |
| N ₂ | 92 | 22 | 42 | 1.0 |
| H ₂ | 1300 | 1700 | 7.6 | 14 |
| CO ₂ | 2300 | 26 | 880 | 25 |
| CH ₄ | 125 | 6.8 | 180 | 1.4 |

* P: Permeability coefficient (1 Barrer= $10^{-10}\text{cm}^3[\text{STP}]\text{cmcm}^{-2}\text{s}^{-1}\text{cmHg}^{-1}$), D: Diffusion coefficient, S: Solubility coefficient, α (x/N₂) is selectivity: The ratio of the gas to the nitrogen permeability

The unique ladder-type structure with contorted sites of PIM-1 leads to hinder the polymer chains rotate and to pack insufficiently, resulting the formation of high fractional free volume (24-26%) and large surface areas to promote remarkable gas transport performance [101]. Studies on PIM-1 revealed that the gas solubility of PIM-1 can be even higher than poly(trimethylsilyl propyne) (PTMSP) which is considered very permeable polymer [102]. This makes PIM-1 a very promising candidate for gas separation applications such as separation oxygen from air for enhanced combustion or removal carbon dioxide from methane [94].

3.6.3.2. Pervaporation

Pervaporation is another separation technique where PIM-1 is extensively studied. It has been found that PIM-1 can play a significant role in liquid phase separations such as the removal of unwanted or harmful compounds in wastewater streams. The removal of phenol from water was the first study of application of PIM-1 [89]. As mentioned in the previous section, pervaporation is dominated by a solution-diffusion mechanism and sorption selectivity is important for transport performance. The molecules which have higher affinity can be located within the free volume regions of PIM-1 causing a small swelling of the polymeric matrix. This leads to the escalated sorption capacity compared to conventional glassy polymers and rubbery polymers. Simultaneously, the presence of a microporous structure of PIM-1 facilitates enhanced diffusion of molecules through the membrane [103]. Moreover, if the polymer possesses larger free volume elements, it addresses directly to enhance the pervaporation flux and to reduce the membrane area required for the pervaporation. Therefore, PIM-1 that is characterized by its hydrophobicity and

high free volume elements, is a very suitable candidate to meet pervaporation requirements, especially for the separation of organics from aqueous solutions [104].

3.6.3.3. Nanofiltration

Owing to its unique properties, PIM-1 is being studied for nanofiltration and organic solvent nanofiltration applications. Several studies have investigated the performance of PIM-1 in nanofiltration applications. To give an example, some studies have focused on the dye sorption and filtration properties of PIM-1 in solvents such as ethanol [105]. Another study reported the development of ultrathin PIM-1 films supported on substrates such as polyacrylonitrile for enhancement of heptane permeation [106]. Furthermore, PIM-1 modifications including crosslinking and incorporation of metal-organic frameworks (MOFs) have been explored to improve solvent stability and functionality by targeting specific applications such as heavy metal or dye removal [107, 108]. Despite these advances, the application of PIM-1 membranes remains rather limited due to the challenge such as low solvent stability since PIM-1 swells or is being dissolved in some organic solvents.

3.6.4. Fractional free volume theory

One of the most important factors of polymer membrane transport theory is the free volume of the polymers. Although there are many different definitions, free volume in polymers is an empirical dimensionless parameter and generally can be defined as the amount of void space not occupied by the molecules of the polymer chains [109]. Free volume in polymers usually results from insufficient packing of the polymer chains which causes the formation of voids which are enough for the gas molecules to permeate through local segmental motion. In this point, there is a strong relation between glass transition temperature (T_g) and free volume. The glass transition can be considered to occur when the thermal energy is enough to disrupt the chain packing leaving an excess free volume in solid state. In the rubbery state, free volume increases along with the temperature. However, when the polymer is quenched from rubbery state to the glassy region, the excess volume is trapped. This free volume is a non-equilibrium quantity and decreases over time due to the relaxation of polymer chains towards equilibrium state [91, 110]. This process is called *physical aging* and is discussed in the next section in detail. The relation of glass transition between rubbery and glassy states of the polymer is illustrated in **Figure 13** [111].

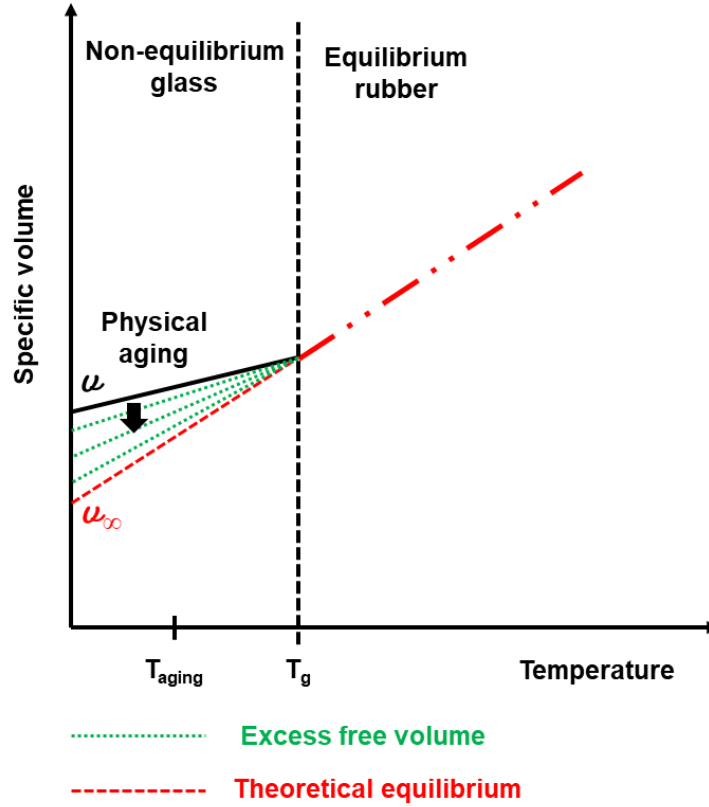


Figure 13: Representation of glass transition from rubbery to glassy state.

Usually, fractional free volume (FFV) which is expressed as percentage can be defined as the ratio of free volume of the polymer, V_f (cm³/g) to the specific volume of the polymer, V_{sp} (cm³/g). The value of V_f can be calculated by using Bondi's equation [112] (**Equation 21**).

$$V_f = V_{sp} - V_{oc} \quad (21)$$

where V_{oc} is the occupied free volume and can be estimated as follows (**Equation 22**)

$$V_{oc} = 1.3V_w \quad (22)$$

where V_w is the van der Waals volume of the repeating unit of the polymer. Taking Equation 18 and Equation 19 into definition of FFV, it is simplified as follows (**Equation 23**).

$$FFV = \frac{V_f}{V_{sp}} = 1 - \frac{1.3V_w}{V_{sp}} \quad (23)$$

Gas transport properties such as diffusion coefficient and permeability are related to FFV which can be explained by Arrhenius type dependence. The free volume created by insufficient packing

of the polymer promotes the diffusion of permeants across the membrane, leading to an increase in the diffusion coefficient (**Equation 24**) and hence permeability [113].

$$D = Ae^{\frac{-B}{FFV}} \quad (24)$$

where A and B are specific gas and polymer constants, respectively. Consequently, there is a correlation which can be plotted as permeability versus 1/FFV. This relationship plays a significant role in regards of the development of polymeric membranes which is aimed to sustain or increase the size-sieving capacity. Free volume is a pivotal element for high free volume glassy polymers such as PIMs. The gas solubility selectivity of PIM-1 is typically close to those of common glassy polymers, whereas the gas solubility coefficients of PIM-1 show higher values. This can be attributed their high free volume encourages the solubility in addition to diffusivity resulting an overall upgrading in permeability [114].

FFV of high free volume glassy polymer can be estimated by various methods including positron annihilation lifetime spectroscopy, inverse gas chromatography, cryogenic physisorption (N₂ sorption), ¹²⁹Xe nuclear magnetic resonance spectroscopy, group contribution method, molecular modeling and scattering methods such as small-angle X-ray scattering and X-ray diffraction [115].

3.6.5. Physical aging

Physical aging is a well-known phenomenon that can be defined as the relaxation of non-equilibrium free volume and is caused by volumetric condensation of the matrix, which is mainly attributed to small-scale molecular motions below T_g [116]. The transport properties of high free volume glassy polymers such as PTMSP and PIM-1 can be severely affected by physical aging since it causes drastically reduction of gas permeability over time. Therefore, numerous studies have been focused on mitigating physical aging of such glassy polymers [117-120]. There are several factors causing physical aging including film thickness, temperature, storage conditions, polymer structure and membrane treatment. Research has shown that physical aging can be reprieved by UV-treatment, UV-photo-oxidation, surface modification, crosslinking, incorporation of fillers and solvent treatments [121]. The effect of physical aging on gas permeability is usually specified in free-standing thin films. Nevertheless, the effects occur at different rates depending on their specific morphology and mainly on the sample thickness.

Typically, as the thickness of the film increases, aging is delayed. Consequently, thin films are subjected to faster physical aging than thick films [122].

PIM-1 has different physical aging pattern than those of conventional glassy polymers. Below the decomposition temperature, T_g of PIM-1 cannot be detected. The absence of single bonds in the backbone of PIM-1 which can promote the rotation, large-scale conformational changes in this polymer are not possible. This can be attributed to why T_g is not observed under decomposition temperature. Following film formation, PIM-1 tends to age faster than conventional glassy polymers due to their high free volume. Studies reported that the physical aging rate is correlated with the T_g of the polymer and that T_g increases along with physical aging [115]. This phenomenon is one of the main reasons why PIM-1 cannot be commercialized.

3.6.6. Further studies on PIM-1

Although PIM-1 has superior transport properties in membrane applications for short times, it suffers from physical aging as mentioned before and selectivity of certain gas pairs. Several strategies have been employed to suppress the physical aging and to improve the gas transport performance of PIM-1. One of the approach to ameliorate gas transport performance is the post-modification of PIM-1 by the introduction of CO₂-philic groups such as amide [123], amine [99], carboxylic acid [124], hydroxyl [125], tetrazole [126], thioamide [127] and vinyl [128]. The cornerstone of these studies hinge upon the utilization of CO₂-philic groups by increasing CO₂ solubility, thus improving the selectivity without compromising permeability. The selectivity in these studies is governed by the solubility selectivity of CO₂ rather than diffusivity selectivity.

A more straightforward approach than post-modification of PIM-1 is the preparation of mixed matrix membranes to improve the gas transport performance and to overcome the physical aging behavior of PIM-1. Studies on this topic include the preparation of PIM-1 mixed matrix membranes with fillers such as fused silica nanoparticles [129], zeolites [130], carbon nanotubes [131], ionic liquid fillers [132], metal organic frameworks (MOFs) [133] and polyhedral oligomeric silsesquioxane (POSS) [134]. Although improvements in permeability or selectivity were demonstrated in almost all these studies, further research in this area is expected to improve the performance of PIM-1 membranes in the field of gas separation.

Another method of enhancing the selectivity without compromising the surface area of the high free volume is to develop a shape-persistent polymer backbone by introducing rigid or non-coplanar monomers. The introduction of rigid groups into the polymer backbone breaks the chain packing resulting the increase of free volume. In this regard, Tröger's base [135] and ethanoanthracene [136] were introduced into PIM structures. It is stated that the sieving property of the polymer increased owing to these rigid units. Further attempts to promote rigidity is to replace spirobisindane group with more rigid spirobifluorene showing good permeability-selectivity data [137]. Likewise, introduction of the roof-shape triptycene unit which was studied by Rose et al. showed also encouraging results [138]. Moreover, a further effective way to ameliorate gas transport is to insert bulky side groups, which create additional free volume. The use of bulky groups e.g. tert-butyl [139] allow better size discrimination ability, thus, greater selectivity.

4. Objective of this work

Membrane processes are one of the most effective technologies for accessing clean water, which is one of the biggest problems of our era. Membrane process such as membrane distillation and pervaporation utilize industrial wastewater, brine or water-solvent mixtures as a source to obtain clean water. In addition, gas and vapor separation processes are among the processes that support water treatment technologies. Polymer membranes are a versatile material often used in this regard due to their advantages of easy processing and low-cost scale-up. Although polymers such as polyethylene, polypropylene, polyvinylidene fluoride, polysulfone and polyimide are commonly used today, other polymers are also the subject of membrane studies to develop more functional materials by modifications on different polymers or developing composites. Polymers of intrinsic microporosity (PIM) have been widely studied in this field in recent years. The main properties that make the PIM-1 polymer attractive are easy processability, easy solubility in common solvents and high fractional free volume due to its contorted molecular structure. These properties make it possible not only to use PIM-1 as it is, but also to functionalize it according to its application. PIM-1, which has been the subject of many membrane studies to date, has mostly been the focus of gas separation and pervaporation studies. The biggest challenge of gas and water vapor separation processes is to overcome the permeability-selectivity trade-off. High free volume polymers are often used for this purpose. However, the main disadvantage of such polymers is that they are significantly affected by the collapse of the free volume over time, so-called “physical aging”. One of the approaches to tackle with physical aging is to make chemical modification on polymer. Studies to increase the fractional free volume by modifying rigid and bulky structures to the contorted molecular structure of PIM-1 are available in the literature and are discussed in the theory section of this dissertation. In addition to hindering physical aging, modifying functional groups in the polymer to increase the solubility of penetrant in the polymer is another method to increase the efficiency of the gas separation technique based on the solution-diffusion model.

Based on these methods, in the first part of this study, various modifications were made to the chemical structure of PIM-1. Accordingly, a series of homopolymer and copolymer series were synthesized by modifying the PIM chemical backbone using anthracene-maleimide monomers

with different side groups, which have roof shaped structure in order to improve rigidity and free volume. The different side groups were investigated from different perspectives: linear and bulky components in terms of their effect on free volume, and aliphatic and aromatic groups in terms of their effect on water solubility. This investigation was achieved by preparation of the novel polymers as a thick film and then evaluating their gas and water vapor permeability using the “time-lag” method. The first published paper of this dissertation covers this work and discusses the results in detail.

Since one of the objectives of this dissertation was to investigate the possible use of PIM-1 polymer in water separation techniques, the second study aimed to develop PIM-1 polymer for use in membrane distillation. In the literature, there are very few studies in which PIM-1 polymer was used in membrane distillation application. One of the main reasons for this is the difficulty of the preparation of PIM-1 as a porous membrane. For this reason, the second study pursued to obtain PIM-1 as a porous membrane by phase inversion. The performance of PIM-1 in membrane distillation was assessed by measuring the water flux of the membranes prepared by trying different solvent-nonsolvent combinations. Furthermore, a PIM-1 thin film composite membrane was prepared, and the effect of membrane morphology was investigated by comparing water vapor permeability of a thin film composite membrane and porous membranes.

In the light of the experiences and findings from these two studies, the third study focused on the use of PIM-1 in pervaporation application. Thin film composite membranes were prepared using homopolymers from the first study and their pervaporation performance was investigated. Moreover, water vapor permeability measurements were performed to evaluate the performance of PIM-1 in the transport of water in liquid or vapor form.

In summary, this dissertation has made an effort to examine in detail the potential uses of PIM-1 in water separation technologies. PIM-1 and PIM modified polymers were used in different membrane applications and their transport properties were discussed in detail in order to make a scientific contribution to water separation technologies.

5. Cumulative part

5.1. Article 1: Investigation of the side chain effect on gas and water vapor transport properties of anthracene-maleimide based polymers of intrinsic microporosity

Authors: Esra Caliskan, Sergey Shishatskiy, Silvio Neumann, Volker Abetz, Volkan Filiz

In the first part of this dissertation, modifications were made to PIM to increase the free volume as described in the objective section. Accordingly, anthracene maleimide monomers with different aliphatic side groups synthesized via Diels-Alder reactions were successfully used as precursors for the synthesis of PIM-based homo- and copolymers. These polymers using aliphatic and aromatic side groups of different sizes and shapes have been characterized in detail using size exclusion chromatography, nuclear magnetic resonance, Fourier-transform-infrared spectroscopy, thermogravimetric analysis, and density measurements. The gas and water vapor transport properties of homopolymers and copolymers were evaluated by "time-lag" measurement methods. Homopolymers with bulky side groups had a significant effect on fractional free volume and penetrant permeability compared to homopolymers containing linear alkyl side chains. The effects of different aliphatic side groups of anthracene maleimide derivatives on water vapor transport were studied in detail. The presence of maleimide group and aromatic side group increased the water affinity of homopolymers. The copolymers with short alkyl side groups presented higher CO₂ and CH₄ permeability compared to PIM-1. In summary, the addition of bulky substituents increased the free volume and permeability of the polymers, while the maleimide group increased the affinity of the polymers with water vapor.

5.1.1. Author contributions

Esra Caliskan (E.C.), Sergey Shishatskiy (S.S.), Silvio Neumann (S.N.), Volker Abetz (V.A.), Volkan Filiz (V.F.)

Table 11: List publication: Publication-1

| Contribution | Authors | | | | |
|-----------------------------------|---------|------|------|------|------|
| | E.C. | S.S. | S.N. | V.A. | V.F. |
| First author | + | | | | |
| Corresponding author | | | | | + |
| Methodology and conceptualization | + | + | + | | |
| Experimental work | + | | | | |
| Material characterization | + | | + | | |
| Investigation | + | | | | |
| Writing original draft | + | | | | |
| Writing-reviewing and editing | + | + | + | + | + |
| Scientific supervision | | | | + | |

5.1.2. Funding and acknowledgements

The Federal Ministry of Education and Research of Germany (BMBF) financially supported this work via the project NAMED (FKZ: 03XP0151A).

The authors would like to appreciatively thank to Silke Dargel for her valuable help with polymerization; Maren Brinkmann for her kind support on size exclusion chromatography; Carsten Scholles for his great input of time-lag measurements.

5.1.3. Publication



polymers

IMPACT
FACTOR
4.7

Indexed in:
PubMed

CITESCORE
8.0

Article

Investigation of the Side Chain Effect on Gas and Water Vapor Transport Properties of Anthracene-Maleimide Based Polymers of Intrinsic Microporosity

Esra Caliskan, Sergey Shishatskiy, Silvio Neumann, Volker Abetz and Volkan Filiz

Special Issue

Advanced Polymer Membranes

Edited by

Dr. Yu-Hsuan Chiao and Prof. Dr. Ranil Wickramasinghe



<https://doi.org/10.3390/polym14010119>

Article

Investigation of the Side Chain Effect on Gas and Water Vapor Transport Properties of Anthracene-Maleimide Based Polymers of Intrinsic Microporosity

Esra Caliskan ¹, Sergey Shishatskiy ¹, Silvio Neumann ¹, Volker Abetz ^{1,2} and Volkan Filiz ^{1,*}

¹ Institute of Membrane Research, Helmholtz-Zentrum Hereon, Max-Planck-Str. 1, 21502 Geesthacht, Germany; esra.caliskan@hereon.de (E.C.); sergey.shishatskiy@hereon.de (S.S.); silvio.neumann@hereon.de (S.N.); volker.abetz@hereon.de (V.A.)

² Institute of Physical Chemistry, University of Hamburg, Martin-Luther-King-Platz 6, 20146 Hamburg, Germany

* Correspondence: volkan.filiz@hereon.de; Tel.: +49-41-5287-2425

Abstract: In the present work, a set of anthracene maleimide monomers with different aliphatic side groups obtained by Diels Alder reactions were used as precursors for a series of polymers of intrinsic microporosity (PIM) based homo- and copolymers that were successfully synthesized and characterized. Polymers with different sizes and shapes of aliphatic side groups were characterized by size-exclusion chromatography (SEC), (nuclear magnetic resonance) ¹H-NMR, thermogravimetric (TG) analysis coupled with Fourier-Transform-Infrared (FTIR) spectroscopy (TG-FTIR) and density measurements. The TG-FTIR measurement of the monomer-containing methyl side group revealed that the maleimide group decomposes prior to the anthracene backbone. Thermal treatment of homopolymer methyl-100 thick film was conducted to establish retro-Diels Alder rearrangement of the homopolymer. Gas and water vapor transport properties of homopolymers and copolymers were investigated by time-lag measurements. Homopolymers with bulky side groups (*i*-propyl-100 and *t*-butyl-100) experienced a strong impact of these side groups in fractional free volume (FFV) and penetrant permeability, compared to the homopolymers with linear alkyl side chains. The effect of anthracene maleimide derivatives with a variety of aliphatic side groups on water vapor transport is discussed. The maleimide moiety increased the water affinity of the homopolymers. Phenyl-100 exhibited a high water solubility, which is related to a higher amount of aromatic rings in the polymer. Copolymers (methyl-50 and *t*-butyl-50) showed higher CO₂ and CH₄ permeability compared to PIM-1. In summary, the introduction of bulky substituents increased free volume and permeability whilst the maleimide moiety enhanced the water vapor affinity of the polymers.

Keywords: polymers of intrinsic microporosity (PIM-1); membranes; gas separation; water vapor transport; Diels Alder reaction



Citation: Caliskan, E.; Shishatskiy, S.; Neumann, S.; Abetz, V.; Filiz, V. Investigation of the Side Chain Effect on Gas and Water Vapor Transport Properties of Anthracene-Maleimide Based Polymers of Intrinsic Microporosity. *Polymers* **2022**, *14*, 119. <https://doi.org/10.3390/polym14010119>

Academic Editor: Yu-Hsuan Chiao

Received: 25 November 2021

Accepted: 22 December 2021

Published: 29 December 2021

Publisher's Note: MDPI stays neutral with regard to jurisdictional claims in published maps and institutional affiliations.



Copyright: © 2021 by the authors. Licensee MDPI, Basel, Switzerland. This article is an open access article distributed under the terms and conditions of the Creative Commons Attribution (CC BY) license (<https://creativecommons.org/licenses/by/4.0/>).

1. Introduction

Membrane technology has drawn great attention owing to its advantages of being ecologically favorable, cost-efficient and easy to operate. Polymers are encouraging materials for gas separation membranes due to their benign processability and low upscaling costs [1]. In gas separation, there are two significant parameters that define membrane performance, permeability (P) and selectivity ($\alpha = P_A/P_B$). Permeability is a product of solubility (S) and diffusivity (D) (Equation (1)) according to the solution-diffusion model [2]. The selectivity parameter, therefore, is an indirect function of solubility and diffusivity of the membrane. The aforementioned transport parameters are directly affected by the state and microstructure of the membrane material; thus, it is crucial to develop particularly tailored polymers for gas separation application [3]. Usually, glassy polymers are used for the separation of non-condensable gases, and for these polymers, a trade-off between

permeability and selectivity is known to cause limits to the use of polymers in practical gas separation [4]. In general, gas transport takes place through interconnected free volume elements formed by non-perfect packing of macromolecular chains of amorphous polymers. Consequently, polymer membranes have difficulties in offering both high permeability and high selectivity, which are mostly defined by large free volume size and narrow size distribution, respectively [5].

$$P = DS \quad (1)$$

Researchers endeavor to overcome permeability and selectivity trade-offs by developing new polymeric materials based on the consideration of empirical structure/property interconnections. A breakthrough discovery addressing this issue was the development of polymers of intrinsic microporosity (PIM) by Budd and McKeown, which have a fractional free volume comparable to disubstituted polyacetylenes [6]. Among the polyacetylenes, poly(trimethylsilylpropyne) (PTMSP) is known to be the most permeable polymer so far. Nevertheless, PTMSP has selectivity drawbacks due to its insufficient rigid structure, which leads to failure of size discrimination [7,8]. Hence, PIMs have drawn attention during the past years owing to their unique properties. The term intrinsic microporosity refers to a network of interconnected free volume voids formed by highly inefficient packing of rigid and contorted macromolecules [9]. The essence of the existence of microporosity in a polymer lies in the presence of a contortion site in the monomeric unit, which could be obtained either by the introduction of a spiro-center, a non-planar rigid conformation or a single covalent bond that limits the rotation within the polymer chain [10]. Bearing these specificities in mind, researchers have focused on the development of different PIMs. PIM-1 is the most extensively studied polymer among the PIM family, which is obtained by the polycondensation of 5,5',6,6'-tetrahydroxy-3,3,3',3'-tetra-methylspirobisindane (TTSBI) and 2,3,5,6-tetrafluoroterephthalonitrile (TFTPN) [11]. Since its discovery, PIM-1 has become attractive due to its high solubility in low boiling point solvents such as tetrahydrofuran (THF) or chloroform (CHCl₃), accessibility to chemical modifications, high surface area accompanied by attractive gas separation properties [10]. Owing to its splendid features, PIM-1 has been studied in many membrane applications such as gas separation [12–15], hydrogen storage [16], pervaporation [6] and water separation [17,18]. Although extensive research has been carried out on PIMs, a development of tailoring PIM for membrane applications, especially for gas separation, is still necessary.

The literature on intrinsic microporosity has highlighted several ways to ameliorate gas transport performance. Previous research focused on post-modification of PIMs to enhance selectivity by the introduction of CO₂ affine functionalities such as amide [19], amine [20], carboxylic acid [21], hydroxyl [22], tetrazole [23], thioamide [24] and vinyl [25]. The cornerstone of these studies is based on the exploitation of CO₂-philic groups by increasing CO₂ solubility, thus upgrading the selectivity without compromising permeability. Further studies examined blend preparation with microporous fillers, e.g., carbon nanotubes [26], graphene oxide [27], MOF [28] and POSS [29]. One of the other aims of these studies was to tackle physical aging, a common problem with glassy polymers.

In addition to the abovementioned studies, a different approach employed by a vast number of researchers is to develop a shape-persistent polymer backbone by introducing rigid or non-coplanar monomers [30,31]. The incorporation of rigid groups into the polymer backbone disrupts the chain packing and consequently increases the free volume [32]. Considering this approach, Bezzu et al. [15] replaced the spirobisindane group with a relatively more rigid spirobifluorene and succeeded in ensuring good permeability-selectivity interrelation. The introduction of Tröger's base and ethanoanthracene into PIM structures (PIM-SBI-TB [8,33] and PIM-EA-TB [33], respectively) enhanced the sieving property of the polymer owing to inflexible, rigid units. Another attempt to promote rigidity, and consequently, free volume was the exploitation of the roof-shaped triptycene unit, which revealed encouraging results [34,35]. Moreover, it has been established that a further effective way to improve gas separation performance is to insert bulky side groups, which create high free volume. The use of rigid, bulky groups provides better size discrimination ability,

thus, greater selectivity [36]. Numerous researchers studied the effect of bulky groups, e.g., *tert*-butyl or trimethylsilyl, introduced in different polymers such as polyimide [36,37], polynorbornene [38] and polyacetylene [39–41]. The studies showed that the incorporation of bulky substituents increases free volume and, thus, the gas permeability coefficient.

Despite the abundant studies of PIM on gas separation, there remains a paucity of research on water transport properties since it is intricate in using the hydrophobic nature of PIM-1 to pass water molecules through the micropores [17]. However, water scarcity is a crucial problem directly affecting our living standards; therefore, a strong need has emerged to develop energy-efficient and ecofriendly methods of water separation [42]. Conventional water separation methods are forward osmosis, reverse osmosis, ultrafiltration, nanofiltration and membrane distillation (MD). Considering the low operating temperature, MD is a promising and energy-efficient technique in which only water vapor molecules are able to pass through the hydrophobic porous membrane [43]. In comparison to the transport of ideal gases, water vapor transport could be discussed from a different point of view due to its unique transport mechanism stemming from water molecule-polymer and water-water molecules interactions. Up to now, far too little investigation has been done on water vapor transport in PIMs.

This study contributes to the aforementioned works by the investigation of the influence of aliphatic side-chain group size and shape of new anthracene maleimide polymers on their properties. It was expected that the roof shape of anthracene-maleimide could provide a rigid and non-coplanar structure that restricts chain packing of the polymer [35]. In this study, new anthracene-maleimide monomers were employed for the synthesis of homopolymers and copolymers with spiro-bisindane comonomers, which were further studied for gas transport properties. The change in aliphatic chain length (methyl-, ethyl- and *n*-propyl-), change in group geometry (propyl-, *i*-propyl- and *t*-butyl-) and difference between cycloaliphatic and aromatic cycles (cyclohexyl- and phenyl-) are the main subjects able to reveal a trend between the change in the structure of the side group and the transport parameters of gaseous penetrants. To this end, the thermal treatment of homopolymer methyl-100 thick film was conducted to establish retro-Diels-Alder rearrangement of the homopolymer. In a previous research article, Khan et al. [44] studied the effect caused by different aromatic substituents on the gas properties of polymers.

To our knowledge, there is a lack of published data correlating regular polymer structure change in substituted anthracene maleimides with gas and vapor transport properties. It is further anticipated that the introduction of the maleimide group into the monomer would increase the polarity of the polymer and subsequently improve water vapor permeability coefficient.

2. Materials and Methods

2.1. Materials

5,5',6,6'-tetrahydroxy-3,3,3',3'-tetramethyl-1,1'-spirobisindane (TTSBI, 98%) was purchased from ABCR GmbH (Karlsruhe, Germany). 2,3,5,6-tetrafluoro-terephthalonitrile (TFTPN, 99%) was obtained from Lanxess (Cologne, Germany). TFTPN was sublimated twice at 70 °C under vacuum before use. Cyclohexyl maleimide (98%) was purchased from TCI (Portland, OR, USA). *t*-Butyl maleimide was purchased from Specific Polymers (Castries, France). Boron tribromide (BBr₃, 99%) was obtained from Acros Organics (Geel, Belgium). Potassium carbonate (K₂CO₃, 99%), methyl maleimide (98%), dimethyl acetamide (DMAc, 99%) and dichloromethane (DCM, 99%) were purchased from Alfa Aesar (Kandel, Germany). All other commercially available reagents were obtained from Merck (Darmstadt, Germany) and were used without further treatment.

2.2. Monomer Synthesis

2.2.1. 2,3,6,7-Tetramethoxy-9,10-Dibutylanthracene

At first, 1,2-dimethoxybenzene (43.4 g, 314 mmol) was added to 100 mL concentrated H₂SO₄ (70% in water) at 0–5 °C. Afterward, pentanal (46 g, 534 mmol) was added dropwise

over a period of 1 h. The viscous violet mixture was stirred at room temperature for 4 days. The highly viscous blackish reaction mixture was poured into a mixture of 2 L ethanol-water (1:1), and the precipitate was collected by filtration. Subsequently, washing with acetone and drying at 70 °C in vacuum yielded 13 g of light yellow powder (20%), Mp. 325 °C. ¹H-NMR (500 MHz, CDCl₃): δ (ppm): 0.98 (t, 6 H), 1.50 (m, 4 H), 1.72 (m, 4 H), 3.35 (m, 4 H), 3.98 (s, 12 H), 7.33 (s, 4 H).

2.2.2. 2,3,6,7-Tetrahydroxy-9,10-Dibutylanthracene

Boron tribromide (BBr₃) (15.8 g, 63 mmol) dissolved in 90 mL dichloromethane (DCM) was added slowly to a cooled mixture of 10 g 2,3,6,7-tetramethoxy-9,10-dibutylanthracene (24 mmol) in 265 mL DCM under argon atmosphere. After the complete addition of BBr₃, the reaction was stirred for approximately 18 h and was terminated by the addition of 60 mL of water. After pouring an excess of water, the mixture was stirred for 2 days. The precipitate was filtered, washed with water and dried at 60 °C in vacuum to give 11 g grey powder (98%), Mp. 220 °C. ¹H-NMR (500 MHz, DMSO-d₆): δ (ppm): 1.01 (t, 6 H), 1.54 (m, 4 H), 1.61 (m, 4 H), 3.18 (t, 4 H), 7.32 (s, 4 H), 9.38 (s, 4 H).

2.2.3. Methyl-Comonomer

A mixture of 1 g 2,3,6,7-tetrahydroxy-9,10-dibutylanthracene (2.8 mmol) and 0.35 g methyl maleimide (3.1 mmol) in 19 mL o-xylene was refluxed at 150 °C for 5 h. The brown reaction suspension was poured into cyclohexane. Filtration and drying at 65 °C under vacuum gave 1.20 g of a dark brown powder, (92%), ¹H-NMR (500 MHz, DMSO-d₆): δ (ppm): 1.13 (t, 6 H), 1.70 (m, 6 H), 1.94 (m, 2 H), 2.11 (m, 2 H), 2.42 (s, 3 H), 2.67 (m, 2 H), 3.18 (s, 2 H), 6.58 (s, 2 H), 6.69 (s, 2 H), 8.60 (s, 2 H), 8.70 (s, 2 H).

2.2.4. Ethyl-Comonomer

Ethyl-comonomer was synthesized by the same method as the methyl-comonomer, using ethyl maleimide instead of methyl maleimide to give a dark brown solid, (83%), ¹H-NMR (500 MHz, DMSO-d₆): δ (ppm): 0.41 (t, 3 H), 1.10 (t, 6 H), 1.70 (m, 6 H), 1.91 (m, 2 H), 2.06 (m, 2 H), 2.64 (m, 2 H), 2.97 (m, 2 H), 3.12 (s, 2 H), 6.57 (s, 2 H), 6.68 (s, 2 H), 8.56 (s, 2 H), 8.68 (s, 2 H).

2.2.5. Propyl-Comonomer

Propyl-comonomer was synthesized by the same method as the methyl-comonomer, using propyl maleimide instead of methyl maleimide to give a dark brown solid, (74 %), ¹H-NMR (500 MHz, DMSO-d₆): δ (ppm): 0.41 (t, 3H), 0.88 (m, 6H), 1.10 (t, 6H), 1.70 (m, 2H), 1.93 (t, 2H), 2.11 (m, 2H), 2.67 (m, 4H), 2.96 (t, 2H), 3.16 (m, 2H), 6.59 (s, 2H), 6.69 (s, 2H), 8.57 (s, 2H), 8.69 (s, 2H).

2.2.6. *i*-Propyl-Comonomer

A solution of 3 g isopropyl amine (50.7 mmol) in 54 mL THF was added dropwise to a solution of 5.5 g maleic anhydride (55.8 mmol) in THF, and then the mixture was stirred for 5 h at room temperature. The reaction mixture was filtrated and residual THF was removed under reduced pressure to obtain 66.4 g 4-oxo-4-(propan-2-ylamino)but-2-enoic acid as a white powder, (80%), ¹H-NMR (500 MHz, DMSO-d₆): δ (ppm): 1.18 (m, 6H), 4.05 (m, H), 6.18 (d, H), 6.25 (d, H), 8.39 (s, H), 15.49 (s, H).

Sixty-six grams of 4-oxo-4-(propan-2-ylamino)but-2-enoic acid (38.17 mmol) was dissolved in 46 mL acetic acid, and the solution was immersed in an oil bath at 80 °C. The reaction mixture was kept stirring for 24 h at 80 °C and was terminated by pouring into water. The resulting emulsion was then extracted with *n*-pentane. A colorless liquid product of isopropyl maleimide was obtained after pentane removal under reduced pressure, (21%), ¹H-NMR (500 MHz, DMSO-d₆): δ (ppm): 1.37 (d, 6 H), 4.25 (m, H), 7.03 (s, 2 H).

Further, the *i*-propyl-comonomer was synthesized by the same method as the methyl-comonomer, using isopropyl maleimide instead of methyl maleimide to give a dark brown

solid, (81%), $^1\text{H-NMR}$ (500 MHz, DMSO- d_6): δ (ppm): 0.83 (d, 6 H), 1.10 (t, 6 H), 1.68 (m, 6 H), 1.91 (m, 2 H), 2.08 (m, 2 H), 2.65 (m, 2 H), 3.08 (s, 2 H), 3.76 (m, H), 6.59 (s, 2 H), 6.68 (s, 2 H), 8.57 (s, 2 H), 8.69 (s, 2 H).

2.2.7. *t*-Butyl-Comonomer

t-Butyl-comonomer was synthesized by the same method as the methyl-comonomer, using *t*-butyl maleimide instead of methyl maleimide to give a dark brown solid, (95%), $^1\text{H-NMR}$ (500 MHz, DMSO- d_6): δ (ppm): 1.07 (m, 15 H), 1.63 (m, 6 H), 1.90 (m, 2 H), 2.04 (m, 2 H), 2.56 (m, 2 H), 2.95 (s, 2 H), 6.59 (s, 2 H), 6.66 (s, 2 H), 8.57 (s, 2 H), 8.66 (s, 2 H).

2.2.8. Cyclohexyl-Comonomer

Cyclohexyl-comonomer was synthesized by the same method as the methyl-comonomer, using cyclohexyl maleimide instead of methyl maleimide to give a dark brown solid, (91%), $^1\text{H-NMR}$ (500 MHz, DMSO- d_6): δ (ppm): 0.85 (d, 2 H), 1.11 (m, 10 H), 1.68 (m, 10 H), 1.92 (m, 2 H), 2.09 (m, 2 H), 2.67 (m, 2 H), 3.10 (s, 2 H), 3.40 (m, 1 H), 6.59 (s, 2 H), 6.69 (s, 2 H), 8.58 (s, 2 H), 8.69 (s, 2 H).

2.2.9. Phenyl-Comonomer

This comonomer and the associated homo- and copolymers were obtained by a procedure published elsewhere [44].

2.3. Polymer Synthesis

2.3.1. PIM-1 Synthesis

PIM-1 was synthesized by using the fast synthesis method reported elsewhere [45–47]. A slight modification of the reported method was employed in this study. A three-necked round bottom flask was charged with TTSBI (20 mmol) and TFTP (20 mmol) and dissolved in 65 mL dimethylacetamide (DMAc) under argon atmosphere. Addition of K_2CO_3 (44 mmol) turned the reaction mixture from orange to yellow. The reaction flask was immediately immersed into a preheated oil bath (150 °C). The gradual addition of diethylbenzene (DEB) (15 mL) prevented the precipitation of PIM-1 and promoted the formation of a polymer with higher molecular weight. The reaction mixture was stirred for 30 min and was quenched by precipitation in methanol. After filtration, the solid was dried at 80 °C in vacuum. The dried polymer was dissolved in CHCl_3 and re-precipitated in methanol. The solid was collected by filtration and dried under high vacuum at 80 °C to give the final product as a yellow solid (90%). The apparent molecular weight (M_w) of the purified polymer and dispersity (\bar{D}) were determined by size-exclusion chromatography, giving an apparent average molecular weight of $M_w = 132.5$ kg/mol and $\bar{D} = 4.9$.

2.3.2. Synthesis of Homo- and Copolymers

Copolymers were synthesized by polycondensation of new comonomers/TTSBI (1 mmol/1 mmol) and TFTP (2 mmol) using the earlier described procedure similar to that of PIM-1 synthesis. Copolymers will be referred to as methyl-/ethyl-/propyl-/*i*-propyl-/*t*-butyl-/cyclohexyl-/phenyl-50 where the suffix –50 indicates the comonomer/TTSBI mol ratio in the copolymers (e.g., methyl-50 consists 50 mol% TTSBI and 50 mol% comonomer unit).

Homopolymers were synthesized by polycondensation of new comonomers and TFTP (equimolar amount) using a similar procedure to that of PIM-1. Homopolymers will be referred to as methyl-/ethyl-/propyl-/*i*-propyl-/*t*-butyl-/cyclohexyl-/phenyl-100 where the suffix –100 stands for the comonomer/TTSBI mol ratio in the homopolymers (e.g., methyl-100 consists of 100 mol% comonomer unit). A slight modification of the abovementioned PIM-1 synthesis was carried out for homopolymerization, which is that, instead of the addition of DEB, DMAc was used in 2-fold excess volume, and the reaction time was increased for an additional 1 h.

2.4. Film Preparation

Thick polymer films were obtained by casting from a solution containing 3–5% wt. of polymer dissolved in CHCl_3 . The homogenous solution was obtained by stirring for at least 2 h followed by casting into a leveled Teflon[®] circular dish. The solution in the dish was covered with a glass lid, and the system was purged gently with an argon stream for 24 h to evaporate CHCl_3 at room temperature. After solvent evaporation, the thick film was removed from the Teflon[®] surface and further dried for 24 h in vacuum at 80 °C. The thickness of the obtained films was in the 60–80 μm range as determined by a digital micrometer Deltascope FMP10 (Helmut Fisher GmbH, Sindelfingen, Germany).

2.5. Methods

2.5.1. Size-Exclusion Chromatography (SEC)

For SEC measurements, a column combination (precolumn-SDV-linear, SDV-linear and SDV 102 nm with inner diameter = 4.6 mm and length = 53 cm, Polymer Standard Service GmbH, Mainz, Germany) was used at a flow rate of 1.0 mL min^{-1} running CHCl_3 as eluent at 30 °C. A combination of refractive index (RI) and ultraviolet (UV) detectors were used for concentration detection. Polystyrene standards of different molecular weights were used for the evaluation of apparent weight average molecular weight (M_w) and dispersity index (D) of the prepared polymers.

2.5.2. ^1H Nuclear Magnetic Resonance (^1H -NMR)

NMR spectra were collected on a Bruker AV500 NMR spectrometer (Bruker Biospin, Ettlingen, Germany) operating at a field of 7T (500 MHz) using a 5 mm $^1\text{H}/^{13}\text{C}$ TXI probe and a sample temperature of 298 K. ^1H NMR spectra were recorded applying a 10 ms 90° pulse.

2.5.3. Thermal Gravimetric Analysis (TGA)

TGA measurements were performed using TGA/DSC 2 Mettler-Toledo, Giessen, Germany). The analysis was performed under argon flow (20 mL/min) in the temperature range 30 to 800 °C at a heating rate of 5 K min^{-1} .

2.5.4. Thermogravimetric Analysis Coupled with Fourier Transform Infrared Spectroscopy (TG-FTIR)

The evolved gases were measured using a thermogravimetric analyzer coupled with an FT-IR spectrometer Nicolet iS50 (Thermo Scientific, Darmstadt, Germany), which was recorded in the spectral range of 400–4000 cm^{-1} with a resolution of 4 cm^{-1} and an average of 8 scans. All measurements were performed in the temperature range 30 to 800 °C at a heating rate of 5 K min^{-1} .

2.5.5. Fourier Transform Infrared Spectroscopy (FTIR)

FTIR spectra were collected on an ALPHA FTIR spectrometer (Bruker Optics, Bremen, Germany) in attenuated total reflectance mode (ATR, diamond crystal). The measurements were done at ambient temperature in a spectral range of 400 to 4000 cm^{-1} with a resolution of 4 cm^{-1} and an average of 64 scans.

2.5.6. Density Measurement

The density measurements were performed based on the buoyancy method, as described elsewhere [45]. FC-770, Fluorinert (3M, Saint Paul, MN, USA) was used as an immersion liquid because it has the least affinity to the polymers under study and would not diffuse into the free volume of the polymer during measurement. The density was determined according to Equation (2):

$$\rho = \frac{\chi(\rho_o - \rho_l)}{\chi - \beta} + \rho_l \quad (2)$$

where, χ is weight of the sample in air, β is weight of the sample in displaced liquid, ρ_o is density of fluorinated liquid (1.79 g cm^{-3} determined at conditions of the experiment) ρ_l is density of air (0.001 g cm^{-3}).

2.5.7. Determination of Fractional Free Volume (FFV)

The fractional free volume (FFV) of polymers under study was determined by the combination of experimental and molecular modeling data, which were applied to Equation (3):

$$FFV = \frac{V - 1.3V_w}{V} \quad (3)$$

where V is the polymer specific volume, and V_w is the specific van der Waals volume obtained by molecular modeling [48]. The specific volume of the polymers was obtained from density measurements. Van der Waals volume can be obtained using the group contribution method by Bondi [49], summarized by van Krevelen [50]. In the current work, a molecular modeling approach was utilized where a polymer chain consisting of 3 monomeric units was equilibrated by geometry optimization functions of HyperChem 8.0 (Hypercube Inc, Gainesville, FL, USA) software. After full molecule optimization, the QSAR function of HyperChem was called out and molecular weight and van der Waals volume of a single monomeric unit was derived. Modeling of the chain consisting of 3 monomeric units allowed for the reduction of the end group effect on the final result. The validity of volume calculation was confirmed by a comparison of results with that obtained in Materials Studio (BIOVIA, San Diego, CA, USA) [46]. Since HyperChem is easier to use for this simple task, it was decided to model all polymers using this software.

2.5.8. Gas Transport Properties Measurement

The gas transport properties of synthesized polymers were investigated by the “time-lag” method utilizing the constant volume/variable pressure approach on the facility described elsewhere [51]. H_2 , N_2 , O_2 , CH_4 and CO_2 were considered as permanent gases at conditions of experiment: 30°C , 1000 mbar feed pressure, 0–10 mbar permeate pressure and 238 cm^3 constant permeate volume. The effective membrane area was 1.15 cm^2 . Transport properties of H_2O vapor were investigated as well; the feed pressure, in this case, was ca. 60% of saturated vapor pressure but, despite the fact that water vapor is very close to the saturation point, the data were treated the same way as for the other gases, not taking into account the fugacity coefficient. Each gas was applied to the thoroughly evacuated polymer film 3 times, and average values were taken. In case the difference in values was bigger than 5%, the measurement was repeated. The time lag measurements were conducted without any further treatment right after film preparation to minimize the physical aging effect.

The permeability (P), diffusion (D) and solubility (S) coefficients and ideal permeability selectivity ($\alpha_{x/y}$) for gases x and y were determined from the linear part of the “time-lag” curve by the following equations:

$$P = DS = \frac{V_p l (P_{p2} - P_{p1})}{ART \Delta t (p_f - (p_{p2} + p_{p1})/2)} \quad (4)$$

$$D = \frac{l^2}{6\theta} \quad (5)$$

where V_p is the constant permeate volume (cm^3), l is the film thickness (cm), A is the effective area of the membrane (cm^2), R is the universal gas constant ($8.314 \text{ J mol}^{-1} \text{ K}^{-1}$), T is the absolute temperature of experiment ($^\circ\text{C}$), Δt is the time for the permeate pressure change from p_{p1} to p_{p2} (s), p_f is the feed pressure (cmHg) and θ is the time lag(s). The accuracy of the gas transport parameters depends strongly on the film preparation quality for the diffusion coefficient and on the pressure applied to the o-ring sealing of the measurement cell for the permeability coefficient. The thickness of studied films was in the range of

80 μm with a thickness spread $\pm 2 \mu\text{m}$ which gives ca. 2.5% error for the diffusion coefficient determination. The experimental error of permeability coefficient determination can be considered as 4% for the case of film area of 1.15 cm^2 exposed to penetrant and 1 mm diameter Viton[®] O-ring used for sample sealing. Other parameters, e.g., accuracy of pressure and temperature sensors, can be considered insignificant in comparison to these two parameters.

3. Results and Discussions

3.1. Comonomer Synthesis

Comonomers were synthesized following the multi-stage synthesis route as shown in Figure 1, inspired by the procedure published by Khan et al. [44]. However, a slight modification of the reported procedure was employed in this study. The first step in this process is the condensation reaction of 1,2-dimethoxybenzene and pentanal to obtain tetramethoxy anthracene. The decision to use pentanal was based on the improved solubility of the reaction product. The hydroxylation of the tetramethoxy anthracene intermediate was the next step to obtain the tetrahydroxy anthracene derivative. After the successful conversion of tetramethoxy to tetrahydroxy anthracene, a Diels-Alder reaction was carried out using maleimides, which contain different substituents attached to the nitrogen atom. In comparison to the procedure established by Khan et al. [44], the anthracene-maleimide comonomers were obtained in a shorter reaction time but with a higher yield in this study.

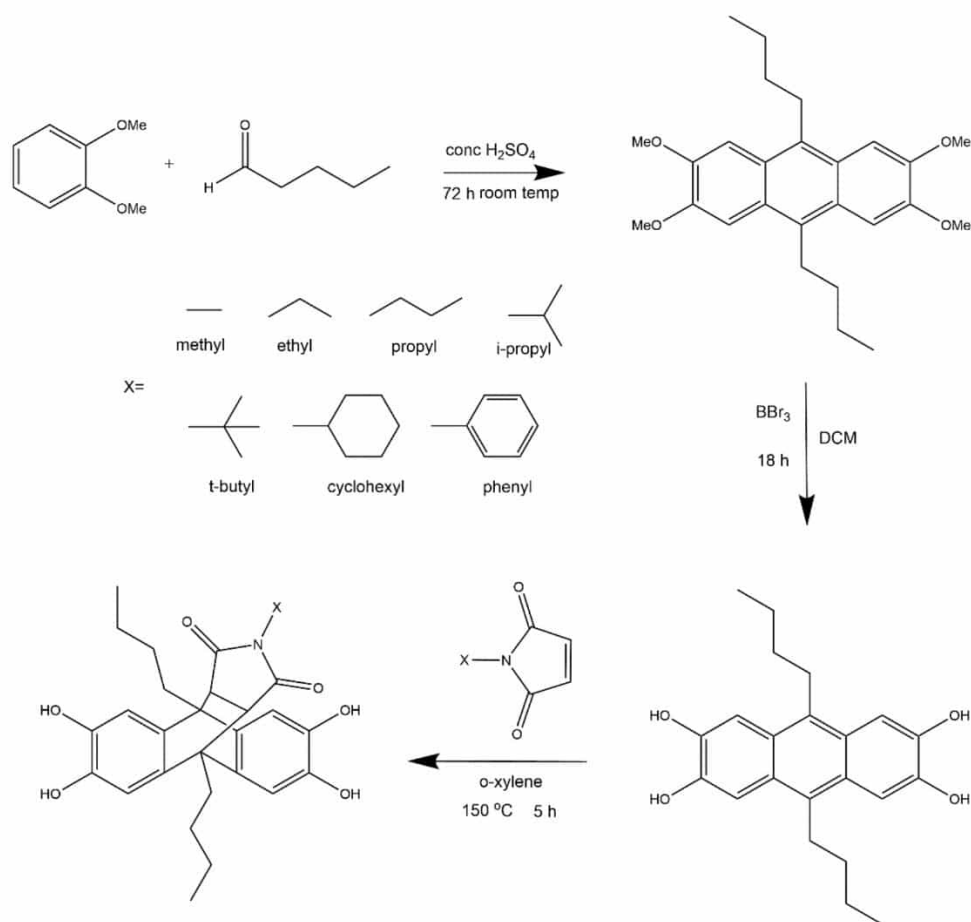


Figure 1. Synthesis route of the new comonomers.

The success of all comonomer syntheses was shown by ^1H NMR measurements (Figure S1). As an example, the ^1H NMR spectrum of the methyl-comonomer is shown in

more detail in Figure 2. The spectrum exhibits two singlets at 8.69 and 8.61 ppm, assigned to the hydroxyl protons, and two singlets at 6.67 and 6.59 ppm, corresponding to the aromatic protons. The signal split is due to the asymmetrical structure of the monomer, which arises from the formation of a “roof-like structure” and the tilting of this group towards one side of the anthracene backbone. The two characteristic protons, which appear after successful Diels-Alder reaction and the formation of the “roof-like structure”, are present at 3.18 ppm, whereas one sharp singlet appears at 2.41 ppm assigned to the aliphatic protons of the *N*-methyl substituent. The protons attributed to the butyl groups appear in the range of 2.74 to 1.09 ppm. The other comonomers show similar spectra regarding the monomer backbone protons (aromatic, hydroxyl, butyl and maleimide groups linked to anthracene backbone). The residual spectra show that variations and signals overlap depending on the size of the substituent (Figure S1).

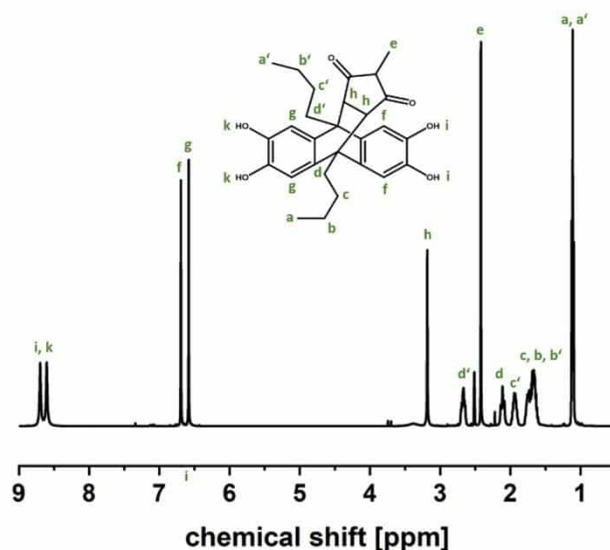


Figure 2. ^1H NMR spectrum of the methyl-comonomer.

TGA was carried out to determine the decomposition temperature of the comonomers since polymerization takes place at 150 °C, and a retro-Diels-Alder reaction was reported for aromatic substituents [44]. TG-FTIR analysis was performed in the temperature range from 30 °C to 800 °C. Figure 3 depicts that the methyl-comonomer remains stable up to approximately 250 °C and degradation of the monomer takes place in two clearly visible steps. In order to identify the early degradation products, gas-phase FTIR spectra were obtained at 265 °C and 300 °C. The gas-phase spectra show FTIR bands at 2953 cm^{-1} related to C-H stretching vibration of the methyl group, 1737 cm^{-1} due to C=O stretching and 697 cm^{-1} related to the H-C=C-H bending vibration of methyl maleimide, which is in very good accordance to a gas-phase spectrum, collected from a TG-FTIR measurement of neat *N*-methyl maleimide and verifies the occurrence of a retro-Diels-Alder reaction as described for aromatic substituents [44]. Additionally, the extracted spectrum obtained for the sample taken at 300 °C shows the appearance of *n*-butane. According to these results, we can infer that the decomposition of the maleimide group takes place prior to the comonomer backbone decomposition. In addition to the methyl-comonomer, also ethyl and *t*-butyl-comonomers show the same behavior regarding the lower retro Diels-Alder temperature. On the other hand, the decomposition of the comonomer backbones of propyl, *i*-propyl, cyclohexyl and phenyl comonomers overlaps with that of the retro Diels-Alder reaction.

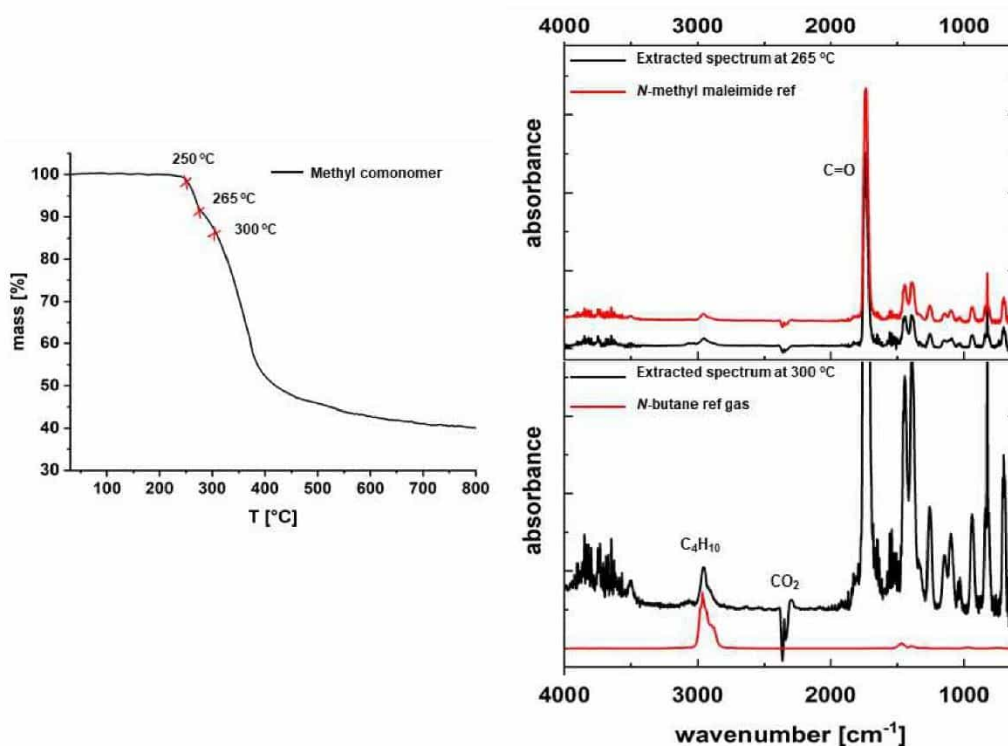


Figure 3. TG-FTIR spectra of methyl-comonomer.

3.2. Polymer Synthesis

After successful monomer synthesis, all comonomers were polymerized in the next step. The homo- and copolymers were synthesized by the polycondensation of comonomers (Figure 4) with TFTP and comonomer/TTSBI (molar ratio 1/1) with TFTP, respectively, by using a procedure similar to PIM-1 synthesis with slight modification [44,47,52]. DEB addition takes place only in the synthesis of copolymers, whereas for homopolymer synthesis, it is not necessary. This discrepancy might be related to the different solubility of homopolymer and copolymer solutions [25]. PIM-1 usually starts to precipitate when the number of repeating units reaches a certain degree of polymerization. Since copolymers also contain the repeating units of PIM-1, a similar situation might occur in this study.

All homo- and copolymers were characterized with respect to their apparent molar masses and dispersity by gel permeation chromatography (GPC) and their compositions by ^1H -NMR spectroscopy (Table S1). Figure 5 depicts ^1H -NMR spectra of methyl-50 and methyl-100 in comparison to PIM-1. The peak seen at 6.45 ppm for PIM-1 and methyl-50 spectra arises from the aromatic protons of TTSBI. The characteristic signal of the comonomer corresponding to the roof-shaped maleimide proton was seen at 3.25 ppm, which indicates the stability of comonomers throughout the polymerization conditions. The integration of allocated peaks of methyl-50 proved that the composition of the copolymer (methyl comonomer/TTSBI) is close to equimolar, as expected. Table S1 shows the entire polymer composition calculations based on the ^1H -NMR spectra.

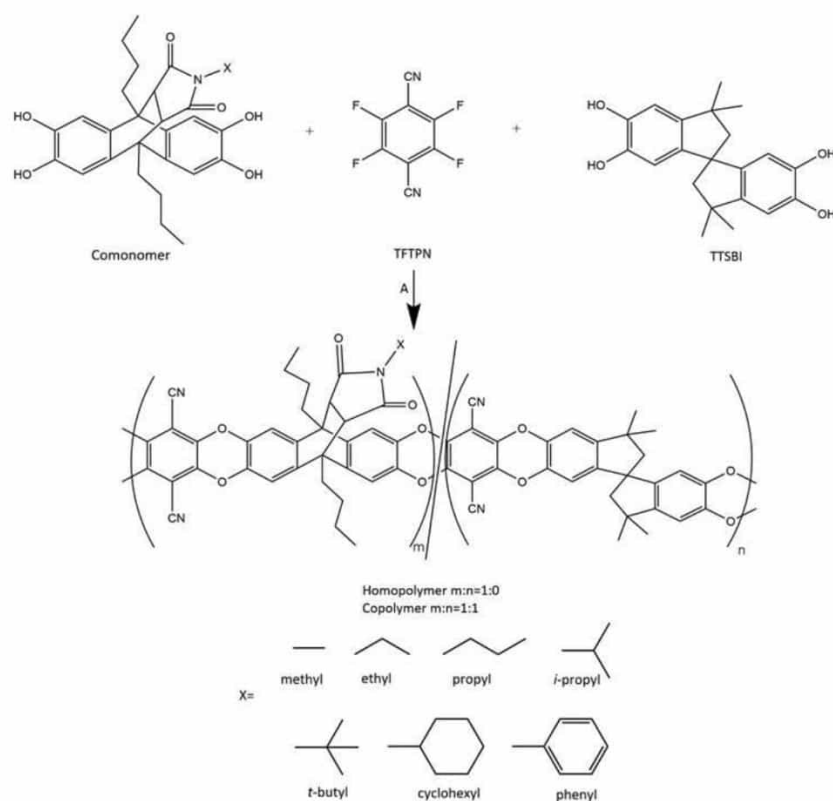


Figure 4. Synthesis of homopolymer and copolymer, A: reagents and conditions DMac, DEB (for copolymer), K_2CO_3 , 150 °C, 30–60 min.

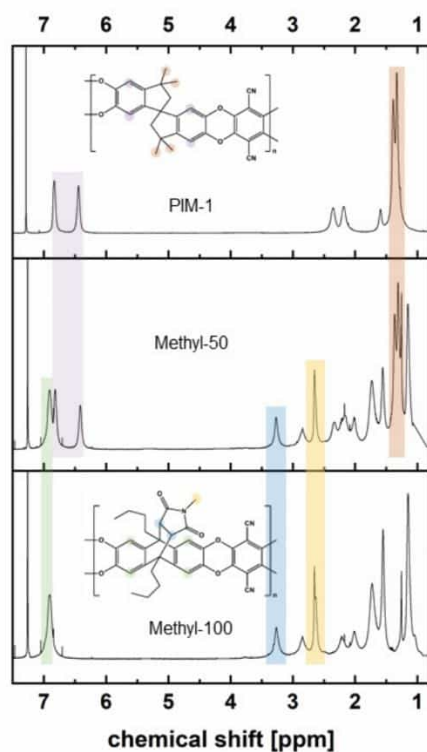


Figure 5. 1H -NMR spectra of PIM-1, methyl-50 and methyl-100.

TG-FTIR analysis was carried out to determine the retro Diels-Alder temperature of homopolymers. TGA curves for all homopolymers exhibit two distinct onset decomposition temperatures (Figure S3). As can be seen from Figure 6, the onset temperature of the first decomposition step of methyl-100 is at approximately 220 °C. It arises from breaking the maleimide moiety, and the second decomposition around 400 °C corresponds to the decaying of the polymer backbone. The evolved gas analysis was conducted at 305 °C, and the extracted spectrum was compared with the reference *N*-methyl maleimide gas-phase spectrum. Additionally, peak height profiles of the carbonyl band at 1730 cm⁻¹ and evolved gases (CO₂ and *n*-butane) revealed that similar to the monomers, retro-Diels-Alder reaction (in the case of the polymers) takes part before butyl group degradation. Moreover, no CO₂ was detected below 350 °C, leading to these inferences: (1) the peak evolved around 300 °C which means, that only retro-Diels-Alder takes part and there is no further degradation from maleimide or group disintegration; (2) the peaks evolving above 400 °C correspond to CO₂ (2350 cm⁻¹) and C₄H₁₀ (2900 cm⁻¹) caused by the degradation of the polymer backbone. These features indicate that the retro Diels-Alder reaction occurs at lower temperatures than the decomposition of the polymer backbone chain and does not overlap with the butane release correlated with decomposition of the polymer backbone.

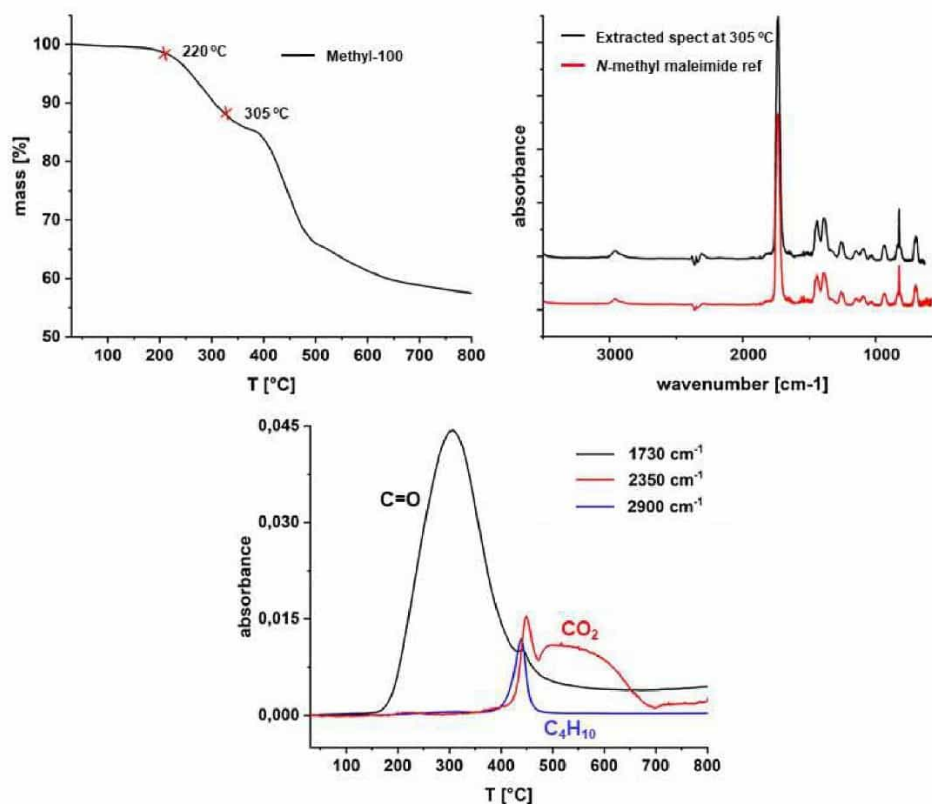


Figure 6. TG-FTIR spectrum of methyl-100.

These findings offer further opportunity for a post-thermal treatment of polymer films, which would lead to materials with structures shown in Figure 7. Although it is not a focus of this study, the effect of the thermal conversion was tested on the example of methyl-100. In order to quantify the extent of the thermal conversion, four additional polymers were synthesized. These polymers consist of 2,3,6,7-tetrahydroxy-9,10-dibutylanthracene (synthesis described earlier) and methyl-comonomer in different molar ratios (0:1, 0.9:0.1, 0.75:0.25, 0.5:0.5, 1:0) and were used for establishing a calibration graph by means of FT-IR (Figure 8). After synthesis, it was observed that all materials are not soluble in common solvents (THF, CHCl₃) that are normally used for the processing of PIMs. This means that

the thermal conversion of the materials does not only change the structure, but also the solubility properties of the polymers.

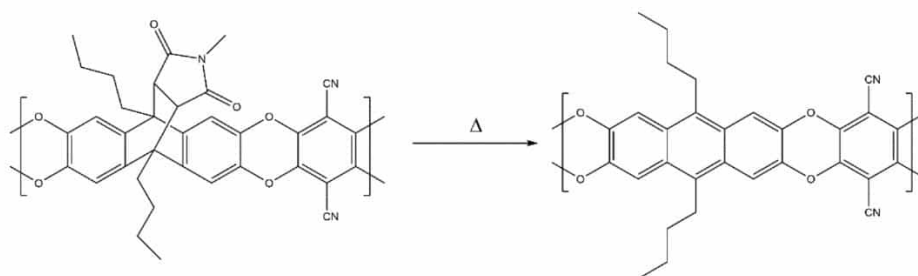


Figure 7. Expected thermal conversion of methyl-100 at 250 °C.

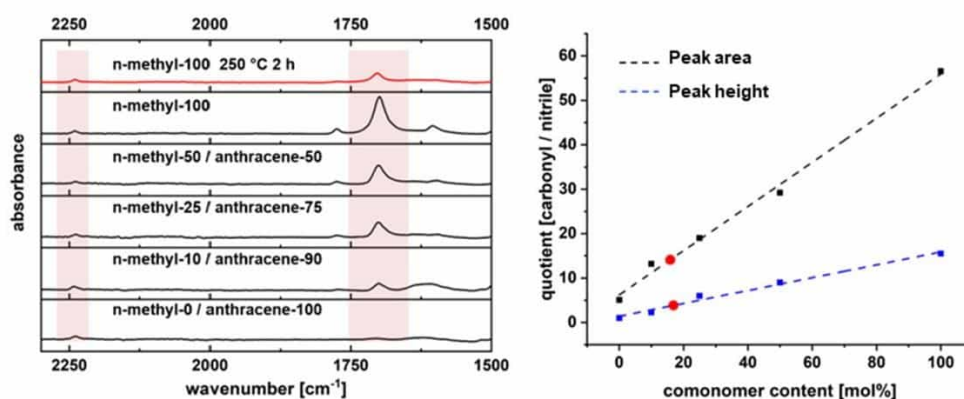


Figure 8. Quantification of conversion by means of FT-IR.

After thermal treatment at 250 °C for 2 h in a nitrogen atmosphere, the polymer film was measured by means of FT-IR (ATR). The ratios of the integrated peak areas and the peak height of the nitrile and carbonyl groups were used for quantification. Both methods gave approximately 16% residual methyl maleimide. Therefore, 84% of the maleimide groups were removed at 250 °C, while the polymer film remained mechanically stable. The optical images of methyl-100 films before and after thermal treatment can be seen in Figure S4.

In this study, differential scanning calorimetry measurement (DSC) of homo- or copolymers was not conducted since the decomposition temperature is lower than PIM-1. It is known that the glass transition temperature (T_g) of PIM-1 cannot be detected before its thermal decomposition using conventional DSC [53].

3.3. Gas and Water Vapor Transport Properties

All polymer films prepared from the synthesized polymers were transparent and mechanically stable enough to be sealed in the measurement cell of the “time-lag” facility with a Viton® O-ring. Films were placed into the experimental facility after the same, shortest possible time after solvent evaporation in order to keep all polymers at a similar state in respect to possible physical aging. No additional experiments on thick polymer film aging were carried out since this topic was investigated earlier [54] and was not intended for the current study. Before this, the gas transport measurement films were evacuated to the state when the permeate pressure sensor did not show any signs of pressure increase due to the desorption of volatile impurities from the polymer film. After the evacuation step, films were exposed to penetrants in the following sequence: H₂, N₂, O₂, CH₄, CO₂ and H₂O. The gas was taken from the gas line or from the liquid water container into the feed pressure vessel and brought to the temperature of the thermostated part of the

“time-lag” facility. The gas permeability, diffusion and solubility coefficients of gases and vapor for films of PIM-1, copolymers and homopolymers are presented in Tables S2–S4. In the further discussion, gas transport parameters will be analyzed mostly on the examples of CH₄ and CO₂ as penetrants with a significant difference in kinetic diameters and state in respect to critical pressure and temperature, and water vapor as an example of a penetrant very close to the condensation under experimental conditions.

3.3.1. Gas Transport Properties of Homopolymers and Copolymers

An initial objective of using different substituted maleimides was to investigate the effect of aliphatic groups of different sizes and shapes on gas and water vapor transport properties. The change in linear aliphatic chain length (methyl-, ethyl- and propyl-), change in group geometry (propyl-, *i*-propyl- and *t*-butyl-) and difference between cycloalkyl and aromatic groups (cyclohexyl- and phenyl-) were the main subjects able to reveal a trend between change in the structure of the side group and transport parameters of gaseous penetrants in synthesized polymers.

In comparison to PIM-1, the newly synthesized homopolymers exhibit lower single gas permeability coefficients. Figure 9 shows that there is a gradual reduction of CH₄ and CO₂ permeability coefficients in the line of the methyl-, ethyl- and propyl- substituted homopolymers. When the linear alkyl chain splits, as in the cases of *i*-propyl-100 and *t*-butyl-100 polymers, forming so-called “bulky” side groups [39], permeability starts to increase in comparison to linear side groups. This result is also supported by further observations. By introducing a third methyl group into the alkyl chain, as seen in *t*-butyl-100, there is an improvement in CO₂ and CH₄ permeability, which, in the case of CH₄ in *t*-butyl-100, became even higher than that of PIM-1. This can be associated with an increase of the fractional free volume (FFV) for *i*-propyl-100 and *t*-butyl-100 polymers in comparison to linear side group polymers. It is interesting to observe that the FFV of *t*-butyl-100 polymer is still lower than in the case of PIM-1, but the CH₄ diffusion coefficient is nearly 40% higher while the diffusion coefficient of CO₂ is very similar to PIM-1. This fact can only be related to differences in the structure of the free volume in these two polymers, giving a lower molecular sieving effect for *t*-butyl-100. Introduction of spacious, “bulky” side groups, as in the case of *t*-butyl-100, where flexibility of the side chain is restricted, leads to a desirable change of the FFV even when the size of the group is relatively small in comparison to the size of the monomeric unit. This phenomenon is in accordance with previous studies indicating that the introduction of bulky side groups leads to inefficient chain packing, thus resulting in higher FFV [36,55]. For a better FFV analysis, CH₄ is a good choice considering its biggest kinetic diameter among all other studied penetrants (H₂O: 2.65 Å; H₂: 2.89 Å; CO₂: 3.3 Å; O₂: 3.46 Å; N₂: 3.64 Å; CH₄: 3.8 Å). Figure 9 exhibits that CH₄ and CO₂ diffusion coefficients of homopolymers follow the same pattern. It can be seen that there is a gradual reduction of the relative diffusion coefficient along with side chain length increase. A possible explanation for this might be that the linear side chains, due to their flexibility, probably fill the free volume formed by packing of macromolecular chains but do not create additional free volume, as in the case of *i*-propyl and *t*-butyl groups, causatively reducing diffusion coefficients for both CH₄ and CO₂. As previously mentioned, in cases of *i*-propyl-100 and *t*-butyl-100, as soon as the rigid, bulky side group is introduced into the polymer structure, the diffusion coefficient increases as a consequence of the rise in FFV. Introduction of the cyclic substituent into the polymer structure does not bring benefits nor for FFV value or for gas transport properties of CH₄ or CO₂. Permeability coefficients of gases in cyclohexyl-100 are very similar to that in propyl-100, and significantly lower than for the homopolymer with bulky substitutes. Due to the possible boat and chair molecular conformations, the cyclohexyl substituent can be considered as a flexible side group, which can effectively fill the free volume elements. This implication is suggested by the FFV value of the homopolymer, which for cyclohexyl-100, is almost the same as for propyl-100 and much lower than those of *i*-propyl-100 or *t*-butyl-100. Surprisingly, CH₄ and CO₂ permeability of phenyl-100 is lower compared to other

homopolymers while possessing almost the same FFV of homopolymers with linear side chains. A possible explanation of this finding might be that the phenyl side group can rotate freely and possibly interact with aromatic rings of the main chain by π - π stacking, consequently not increasing the FFV of the polymer as in the case of other spacious groups. In this manner, the phenyl substituent might be addressed as a viably flexible side chain rather than called a rigid, bulky group [44].

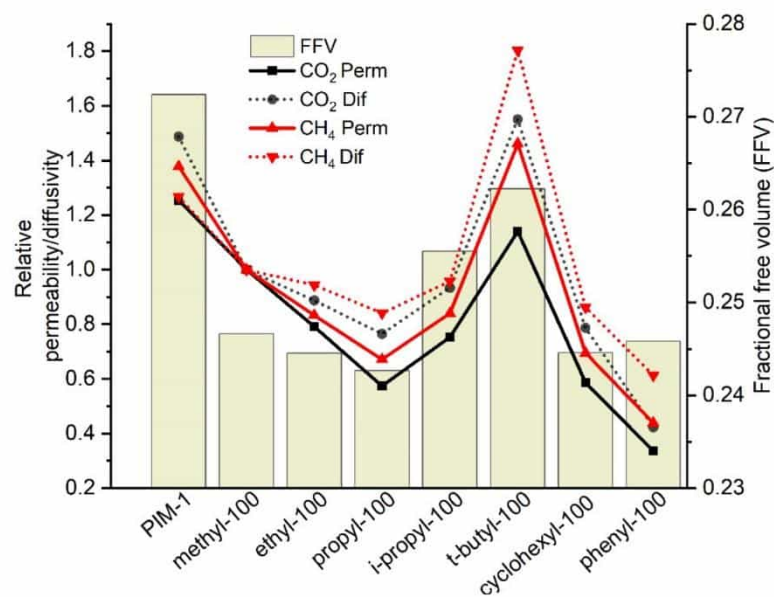


Figure 9. CO₂ and CH₄ relative permeability relative diffusivity and FFV of homopolymers. (Relative permeability or diffusivity: homopolymer gas permeability or diffusivity are normalized to methyl-100 gas permeability or diffusivity.)

Gas transport properties of copolymers are discussed by considering the effect of the introduction of 50 mol% of comonomer units into the PIM-1 polymer backbone. It must be reckoned that the main disadvantage of the polycondensation mechanism for copolymer synthesis is its limitation to control the distribution of the monomeric units along the polymer chain and the formation of oligomers in contrast to addition type polymerizations [47,56]. Consequently, copolymerization of PIM-1 and anthracene maleimide comonomer units leads, probably, to a random distribution of the different units along the polymer chain if the reactivity of their functional groups is similar.

In comparison to PIM-1, methyl-50 and *t*-butyl-50, copolymer presence increased gas permeabilities (Table S2). Figure 10 depicts that the CO₂ permeability in methyl-50 is increased by 14%, while in *t*-butyl-50, it is increased by 18% in comparison to PIM-1. Regarding CH₄ permeability, methyl-50 exhibits 35% and *t*-butyl-50 exhibits 50% higher values compared to PIM-1. It can therefore be assumed that the introduction of methyl or *t*-butyl anthracene maleimide structures into PIM-1 at a 1:1 molar ratio helps to increase permeability by ca. 20% compared to PIM-1, accompanied by an ca. 20% decrease in CO₂/CH₄ selectivity.

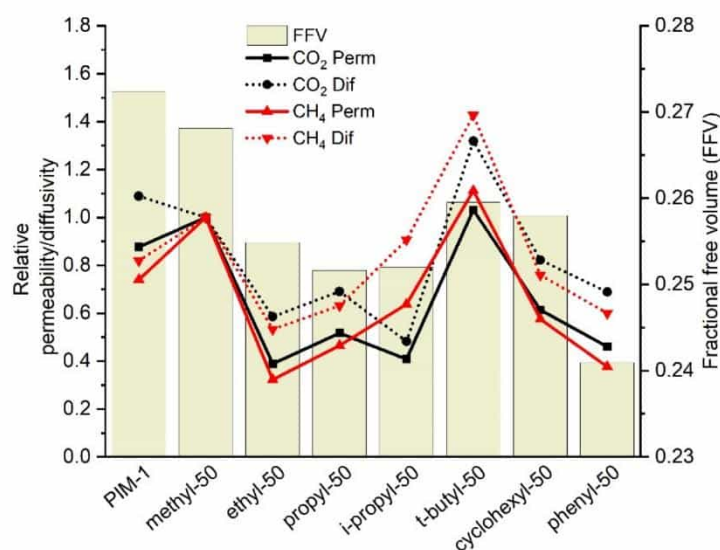


Figure 10. CO₂ and CH₄ relative permeability relative diffusivity and FFV of copolymers. (Relative permeability or diffusivity: copolymer gas permeability or diffusivity are normalized to methyl-50 gas permeability or diffusivity.)

However, the line for permeability of copolymers does not show the same behavior when compared to that for homopolymers. Figure 10 demonstrates that the FFV of copolymers does not follow the same trend, which was attributed to the linear and bulky side group effect, as discussed in the homopolymer case. An unanticipated finding is that methyl-50 has a higher FFV than *t*-butyl-50. One can conclude that the aforementioned random copolymerization results in the mixing of geometrically different PIM-1 and substituted maleimide monomers play an important role in polymer chain packing, making it especially inefficient in the case of methyl-50 polymer and resulting in higher free volume and permeability coefficients. Unfortunately, it is difficult to have a clear knowledge of the comonomer distribution within the copolymers. Herein, further research is required to evaluate reaction kinetics for maleimide and spirobisindane units and to understand whether copolymerization is truly random or block formation is possible. The ambiguity of the reaction kinetics could lead to a non-uniform arrangement of the polymer packing, hereby causing the formation of an irregular structure of the FFV.

Furthermore, N₂, H₂ and O₂ transport data of homopolymers and copolymers can be found in the supporting information. Figures S5 and S6 clearly show that N₂, H₂ and O₂ permeability and diffusivity lines follow the same trend as those of CO₂ and CH₄ for homopolymer and copolymer.

3.3.2. Water Vapor Transport Properties of Homo- and Copolymers

The outcome of water transport in synthesized homo- and copolymers indicates that the introduction of an anthracene maleimide derivative with different side chains plays a significant role in water transport through the polymer matrix. Numerous publications report that imide-based membranes are extensively used for water separation since they possess good mechanical stability, high thermal resistance and high water vapor permeability [57–59]. It is known that the imide group increases the polarity of the molecule and provides an environment for water molecules to form hydrogen bonding [60–62]. Hence, the introduction of this group into the polymer chain would lead to an improvement in the interaction between the water molecule and the polymer. This estimation is supported by the results of water transport in homopolymers displayed in Table 1.

Table 1. Water vapor permeability of homopolymers and copolymers.

| | PIM-1 | Methyl-100 | Ethyl-100 | Propyl-100 | <i>i</i> -Propyl-100 | <i>t</i> -Butyl-100 | Cyclohexyl-100 | Phenyl-100 |
|-------------------------------|--------|------------|-----------|------------|----------------------|---------------------|----------------|------------|
| Water permeability (Barrer *) | 79,300 | 110,000 | 87,800 | 56,300 | 64,100 | 72,500 | 46,800 | 48,600 |
| | | Methyl-50 | Ethyl-50 | Propyl-50 | <i>i</i> -Propyl-50 | <i>t</i> -Butyl-50 | Cyclohexyl-50 | Phenyl-50 |
| Water permeability (Barrer *) | | 114,500 | 62,700 | 60,100 | 54,800 | 88,500 | 60,600 | 56,400 |

* 1 Barrer = 1×10^{-10} (cm³(STP) cm cm⁻² s⁻¹ cmHg⁻¹ = 3.348×10^{-16} mol m m⁻² s⁻¹ Pa⁻¹).

In comparison to PIM-1, methyl-100 and ethyl-100 show higher water permeabilities in accordance with the expectation. Among the substituents, the methyl-imide derivative is assumed to give the most polar comonomer since it has the shortest alkyl side chain, which influences the molecule's polarity, and therefore restricts the interaction of water with the macromolecule less than larger aliphatic substituents. Previous studies show that larger alkyl groups inversely act on water permeability independent of membrane application, e.g., gas separation or pervaporation [63,64]. Along with the increase in alkyl side chain length, water vapor permeability decreases, as can be observed in the line of methyl-100, ethyl-100, and propyl-100 polymers. The reason for this can be attributed to the fact that a longer aliphatic chain reduces the affinity of the imide side-chain group toward H₂O, most probably due to increased hydrophobicity and thus effective blocking of the imide ring vicinity for water molecules. This consideration is confirmed by the absence of the aforementioned bulky group effect on CH₄ and CO₂ permeability for the case of water permeability. Table 1 exhibits that water permeability of *i*-propyl-100 and *t*-butyl-100 increases insignificantly contrary to cases for CO₂ and CH₄ as a result of replacing the linear side chain by bulkier groups accompanied with a significant increase in free volume. Cyclic side groups also did not bring any significant improvement to water permeability. It is obvious to evaluate the permeability data in conjunction with the diffusion and solubility coefficients and fractional free volume of polymers in accordance with the solution-diffusion model. Taking into account both the solubility and diffusivity effects in Figure 11, the water vapor permeability of homopolymers with alkyl side chains mostly follows changes of solubility, while the diffusion coefficient gradually decreases in the line from methyl to propyl side groups along with reduction of free volume. When the linear side group is changing to more spacious *i*-propyl- and *t*-butyl- substituents, the water diffusion coefficient increases following the change of the FFV. At the same time, the water solubility coefficient decreases and reaches minimum values for *t*-butyl and cyclohexyl substituents. In comparison to the methyl case, both of these factors, i.e., changes in solubility and diffusion coefficients, result in relatively low water vapor permeability coefficients, which can be explained only by blocking the access of water molecules to the imide moiety by the bulky substituent.

To understand water transport through polymers better, it is worth mentioning some specific phenomena regarding the penetrant behavior. Generally, when there is an affinity of water penetrant to the polymer (high hydrophilicity), the interaction of water-polymer leads to polymer swelling, which is also called plasticization [65], or even dissolution. On the other hand, if the polymer is rather hydrophobic, the water-water interaction can be more prominent than the water-polymer interaction. As a result of prevailed penetrant-penetrant association, water molecules can form clusters due to hydrogen bonding [65–67]. These two phenomena significantly influence water diffusivity and, consequently, permeability through the membrane in different ways. Kelkar and Paul showed that plasticization causes the polymer chains to move freely on a segmental length scale, thus increasing water diffusivity [68]. However, when the molecule clustering effect overrides the plasticization, water molecule clusters increase in average size; subsequently, the apparent diffusivity of water decreases. Several studies reported the importance of the clustering effect on water transport [67–72]. In this current study, the transport of water molecules in polymers is in

compliance with the solution-diffusion model without strong evidence of specific interactions between the water molecule and polymer. Therefore, the abovementioned clustering of water molecules or polymer swelling are probably not preponderant phenomena—a result based on our “time-lag” experimental results, with the exception of the phenyl-100 case. More concrete, the result of the gas transport parameters revealed a strong deviation of the water vapor solubility coefficient of phenyl-100. Further analysis of the experimental data has clearly shown the presence of at least two time-lags on the curve of permeate pressure increase during the “time-lag” experiment. The presence of at least two time-lags is obviously observed by the analysis curves derived from the experimental data when the time-lag value is plotted with the development of time. In detail, a certain number of experimental points were used to plot a tangential line by using the “least squares method”. In the present case, 37 points were taken since this was the minimum number of points suitable for the analysis of the water permeation curve through phenyl-100, while the same number of points was used for other polymers: PIM-1, methyl-100, *t*-butyl-100 and cyclohexyl-100. The data set of 37 points was moved along the water permeation curve (y_1 -axis), and the corresponding values of the tangential line intersection with time (y_2 -axis) were plotted along with the time-lag development with the time of the experiment (x-axis). As can be seen from Figure 12, the experimental curves for PIM-1 and phenyl-100 in the range of 1–3 time lags have a slight difference in shape. However, the curves of the time-lag development have a significant difference. The red dotted line in Figure 12 corresponding to PIM-1 shows a proper time-lag curve, which reaches its maximum value of 9.5 s at 4.4 time-lags (42.2 s after experiment started). On the other hand, the curve for phenyl-100 exhibits the presence of at least two time-lags which occur at ca. two time-lags (89.6 s of experiment) and at 7.16 time-lags (320 s of experiment), where the curve reaches its maximum of 44.8 s. Remarkably, the analysis was carried out according to the maximum time-lag values observed from which diffusion and the corresponding solubility coefficients are derived. These diffusion and solubility coefficients can be considered as “effective” coefficients, indicating the behavior of the polymer during the water vapor permeation and thus the collection of the water vapor in the permeate side of the facility. Further analysis of obtained results should be carried out according to, e.g., Jansen et al. [73].

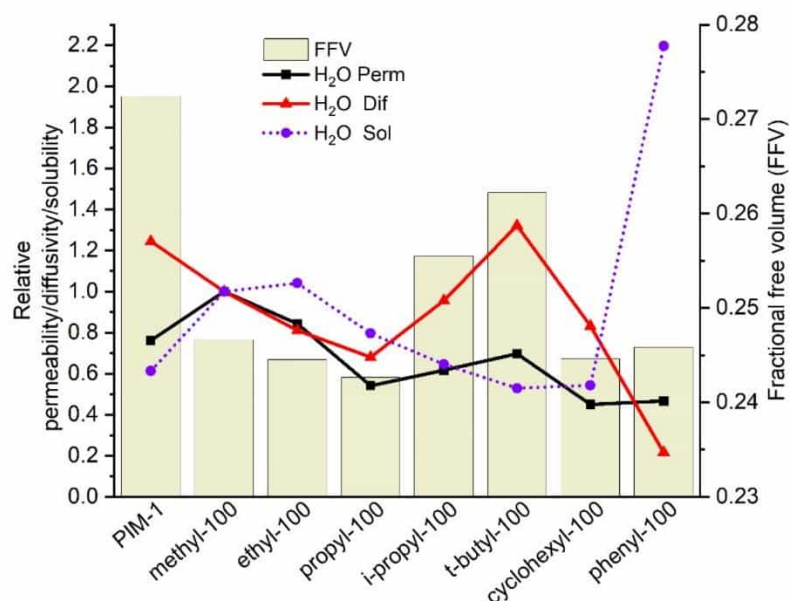


Figure 11. H₂O relative permeability relative diffusivity, relative solubility and FFV of homopolymers. (Relative permeability or diffusivity or solubility: homopolymer water permeability or diffusivity or solubility are normalized to methyl-100 water permeability or diffusivity or solubility.)

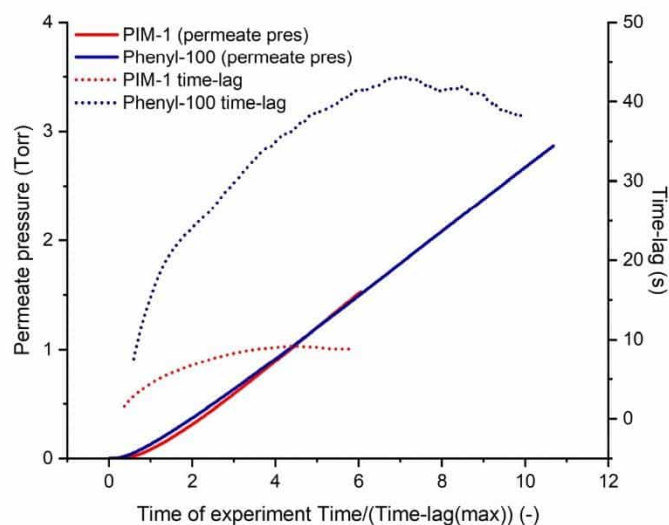


Figure 12. Time-lag curve analysis of PIM-1 and phenyl-100.

As mentioned before, the increase of the permeate pressure curves was analyzed for several polymers. Table 2 shows the comparison of the moments when the time-lag values of polymers reach their maximum. It can be seen from the table data that the maximum time-lag of the polymers was reached at 4.5 ± 0.4 time-lags after the experiment started. However, phenyl-100 is an exceptional case in which the maximum time-lag is reached at 7.16. A possible explanation for this might be the presence of at least two diffusion coefficients for water vapor in phenyl-100 attributed to the formation of water molecule clusters in free volume elements of this polymer. These findings raise intriguing questions regarding the difference between phenyl-100 and the other homopolymers such as methyl-100 or cyclohexyl-100, which lead to this discrepancy. Similar to findings in a previous study [73,74] referring to the diffusion of alcohol vapors through Teflon[®] AF and Hyflon[®] AD, the presence of several diffusion coefficients can be explained by the water molecules clustering in the free volume of hydrophobic polymers. Moreover, if the phenyl substitution leads to a specific interaction between the functional groups of the polymer located on the “surface” of the free volume elements, it could explain the confounding information stored in the “time-lag” curve. In relation to that, prior studies have noted the importance of the interaction of water with aromatic rings [75–77]. Levitt and Perutz claimed that aromatic groups might act as hydrogen bond acceptors due to their electrostatic interaction arising from carbon and hydrogen atoms of aromatic rings [75]. Moreover, Vojislavljevic et al. [76] emphasized the position of the water molecule accommodated near an aromatic ring, highlighting the OH- π electron interactions between water and aromatic rings. Answers to these questions should be examined by investigation of phenyl-100 in the presence of water vapor by solid-state NMR or other spectroscopic methods able to reveal either change in water self-diffusion or shift in peaks characteristic for the bonds able to interact with water. It is also suggested to develop a detailed analysis tool of the time-lag data similar to the one reported by Friess et al. [74]. Further investigation of water vapor transport in synthesized polymers or their analogs is also interesting since phenyl-50 copolymer does not show any evidence of multiple diffusion coefficients, the solubility coefficient of water is in the usual range as in, e.g., PIM-1.

The water vapor permeability trend for copolymers is consistent with the trend of water solubility. Figure 13 depicts that the shift in water permeability follows nearly the same pattern with solubility, except for *i*-propyl-50. It can be seen that methyl-50 has higher water vapor permeability than PIM-1, similar to the case of methyl-100. The aforementioned effect of affinity toward water might be the reason for this behavior. Since imide with

methyl side group is assumed to be the most polar among all substituents, the observation of the highest water vapor permeability and solubility fits the assumption.

Table 2. Comparison of the moments where the time-lags of polymers reach their maximum values.

| Polymer | Time [Time-Lags] |
|---------------------|------------------|
| PIM-1 | 4.44 |
| Methyl-100 | 4.49 |
| <i>t</i> -Butyl-100 | 4.90 |
| Cyclohexyl-100 | 4.17 |
| Phenyl-100 | 7.16 |
| Phenyl-50 | 3.80 |

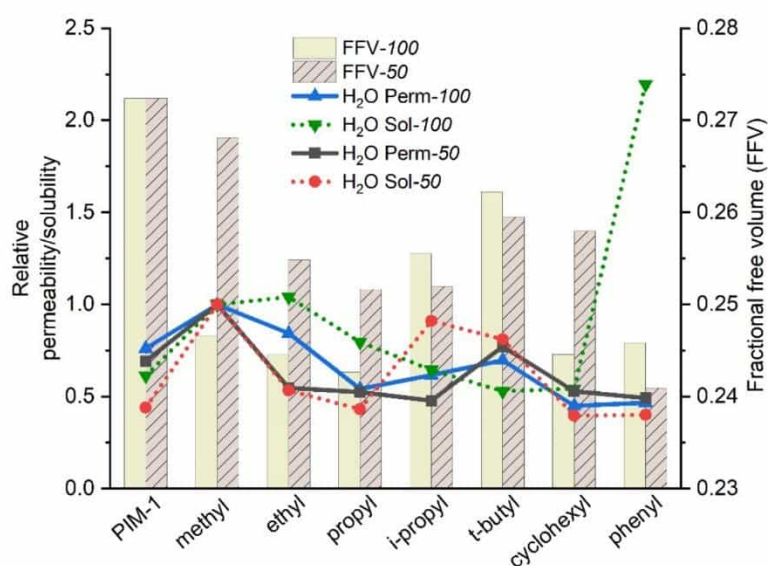


Figure 13. H₂O relative permeability and relative solubility and FFV of copolymer and homopolymers. (Relative permeability/ solubility: polymer water permeability or solubility are normalized to methyl- water permeability or solubility.)

Surprisingly, the water solubility peak seen in phenyl-100 does not demonstrate a similar leap in phenyl-50. Random distribution of monomer units could be responsible for such a discrepancy, as was discussed before. Taking into consideration that such random chain packing exists, the spirobisindane monomer unit, which is more hydrophobic, might hinder or stultify the effect of the phenyl side group on water interaction. Whether the increment of water vapor permeability is attributed to FFV or substituents affinity to water vapor remains a matter of question. Furthermore, the FFV of the copolymer is mostly higher than those of the homopolymer, as expected. This is attributed to the contorted structure resulting from the spirobisindane unit of PIM-1, which causes enhancement on interconnected voids. However, the FFV of *i*-propyl-50 and *t*-butyl-50 are slightly higher than those of related homopolymers. Such behavior might occur due to the high impact of bulky side groups. Overall, it is important to point out the fact that a random distribution of copolymer units plays a prominent role in the arrangement of FFV and also polymer-molecule affinity.

Gas transport properties of methyl-100 after thermal treatment (methyl-100-TT) were tested by a time-lag measurement (Table S5). The results revealed a significant permeability and diffusivity drop of all single gases and water vapor. These results are likely due to the physical aging of the polymer films because of their exposure to high temperature.

Nevertheless, it would be misleading to compare the permeability and diffusion coefficients of polymer films before and after thermal treatment, since they were not exposed to the same conditions. Taking this fact into account, one interesting finding can still be sorted out of these results—the water vapor solubility of methyl-100-TT increased more than two folds compared to methyl-100. This observation may support the hypothesis that was mentioned before regarding the aromatic ring-water molecule affinity. After thermal treatment, the polymer structure was rearranged, and the roof-shaped maleimide moiety was removed by the formation of the third aromatic ring in the backbone. It can be therefore assumed that water solubility escalated due to the increase of aromatic groups. However, since the vapor diffusion coefficient decreased, possibly due to the collapse of FFV arising from physical aging, water vapor permeability does not show an increase, as does the solubility. To develop a full picture of the gas transport properties of thermally treated polymer films, additional studies are needed.

4. Conclusions

The aim of the present research was to examine the effect of different alkyl chains on gas and water vapor transport. Anthracene maleimide-based comonomers with different alkyl side chains were successfully synthesized by the Diels-Alder reaction. ^1H -NMR and TG-FTIR characterizations of comonomers were properly established. TG-FTIR results of methyl, ethyl and *t*-butyl comonomers revealed that the decomposition temperature of the maleimide unit occurs prior to that of the anthracene unit. Consequently, the outcome provided the further possibility to employ the retro-Diels Alder rearrangement of homopolymers. New comonomers were further used for homopolymerization with TFTPn and then used for copolymerization in the combination of TFTPn and TTSBI monomer units. All polymers were characterized via ^1H -NMR, GPC and TG-FTIR. ^1H -NMR spectra of copolymers confirmed the 1:1 molar ratio of the comonomer TTSBI. TG-FTIR analysis of methyl-100 revealed that the retro-Diels Alder reaction of the maleimide group occurs earlier than the decomposition of the homopolymer backbone. Based on this finding, post-thermal treatment of methyl-100 and gas transport measurements were tested to set an example of structure rearrangement by retro-Diels Alder reaction.

Gas and water vapor transport properties of all newly synthesized polymers were established by the time-lag method. Methyl-50 and *t*-butyl-50 exhibit higher CO_2 and CH_4 permeability than PIM-1. The distinguished effect of linear alkyl and bulky side chains on the fractional free volume was discussed, and it was shown that bulky side groups lead to a better permeability of these gases. The influence of the anthracene maleimide unit with different side groups revealed that the affinity of the side group strongly affects water vapor transport. Methyl-100 and ethyl-100 show higher water vapor permeability and solubility than PIM-1 and other homopolymers. However, phenyl-100 showed a jump in water vapor solubility with a low diffusion coefficient, which is attributed to the formation of the water molecule clusters located in the free volume elements of the polymer. This research provides a framework for the exploration of employment of the new polymer series with anthracene maleimide for water vapor transport studies in a broader concept of water treatment applications. Nevertheless, it is recommended that further research be undertaken in order to validate the water vapor transport parameters of these glassy polymers.

Supplementary Materials: The following are available online at <https://www.mdpi.com/article/10.3390/polym14010119/s1>, Figure S1: ^1H NMR spectra of all comonomers; Figure S2: TGA curves of comonomers; Figure S3: TGA curves of homopolymers; Figure S4: Optical images of methyl-100 before and after thermal treatments; Figure S5: N_2 , O_2 , H_2 transport properties of homopolymers; Figure S6: N_2 , O_2 , H_2 transport properties of copolymers; Table S1: Molecular weight data of polymers by GPC and polymer compositions calculated by ^1H NMR; Table S2: Permeability coefficients of PIM-1, homo- and copolymers determined at 30 °C; Table S3: Diffusion coefficients of PIM-1, homo- and copolymers determined at 30 °C; Table S4: Solubility coefficient of PIM-1, homo- and copolymers determined at 30 °C; Table S5: Gas transport properties of methyl-100-TT* determined at 30 °C.

Author Contributions: Conceptualization, E.C. and S.S.; methodology, E.C., S.S. and S.N.; investigation, E.C.; writing-original draft preparation, E.C.; writing-review and editing, E.C., S.S., S.N., V.F. and V.A.; supervision, V.A.; project administration, V.F. All authors have read and agreed to the published version of the manuscript.

Funding: We gratefully acknowledge financial support from the Federal Ministry of Education and Research of Germany (BMBF) via the project NAMED (FKZ: 03XP0151A).

Institutional Review Board Statement: Not applicable.

Informed Consent Statement: Not applicable.

Data Availability Statement: The data presented in this study are available on request from the corresponding author.

Acknowledgments: The authors would like to thank Silke Dargel, Maren Brinkmann and Carsten Scholles for their help with polymerization, SEC and time-lag measurements, respectively.

Conflicts of Interest: The authors declare no conflict of interest.

References

- Budd, P.M.; McKeown, N.B. Highly permeable polymers for gas separation membranes. *Polym. Chem.* **2010**, *1*, 63–68. [\[CrossRef\]](#)
- Wijmans, J.G.; Baker, R.W. The solution-diffusion model: A review. *J. Membr. Sci.* **1995**, *107*, 1–21. [\[CrossRef\]](#)
- Xiao, Y.; Zhang, L.; Xu, L.; Chung, T.-S. Molecular design of Tröger's base-based polymers with intrinsic microporosity for gas separation. *J. Membr. Sci.* **2017**, *521*, 65–72. [\[CrossRef\]](#)
- Park, H.B.; Kamcev, J.; Robeson, L.M.; Elimelech, M.; Freeman, B.D. Maximizing the right stuff: The trade-off between membrane permeability and selectivity. *Science* **2017**, *356*, eaab0530. [\[CrossRef\]](#)
- Corrado, T.; Guo, R. Macromolecular design strategies toward tailoring free volume in glassy polymers for high performance gas separation membranes. *Mol. Syst. Des. Eng.* **2020**, *5*, 22–48. [\[CrossRef\]](#)
- Budd, P.M.; Elabas, E.S.; Ghanem, B.S.; Makhseed, S.; McKeown, N.B.; Msayib, K.J.; Tattershall, C.E.; Wang, D. Solution-Processed, Organophilic Membrane Derived from a Polymer of Intrinsic Microporosity. *Adv. Mater.* **2004**, *16*, 456–459. [\[CrossRef\]](#)
- Rose, I.; Bezzu, C.G.; Carta, M.; Comesana-Gandara, B.; Lasseguette, E.; Ferrari, M.C.; Bernardo, P.; Clarizia, G.; Fuoco, A.; Jansen, J.C.; et al. Polymer ultrapermeability from the inefficient packing of 2D chains. *Nat. Mater.* **2017**, *16*, 932–937. [\[CrossRef\]](#) [\[PubMed\]](#)
- Guiver, M.D.; Lee, Y.M. Polymer Rigidity Improves Microporous Membranes. *Science* **2013**, *339*, 284–285. [\[CrossRef\]](#)
- McKeown, N.B.; Budd, P.M. Exploitation of Intrinsic Microporosity in Polymer-Based Materials. *Macromolecules* **2010**, *43*, 5163–5176. [\[CrossRef\]](#)
- Budd, P.M.; McKeown, N.B.; Fritsch, D. Free volume and intrinsic microporosity in polymers. *J. Mater. Chem.* **2005**, *15*, 1977–1986. [\[CrossRef\]](#)
- Budd, P.M.; Ghanem, B.S.; Makhseed, S.; McKeown, N.B.; Msayib, K.J.; Tattershall, C.E. Polymers of intrinsic microporosity (PIMs): Robust, solution-processable, organic nanoporous materials. *Chem. Commun.* **2004**, 230–231. [\[CrossRef\]](#)
- Budd, P.M.; McKeown, N.B.; Ghanem, B.S.; Msayib, K.J.; Fritsch, D.; Starannikova, L.; Belov, N.; Sanfirova, O.; Yampolskii, Y.; Shantarovich, V. Gas permeation parameters and other physicochemical properties of a polymer of intrinsic microporosity: Polybenzodioxane PIM-1. *J. Membr. Sci.* **2008**, *325*, 851–860. [\[CrossRef\]](#)
- Alberto, M.; Bhavsar, R.; Luque-Alled, J.M.; Vijayaraghavan, A.; Budd, P.M.; Gorgojo, P. Impeded physical aging in PIM-1 membranes containing graphene-like fillers. *J. Membr. Sci.* **2018**, *563*, 513–520. [\[CrossRef\]](#)
- Bengtson, G.; Neumann, S.; Filiz, V. Membranes of Polymers of Intrinsic Microporosity (PIM-1) Modified by Poly(ethylene glycol). *Membranes* **2017**, *7*, 28. [\[CrossRef\]](#)
- Bezzu, C.G.; Carta, M.; Tonkins, A.; Jansen, J.C.; Bernardo, P.; Bazzarelli, F.; McKeown, N.B. A Spirobifluorene-Based Polymer of Intrinsic Microporosity with Improved Performance for Gas Separation. *Adv. Mater.* **2012**, *24*, 5930–5933. [\[CrossRef\]](#)
- Tian, M.; Rochatz, S.; Fawcett, H.; Burrows, A.D.; Bowen, C.R.; Mays, T.J. Chemical modification of the polymer of intrinsic microporosity PIM-1 for enhanced hydrogen storage, (in English). *Adsorpt.-J. Int. Adsorpt. Soc.* **2020**, *26*, 1083–1091. [\[CrossRef\]](#)
- Kim, H.J.; Kim, D.G.; Lee, K.; Baek, Y.; Yoo, Y.; Kim, Y.S.; Kim, B.G.; Lee, J.C. A Carbonaceous Membrane based on a Polymer of Intrinsic Microporosity (PIM-1) for Water Treatment. *Sci. Rep.* **2016**, *6*, 36078. [\[CrossRef\]](#) [\[PubMed\]](#)
- Madrid, E.; Cottis, P.; Rong, Y.; Rogers, A.T.; Stone, J.M.; Malpass-Evans, R.; Carta, M.; McKeown, N.B.; Marken, F. Water desalination concept using an ionic rectifier based on a polymer of intrinsic microporosity (PIM). *J. Mater. Chem. A* **2015**, *3*, 15849–15853. [\[CrossRef\]](#)
- Du, N.; Cin, M.M.; Pinna, I.; Nicalek, A.; Robertson, G.P.; Guiver, M.D. Azide-based cross-linking of polymers of intrinsic microporosity (PIMs) for condensable gas separation. *Macromol. Rapid Commun.* **2011**, *32*, 631–636. [\[CrossRef\]](#)
- Mason, C.R.; Maynard-Atem, L.; Heard, K.W.J.; Satilmis, B.; Budd, P.M.; Friess, K.; Lanč, M.; Bernardo, P.; Clarizia, G.; Jansen, J.C. Enhancement of CO₂ Affinity in a Polymer of Intrinsic Microporosity by Amine Modification. *Macromolecules* **2014**, *47*, 1021–1029. [\[CrossRef\]](#) [\[PubMed\]](#)

21. Du, N.; Robertson, G.P.; Song, J.; Pinnau, I.; Guiver, M.D. High-Performance Carboxylated Polymers of Intrinsic Microporosity (PIMs) with Tunable Gas Transport Properties†. *Macromolecules* **2009**, *42*, 6038–6043. [\[CrossRef\]](#)
22. Ma, X.; Swaidan, R.; Belmabkhout, Y.; Zhu, Y.; Litwiller, E.; Jouiad, M.; Pinnau, I.; Han, Y. Synthesis and Gas Transport Properties of Hydroxyl-Functionalized Polyimides with Intrinsic Microporosity. *Macromolecules* **2012**, *45*, 3841–3849. [\[CrossRef\]](#)
23. Du, N.; Park, H.B.; Robertson, G.P.; Dal-Cin, M.M.; Visser, T.; Scoles, L.; Guiver, M.D. Polymer nanosieve membranes for CO₂-capture applications. *Nat. Mater.* **2011**, *10*, 372–375. [\[CrossRef\]](#)
24. Mason, C.R.; Maynard-Atem, L.; Al-Harbi, N.M.; Budd, P.M.; Bernardo, P.; Bazzarelli, F.; Clarizia, G.; Jansen, J.C. Polymer of Intrinsic Microporosity Incorporating Thioamide Functionality: Preparation and Gas Transport Properties. *Macromolecules* **2011**, *44*, 6471–6479. [\[CrossRef\]](#)
25. Halder, K.; Neumann, S.; Bengtson, G.; Khan, M.M.; Filiz, V.; Abetz, V. Polymers of Intrinsic Microporosity Postmodified by Vinyl Groups for Membrane Applications. *Macromolecules* **2018**, *51*, 7309–7319. [\[CrossRef\]](#)
26. Khan, M.M.; Filiz, V.; Bengtson, G.; Shishatskiy, S.; Rahman, M.; Abetz, V. Functionalized carbon nanotubes mixed matrix membranes of polymers of intrinsic microporosity for gas separation. *Nanoscale Res. Lett.* **2012**, *7*, 504. [\[CrossRef\]](#)
27. Aliyev, E.M.; Khan, M.M.; Nabyev, A.M.; Alosmanov, R.M.; Bunyad-zadeh, I.A.; Shishatskiy, S.; Filiz, V. Covalently Modified Graphene Oxide and Polymer of Intrinsic Microporosity (PIM-1) in Mixed Matrix Thin-Film Composite Membranes. *Nanoscale Res. Lett.* **2018**, *13*, 359. [\[CrossRef\]](#) [\[PubMed\]](#)
28. Aliyev, E.; Warfsmann, J.; Tokay, B.; Shishatskiy, S.; Lee, Y.J.; Lillepaerg, J.; Champness, N.R.; Filiz, V. Gas Transport Properties of the Metal–Organic Framework (MOF)-Assisted Polymer of Intrinsic Microporosity (PIM-1) Thin-Film Composite Membranes. *ACS Sustain. Chem. Eng.* **2020**, *9*, 684–694. [\[CrossRef\]](#)
29. Kinoshita, Y.; Wakimoto, K.; Gibbons, A.H.; Isfahani, A.P.; Kusuda, H.; Sivaniah, E.; Ghalei, B. Enhanced PIM-1 membrane gas separation selectivity through efficient dispersion of functionalized POSS fillers. *J. Membr. Sci.* **2017**, *539*, 178–186. [\[CrossRef\]](#)
30. Lee, W.H.; Seong, J.G.; Hu, X.; Lee, Y.M. Recent progress in microporous polymers from thermally rearranged polymers and polymers of intrinsic microporosity for membrane gas separation: Pushing performance limits and revisiting trade-off lines. *J. Polym. Sci.* **2020**, *58*, 2450–2466. [\[CrossRef\]](#)
31. Low, Z.-X.; Budd, P.M.; McKeown, N.B.; Patterson, D.A. Gas Permeation Properties, Physical Aging, and Its Mitigation in High Free Volume Glassy Polymers. *Chem. Rev.* **2018**, *118*, 5871–5911. [\[CrossRef\]](#)
32. Hart, K.E.; Colina, C.M. Estimating gas permeability and permselectivity of microporous polymers. *J. Membr. Sci.* **2014**, *468*, 259–268. [\[CrossRef\]](#)
33. Carta, M.; Malpass-Evans, R.; Croad, M.; Rogan, Y.; Jansen, J.C.; Bernardo, P.; Bazzarelli, F.; McKeown, N.B. An Efficient Polymer Molecular Sieve for Membrane Gas Separations. *Science* **2013**, *339*, 303–307. [\[CrossRef\]](#) [\[PubMed\]](#)
34. Rose, I.; Carta, M.; Malpass-Evans, R.; Ferrari, M.C.; Bernardo, P.; Clarizia, G.; Jansen, J.C.; McKeown, N.B. Highly Permeable Benzotriptycene-Based Polymer of Intrinsic Microporosity. *ACS Macro Lett.* **2015**, *4*, 912–915. [\[CrossRef\]](#)
35. Carta, M.; Croad, M.; Malpass-Evans, R.; Jansen, J.C.; Bernardo, P.; Clarizia, G.; Friess, K.; Lanc, M.; McKeown, N.B. Triptycene induced enhancement of membrane gas selectivity for microporous Troger’s base polymers. *Adv. Mater.* **2014**, *26*, 3526–3531. [\[CrossRef\]](#) [\[PubMed\]](#)
36. Calle, M.; Lozano, A.E.; de Abajo, J.; de la Campa, J.G.; Álvarez, C. Design of gas separation membranes derived of rigid aromatic polyimides. 1. Polymers from diamines containing di-tert-butyl side groups. *J. Membr. Sci.* **2010**, *365*, 145–153. [\[CrossRef\]](#)
37. Rodriguez-Gonzalez, F.E.; Perez, G.; Niebla, V.; Jessop, I.; Martin-Trasanco, R.; Coll, D.; Ortiz, P.; Aguilar-Vega, M.; Tagle, L.H.; Terraza, C.A.; et al. New Poly(imide)s Bearing Alkyl Side-Chains: A Study on the Impact of Size and Shape of Lateral Groups on Thermal, Mechanical, and Gas Transport Properties. *Membranes* **2020**, *10*, 141. [\[CrossRef\]](#)
38. Bermeshev, M.V.; Syromolotov, A.V.; Starannikova, L.E.; Gringolts, M.L.; Lakhtin, V.G.; Yampolskii, Y.P.; Finkelshtein, E.S. Glassy Polynorbornenes with Si–O–Si Containing Side Groups. Novel Materials for Hydrocarbon Membrane Separation. *Macromolecules* **2013**, *46*, 8973–8979. [\[CrossRef\]](#)
39. Yampolskii, Y.P.; Banerjee, S. Effects of Bulky Substituents on Transport Properties of Membrane Gas Separation Materials. *Pet. Chem.* **2018**, *57*, 1195–1206. [\[CrossRef\]](#)
40. Masuda, T. Substituted polyacetylenes. *J. Polym. Sci. Part A Polym. Chem.* **2007**, *45*, 165–180. [\[CrossRef\]](#)
41. Pinnau, I.; He, Z.; Morisato, A. Synthesis and gas permeation properties of poly(dialkylacetylenes) containing isopropyl-terminated side-chains. *J. Membr. Sci.* **2014**, *241*, 363–369. [\[CrossRef\]](#)
42. Deshmukh, A.; Boo, C.; Karanikola, V.; Lin, S.; Straub, A.P.; Tong, T.; Warsinger, D.M.; Elimelech, M. Membrane distillation at the water-energy nexus: Limits, opportunities, and challenges. *Energy Environ. Sci.* **2018**, *11*, 1177–1196. [\[CrossRef\]](#)
43. Drioli, E.; Ali, A.; Macedonio, F. Membrane distillation: Recent developments and perspectives. *Desalination* **2015**, *356*, 56–84. [\[CrossRef\]](#)
44. MKhan, M.; Bengtson, G.; Neumann, S.; Rahman, M.M.; Abetz, V.; Filiz, V. Synthesis, characterization and gas permeation properties of anthracene maleimide-based polymers of intrinsic microporosity. *RSC Adv.* **2014**, *4*, 32148–32160. [\[CrossRef\]](#)
45. Halder, K.; Khan, M.M.; Grünauer, J.; Shishatskiy, S.; Abetz, C.; Filiz, V.; Abetz, V. Blend membranes of ionic liquid and polymers of intrinsic microporosity with improved gas separation characteristics. *J. Membr. Sci.* **2017**, *539*, 368–382. [\[CrossRef\]](#)
46. Halder, K.; Georgopoulos, P.; Shishatskiy, S.; Filiz, V.; Abetz, V. Investigation of gas transport and other physical properties in relation to the bromination degree of polymers of intrinsic microporosity. *J. Polym. Sci. Part A Polym. Chem.* **2018**, *56*, 2752–2761. [\[CrossRef\]](#)

47. Du, N.; Song, J.; Robertson, G.P.; Pinnau, I.; Guiver, M.D. Linear High Molecular Weight Ladder Polymer via Fast Polycondensation of 5,5',6,6'-Tetrahydroxy-3,3',3'-tetramethylspirobisindane with 1,4-Dicyanotetrafluorobenzene. *Macromol. Rapid Commun.* **2008**, *29*, 783–788. [\[CrossRef\]](#)
48. Nagai, K.; Freeman, B.D.; Hill, A.J. Effect of physical aging of poly(1-trimethylsilyl-1-propyne) films synthesized with TaCl₅ and NbCl₅ on gas permeability, fractional free volume, and positron annihilation lifetime spectroscopy parameters. *J. Polym. Sci. Part B Polym. Phys.* **2000**, *38*, 1222–1239. [\[CrossRef\]](#)
49. Bondi, A. Van der Waals Volumes and Radii. *J. Phys. Chem.* **1964**, *68*, 441–451. [\[CrossRef\]](#)
50. Krevelen, D.W.V.; Nijenhuis, K.T. *Properties of Polymers: Their Correlation with Chemical Structure; Their Numerical Estimation and Prediction from Additive Group Contributions*, 4th ed.; Elsevier: Amsterdam, The Netherlands, 2009; p. 1032.
51. Liljeberg, J.; Georgopoulos, P.; Emmeler, T.; Shishatskiy, S. Effect of the reactive amino and glycidyl ether terminated polyethylene oxide additives on the gas transport properties of Pebax[®] bulk and thin film composite membranes. *RSC Adv.* **2016**, *6*, 11763–11772. [\[CrossRef\]](#)
52. Fritsch, D.; Bengtson, G.; Carta, M.; McKeown, N.B. Synthesis and Gas Permeation Properties of Spirobischromane-Based Polymers of Intrinsic Microporosity. *Macromol. Chem. Phys.* **2011**, *212*, 1137–1146. [\[CrossRef\]](#)
53. Yin, H.; Yang, B.; Chua, Y.Z.; Szymoniak, P.; Carta, M.; Malpass-Evans, R.; McKeown, N.B.; Harrison, W.J.; Budd, P.M.; Schick, C.; et al. Effect of Backbone Rigidity on the Glass Transition of Polymers of Intrinsic Microporosity Probed by Fast Scanning Calorimetry. *ACS Macro Lett.* **2019**, *8*, 1022–1028. [\[CrossRef\]](#)
54. Harms, S.; Rätzke, K.; Faupel, F.; Chaukura, N.; Budd, P.M.; Egger, W.; Ravelli, L. Aging and Free Volume in a Polymer of Intrinsic Microporosity (PIM-1). *J. Adhes.* **2017**, *88*, 608–619. [\[CrossRef\]](#)
55. Guiver, M.D.; Yahia, M.; Dal-Cin, M.M.; Robertson, G.P.; Saeedi Garakani, S.; Du, N.; Tavajohi, N. Gas Transport in a Polymer of Intrinsic Microporosity (PIM-1) Substituted with Pseudo-Ionic Liquid Tetrazole-Type Structures. *Macromolecules* **2020**, *53*, 8951–8959. [\[CrossRef\]](#)
56. Song, J.; Du, N.; Dai, Y.; Robertson, G.P.; Guiver, M.D.; Thomas, S.; Pinnau, I. Linear High Molecular Weight Ladder Polymers by Optimized Polycondensation of Tetrahydroxytetramethylspirobisindane and 1,4-Dicyanotetrafluorobenzene. *Macromolecules* **2008**, *41*, 7411–7417. [\[CrossRef\]](#)
57. Xu, Y.; Chen, C.; Zhang, P.; Sun, B.; Li, J. Pervaporation Properties of Polyimide Membranes for Separation of Ethanol + Water Mixtures. *J. Chem. Eng. Data* **2006**, *51*, 1841–1845. [\[CrossRef\]](#)
58. Huang, J.; Cranford, R.J.; Matsuura, T.; Roy, C. Water vapor permeation properties of aromatic polyimides. *J. Membr. Sci.* **2003**, *215*, 129–140. [\[CrossRef\]](#)
59. Jiang, L.Y.; Wang, Y.; Chung, T.-S.; Qiao, X.Y.; Lai, J.-Y. Polyimides membranes for pervaporation and biofuels separation. *Prog. Polym. Sci.* **2009**, *34*, 1135–1160. [\[CrossRef\]](#)
60. Petrov, A.V.; Smirnov, M.A.; Sokolova, M.P.; Toikka, A.M. Influence of Water Concentration on Its Mobility in Matrimid[®]. *Coatings* **2019**, *9*, 466. [\[CrossRef\]](#)
61. Maya, E.M.; Benavente, J.; de Abajo, J. Effect of the carboxylic acid groups on water sorption, thermal stability and dielectric properties of polyimide films. *Mater. Chem. Phys.* **2012**, *131*, 581–588. [\[CrossRef\]](#)
62. Kim, J.W.; Chang, J.-H. Syntheses of Colorless and Transparent Polyimide Membranes for Microfiltration. *Polymers* **2020**, *12*, 1610. [\[CrossRef\]](#)
63. Stern, S.A.; Shah, V.M.; Hardy, B.J. Structure-permeability relationships in silicone polymers. *J. Polym. Sci. Part B Polym. Phys.* **1987**, *25*, 1263–1298. [\[CrossRef\]](#)
64. Borisov, I.L.; Ushakov, N.V.; Volkov, V.V.; Finkel'shtein, E.S. Polydimethylsilalkylene-dimethylsiloxanes as advanced membrane materials for thermopervaporative recovery of oxygenates from aqueous reaction media. *Pet. Chem.* **2016**, *56*, 798–804. [\[CrossRef\]](#)
65. Chen, G.Q.; Scholes, C.A.; Qiao, G.G.; Kentish, S.E. Water vapor permeation in polyimide membranes. *J. Membr. Sci.* **2011**, *379*, 479–487. [\[CrossRef\]](#)
66. Barrie, J.A.; Platt, B. The diffusion and clustering of water vapour in polymers. *Polymer* **1963**, *4*, 303–313. [\[CrossRef\]](#)
67. Modesti, M.; Dall'Acqua, C.; Lorenzetti, A.; Florian, E. Mathematical model and experimental validation of water cluster influence upon vapour permeation through hydrophilic dense membrane. *J. Membr. Sci.* **2004**, *229*, 211–223. [\[CrossRef\]](#)
68. Kelkar, A.J.; Paul, D.R. Water vapor transport in a series of polyarylates. *J. Membr. Sci.* **2001**, *181*, 199–212. [\[CrossRef\]](#)
69. Arce, A.; Fornasiero, F.; Rodríguez, O.; Radke, C.J.; Prausnitz, J.M. Sorption and transport of water vapor in thin polymer films at 35 °C. *Phys. Chem. Chem. Phys.* **2004**, *6*, 103–108. [\[CrossRef\]](#)
70. Kanehashi, S.; Tomita, Y.; Obokata, H.; Kidesaki, T.; Sato, S.; Miyakoshi, T.; Nagai, K. Effect of substituted groups on characterization and water vapor sorption property of polyhedral oligomeric silsesquioxane (POSS)-containing methacryl polymer membranes. *Polymer* **2013**, *54*, 2315–2323. [\[CrossRef\]](#)
71. Du, A.; Koo, D.; Theryo, G.; Hillmyer, M.A.; Cairncross, R.A. Water transport and clustering behavior in homopolymer and graft copolymer polylactide. *J. Membr. Sci.* **2012**, *396*, 50–56. [\[CrossRef\]](#)
72. Davis, E.M.; Minelli, M.; Baschetti, M.G.; Sarti, G.C.; Elabd, Y.A. Nonequilibrium Sorption of Water in Polylactide. *Macromolecules* **2012**, *45*, 7486–7494. [\[CrossRef\]](#)
73. Jansen, J.C.; Friess, K.; Drioli, E. Organic vapour transport in glassy perfluoropolymer membranes: A simple semi-quantitative approach to analyze clustering phenomena by time lag measurements. *J. Membr. Sci.* **2011**, *367*, 141–151. [\[CrossRef\]](#)

-
74. Friess, K.; Jansen, J.C.; Poživil, J.; Hanta, V.; Hynek, V.; Vopička, O.; Zgažar, M.; Bernardo, P.; Izák, P.; Drioli, E. Anomalous Phenomena Occurring during Permeation and Sorption of C₁–C₆ Alcohol Vapors in Teflon AF 2400. *Ind. Eng. Chem. Res.* **2013**, *52*, 10406–10417. [[CrossRef](#)]
 75. Levitt, M.; Perutz, M.F. Aromatic rings act as hydrogen bond acceptors. *J. Mol. Biol.* **1988**, *201*, 751–754. [[CrossRef](#)]
 76. Vojislavljević, D.Z.; Janjić, G.V.; Ninković, D.B.; Kapor, A.; Zarić, S.D. The influence of water molecule coordination onto the water–aromatic interaction. Strong interactions of water coordinating to a metal ion. *CrystEngComm* **2013**, *15*, 2099–2105. [[CrossRef](#)]
 77. Jain, A.; Ramanathan, V.; Sankararamkrishnan, R. Lone pair . . . pi interactions between water oxygens and aromatic residues: Quantum chemical studies based on high-resolution protein structures and model compounds. *Protein Sci.* **2009**, *18*, 595–605.

5.2. Article 2: Pioneering the preparation of porous PIM-1 membranes for enhanced water vapor flow

Authors: Esra Caliskan, Sergey Shishatskiy, Volker Abetz, Volkan Filiz

In the second part, PIM-1 membranes were prepared by nonsolvent induced phase separation (NIPS) method and investigated for water vapor transport for membrane distillation. By trying several solvent-nonsolvent combinations, it was determined that a mixture of tetrahydrofuran (THF) and N-methyl-2-pyrrolidone (NMP) was the most suitable solvent system for the formation of membranes with enhanced pores. Scanning electron microscopy (SEM) images showed that the membrane obtained from high molecular weight PIM-1 polymer exhibited a structure with large voids, while the other membranes presented more homogeneous porous structures. Contact angle measurements showed that all membranes were highly hydrophobic, while water flux measurements showed high results for PIM-1 with a large porous structure. In addition, water vapor transport tests confirmed that all membranes exhibited high permeability. Furthermore, a thin film composite (TFC) membrane was prepared and compared with porous membranes. The TFC membrane showed about four times lower vapor permeability. The results show that porous PIM-1 membranes can be a good candidate for membrane distillation due to their hydrophobic properties and nature that only allows vapor permeability.

5.2.1. Author contributions

Esra Caliskan (E.C.), Sergey Shishatskiy (S.S.), Volker Abetz (V.A.), Volkan Filiz (V.F.)

Table 12: List of contribution: Publication-2

| Contribution | Authors | | | |
|-----------------------------------|----------------|-------------|-------------|-------------|
| | E.C. | S.S. | V.A. | V.F. |
| First author | + | | | |
| Corresponding author | | | | + |
| Methodology and conceptualization | + | + | | |
| Experimental work | + | | | |
| Material characterization | + | | | |
| Investigation | + | | | |
| Writing original draft | + | | | |
| Writing-reviewing and editing | + | + | + | + |
| Scientific supervision | | + | + | |

5.2.2. Funding and acknowledgements


We gratefully grant the financial support from the Federal Ministry of Education and Research of Germany (BMBF) *via* the project NAMED (FKZ: 03XP0151A).

The authors would like to thank to Dr. Evgeni Sperling for his exceptional contribution of SEM visualization; Dr. Erik Schneider for invaluable support on membrane morphology analysis.

5.2.3. Publication


Cite this: *RSC Adv.*, 2024, 14, 9631

Pioneering the preparation of porous PIM-1 membranes for enhanced water vapor flow†

Esra Caliskan,^a Sergey Shishatskiy,^a Volker Abetz^{ab} and Volkan Filiz  ^{*a}

In this study, porous polymers of intrinsic microporosity (PIM-1) membranes were prepared by non-solvent induced phase inversion (NIPS) and investigated for water vapor transport in view of their application in membrane distillation (MD). Due to the lack of high boiling point solvents for PIM-1 that are also water miscible, the mixture of tetrahydrofuran (THF) and *N*-methyl-2-pyrrolidone (NMP) was found to be optimal for the formation of a membrane with a developed porous system both on the membrane surface and in the bulk. PIM-1 was synthesized by using low and high temperature methods to observe how molecular weight effects the membrane structure. Low molecular weight PIM-1 was produced at low temperatures, while high molecular weight PIM-1 was obtained at high temperatures. Several membranes were prepared, including PM-6, PM-9, and PM-11 from low molecular weight PIM-1, and PM-13 from high molecular weight PIM-1. Scanning electron microscopy (SEM) was used to image the surface and cross-section of different porous PIM-1 membranes. Among all the PIM-1 membranes (PM) obtained, PM-6, PM-9, PM-11 and PM-13 showed the most developed porous structure, while PM-13 showed large voids in the bulk of the membrane. Contact angle measurements showed that all PIM-1 porous membranes are highly hydrophobic. Liquid water flux measurements showed that PM-6, PM-9 and PM-11 showed minimal water fluxes due to small surface pore size, while PM-13 showed a high water flux due to a large surface pore size. Water vapor transport measurements showed high permeance values for all membranes, demonstrating the applicability of the developed membranes for MD. In addition, a thin film composite (TFC) membrane with PIM-1 selective layer was prepared and investigated for water vapor transport to compare with porous PIM-1 membranes. The TFC membrane showed an approximately 4-fold lower vapor permeance than porous membranes. Based on these results, we postulated that the use of porous PIM-1 membranes could be promising for MD due to their hydrophobic nature and the fact that the porous membranes allow vapor permeability through the membrane but not liquid water. The TFC membrane can be used in cases where the transfer of water-soluble contaminants must be absolutely avoided.

Received 8th December 2023

Accepted 13th March 2024

DOI: 10.1039/d3ra08398e

rsc.li/rsc-advances

1. Introduction

Water scarcity is one of the biggest hurdles that science is trying to overcome today. According to a report published by the United Nations in 2023, it is estimated that the global urban population suffering from water scarcity could reach 1.7 to 2.4 billion by 2050.¹ Global population growth, industrialization, wars and climate change are making access to water resources more difficult, while freshwater reserves and conventional energy sources are rapidly depleting.² In other words, due to the lack of cost-effective technologies to remove unwanted solutes such as ions, organics and particles, the vast majority of water

in natural sources is unsuitable for human consumption or many other industrial uses.³ As a result, the development of efficient and sustainable water treatment technologies is the focus of research by many groups around the world.⁴ Membrane processes are among the leading water treatment technologies due to their higher energy efficiency and smaller footprint compared to other available, mostly thermal options.^{5,6} Pressure-driven processes, such as reverse osmosis (RO) and nanofiltration (NF), are the conventional membrane technologies currently in use.⁷ However, the transport of water through the molecular-sized 'pores' of the membrane in both RO and NF technologies requires a significant amount of pressure, which results in high-energy penalties and consequently high operating costs. Despite being a less energy-intensive process than RO, NF has a lower rejection rate for sodium and chloride ions, which are the main dissolved substances in saline water.^{8,9} However, novel membrane technologies that use low-grade energy as the driving force for separation are being extensively

^aInstitute of Membrane Research, Helmholtz-Zentrum Hereon, Max-Planck-Str. 1, Geesthacht 21502, Germany. E-mail: volkan.filiz@hereon.de; Tel: +49-41-5287-2425

^bInstitute of Physical Chemistry, University of Hamburg, Martin-Luther-King-Platz 6, Hamburg 20146, Germany

† Electronic supplementary information (ESI) available. See DOI: <https://doi.org/10.1039/d3ra08398e>


studied and developed. One such technology is membrane distillation (MD), which has attracted considerable interest. Conventionally, MD is a thermal-membrane process driven by the vapor pressure difference between hot and cold sides of a hydrophobic porous or non-porous membrane. The vapor pressure difference between the feed and permeate sides of the membrane, and a chemical potential gradient too low for other components, results in only vapor molecules being able to pass across the membrane followed by condensation of the vapor molecules in the cold permeate side of the membrane module.^{10,11} The use of MD has several advantages, including lower operating temperatures compared to conventional processes, which means that the feed solution does not need to be heated to its boiling point. In addition, the feed hydrostatic pressure in MD is significantly lower than in pressure-driven membrane processes such as RO, making it a potentially cost-effective process with lower requirements for membrane mechanical properties.^{12,13} Moreover, the pore size of the membrane used in MD is relatively larger than those for other membrane separation applications which makes MD less affected by fouling.¹⁴

There are several types of MD configurations:^{15,16}

- Direct contact membrane distillation (DCMD) involves direct contact between the hot feed solution and the hot membrane surface. Water vapor passes through the membrane by the gradient of chemical potential between the feed and the permeate sides of the membrane.
- Air gap membrane distillation (AGMD) contains stagnant air gap present between permeate side of the membrane and the condensation surface meanwhile feed solution is in direct contact with the feed side of the membrane.
- Sweeping gas membrane distillation (SGMD) uses a gas stream to sweep the vapor on the permeate side and to drive it to a condenser.
- Vacuum membrane distillation (VMD) employs a pump to create the vacuum on the permeate side in order to enhance the mass transfer rate.

A variety of polymers are used in MD depending on the specific process conditions. Some examples of polymers commonly used for MD membranes include polytetrafluoroethylene (PTFE), poly(vinylidene fluoride) (PVDF) and polypropylene (PP) due to their low surface tension and high hydrophobicity.¹⁷ The membranes typically have a volume porosity in the range of 0.60–0.95, which is determined by the absence of the need to withstand an absolute pressure gradient across the membrane, while the surface pore size is in the range of 0.2–1.0 μm .¹⁵ Moreover, hydrophobized ceramic membranes and carbon nanotubes are being used in MD owing to their hydrophobicity and porosity.¹⁸

There are also several challenges that need to be addressed to make MD more practical and economically viable. Two key factors significantly affect the performance of MD. The first is 'membrane wetting', which occurs when water vapor condenses in the pores of the membrane.¹⁹ The accumulation of condensed water in the membrane pores causes a reduction in permeability, while at the same time changing the surface property of the membrane, making it less hydrophobic and

increasing its affinity for water molecules.²⁰ The other factor hindering MD performance is 'membrane fouling', which is caused by the accumulation of organic or inorganic substances, dissolved or colloidal in the feed water, on the membrane surface or in the pores of the membrane, resulting in a reduction in vapor flux and a breakthrough of the feed mixture to the permeate side.^{21,22} These two main factors limit the choice of a suitable polymer for MD. As mentioned above, the MD process requires hydrophobic and porous membranes in order to restrict all molecules except water from passing through the membrane while avoiding membrane wetting. In addition to conventional polymers such as PTFE, PVDF and PP, the availability of other effective polymers that meet these requirements for MD applications is being investigated.

In the last two decades, there has been considerable interest in polymers of intrinsic microporosity (PIMs), a new class of microporous polymers with many attractive properties such as excellent solubility in organic solvents and thus processability, high glass transition temperature, good thermal stability, and exceptional mechanical and film-forming properties.^{23–26} In addition to these features, PIM-1 acquires two key properties, which are 'hydrophobicity' and 'high free volume', which can be exploited in favor of MD applications. Although, there is a substantial amount of research on gas separation using PIM-1,^{27–29} there are not many studies specifically focusing on PIM-1 for water separation.

Previous studies on PIM-1 for water separation have been focused on various modifications of this polymer.^{30,31} Kim *et al.*³⁰ studied the carbonization of PIM-1 resulting in an increase of water flux in nanofiltration application. Furthermore, Jeon *et al.*³¹ reported on the study of carboxylate-functionalized PIM-1 developed for nanofiltration as well. In addition to these studies, there are some researches focused on the development of PIM-1 hollow fiber membranes, which may be related to the current study in terms of aiming to obtain similar morphological aspects of PIM-1. For example, Jue *et al.*³² developed PIM-1 hollow fiber membrane used for gas separation where they attempted to obtain integrally asymmetric membrane by phase inversion. In another study, Hao *et al.*³³ described the study of ultem/PIM-1 hollow fiber membrane obtained by electrospinning. However, none of these studies were focused on the water separation application of PIM-1 with membranes obtained by NIPS.

Despite the versatile properties of PIM-1, there is still a lack of studies on porous PIM-1 membranes for water separation applications. Considering this knowledge deficit in the literature, the aim of this paper is to describe asymmetric porous PIM-1 membrane supported by a nonwoven for prospective use in membrane distillation. For this purpose, the phase inversion method, which is the most common method of porous membrane formation, was implemented. The choice of solvent and non-solvent is critical for the preparation of porous PIM-1 membranes by NIPS as it can affect the morphology, pore size, and overall performance of the resulting PIM-1 membranes.^{34,35} In general, the solvent should dissolve the polymer and acquire a high boiling point in order not to evaporate during the membrane formation process, while the non-solvent should not



dissolve the polymer and induce phase separation. There is an exiguity of solvents for PIM-1 that acquire a high boiling point. For this reason, an attempt was made to use a mixture of tetrahydrofuran (THF) and *N*-methyl-2-pyrrolidone (NMP), although NMP is a weak solvent for PIM-1. Water was preferred as the coagulation bath as it is the most environmentally friendly and widely available liquid. After casting the porous PIM-1 membrane, water vapor and water flux analyses were carried out. In addition, a TFC membrane with a dense PIM-1 selective layer was fabricated, and water vapor transport data was obtained and compared with that of the porous membrane.

2. Materials and methods

2.1 Materials

5,5',6,6',-Tetrahydroxy-3,3,3',3'-tetramethyl-1,1'-spirobisindane (TTSBI, 98%) was purchased from ABCR GmbH. 2,3,5,6-tetrafluoro-terephthalonitrile (TFTPN, 99%) was purchased from Lanxess. TFTPN was sublimated twice at 70 °C under vacuum prior to use. Potassium carbonate (K_2CO_3 , 99%) was purchased from Alfa Aesar. The rest of the commercially available compounds as chloroform ($CHCl_3$), dichlorobenzene (DCB), dimethylacetamide (DMAc), ethanol (EtOH), NMP, THF were obtained from Merck Millipore and were used without further treatment.

2.2 Synthesis of PIM-1

In the current study, PIM-1 was synthesized three times using different methods. The first batch was synthesized according to the high temperature method³⁶ to achieve higher polymer molecular weight. The next two batches were synthesized according to the low temperature method³⁷ yielding polymers with lower molecular weight. Since the low temperature method ensures more reproducible molecular weight³⁸ it has been chosen for the trials on porous membrane formation. In the low temperature method, it is assumed that if the molecular weights of the polymer are close to each other, the properties of the polymer will not change significantly.

The polymers resulted from two synthesis methods had characteristic yellow color. Polymers were characterized by size-exclusion chromatography calibrated to polystyrene standards for apparent average molecular weight (M_w) and dispersity (\bar{D}) summarized in Table 1.

2.3 Preparation of membranes

2.3.1 Membrane obtained by non-solvent induced phase separation. The choice of the membrane casting method is

critical to the production of polymeric membranes for use in various membrane applications such as gas separation and water treatment. There are several techniques to form polymeric membranes, which can be porous, dense, or porous with a dense thin layer on top. In particular, there are numerous techniques to fabricate porous membranes, such as sintering, stretching, track-etching.³⁹ In addition to these techniques, phase inversion is the most widely used method for producing porous membranes due to its simplicity, low cost and scalability.⁴⁰ In this method, a homogeneous polymer solution is first cast onto a nonwoven fabric using a doctor blade to obtain a polymer solution layer of uniform thickness. The resulting solution coated nonwoven is then immersed in a non-solvent or subjected to a rapid temperature change in order to induce phase separation.⁴¹ If a non-solvent is used, phase separation occurs due to the diffusion of the non-solvent into the thermodynamically stable polymer solution, causing a rapid decay of solvent system's ability to dissolve a polymer with consequent precipitation of a polymer and thus formation of polymer-rich and polymer-poor phases. At the same time, solvents of the casting solution diffuse out of the area of two phases. Basically, the polymer-rich phase forms the membrane matrix, while the polymer-poor phase forms the pores of the membrane.⁴² A high concentration of a volatile solvent in the casting solution can promote the formation of a dense skin layer over an underlying porous structure when the polymer solution is exposed to air after deposition onto nonwoven, allowing some solvent to be evaporated. If a porous membrane is desired, it is necessary to minimize the time the solution is exposed to the air. The composition of the casting solution, especially the amount of highly volatile solvents, the duration of solvent evaporation prior to precipitation, and the type of precipitation bath, its temperature, are crucial parameters for achieving the desired membrane structure.^{43,44}

In this study, various solvents were tested in order to prepare a suitable polymer-solvent composition considering the factors mentioned above. Table 2 shows the most suitable polymer composition of the casting solutions used in this study for the non-solvent induced phase inversion method and the casting parameters for membrane formation. On the other hand, other polymer solutions prepared and membranes cast are shown in the ESI, Table S1.†

The concentration of PIM-1 polymer in the casting solutions was adjusted to be between 10 and 17.5 wt% depending on the solvents used. After stirring for 2 days, the solution was directly cast on a polyester nonwoven support using an in-house designed casting machine with a doctor blade set at a specified gap height (some membranes were cast directly onto glass as substrate, see Table 2). On the casting machine, the speed of the take-up reel is adjustable to control the evaporation time before the solution cast film is immersed in the non-solvent (precipitation) bath. The cast membranes were left in the precipitation bath for 20 min, pulled out of the water and dried under vacuum at 60 °C for 2 days to remove all residual solvents. Due to the lack of high boiling point solvents suitable for PIM-1 dissolution, THF was chosen as a component of all polymer solutions except those with DCB. NMP is one of the most used

Table 1 Molecular weight and dispersity of different synthesis of PIM-1

| Method | Name of batch | M_w (kg mol ⁻¹) | \bar{D} |
|------------------|---------------|-------------------------------|-----------|
| High temperature | PIM-HT | 142 | 5.5 |
| Low temperature | PIM-LT-1 | 76 | 4.4 |
| Low temperature | PIM-LT-2 | 76 | 2.8 |

Table 2 Composition of casting solutions and membrane casting parameters

| Name | Composition (% wt) | Precipitation bath | Batch | Membrane casting thickness | M_w (kDa) |
|-------|--------------------------|--------------------|----------|----------------------------|-------------|
| PM-6 | PIM/NMP/THF:12.5/69.5/18 | Water | PIM-LT-2 | 150 μm | 76 |
| PM-9 | PIM/NMP/THF:12.5/69.5/18 | Water | PIM-LT-2 | 150 μm | 76 |
| PM-11 | PIM/NMP/THF:15/77/8 | Water | PIM-LT-1 | 150 μm | 76 |
| PM-13 | PIM/NMP/THF:11.5/72/16.5 | Water | PIM-HT | 150 μm | 142 |

nonvolatile solvents for membrane formation by NIPS. As NMP is a weak solvent of PIM-1, the combination of NMP and THF was essential and gave the best results among other investigated solvent systems. Chlorinated solvents, as *e.g.*, chloroform, which is one of the best solvents for PIM-1, were considered environmentally harmful and not suitable for potential large-scale membrane production. Another argument against using chlorinated solvents is their immiscibility with water, the most desirable liquid to use as a non-solvent in the quenching bath.

A further treatment was applied to one of the membranes (PM-6) to investigate the permeance of liquid water while the membrane was initially fully wetted with a liquid. For that purpose, isopropanol was used as wetting agent to reduce the contact angle of the membrane toward water. After membrane preparation by phase inversion method, dry PM-6 membrane was immersed in 50 : 50 (wt%) isopropanol–water mixture for 1 hour. Afterwards, the membrane was taken out of the solution and subjected immediately to water flux measurement.

2.3.2 Thin film composite membrane. The preparation of the TFC membrane was carried out by a coating method, which is widely used for the formation of TFC membranes. The porous support was brought into the contact with the polymer solution and drawn from the contact point at a certain speed to achieve uniform polymer solution distribution on the ultrafiltration membrane used as a support.⁴⁵ In this study, a PIM-1 dense selective layer was formed on a porous polyacrylonitrile (PAN) membrane using a laboratory scale membrane casting machine developed in-house. The solution of PIM-1 was prepared as 1% by weight in THF. The polymer solution was poured into the bath of specific shape and the PAN membrane was brought into contact with the solution. A meniscus of polymer solution was then formed by lowering the bath with the solution for *ca.* 2 mm. A thin layer of solution on the support surface was obtained by pulling the porous support out of the meniscus at a constant speed. The drying of the TFC membrane was carried out under ambient conditions without controlling of the solvent evaporation. The procedure was carried out in a hood with a high air exchange rate to ensure that no accountable solvent vapor was present in the vicinity of the membrane casting machine, except where the polymer solution bath was placed.

2.4 Characterization methods

2.4.1 Size-exclusion chromatography (SEC). SEC measurements were performed at 30 °C in CHCl_3 using a column combination (precolumn-SDV-linear, SDV-linear and SDV 102 nm with inner diameter = 4.6 mm and length = 53 cm, Polymer Standard Service GmbH, Mainz, Germany) at a flow

rate 1.0 mL min^{-1} . A combination of refractive index (RI) and ultraviolet (UV) detectors was used for concentration detection. The system was calibrated to polystyrene standards for the evaluation of apparent weight average molecular weight (M_w) and dispersity index (\bar{D}) of the prepared polymers.

2.4.2 Scanning electron microscopy (SEM). The morphology of the membranes was studied using a MERLIN SEM (ZEISS, Oberkochen, Germany) at accelerating voltages between 1.5 kV and 3 kV. The samples were coated with 1–1.5 nm platinum. The cross-section morphology was examined on cryogenically (liquid nitrogen) fractured samples.

2.4.3 Fourier transform infrared spectroscopy (FTIR). FTIR spectra was measured on an ALPHA FTIR spectrometer (Bruker Optics, Bremen, Germany) in attenuated total reflectance mode (ATR, diamond crystal). The measurements were conducted at ambient temperature in a spectral range of 400 to 4000 cm^{-1} with a resolution of 4 cm^{-1} and an average of 64 scans.

2.4.4 Water contact angle. Dynamic contact angle measurements were conducted by using Krüss Drop Shape Analysis System DSA 100. The computational analysis was done using Advance software. Prior to each measurement, the baseline detection was done manually. Deionized water was taken to glass syringe and placed onto PIM-1 samples. Average value of first 30 measurement was recorded for each sample.

2.4.5 Water flux measurement. Water flux measurements were performed at ambient conditions using an in-house designed automatic testing facility where dead-end mode of filtration was utilized. The transmembrane pressure (Δp) was set to 4 bar. This pressure was chosen in order to compare results with parameters obtained for other membranes developed at Hereon. The diameter of the membrane was 1.45 cm ($A = 1.65 \text{ cm}^2$). Ultrapure water with conductivity $\leq 0.055 \mu\text{S cm}^{-1}$ from Siemens LaboStar was used for this measurement. The volume of water (ΔV) permeated through the membrane was determined every 60 s using build-in microbalance (Δt). The normalized permeance (J) was calculated according to following equation:

$$J = \frac{\Delta V}{A \Delta p \Delta t} \quad (1)$$

In general, pore wetting should be avoided in order to maintain an efficient MD operation. Membrane wetting is obtained when applied pressure exceeds the liquid entry pressure (LEP) which can be defined as the highest applied transmembrane hydrostatic pressure before the liquid in the feed penetrates the larger pores and passes through the hydrophobic membrane. LEP can be calculated by the Young–Laplace equation as seen in (eqn (2)).⁴⁶



$$\text{LEP} = \frac{-4B\gamma_L \cos\theta}{d_{\max}} \quad (2)$$

where B is the geometric factor of the membrane pores ($B = 1$ for assumed cylindrical pores), γ_L is surface tension of the liquid, θ is the contact angle of the liquid and d_{\max} the largest pore size. In theory, when transmembrane pressure is kept below the LEP during the operation, the liquid in the feed does not penetrate the pores, thus, only vapor diffusion across the membrane occurs.⁴⁷ LEP for membranes under investigation was assessed during experiment where feed pressure was stepwise increased until constant water flow was detected.

2.4.6 Water vapor permeance test. In the MD water is transported across the membrane in the vapor state, unless there is no liquid breakthrough. It was decided to investigate vapor transport of PIM-1 porous and TFC membranes using an in-house designed pressure increase facility to have parameters comparison to other membranes developed at Hereon. This facility uses the same “constant volume/variable pressure” measurement method as the time-lag facility, which is widely used to determine gas transport parameters of thick isotropic polymer films.⁴⁸ The software of the pressure increase facility is optimized for the characterization of membranes with negligible thickness for which no time-lag can be determined. All membranes were characterized at 40 °C, feed vapor pressure lower than 60 kPa and permeate pressure changing in the range 10–130 Pa. The permeance was determined as the average of at least 10 measurements within each data accumulation set.⁴⁹ The foreseen and accepted disadvantage of the pressure increase facility is the lack of ability to determine vapor permeance at saturated vapor conditions. This disadvantage arises from the fact that the gas or vapor to be studied is accumulated and conditioned to the temperature of the experiment in the feed pressure vessel and is isolated from the external supply line at the start of the experiment. When an experiment starts, the valve on the feed side of the membrane is opened and the membrane is exposed to the penetrant. This results in a small pressure drop, approximately 10% of the pressure at which gas or vapor was accumulated in the feed vessel. At the same time, this method allows the behavior of the membrane to be studied as it is subjected to a steadily decreasing feed pressure of the penetrant. In the case of highly soluble or condensable penetrants, the results of such an experiment are of great importance.

3. Results and discussion

3.1 Porous membrane development

The aim of this work was to develop porous PIM-1 membranes by NIPS for use in water purification processes, preferably in MD. There is a lack of studies on this subject, as PIM-1 is a difficult polymer to use in the phase inversion process. The solvent choice is crucial for the phase separation method and when the subject is PIM-1, there is a limitation in solvents suitable for this membrane formation process, especially when water is used as phase separation inducing liquid. The most prevalent solvents used to cast PIM-1 membranes or films are THF, CHCl_3 , dichloromethane (DCM) and DCB but not all of them can be used in the phase inversion method because

CHCl_3 , DCB and DCM are immiscible with water, and high volatility of CHCl_3 and DCM can easily induce dense layer formation when polymer solution is exposed to air during membrane casting. Considering these limitations, there are not many options left but to use THF as a solvent. However, it is important to use as much of the high boiling point solvent in the polymer solution that is well miscible with water to facilitate the phase inversion process. With this in mind, we have tried several solvent/non-solvent combinations to prepare polymer solutions and then the porous membrane itself. Some of these membranes were further investigated as their surface and cross-sectional morphologies allowed us to delve into the membrane performance.

In this study the ternary phase diagrams were not determined, instead of this, the previous studies^{32,50} were taken into account to gain insight into the starting point of the polymer solution formulation. Jue *et al.*³² reported the preparation of the hollow fiber PIM-1 membrane using THF, DMAc and ethanol in the dope composition for the electrospinning. It was observed that the pore formation starts below a dense layer on top of the membrane cross-section. This fact might be attributed to the presence of THF: as THF has a low boiling point (64 °C), it evaporates rapidly when the polymer solution is exposed to the air, resulting in the formation of a dense film on top of the membrane. Taking this situation into account, this current study aimed to use the lowest possible amount of THF in the casting solution.³³ Therefore, another solvent with a high boiling point was needed to be used together with THF to facilitate pore formation at the desired moment. At this point, the most common non-volatile solvent NMP is the best candidate due to its excellent miscibility with water. However, NMP can only dissolve PIM-1 at low concentrations to achieve one phase solution. In this study, PIM-1/NMP/THF solutions were prepared, and our observations showed that the optimum concentration to obtain one phase solution is PIM-1/NMP/THF:12.5/69.5/18 wt%, which is the case for PM-6 and PM-9. Higher NMP loading in the casting solution caused insufficient dissolution of PIM-1.

The characterization of PM-6, PM-9, PM-11 and PM-13 porous PIM-1 membranes were carried out by FTIR measurement. FTIR spectrum of each membranes showed the characteristic peaks corresponding to each functional group. FTIR spectrum of the membranes can be found in ESI, Fig. S1.†

3.2 Membrane morphology

The SEM images of PIM-1 membranes are shown in this section to demonstrate the internal and surface morphology of the membranes. Fig. 1 shows the cross-sectional morphology of PM-6, PM-9, PM-11 and PM-13 with well-developed internal porosity of the membranes. Fig. 1a and b show the presence of the interconnected pores within the membrane, which are covered by a denser but still visibly porous layer on top of the membrane. According to the generally accepted classification, microfiltration membranes have a pore size of 100–10000 nm, while ultrafiltration membranes have a pore size in the range of 2–100 nm.³⁹ The membrane PM-11 shown in Fig. 1c has a much



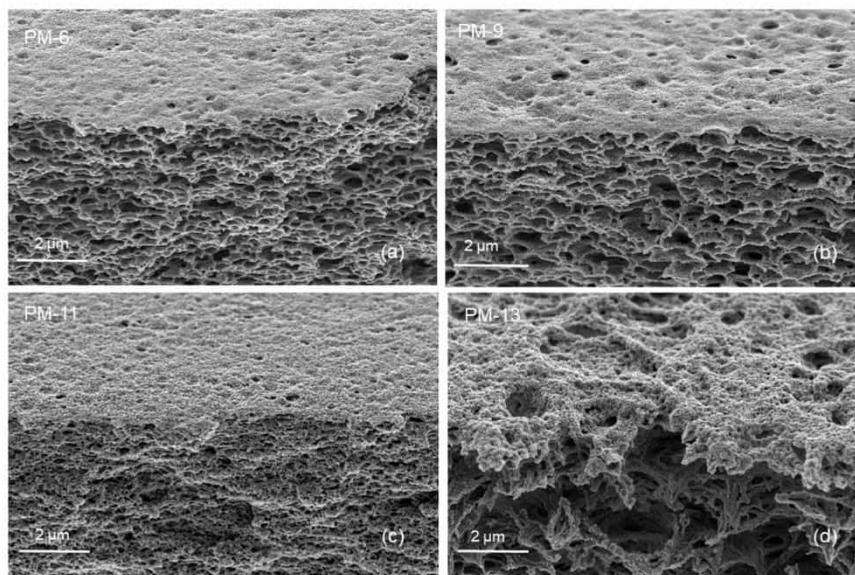


Fig. 1 Cross-sectional images of PM-6 (a), PM-9 (b), PM-11 (c) and PM-13 (d) (2 μm).

more compact morphology with smaller voids than PM-6 and PM-9. In case of PM-11 8 wt% THF resulted in very different morphology of the membrane in the vicinity to the surface exposed to the air during the membrane formation. One can speculate that a small THF content in the polymer solution led to smaller changes in polymer concentration when THF was unavoidably evaporated from the polymer solution surface, and this prevented the formation of a distinctive “crust” as on the surface of PM-6 and PM-9. Yong *et al.*⁵¹ pointed out that a higher polymer concentration in the casting solution suppresses the formation of macrovoids, resulting in the formation a compact porous structure. The formation of internal pores increases in PM-13 compared to PM-6, PM-9 and PM-11 as shown in Fig. 1d. In this case the polymer concentration is slightly lower than in

PM-6 and PM-9, but in addition the polymer used to cast PM-13 is from the different batch (PM-HT, see Table 1), which has a high molecular weight. PM-13 therefore clearly demonstrates the effect of molecular weight on the membrane formation process, where a higher molecular weight of the polymer leads to the formation of a very open porous structure both on the surface and within the membrane.

Fig. 2 provides a magnified visualization of the cross-sectional morphology of the membranes. From Fig. 2a and b it can be said that PM-6 and PM-9 have similar pores both in shape and in size as one can expect for membranes formed of the same polymer and from the polymer solution of the same composition. On the other hand, PM-11 has smaller voids that are well interconnected (Fig. 2c). This difference in porous

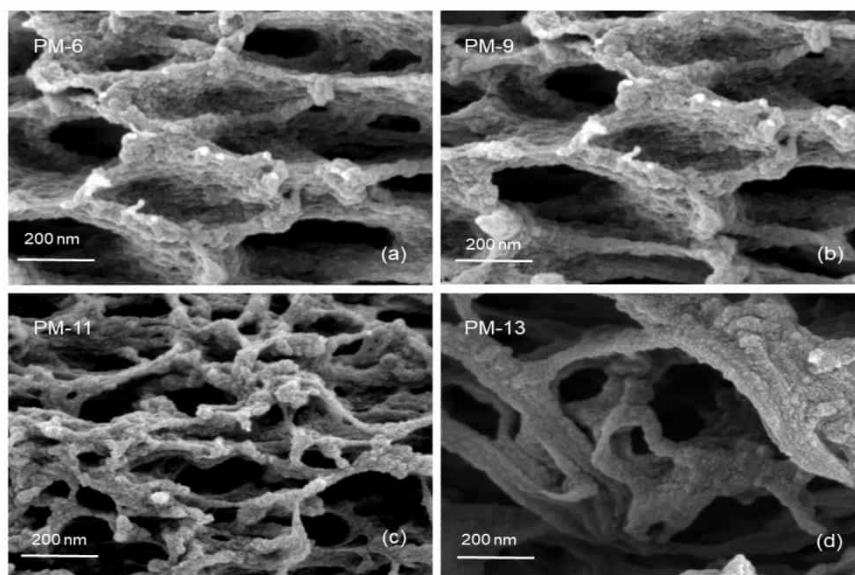


Fig. 2 Cross-sectional images of PM-6 (a), PM-9 (b), PM-11 (c) and PM-13 (d) (scale bars: 200 nm).



structure should result from the difference in polymer concentration between 12.5 wt% for PM-6 and PM-9, and 15 wt% for PM-11. PM-13 on Fig. 2d shows large pores with walls formed of a denser, fiber-like polymer. The difference of PM-13 to other membranes is high molecular weight of the polymer. Presumably, this parameter even at the lowest polymer concentration and the highest THF concentration in the casting solution, has led to changes in the interaction of PIM-HT with water during the phase inversion process, resulting in both a highly porous internal structure of the PM-13 and large pores on the membrane surface (Fig. 1d).

Fig. 1 already showed that the cross-sectional morphology of the membranes is anisotropic, the feed side of the membranes is covered by a layer denser than the bulk of the membrane. For a better understanding of the surface porosity of the membrane, SEM images of the membrane surface are shown in Fig. 3. Fig. 4 shows SEM images of the membrane surface with enlarged magnification. Fig. 3a–c, corresponding to PM-6, PM-9 and PM-11 respectively, clearly demonstrate the presence of small pores of different sizes with the smallest visible pore size in case of PM-11, while PM-13 in Fig. 4d shows large surface pores through which the internal structure of the membrane can be observed. The major difference of PM-13 that distinguishes it

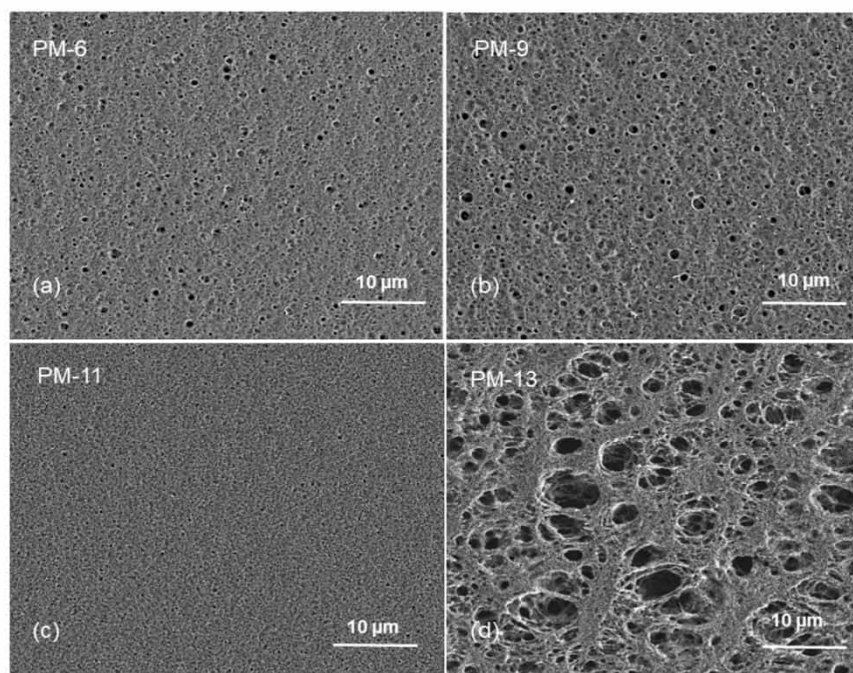


Fig. 3 Surface morphology of PM-6 (a), PM-9 (b), PM-11 (c) and PM-13 (d) (scale bars: 10 μm).

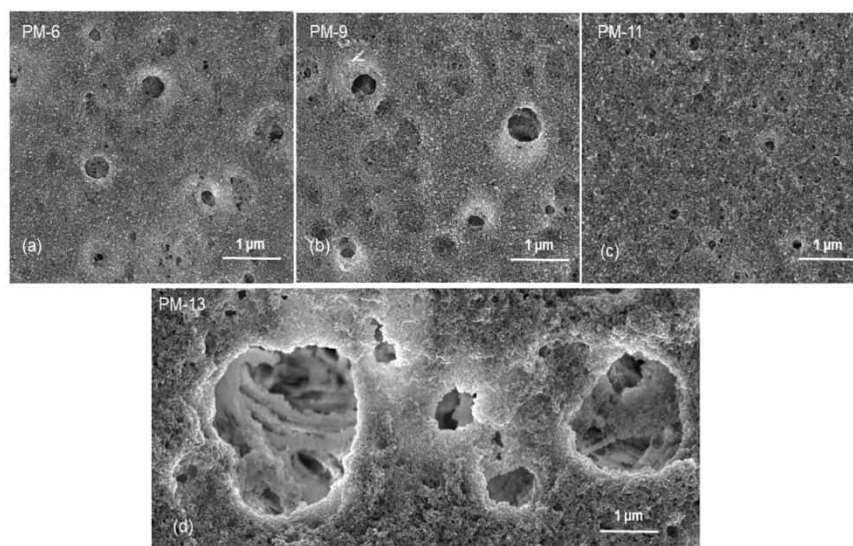


Fig. 4 Surface morphology of PM-6 (a), PM-9 (b), PM-11 (c) and PM-13 (d) (scale bars: 1 μm).



from PM-6, PM-9 and PM-11 is the higher molecular weight of the PIM-HT (Table 1). It is a questionable whether the formation of big pores is due to the higher molecular weight of the polymer, as the membrane casting technique is the same for all membranes. The polymer content in the PM-13 case is the lowest of all the membranes and the THF content in the polymer solution is the highest. The high THF content should have led to an increase in the polymer concentration near the surface of the polymer solution exposed to the air due to the intensive evaporation of the solvent. At the same time, the decrease in THF concentration should lead to a lower polymer solubility in the NMP/THF system, since, as mentioned above, the PIM-HT has limited solubility, due to its high molecular weight. The combination of these factors with the highest weight factor of the polymer molecular weight resulted in the formation of the membrane with the largest surface pores and voids within the membrane. Prior studies have noticed the effect of the molecular weight on the structure and performance of ultrafiltration membranes.^{52–55} Zhou *et al.* showed that increasing PES molecular weight led to the formation of larger pores on the membrane surface.⁵³ However, Miyano *et al.* asserted that the molecular weight is the least factor, which influences the pore size of the membrane while the concentration of polymer solution and solvent choice are more dominant parameters.⁵⁴ Another remark on molecular weight influence on membrane morphology was made by Haponska *et al.*, who claimed that lower molecular weight caused a compact morphology of the membrane cross-section while higher molecular weight led to a more spongy-like porous structure.⁵⁵ Taking these findings into consideration, it can be concluded that the molecular weight has a strong impact on the formation of the membrane structure, especially in case when the polymer is only partly soluble in the main solvent of the solvent system.

3.3 Water flux measurement

Experiments on the liquid water flow transport through porous membrane pursued two aims: determination of LEP and investigation of water transport at 4 bar pressure as driving force to be able to compare results with other developed microfiltration (MF) and ultrafiltration (UF) membranes. Unfortunately, the experimental LEP determination did not give conclusive results, at transmembrane pressure as low as 0.5 bar minor water flow was determined. It is in the line with the theoretically determined LEP values listed in Table 3. The transmembrane pressure for continuous water permeance measurements was chosen based on the pore size of the

membranes used in this study. The average pore sizes calculated by SEM are between 0.1 and 0.2 μm as seen in Table 3. This range corresponds to the pore sizes of membranes used in microfiltration (10–0.1 μm) and ultrafiltration (0.1–0.002 μm).⁵⁶ On the other hand, the transmembrane pressure can reach up to 4 bar in microfiltration and 2.5–5 bar in ultrafiltration.^{57,58} Considering that, the average pore size of the membranes in this study is in the MF and UF range, the transmembrane pressure was set to 4 bar to be in an application range. In addition, since there is a direct relationship between the applied transmembrane pressure and the permeate flux, this value was not set too low.⁵⁹ Another reason for determining the transmembrane pressure is to prevent membrane compaction. In the case of transmembrane pressure between 2 and 70 bar, membrane compaction is considered negligible.⁶⁰ All these reasons led to set the transmembrane pressure to 4 bar.

In addition to average pore size determination, Table 3 shows contact angle, largest pore size for each membrane and theoretical LEP values calculated from aforementioned parameters. It can be seen that the sequence of the largest pore size is consistent with the morphology images as PM-11 < PM-6 < PM-9 < PM-13. The theoretically calculated LEP follows the order of PM-13 < PM-11 < PM-9 < PM-6.

Fig. 5 shows the time dependence of the water permeance for four membrane samples. These samples were chosen from a set of many developed in the current study (ESI, Table S1†). The decision to focus on PM-6, PM-9, PM-11 and PM-13 was taken based on the analysis of SEM images, which showed the developed porous structure both on the membrane surface and in the bulk of the membrane.

Water flux measurements were carried out using ultra-pure water. The applied transmembrane pressure of 4 bar is above the theoretical LEP for all samples and anyway water flow through PM-6, PM-9 and PM-11 is on the level of the measurement system resolution. The fact that water penetrates through the membrane shows that on the membrane surface pores are larger than those presented in the Table 3 and not identified by SEM investigation. The quantity of these pores is extremely small since no significant water flux can be observed under 4 bar pressure. Most of the membrane surface does not allow liquid water to pass through. In that point, membrane hydrophobicity or hydrophilicity should be considered since it significantly influences membrane performance. Contact angle of a dense PIM-1 film is about 90° (ref. 30 and 62) and measurements done for porous membranes under study revealed that the contact angle of porous PIM-1 membranes are

Table 3 Contact angle, pore size analysis and theoretical LEP of the porous membranes

| | Contact angle (θ) | Average pore size (μm) | Largest pore (μm) | LEP (bar) |
|----------------------|---------------------------------|-------------------------------------|--------------------------------|-----------|
| PM-6 | 106.9 | 0.14 ± 0.13 | 0.83 | 1.01 |
| PM-9 | 113.4 | 0.21 ± 0.22 | 1.42 | 0.80 |
| PM-11 | 97.9 | 0.11 ± 0.08 | 0.75 | 0.52 |
| PM-13 | 129.6 | — | 5.36 | 0.34 |
| PIM-1 (TFC membrane) | 70 (in this study) 89 (ref. 61) | — | — | — |



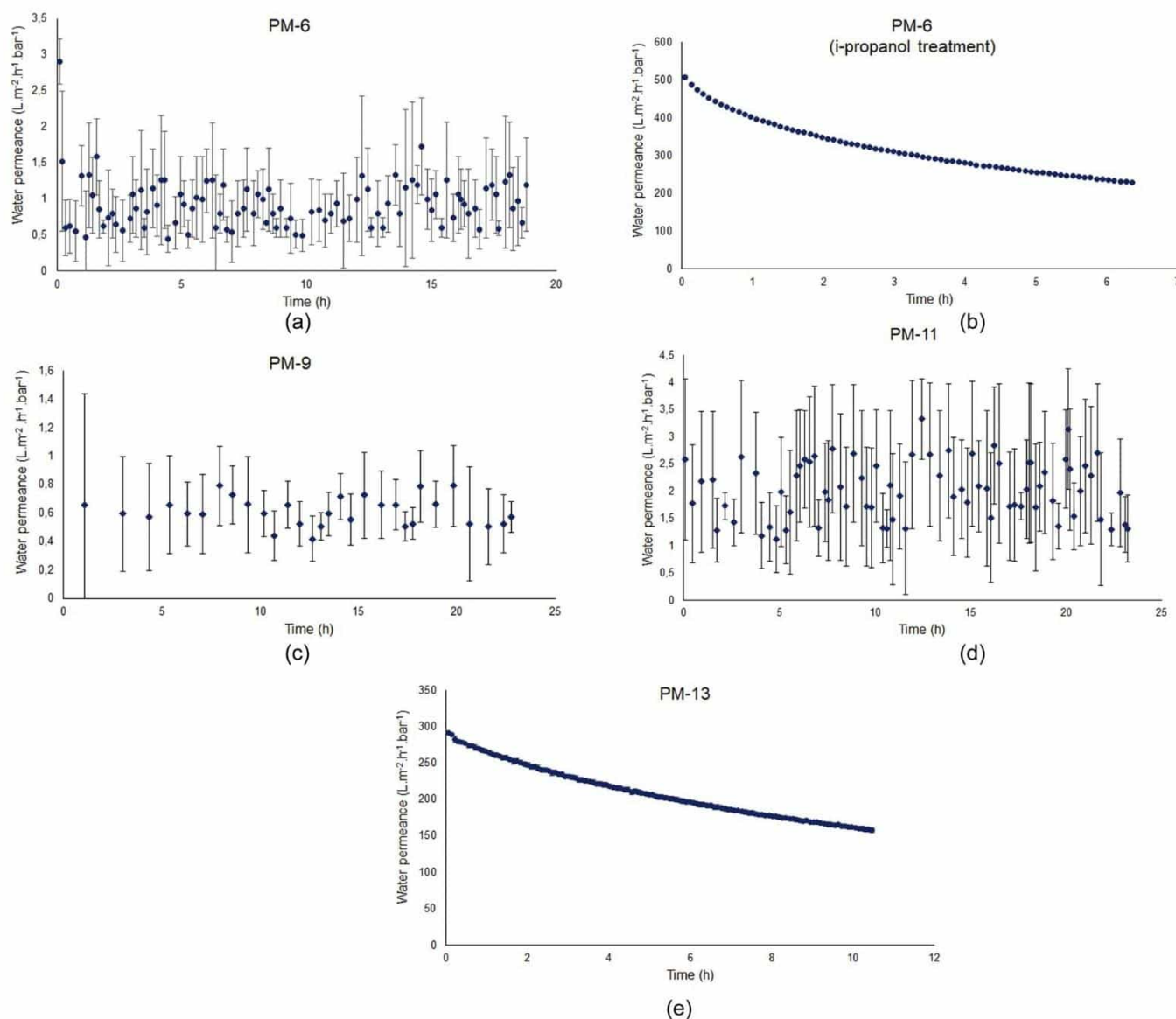


Fig. 5 Water flux data of PM-6, PM-9, PM-11 and PM-13. Due to the resolution of the measuring range, it was difficult to record a constant flow. In order to show the deviations within a measurement error bars are shown.

higher (Table 3, 97–130°) than that of a dense film. The reason for this could be that the contact angle can vary depending on the surface morphology.^{63,64} For highly hydrophobic membranes, it is hard to evaluate the accessibility of the porous system for liquid water and its ability to transport water.

To understand the ability of the developed porous membranes to the transport of liquid water, one of the samples, PM-6, was immersed in the isopropanol–water mixture and soaked with the liquid. The alcohol–water mixture has a low surface tension and low contact angle toward PIM-1 and it allowed for effective impregnation of the pores with water miscible liquid.⁶⁵ Several publications have shown that membranes treated with wetting agents such as ethanol or isopropanol demonstrate higher water flux even after alcohol evaporation.^{66–68} It should be noted that the pore activation by alcohols is a temporary effect since the wetting agent adsorbs only physically on the pore surface and do not cause any

chemical modification. Nevertheless, it would be beneficial to investigate a PIM-1 membrane treated by a wetting agent in order to discuss its porosity. Therefore, we conducted an additional post-treatment for PM-6 which exhibits the smallest pore size according to SEM results. For this reason, PM-6 was soaked into an isopropanol–water mixture in order to make the membrane hydrophilic to investigate whether the pore openings occur. Fig. 5b depicts that the water flux of PM-6 significantly escalates to 500 L m⁻² h⁻¹ bar⁻¹ after the membrane were exposed to isopropanol–water treatment, which triggered the interconnection of the small pores. It might be explained by the fact that small pores do not take part in filtration at the beginning, since the surface tension between liquid–solid is less than that of liquid–air. After the wetting treatment, cohesive forces between water molecules becomes weaker, therefore, water can penetrate into pores.⁶⁸ If we want to compare this result with a reference polymeric membrane, a polyethersulfone

(PES) membrane can be considered. This polymer membrane is widely used in ultrafiltration and microfiltration and a vast amount of studies on PES membranes can be found in the literature. Studies have shown that PES membranes exhibit water flux in the range of $300\text{--}500\text{ L m}^{-2}\text{ h}^{-1}\text{ bar}^{-1}$.^{69,70} Therefore, PM-6 can show a water flux at the level of PES membranes, by virtue of pore activation after isopropanol–water treatment. If it is to be compared with polymers used in membrane distillation, the example of PVDF and PTFE can be given. Nawi *et al.*⁷¹ recorded the pure water flux value of pristine PVDF membrane as approximately 200 L, while Yu *et al.*,⁷² in their work on PTFE for MD applications, reported a pure water flux value of approximately 900 L. Based on these reference values, it can be stated that the PM-6 membrane after isopropanol treatment exhibited a notable water flux of $500\text{ L m}^{-2}\text{ h}^{-1}\text{ bar}^{-1}$. According to this result, it can be inferred that PM-6 acquires pores but relatively in small size which hinders the liquid water transport through the virgin membrane. It should be noted that since the polymer was casted on a porous nonwoven support, the actual thickness of the polymer cannot be determined in this study by excluding the nonwoven support. Therefore, we are limited to determine of the membrane porosity. Yet, it allows us to interpret the effect of isopropanol–water treatment on the pore activation and water flux.

A similar water flux result was obtained from PM-9 as expected since it is the same PIM-1 which was used in PM-6, yet PM-9 was obtained from another membrane casting in order to reproduce the results. Fig. 5c exhibits the absence of water flux. As mentioned before, water molecules are not able to transfer through the membrane pores at 4 bar transmembrane pressure in this study. Likewise, PM-11 demonstrates also scattered but extremely low water flux values as seen in Fig. 5d, what cannot be considered as water flux. This finding is anticipated due to the surface morphology and internal porosity of PM-11 are not appropriate to transfer the water molecules across the membrane. Experimentally, although the transmembrane pressure is actually above the theoretically calculated LEP for all membranes, PM-6, PM-9, and PM-11 showed basically no water flux (only noise). This can be attributed to the deviation of the experimental LEP from its theoretical value. Despite operating the water flux experiments with a transmembrane pressure higher than the theoretical LEP, the reason for the water flux remaining only as noise could be the variations in the actual values according to the operating conditions. For example, the presence of defects in pore structure or the pore shape not being uniformly cylindrical as assumed in reality can cause deviations between calculated values based on theory and experimental results.^{73,74} However, the observed difference in water flux measurements is associated to PM-13. Unlike the other membranes studied in this work, Fig. 5e shows that PM-13 provides a significantly high water flux of $300\text{ L m}^{-2}\text{ h}^{-1}\text{ bar}^{-1}$. This result might be attributed to the large pores of PM-13 on the surface and cross-section of the membrane and therefore PM-13 possesses the lowest LEP value. It can therefore be assumed that 4 bar transmembrane pressure is enough for PM-13 to press the water molecules through the membrane pores without the necessity of a wetting treatment.

Isopropanol–water treatment was not applied to all membranes. Since PM-13, which has the largest pore according to SEM results, already showed some water flux, it was concluded that the membrane with the smallest pore could be used to see if such a treatment would have an effect, and therefore only PM-6 was exposed to isopropanol soaking.

3.4 Water vapor permeance

MD is the method of water purification by transport of water molecules as vapor through the porous structure of the membrane. The ability of the developed membranes to transport water in a vapor form was studied on an in-house designed “pressure increase” facility. On this facility it is possible to study transport of gases and vapor through flat and hollow fiber shaped membranes in relation to temperature in the range of $4\text{--}120\text{ }^{\circ}\text{C}$ and feed pressure in the range of $20\text{--}1200\text{ mbar}$. For water vapor, the maximum achievable feed pressure applied to the membrane was *ca.* 95% of vapor activity at the temperature of experiment. Permeate pressure range in which permeance data points are acquired can be chosen in accordance with membrane performance. For slow membranes it can be $0.1\text{--}0.2\text{ mbar abs}$, for “fast” membranes $1\text{--}13\text{ mbar abs}$. From the MD point of view, the obvious drawback of this facility is the inability to start an experiment at saturated vapor pressure. At the same time, the feed vapor activity can be as high as 95%, very close to the saturation pressure and at the same time the membrane can not be exposed to liquid water due to *e.g.* condensation caused by a temperature drop on the membrane surface as a result of the Joule-Thomson effect.⁷⁵

Each membrane was exposed several times to the same pressure of vapor; during each exposure, several points were collected to have statistically relevant data and the experiment was repeated after the membrane was fully evacuated. Fig. 6 shows that all membranes have significant permeance for water in a vapor form while Fig. 5 showed that membranes PM-6, PM-9 and PM-11 had extremely limited transport when liquid water was applied under a transmembrane pressure of 4 bar.

Fig. 6 shows that PM-6, PM-9 and PM-11 show high water vapor permeance with the highest value for PM-6. This difference can be considered insignificant since these are handmade casted membranes and THF evaporation is not controlled. On the other hand, PM-13 exhibits dramatically higher water vapor permeance which is almost 3-fold of PM-6. This result can be attributed to large surface pores of PM-13 and well interconnected inner porosity which allows water transport without any obstruction. To compare water transport in vapor and liquid forms, vapor permeance was converted to a comparable unit as shown in Table 4. It is seen that the vapor/liquid permeance ratio is tremendous. Especially in case of PM-6 and PM-9 which have the smallest pores, this comparison vividly demonstrates how water permeance differs in the vapor and liquid phases. In particular, our findings up to this point are supportive of the use of porous PIM-1 membranes in MD considering that this process requires a hydrophobic membrane which would allow only vapor to permeate. As it can be seen from Table 4 measures to prevent membrane wetting



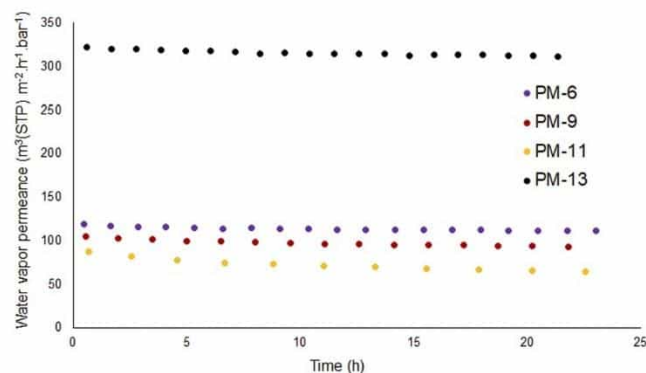


Fig. 6 Water vapor permeance of PM-6, PM-9, PM-11 and PM-13.

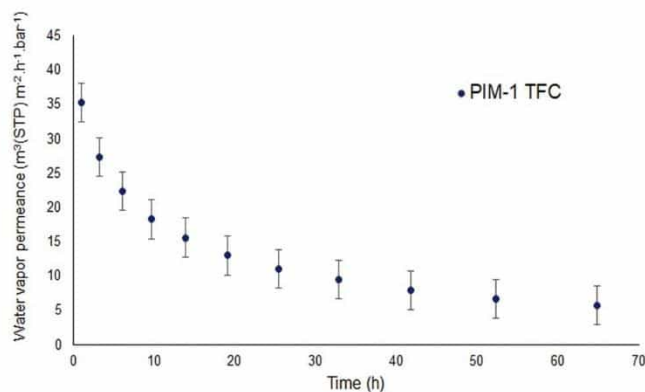


Fig. 7 Water vapor permeance of the PIM-1 thin film composite (TFC) membrane.

are essential since as soon as the membrane is impregnated with water the flux of liquid contaminated liquid will be significantly higher than that of vapor.

To better understand the water vapor characteristics of porous PIM-1 membranes, it is beneficial to make a comparison with water vapor properties of a PIM-1 thin film composite (TFC) membrane. Fig. 7 depicts the water vapor permeance of PIM-1 TFC membrane determined at 40 °C. It should be noted that water permeance could not be measured at saturated vapor pressure due to the facility conditions. The water permeance shown in Fig. 7 was obtained at 91% of vapor activity. The permeance starts around 30 m³(STP) m⁻² h⁻¹ bar⁻¹ and decreases almost 60% over time of 25 h to 10 m³(STP) m⁻² h⁻¹ bar⁻¹. This drop in permeance reveals physical aging of the PIM-1 selective layer. However, it is observed that porous PIM-1 membranes sustain the water vapor permeance over time unlike the PIM-1 TFC membrane. Moreover, porous membranes demonstrate significantly higher water vapor permeance than the PIM-1 TFC membrane. However, in case of extreme water purity is required, a dense PIM-1 membrane might be better candidate.

In this study, the porosity of the membranes was not investigated by an analytical method. Nevertheless, prior studies have shown that Knudsen diffusion is an indication of membrane porosity. Basically gas transport in membranes might take place in different ways: poiseuille diffusion (wide pore size), Knudsen diffusion (intermediate pore size), molecular sieving and surface diffusion (small pore size) and solution-diffusion (dense membrane).⁷⁶ In some cases, two or more of these diffusion mechanisms can occur concurrently. Among

them, Knudsen diffusion occurs if the mean free path of the gas molecule is larger than the pore size of the membrane. Moreover, gas transport in Knudsen diffusion occurs in the gaseous state without participation of adsorption.⁷⁷ Knudsen permeance is expressed as in eqn (3) where ε is the porosity of the membrane, d_p is the pore diameter, τ is the tortuosity, L is the thickness of the membrane, R is gas constant, M is molecular weight and T is the operating temperature.

$$Q = \frac{\varepsilon d_p}{\tau L} \left(\frac{8}{9\pi MRT} \right)^{1/2} \quad (3)$$

According to this equation, Knudsen permeance is proportional to the inverse square root of both the molecular weight and the temperature of the permeate gas. From this point of view, the permeance values of the gases were plotted against the inverse square root of their molecular weight in order to discuss the porosity of the subjected membranes in this study. Fig. 8 shows a strong relationship between the permeance and the square root of the molecular weight of the gas molecules for PM-6, PM-9 and PM-13 which correspond with Knudsen diffusion. It is seen that the permeance of each gas follows in the order of the square root of molecular weight. Further to that, the curves show good regression fits ($R^2 = 0.992$ – 0.9882) which is also attributed to the presence of significant Knudsen diffusion where molecule-pore wall interaction is dominates molecule-molecule interactions.⁷⁸ It is important to bear in mind that Knudsen diffusion describes the gas transport through the pores. Therefore, it is limited by the lack of information on

Table 4 Comparison of water transport through PIM-1 membrane when membrane is exposed to vapor or liquid on the feed side

| Sample | Vapor permeance (m ³ (STP) m ⁻² h ⁻¹ bar ⁻¹) (Fig. 6) | Vapor permeance (kg m ⁻² h ⁻¹ bar ⁻¹) (Fig. 6) | Liquid flux (L m ² h ⁻¹ bar ⁻¹) (Fig. 5) | Permeance ratio |
|-------------------|---|---|---|--------------------|
| PM-6 | 125 | 100 | 1.5 | 67 |
| PM-6 ^a | 125 | 100 | 500 | 0.2 |
| PM-9 | 100 | 80 | 0.65 | 124 |
| PM-11 | 85 | 68 | 2.0 | 34 |
| PM-13 | 320 | 257 | 300 | 0.86 |

^a PM-6 data from Fig. 5b when membrane was impregnated with water miscible fluid and exchanged to water during water flow experiment.



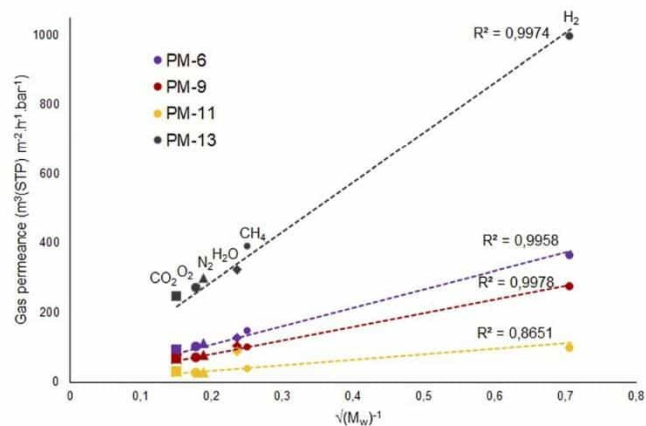


Fig. 8 Knudsen diffusion dependency of PM-6, PM-9, PM-11 and PM-13.

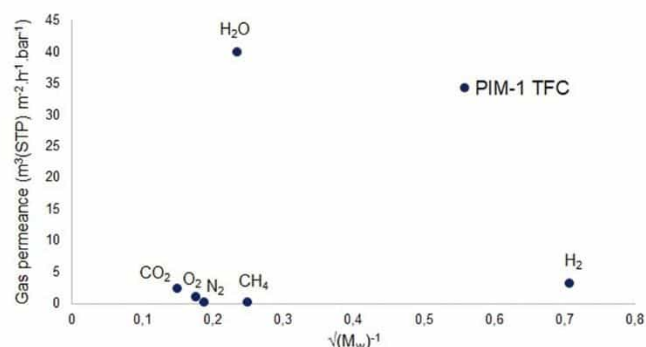


Fig. 9 Knudsen diffusion dependency of the PIM-1 TFC membrane.

surface porosity. From our results it is unfortunately hard to evaluate if a combination of different diffusion mechanisms also exists in the membrane. Nevertheless, it should be noted that both Knudsen and Poiseuille diffusion might take part simultaneously in one membrane.⁷⁹ Among the porous membranes studied in this paper, PM-11 is the exceptional case in terms of Knudsen diffusion. Water vapor permeance does not fit to the Knudsen plot as seen in Fig. 8. This might result from a combination of more than one diffusion mechanism in one membrane.

On the other hand, Fig. 9 shows a different behavior of the PIM-1 TFC membrane. It can be clearly seen that the gas permeance of PIM-1 TFC membrane does not increase in proportion to the square root of the molecular weight of the gases. This can be attributed to the behavior of the membrane with a selective dense layer which is most likely correspondent to solution-diffusion mechanism.⁸⁰

4. Conclusion

This study aimed at a detailed examination of porous PIM-1 membrane formation by non-solvent induced phase separation. Polymer solutions with a variety of solvent and non-solvent combinations were prepared in order to obtain continuous pores from the surface through the cross-section of the

membrane. It is difficult to prepare a PIM-1 polymer solution because of the lack of volatile and water-miscible solvents with a high boiling point that can be used in the phase separation method. To address this, different solvent-non-solvent mixtures including DMAc, EtOH, DCB, NMP and THF were prepared in this study in order to prepare a proper polymer solution. Among the polymer solutions, an NMP/THF combination was found to be the best candidate to cast the membrane from a homogeneous PIM-1 solution, *i.e.* without the formation of a precipitate. Four different PIM-1 membranes (PM-6, PM-9, PM-11 and PM-13) were obtained by NIPS method by using different ratios of the components in the NMP/THF/PIM-1 combination. In order to observe the effect of molecular weight on pore formation, PIM-1 used in PM-6, PM-9 and PM-11 has a low molecular weight, while PIM-1 used in PM-13 has a high molecular weight. Moreover, SEM imaging was performed to examine the morphology of the prepared membranes. Among the membranes studied in this work, PM-6 and PM-9 showed favorable void formation on the surface and cross-section of the membrane. PM-13 exhibits large pores, which was attributed using PIM-1 with high molecular weight. Additionally, water contact angle measurements were performed on membrane surfaces to investigate membrane wetting by LEP correlation. According to that, the distinct patterns in the sequence of the largest pore size and theoretical LEP values were observed consistently across the membranes. Water transport was also discussed in order to understand the membrane performance. Water flux of PM-6, PM-9 and PM-11 were neglectable, while PM-13 showed high water flux which is consistent with the presence of large voids. On the other hand, PM-6 and PM-9 demonstrated higher water vapor permeance compares to PIM-1 TFC membrane which is considered as a dense membrane. It is interesting that PM-6 and PM-9 allow to water vapor pass through the membrane however, liquid water cannot be transferred across the membrane. This membrane configuration might be a good candidate for membrane distillation since it uses hydrophobic membrane which only water vapor can pass through the membrane. These observations help us to raise intriguing questions regarding the applicability of PIM-1 on water separation. For future work, it would be interesting to establish pressure breakthrough measurement in order to deeper investigate the water flux data of PIM-1 membrane. Further experimentation regarding the role of porous PIM-1 membrane would be worthwhile since PIM-1 is easy to handle and favorable polymer which can be promising for water separation applications.

Conflicts of interest

There are no conflicts to declare.

Acknowledgements

The authors would like to thank to Dr Evgeni Sperling and Dr Erik Schneider for the SEM images and membrane morphology analysis. We gratefully acknowledge financial support from the



Federal Ministry of Education and Research of Germany (BMBF) via the project NAMED (FKZ: 03XP0151A).

References

- 1 *The United Nations World Water Development Report 2023: Partnerships and Cooperation for Water*, UNESCO, Paris, 2023.
- 2 E. Drioli, A. Ali and F. Macedonio, Membrane distillation: recent developments and perspectives, *Desalination*, 2015, **356**, 56–84.
- 3 M. R. Landsman, *et al.*, Water treatment: are membranes the panacea?, *Annu. Rev. Chem. Biomol. Eng.*, 2020, **11**(1), 559–585.
- 4 W. N. A. Wan Osman, *et al.*, A review on recent progress in membrane distillation crystallization, *ChemBioEng Rev.*, 2021, **9**(1), 93–109.
- 5 M. Yao, *et al.*, A review of membrane wettability for the treatment of saline water deploying membrane distillation, *Desalination*, 2020, **479**, 114312.
- 6 H. K. Lonsdale, The growth of membrane technology, *J. Membr. Sci.*, 1982, **10**(2), 81–181.
- 7 S. Adham, *et al.*, Membrane applications and opportunities for water management in the oil & gas industry, *Desalination*, 2018, **440**, 2–17.
- 8 B. S. Lalia, *et al.*, A review on membrane fabrication: structure, properties and performance relationship, *Desalination*, 2013, **326**, 77–95.
- 9 L. N. Nthunya, *et al.*, A review of nanoparticle-enhanced membrane distillation membranes: membrane synthesis and applications in water treatment, *J. Chem. Technol. Biotechnol.*, 2019, **94**(9), 2757–2771.
- 10 A. Hussain, *et al.*, Membrane distillation: recent technological developments and advancements in membrane materials, *Emergent Mater.*, 2021, 347–367.
- 11 A. Deshmukh, *et al.*, Membrane distillation at the water-energy nexus: limits, opportunities, and challenges, *Energy Environ. Sci.*, 2018, **11**(5), 1177–1196.
- 12 M. M. A. Shirazi, *et al.*, Characterization of polymeric membranes for membrane distillation using atomic force microscopy, *Desalin. Water Treat.*, 2013, **51**(31–33), 6003–6008.
- 13 S. Parani and O. S. Oluwafemi, Membrane distillation: recent configurations, membrane surface engineering, and applications, *Membranes*, 2021, **11**(12), 1–26.
- 14 A. Alkhudhiri, N. Darwish and N. Hilal, Membrane distillation: a comprehensive review, *Desalination*, 2012, **287**, 2–18.
- 15 L. Camacho, *et al.*, Advances in membrane distillation for water desalination and purification applications, *Water*, 2013, **5**(1), 94–196.
- 16 L. Francis, F. E. Ahmed and N. Hilal, Advances in membrane distillation module configurations, *Membranes*, 2022, **12**(1), 1–22.
- 17 X. Li, *et al.*, Fluoropolymer membranes for membrane distillation and membrane crystallization, *Polymers*, 2022, **14**(24), 1–50.
- 18 B. A. Cinelli, D. M. G. Freire and F. A. Kronemberger, Membrane distillation and pervaporation for ethanol removal: are we comparing in the right way?, *Sep. Sci. Technol.*, 2019, **54**(1), 110–127.
- 19 T. Horseman, *et al.*, Wetting, scaling, and fouling in membrane distillation: state-of-the-art insights on fundamental mechanisms and mitigation strategies, *ACS ES&T Eng.*, 2020, **1**(1), 117–140.
- 20 H. Chang, *et al.*, A critical review of membrane wettability in membrane distillation from the perspective of interfacial interactions, *Environ. Sci. Technol.*, 2021, **55**(3), 1395–1418.
- 21 A. L. Ahmad, *et al.*, Membrane antifouling methods and alternatives: ultrasound approach, *Separat. Purif. Rev.*, 2012, **41**(4), 318–346.
- 22 P. S. Goh, *et al.*, Membrane fouling in desalination and its mitigation strategies, *Desalination*, 2018, **425**, 130–155.
- 23 L. Wang, *et al.*, Polymer of intrinsic microporosity (PIM) films and membranes in electrochemical energy storage and conversion: A mini-review, *Electrochem. Commun.*, 2020, **118**, 1–7.
- 24 G. Bengtson, S. Neumann and V. Filiz, Membranes of polymers of intrinsic microporosity (PIM-1) modified by poly(ethylene glycol), *Membranes*, 2017, **7**(2), 28.
- 25 N. B. McKeown, Polymers of intrinsic microporosity (PIMs), *Polymer*, 2020, **202**, 122736.
- 26 P. M. Budd, *et al.*, Polymers of intrinsic microporosity (PIMs): robust, solution-processable, organic nanoporous materials, *Chem. Commun.*, 2004, (2), 230–231.
- 27 A. Arabi Shamsabadi, *et al.*, Next generation polymers of intrinsic microporosity with tunable moieties for ultrahigh permeation and precise molecular CO₂ separation, *Prog. Energy Combust. Sci.*, 2021, **84**, 1–42.
- 28 M. Tian, *et al.*, Chemical modification of the polymer of intrinsic microporosity PIM-1 for enhanced hydrogen storage, *J. Int. Adsorpt. Soc.*, 2020, **26**(7), 1083–1091.
- 29 Y. Wang, *et al.*, Polymers of intrinsic microporosity for energy-intensive membrane-based gas separations, *Mater. Today Nano*, 2018, **3**, 69–95.
- 30 H. J. Kim, *et al.*, A carbonaceous membrane based on a polymer of intrinsic microporosity (PIM-1) for water treatment, *Sci. Rep.*, 2016, **6**, 36078.
- 31 J. W. Jeon, *et al.*, Carbonization of carboxylate-functionalized polymers of intrinsic microporosity for water treatment, *Macromol. Chem. Phys.*, 2020, **221**(5), 1900532.
- 32 M. L. Jue, V. Breedveld and R. P. Lively, Defect-free PIM-1 hollow fiber membranes, *J. Membr. Sci.*, 2017, **530**, 33–41.
- 33 L. Hao, J. Zuo and T.-S. Chung, Formation of defect-free polyetherimide/PIM-1 hollow fiber membranes for gas separation, *AIChE J.*, 2014, **60**(11), 3848–3858.
- 34 J. Heo, *et al.*, Controlled pore evolution during phase inversion from the combinatorial non-solvent approach: application to battery separators, *J. Mater. Chem. A*, 2016, **4**(24), 9496–9501.
- 35 T. A. Geleta, *et al.*, Recent advances on the fabrication of antifouling phase-inversion membranes by physical blending modification method, *Membranes*, 2023, **13**(1), 1–53.



- 36 N. Du, *et al.*, Linear high molecular weight ladder polymer via fast polycondensation of 5,5',6,6'-tetrahydroxy-3,3,3',3'-tetramethylspirobisindane with 1,4-dicyanotetrafluorobenzene, *Macromol. Rapid Commun.*, 2008, **29**(10), 783–788.
- 37 P. M. Budd, *et al.*, Solution-processed, organophilic membrane derived from a polymer of intrinsic microporosity, *Adv. Mater.*, 2004, **16**(5), 456–+.
- 38 A. B. Foster, *et al.*, Understanding the topology of the polymer of intrinsic microporosity PIM-1: cyclics, tadpoles, and network structures and their impact on membrane performance, *Macromolecules*, 2020, **53**(2), 569–583.
- 39 M. Mulder, Materials and material properties, in *Basic Principles of Membrane Technology*, ed. M. Mulder, Springer Netherlands, Dordrecht, 1996, pp. 22–70.
- 40 X. Tan and D. Rodrigue, A review on porous polymeric membrane preparation. Part I: production techniques with polysulfone and poly(vinylidene fluoride), *Polymers*, 2019, **11**(7), 1–39.
- 41 V. Abetz, Isoporous block copolymer membranes, *Macromol. Rapid Commun.*, 2015, **36**(1), 10–22.
- 42 K. Kimmerle and H. Strathmann, Analysis of the structure-determining process of phase inversion membranes, *Desalination*, 1990, **79**(2), 283–302.
- 43 K. V. Peinemann, V. Abetz and P. F. Simon, Asymmetric superstructure formed in a block copolymer via phase separation, *Nat. Mater.*, 2007, **6**(12), 992–996.
- 44 S. Shishatskiy, *et al.*, Polyimide asymmetric membranes for hydrogen separation: influence of formation conditions on gas transport properties, *Adv. Eng. Mater.*, 2006, **8**(5), 390–397.
- 45 J. Grünauer, *et al.*, Scalable application of thin film coating techniques for supported liquid membranes for gas separation made from ionic liquids, *J. Membr. Sci.*, 2016, **518**, 178–191.
- 46 G. Rácz, *et al.*, Theoretical and experimental approaches of liquid entry pressure determination in membrane distillation processes, *Period. Polytech., Chem. Eng.*, 2014, **58**(2), 81–91.
- 47 S. Claramunt, *et al.*, Membranes for the gas/liquid phase separation at elevated temperatures: characterization of the liquid entry pressure, *Membranes*, 2021, **11**(12), 1–15.
- 48 E. Caliskan, *et al.*, Investigation of the side chain effect on gas and water vapor transport properties of anthracene-maleimide based polymers of intrinsic microporosity, *Polymers*, 2021, **14**(1), 1–25.
- 49 J. Lilleparg, *et al.*, Multicomponent network formation in selective layer of composite membrane for CO₂ separation, *Membranes*, 2021, **11**(3), 1–16.
- 50 S. Wang, *et al.*, Designing intrinsically microporous polymer (PIM-1) microfibers with tunable morphology and porosity via controlling solvent/nonsolvent/polymer interactions, *ACS Appl. Polym. Mater.*, 2020, **2**(6), 2434–2443.
- 51 W. F. Yong, *et al.*, High performance PIM-1/matrimid hollow fiber membranes for CO₂/CH₄, O₂/N₂ and CO₂/N₂ separation, *J. Membr. Sci.*, 2013, **443**, 156–169.
- 52 Z. Chen, *et al.*, Study on structure and vacuum membrane distillation performance of PVDF membranes: II. Influence of molecular weight, *Chem.-Eng. J.*, 2015, **276**, 174–184.
- 53 C. Zhou, *et al.*, Effect of polyethersulfone molecular weight on structure and performance of ultrafiltration membranes, *Ind. Eng. Chem. Res.*, 2010, **49**(20), 9988–9997.
- 54 T. Miyano, T. Matsuura and S. Sourirajan, Effect of polymer molecular weight, solvent and casting solution composition on the pore size and the pore size distribution of polyethersulfone(victrix)membrane, *Chem. Eng. Commun.*, 2010, **95**(1), 11–26.
- 55 M. Haponska, *et al.*, PVDF membrane morphology-influence of polymer molecular weight and preparation temperature, *Polymers*, 2017, **9**(12), 1–14.
- 56 A. I. Cirillo, G. Tomaiuolo and S. Guido, Membrane fouling phenomena in microfluidic systems: from technical challenges to scientific opportunities, *Micromachines*, 2021, **12**, 1–36.
- 57 J. Gyura, Z. Šereš and M. Eszterle, Influence of operating parameters on separation of green syrup colored matter from sugar beet by ultra- and nanofiltration, *J. Food Eng.*, 2005, **66**(1), 89–96.
- 58 D. Wei, M. Hossain and Z. Saleh, Separation of polyphenolics and sugar by ultrafiltration: effects of operating conditions on fouling and diafiltration, *Int. J. Chem. Biomol. Eng.*, 2013, **1**, 10–17.
- 59 K. Karakulski, M. Gryta and M. Sasim, Production of process water using integrated membrane processes, *Chem. Pap.*, 2006, **60**(6), 416–421.
- 60 T. S. Hung, *et al.*, Confounding effect of wetting, compaction, and fouling in an ultra-low-pressure membrane filtration: a review, *Polymers*, 2022, **14**(10).
- 61 B. Qiu, *et al.*, Thin film nanocomposite membranes of PIM-1 and graphene oxide/ZIF-8 nanohybrids for organophilic pervaporation, *Sep. Purif. Technol.*, 2022, **299**, 121693.
- 62 N. A. Belov, *et al.*, Hydrophobic-hydrophilic properties and characterization of PIM-1 films treated by elemental fluorine in liquid perfluorodecalin, *Polymers*, 2022, **14**(23), 1–14.
- 63 I. O. Odidi, J. M. Newton and G. Buckton, The effect of surface treatment on the values of contact angles measured on a compressed powder surface, *Int. J. Pharm.*, 1991, **72**(1), 43–49.
- 64 O. Serenko, Z. Nizamova, M. Kalinin, Y. Ostrovsky, L. Polukhina and A. Muzafarov, Effect of the morphology of leather surface on the hydrophobic-hydrophilic properties, *Adv. Mater. Phys. Chem.*, 2014, **4**(2), 13–19.
- 65 J. Geens, B. Van der Bruggen and C. Vandecasteele, Characterisation of the solvent stability of polymeric nanofiltration membranes by measurement of contact angles and swelling, *Chem. Eng. Sci.*, 2004, **59**(5), 1161–1164.
- 66 H. Molisak-Tolwinska, A. Wencel and Z. Figaszewski, Impedance of polypropylene membranes hydrophelized with ethyl alcohol, *J. Macromol. Sci., Part A: Pure Appl. Chem.*, 1997, **34**(8), 1413–1427.
- 67 H. Molisak-Tolwinska, A. Wencel and Z. Figaszewski*, The effect of hydrophilization of polypropylene membranes



- with alcohols on their transport properties, *J. Macromol. Sci., Part A Pure Appl. Chem.*, 1998, **35**(5), 857–865.
- 68 J. Kochan, *et al.*, Impact of wetting agents on the filtration performance of polymeric ultrafiltration membranes, *Desalination*, 2009, **241**(1), 34–42.
- 69 S. H. Liu, *et al.*, A polyethersulfone-bisphenol sulfuric acid hollow fiber ultrafiltration membrane fabricated by a reverse thermally induced phase separation process, *RSC Adv.*, 2018, **8**(14), 7800–7809.
- 70 H. Susanto, N. Stahra and M. Ulbricht, High performance polyethersulfone microfiltration membranes having high flux and stable hydrophilic property, *J. Membr. Sci.*, 2009, **342**(1–2), 153–164.
- 71 N. I. M. Nawî, *et al.*, Polyvinylidene fluoride membrane *via* vapour induced phase separation for oil/water emulsion filtration, *Polymers*, 2021, **13**(3), 1–17.
- 72 Y. Yu, *et al.*, Multifunctionalization of PTFE membrane surface for biofouling resistance and oil/water separation performance improvement, *J. Environ. Chem. Eng.*, 2023, **11**(1), 1–10.
- 73 A. L. McGaughey and A. E. Childress, Wetting indicators, modes, and trade-offs in membrane distillation, *J. Membr. Sci.*, 2022, **642**, 119947.
- 74 H. Chamani, *et al.*, Pore wetting in membrane distillation: a comprehensive review, *Prog. Mater. Sci.*, 2021, **122**, 100843.
- 75 T. Loimer, K. Setnickova and P. Uchytíl, Consideration of the Joule-Thomson effect for the transport of vapor through anodic alumina membranes under conditions of capillary condensation, *Sep. Purif. Technol.*, 2019, **215**, 548–556.
- 76 S. T. Oyama, *et al.*, Review on mechanisms of gas permeation through inorganic membranes, *J. Jpn. Pet. Inst.*, 2011, **54**(5), 298–309.
- 77 D. Lee and S. T. Oyama, Gas permeation characteristics of a hydrogen selective supported silica membrane, *J. Membr. Sci.*, 2002, **210**(2), 291–306.
- 78 B. Topuz and M. Çiftçioğlu, Sol-gel derived mesoporous and microporous alumina membranes, *J. Sol Gel Sci. Technol.*, 2010, **56**(3), 287–299.
- 79 K. Fu, *et al.*, Efficient estimation of permeate flux of asymmetric ceramic membranes for vacuum membrane distillation, *Molecules*, 2022, **27**(3), 1–12.
- 80 J. Lyu, *et al.*, Separation and purification using GO and r-GO membranes, *RSC Adv.*, 2018, **8**(41), 23130–23151.



5.3. Article 3: Comparative study of polymer of intrinsic microporosity-derivative polymers in pervaporation and water vapor permeance applications

Authors: Esra Caliskan, Sergey Shishatskiy, Volkan Filiz

In the last study of this dissertation, the gas and water vapor permeability of PIM-based TFC membranes were investigated by “pervaporation” and “pressure increase” methods and compared with “time lag” measurements which were obtained from first study. TFC membranes were prepared using PIM-1 and homopolymers modified with rigid and bulky aliphatic side groups which aimed to increase the free volume. Another substituent which is an aromatic group was used to investigate the water affinity. The permeance of CO₂, H₂, CH₄ and water vapor was analyzed by the “pressure increase” method and 20-hour aging behavior was studied. Pervaporation experiments showed higher water vapor transport compared to the “pressure increase” method. The results obtained from “time lag” and “pervaporation” tests showed similar trends.

5.3.1. Author contributions

Esra Caliskan (E.C.), Sergey Shishatskiy (S.S.), Volkan Filiz (V.F.)

Table 13: List of contribution: Publication-3

| Contribution | Authors | | |
|-----------------------------------|---------|------|------|
| | E.C. | S.S. | V.F. |
| First author | + | | |
| Corresponding author | | | + |
| Methodology and conceptualization | + | + | |
| Experimental work | + | | |
| Material characterization | + | | |
| Investigation | + | | |
| Writing original draft | + | | |
| Writing-reviewing and editing | + | + | + |
| Scientific supervision | | + | + |

5.3.2. Funding and acknowledgements

This work had financial support from the Federal Ministry of Education and Research of Germany (BMBF) via the project NAMED (FKZ: 03XP0151A).

The authors gratefully thank to Silvio Neumann for his great support for polymerization of homopolymers and copolymers; Carsten Scholz for his kind help for pervaporation test installment.

5.3.3. Publication

Article

Comparative Study of Polymer of Intrinsic Microporosity-Derivative Polymers in Pervaporation and Water Vapor Permeance Applications

Esra Caliskan, Sergey Shishatskiy and Volkan Filiz



Article

Comparative Study of Polymer of Intrinsic Microporosity-Derivative Polymers in Pervaporation and Water Vapor Permeance Applications

Esra Caliskan , Sergey Shishatskiy  and Volkan Filiz * 

Institute of Membrane Research, Helmholtz-Zentrum Hereon, Max-Planck-Str. 1, 21502 Geesthacht, Germany; esra.caliskan@hereon.de (E.C.); sergey.shishatskiy@hereon.de (S.S.)

* Correspondence: volkan.filiz@hereon.de; Tel.: +49-41-5287-2425

Abstract: This study assesses the gas and water vapor permeance of PIM-derivative thin-film composite (TFC) membranes using pervaporation and “pressure increase” methods, and provides a comparative view of “time lag” measurements of thick films obtained from our previous work. In this study, TFC membranes were prepared using PIM-1 and homopolymers that were modified with different side groups to explore their effects on gas and water vapor transport. Rigid and bulky aliphatic groups were used to increase the polymer’s free volume and were evaluated for their impact on both gas and water transport. Aromatic side groups were specifically employed to assess water affinity. The permeance of CO₂, H₂, CH₄ and water vapor through these membranes was analyzed using the ‘pressure increase’ method to determine the modifications’ influence on transport efficiency and interaction with water molecules. Over a 20 h period, the aging and the permeance of the TFC membranes were analyzed using this method. In parallel, pervaporation experiments were conducted on samples taken independently from the same membrane roll to assess water flux, with particular attention paid to the liquid form on the feed side. The significantly higher water vapor transport rates observed in pervaporation experiments compared to those using the “pressure increase” method underline the efficiency of pervaporation. This efficiency suggests that membranes designed for pervaporation can serve as effective alternatives to conventional porous membranes used in distillation applications. Additionally, incorporating “time lag” results from a pioneering study into the comparison revealed that the trends observed in “time lag” and pervaporation results exhibited similar trends, whereas “pressure increase” data showed a different development. This discrepancy is attributed to the state of the polymer, which varies significantly depending on the operating conditions.

Keywords: polymers of intrinsic microporosity (PIM-1); membranes; gas and vapor permeance; pervaporation



Citation: Caliskan, E.; Shishatskiy, S.; Filiz, V. Comparative Study of Polymer of Intrinsic Microporosity-Derivative Polymers in Pervaporation and Water Vapor Permeance Applications. *Polymers* **2024**, *16*, 2932. <https://doi.org/10.3390/polym16202932>

Academic Editor: Francesco Galiano

Received: 17 September 2024

Revised: 10 October 2024

Accepted: 14 October 2024

Published: 18 October 2024



Copyright: © 2024 by the authors. Licensee MDPI, Basel, Switzerland. This article is an open access article distributed under the terms and conditions of the Creative Commons Attribution (CC BY) license (<https://creativecommons.org/licenses/by/4.0/>).

1. Introduction

One of the most important issues of this century is access to clean water. Factors such as climate change, global population growth, and industrialization issues are increasingly straining water resources, while freshwater reserves and traditional energy sources are rapidly depleting. It is therefore crucial to develop energy-efficient water treatment technologies that are able to utilize energy from renewable sources such as wind and solar light, thus reducing environmental impacts [1–3]. Membrane technology, recognized for its high energy efficiency and low carbon footprint, has garnered significant attention for water treatment applications. Its advantages include easy operability and low cost when compared to traditional thermal processes. Membranes are widely used in all technological stages of the water treatment process starting from micro- and ultrafiltration and up to nanofiltration and reverse osmosis. The last two processes give high-quality water but

are energy-intensive [4–6]. The relatively new process of membrane distillation offers high-quality water production and can utilize lower-quality water sources compared to methods like reverse osmosis. Water desalination is one of the areas where membrane distillation has been used effectively. In recent applications in desalination, it has proven to be particularly effective in producing high-quality fresh water from brackish sources using waste heat from adjacent industrial processes [7,8]. For example, several desalination plants in Middle East regions rich in solar energy resources have integrated solar-powered membrane distillation systems to maximize the use of renewable waste heat [9]. Additionally, desalination requires a lower grade of energy, even allowing for the use of waste heat, to carry out the separation process. It is usual practice to use porous membranes for this process, which requires one to face certain drawbacks such as, e.g., fouling of the porous structure with organic or inorganic matter present in the feed water causing water breakthrough through the membrane and compromising the product. It is considered favorable to develop a new type of membrane with a highly permeable, hydrophobic, defect-free selective layer, which would provide high water flux through the membrane and would not allow any impurities of biological or inorganic nature to move through it [10–12].

One of the widely studied polymer types are polymers of intrinsic microporosity (PIMs). These polymers have received considerable attention in recent years due to their very high free volume, making them desirable for gas separation applications [13]. Despite the primary application of PIM-1 in dense films for gas separation due to its intrinsic microporosity and solvent resistance, its unusual properties have led researchers to explore different membrane preparations and applications, such as pervaporation for toluene recovery [14] or alcohol–water separation [15,16]. In addition to pervaporation, previous studies have explored various modifications of PIM-1 for nanofiltration. One study enhanced water flow by carbonizing PIM-1, while another developed carboxylate-functionalized PIM-1 for similar purposes [17,18].

In our previous study, the hydrophobic and high-free-volume PIM-1 polymer was examined for the possibility to fabricate a porous membrane via the phase-inversion process and its suitability in membrane distillation (MD), which was shown to be promising [19]. Additionally, a thin-film composite (TFC) membrane was formed by deposition of PIM-1 selective layer formation on a PAN ultrafiltration membrane as a support, and its water permeance was compared with that of the porous PIM-1 membrane. While the porous membrane exhibited a higher water vapor permeance of $100 \text{ m}^3(\text{STP}) \text{ m}^{-2} \text{ h}^{-1} \text{ bar}^{-1}$, the TFC membrane displayed a considerable vapor permeance of $35 \text{ m}^3(\text{STP}) \text{ m}^{-2} \text{ h}^{-1} \text{ bar}^{-1}$. Additionally, in another study [20], our research group utilized a set of anthracene maleimide monomers with aliphatic side groups of varying sizes and shapes as precursors for a series of polymer of intrinsic microporosity (PIM)-based homopolymers. These side groups, which did not exceed 7% of the monomer's molecular weight, were investigated for their effect on the gas transport properties of homopolymers. It was observed that particularly the bulky side groups significantly enhanced the gas transport. Accordingly, the permeability coefficients for CO_2 and CH_4 in isotropic films made from the homopolymer derived from the *t*-butyl substituted comonomer (*t*-butyl-100) were the highest among the studied homopolymers.

Building upon aforementioned research, the current study investigates the formation of TFC membranes with a selective layer made of anthracene maleimide-modified PIM homopolymers to examine how polymer gas and water vapor transport properties are retained or altered upon transformation into thin layers, and how these properties change with time. Characterized by minimal polymer usage per unity of membrane surface due to the formation of exceptionally thin selective layers, TFC membranes are widely adopted in industrial gas and water vapor separation applications. This paper utilizes the “pressure increase” method to determine water vapor, carbon dioxide, hydrogen, and methane permeances, allowing for a detailed comparison of the permeation properties of TFC membranes and thick isotropic films reported earlier. Additionally, this study evaluates

how TFC membrane permeance evolves over time in relation to the nature of the penetrant and of the chemical composition of the polymer of the selective layer. Therefore, the research aims to explore how the side groups of these polymers affect membranes' physical aging and overall performance in applications such as pervaporation and general water vapor permeation. By comparing the properties of thin-film composite membranes to those of previously studied PIM membranes, this paper seeks to determine whether modifications in side groups can enhance membrane performance and mitigate the challenges posed by physical aging.

The analysis is enriched by including data from pervaporation experiments, providing a framework to assess vapor permeation data from both pervaporation and "pressure increase" methods. The study addresses challenges in data comparison between these two methods due to differences in measurement units. Moreover, the use of saturated vapor pressure in pervaporation experiments suggests significantly higher permeance values compared to those from "pressure increase" experiments, highlighting the need for an understanding of membrane behavior at the interface where water transitions from a liquid to a vapor state [21]. This dynamic is critical as it implies a potential disparity in how membranes behave under different operational conditions and measurement setups [22]. Overall, this study explores how changes at the molecular level affect the macroscopic properties of membranes, particularly their longevity and efficiency in separation processes. The outcomes could lead to an improved membrane separation process for water treatment technologies that is better suited to meet the demands of modern industrial applications.

2. Materials and Methods

2.1. Materials

5,5',6,6'-tetrahydroxy-3,3,3',3'-tetramethyl-1,1'-spirobisindane (TTSBI, 98%) was purchased from ABCR GmbH (Karlsruhe, Germany). 2,3,5,6-tetrafluoro-terephthalonitrile (TFTPN, 99%) was obtained from Lanxess (Cologne, Germany). TFTPN was sublimated twice at 70 °C under vacuum before use. Potassium carbonate (K_2CO_3 , 99%) and dimethyl acetamide (DMAc, 99%) were purchased from Alfa Aesar (Karlsruhe, Germany). All other commercially available reagents were obtained from Merck (Darmstadt, Germany) and were used without further treatment.

2.2. Synthesis of Polymers

2.2.1. PIM-1 Synthesis

PIM-1 was produced utilizing a rapid synthesis technique as previously described [20,23]. A mixture of TTSBI (20 mmol) and TFTPN (20 mmol) was prepared in a three-necked round bottom flask, dissolved in 65 mL of dimethylacetamide (DMAc) under an argon atmosphere. The addition of K_2CO_3 (44 mmol) changed the color of the reaction from orange to yellow. The flask was then quickly placed in an oil bath preheated to 150 °C. To prevent PIM-1 precipitation and enhance the formation of a higher-molecular-weight polymer, diethylbenzene (DEB) (15 mL) was added gradually. After stirring the mixture for 30 min, the reaction was stopped by precipitating the mixture in methanol. The precipitated solid was filtered and dried at 80 °C under vacuum. This dried polymer was then dissolved in $CHCl_3$, re-precipitated in methanol, collected by filtration, and dried at 80 °C under high vacuum to yield the final yellow solid product with a 90% yield. The molecular weight (Mw) and dispersity (\bar{D}) of the purified polymer were determined using size-exclusion chromatography, resulting in an Mw of 132.5 kg/mol and a \bar{D} of 4.9.

2.2.2. Synthesis of Homopolymers

The synthesis and characterization of anthracene maleimide-structured bulky and linear group monomers, as well as the homopolymers derived from these monomers, were reported in our previous study [20]. Accordingly, the homopolymer series was synthesized through the polycondensation of comonomers, which are essentially TTSBI substitutions, with TFTPN using a method akin to that employed for PIM-1 synthesis. These comonomers

were specifically modified by incorporating an anthracene maleimide structure with various aliphatic side groups. The detailed synthesis scheme is provided in Figure 1. The nomenclature for homopolymers was adapted from the reference study. In order to clarify the nomenclature of the homopolymers used in this study, they were identified as methyl-/propyl-/i-propyl-/t-butyl-/phenyl-100. The suffix “-100” represents the comonomer indicating that, for example, methyl-100 comprises 100 mol% comonomer unit.

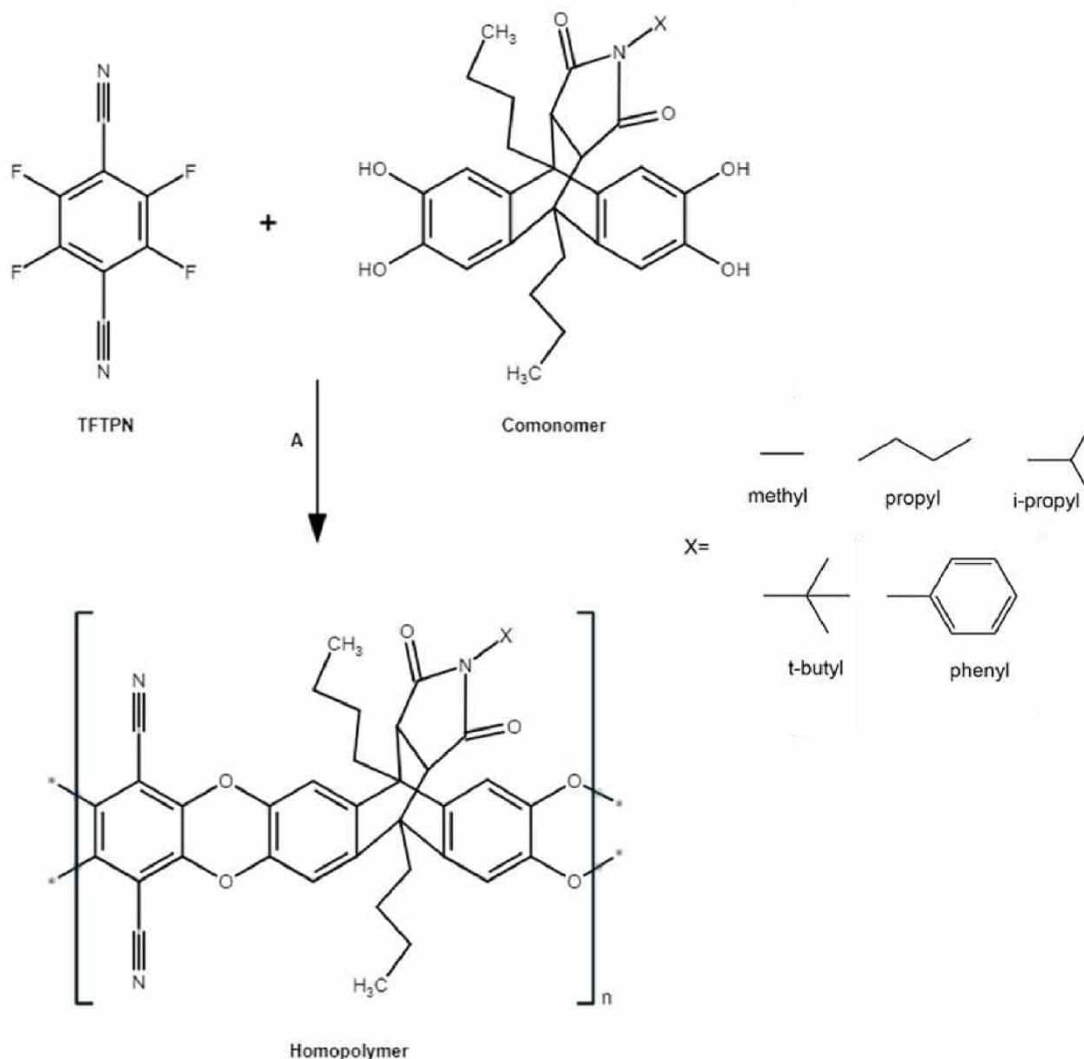


Figure 1. Synthesis of homopolymer. A: reagents and conditions DMAc, K_2CO_3 , 150 °C, 30–60 min.

2.3. Preparation of Thin-Film Composite (TFC) Membranes

The fabrication of the TFC membrane was carried out using a widely adopted dip-coating technique, the most used for TFC membrane formation [24]. This method entailed placing the porous substrate in contact with the polymer solution, then uniformly withdrawing it from the solution at a predetermined speed to ensure an even coating of the polymer solution on the ultrafiltration (UF) membrane used as a support for a selective layer. In our experiment, a dense selective layer of PIM-1 or homopolymer was applied over a porous polyacrylonitrile (PAN) UF membrane using an in-house-designed laboratory scale membrane casting machine. A 1% wt. solution of polymer in THF was prepared, which upon filtration was poured into a uniquely designed bath. Subsequently, the PAN membrane was aligned with this solution. A consistent meniscus of the polymer solution

was formed between the solution surface and PAN membrane by slightly lowering the bath by about 2 mm. By drawing the porous substrate out of the meniscus at a fixed pace, a thin film of the solution was formed on the support's surface. The drying of the TFC membrane was conducted at ambient conditions, letting the solvent evaporate freely without any active control over the process. This step was performed in an enclosure with substantial low-humidity air flow to prevent the accumulation of solvent vapors around the casting device, aside from the immediate area of the polymer solution bath. The prepared membrane was dried for 1 h before gas transport experiments by the "pressure increase" or pervaporation methods were conducted.

2.4. Characterization Methods

2.4.1. Size Exclusion Chromatography (SEC)

Size exclusion chromatography (SEC) analyses were conducted at 30 °C using chloroform (CHCl_3) as the solvent. The chromatographic setup included a series of columns: a precolumn-SDV-linear, an SDV-linear, and an SDV with a 102 nm pore size, each having an inner diameter of 4.6 mm and a length of 53 cm, supplied by Polymer Standard Service GmbH, Mainz, Germany. The flow rate was maintained at 1.0 mL per minute. To detect the concentration of polymers, both refractive index (RI) and ultraviolet (UV) detectors were utilized. Calibration with polystyrene standards allowed for the determination of the apparent weight average molecular weight (M_w) and the dispersity index (\bar{D}) of the synthesized polymers.

2.4.2. Gas and Water Vapor Permeance Measurements: "Pressure Increase" Method

Gas transport properties of thin-film composite (TFC) membranes were measured using a "pressure increase" method, which follows the "constant volume/variable pressure" principle as described elsewhere [25,26]. This technique is especially suitable for membranes with thin selective layers and allows for the investigation of membrane permeances in a wide range of feed pressures and temperatures. Additionally, this method was utilized for water vapor transport studies in TFC membranes under controlled conditions (40 °C, feed vapor pressure below 60 kPa, permeate pressure 1–13 mbar), and the permeance from at least ten measurements were averaged. One limitation of this method is that it cannot assess vapor permeance in saturated vapor conditions because the setup isolates the gas or vapor in the feed vessel from any external supply, leading to a slight pressure drop at the start. This pressure drop prevents the execution of experiments with vapors at activities above 90%. However, isolating the feed volume from the supply line allows experiments to be conducted over a wide range of vapor activities, decreasing from high to low. The lowest feed vapor activity to be investigated is determined by the initial conditions of the experiment. The program conducting the experiment is set to measure the permeance value by collecting penetrant on the permeate side of the setup, within a range of 1 to 10 mbar. This final value determines the lowest feed pressure, as the program is designed to stop the experiment when the feed pressure equals the desired permeate pressure. However, this feature provides vital insights into membrane performance as feed pressure decreases, which is essential for studying substances that are highly soluble or prone to condensation [19,27].

2.4.3. Water Vapor Permeance Measurement: Pervaporation Method

Pervaporation is a separation technique which utilizes the semi-permeable membrane for preferable selective transport of penetrants that are in the liquid phase on the feed side and the gas phase (vapor) on the permeate side, meaning that liquid evaporation occurs on the immediate interphase of the liquid and feed side of the membrane. The driving force for the vapor transport arises from a chemical potential gradient between feed and permeate sides of membranes created by the application of a vacuum or sweep gas to the permeate side of the membrane causing efficient vapor withdrawal [28]. In this study, pervaporation experiments were performed in addition to the "pressure increase"

experiment to provide a comprehensive analysis of membrane performance under different operational conditions with the aim of covering a wide range of feed vapor activity, starting from 100% activity for the case of pervaporation and going from ca. 90 to ca 20% activity in the case of the “pressure increase” experiment. Pervaporation, involving a phase change from liquid to vapor across the membrane, offers distinct insights into the membrane’s efficiency where liquid water is present on the feed side. It is important to note that one of the highlights of this study is the analysis of two water phases, vapor and liquid, that contact the film surface and how this interaction influences vapor transport. Figure 2 shows the schematic flow chart of the pervaporation facility used in this study. A circulation pump provides liquid water circulation from the water tank through the measurement cell containing the membrane under study and back to the water tank. On the permeate side of the measurement cell, a pressure sensor is installed to monitor permeate pressure during the experiment, while the permeate stream is directed into a cold trap cooled with liquid nitrogen for water condensation. To protect the vacuum pump from moisture during the changing of the permeate cold trap, a second cold trap is included in a bypass line. During each measurement session for each membrane sample, 10 measurement points were recorded, with permeate water collected into a cold trap for 5 min at each point. Approximately 15 min were spent between consequent measurements: 5 min for the permeate collection and an additional 10 min to prepare the system for the next measurement, including exchange, evacuation, and accommodation of the new trap to liquid nitrogen temperature. This timing of the experimental sequence is crucial as it was thought to provide an indication of membrane properties’ changes during the experiments. In total, it takes ca. two hours to complete the pervaporation experiment for one membrane. It was assumed that the feed side vapor pressure was 70 mbar, taken as a saturated vapor state at 40 °C, and permeate vapor pressure was considered zero since the vacuum was provided by a rotary pump and additionally by the liquid nitrogen temperature of the cold permeate trap.

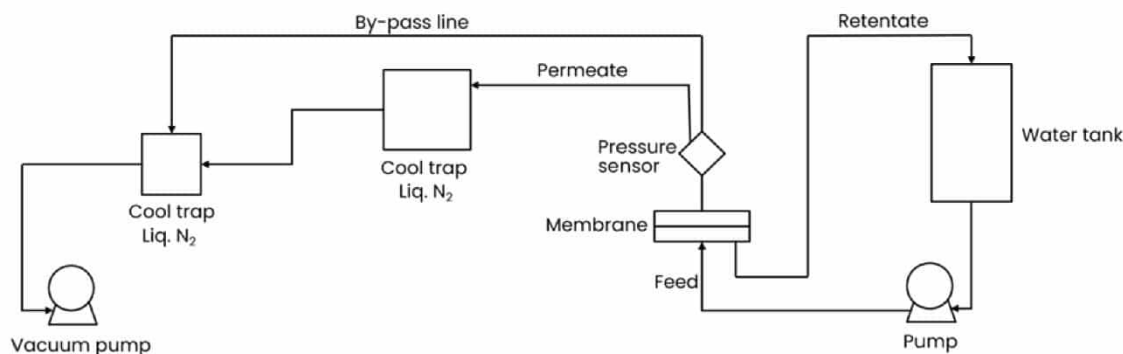


Figure 2. Schematic flow chart of pervaporation.

3. Result and Discussion

3.1. Membrane Formation

The aim of this study was to develop a defect-free TFC membranes by coating a thin dense layer on a porous substrate using anthracene maleimide-modified PIM homopolymers with different side groups initially synthesized and studied as thick isotropic films [20]. We successfully prepared selective TFC membranes using the same coating procedure for each homopolymer.

Typically, any defect in the membrane leading to unintended gas flow through pores would result in a noticeable decrease in the ideal selectivity. However, there was no such decrease in selectivity in the experiments based on the example of CO₂/CH₄ selectivity as shown in Table S1. It was considered important to keep all parameters consistent during the experiments to make sure the results are reliable and comparable. In this study, attention was given to forming TFC membranes in the same conditions and with the same

post-formation treatment, using the same equipment and using the same experimental conditions for all the tests. This careful approach helped avoid errors that could skew the results, ensuring that any observed differences are due to the variables being tested rather than inconsistencies in the setup. This makes the findings accurate and reproducible, providing a solid basis for evaluating the performance and properties of membranes.

3.2. Transport Properties of TFC Membranes

3.2.1. Gas and Water Vapor Permeances by “Pressure Increase” Method

In the Results and Discussion section of our study, we provide a detailed analysis of the permeance decay observed for penetrants—water vapor (H_2O), carbon dioxide (CO_2), hydrogen (H_2), and methane (CH_4)—for thin-film composite membranes studied over a period of at least 20 h. The selection of penetrants for this study was based on specific criteria: H_2O transport was the primary focus, while H_2 , CO_2 , and CH_4 were chosen for their wide range of kinetic diameters and differing interactions with the polymer. Analyzing these variations helps us understand the aging processes in the polymer’s selective layer. For all studied membranes, the order in which penetrants were applied to the membrane sample was the same: CH_4 , H_2 , CO_2 , H_2O . Water, even being close to the saturation state, was considered as penetrant and not able to change the state of the polymer of the selective layer due to, e.g., the formation of molecule clusters within the free-volume elements and, thus, no investigation on this matter was carried out [29,30]. The measurement method involved exposing the membranes to a high vacuum, provided by the turbomolecular pumping unit, for full penetrant desorption during the multiple gas change procedures, which did not occur during the pervaporation experiment and can be a trigger for the fast aging process in the selective layer. As mentioned above, each TFC membrane sample was continuously studied for gas and water vapor transport properties during the period of at least 20 h with multiple full evacuations and exposures to different penetrants and, after this, the sample was removed from the experimental facility. Once removed from the experimental setup, the membrane sample could not be reused due to potential damage to the selective layer. This damage could occur from detaching the layer from the UF support or removing the O-ring from the membrane surface.

In our initial study [20], we observed that the introduction of maleimide derivatives with various side chain groups significantly influenced water vapor transport through the studied polymers. This effect was primarily due to the polymer polarity change caused by the imide groups, which altered facilitated hydrogen bonding with water molecules’ interaction with polymers. These observations were made for the case of dense thick films of homopolymers, where it was noted that the polymers with the “-methyl” side group exhibited the highest water permeability. The “-methyl” side group, having the shortest alkyl side chain, impacted the polymer polarity the most among those tested. The increase in the number of carbon atoms in linear alkyl side groups was found to decrease water permeability.

When compared with examples where linear alkyl groups were replaced with bulkier groups such as “-i-propyl” or “-t-butyl”, it was observed that bulky, in comparison to “-methyl”, side groups influenced both diffusivity and solubility and, hence, gas permeability. The introduction of bulky groups significantly increased the free volume, which consequently increased the diffusion coefficient.

In this study, the experimental results obtained for TFC membranes with selective layers of homopolymers show differences from those obtained for thick isotropic films. Figure 3 shows the gas permeance decay of each homopolymer-based TFC membrane observed over the span of 20 h. The complete measurements for each TFC membrane can be found in Figure S1.

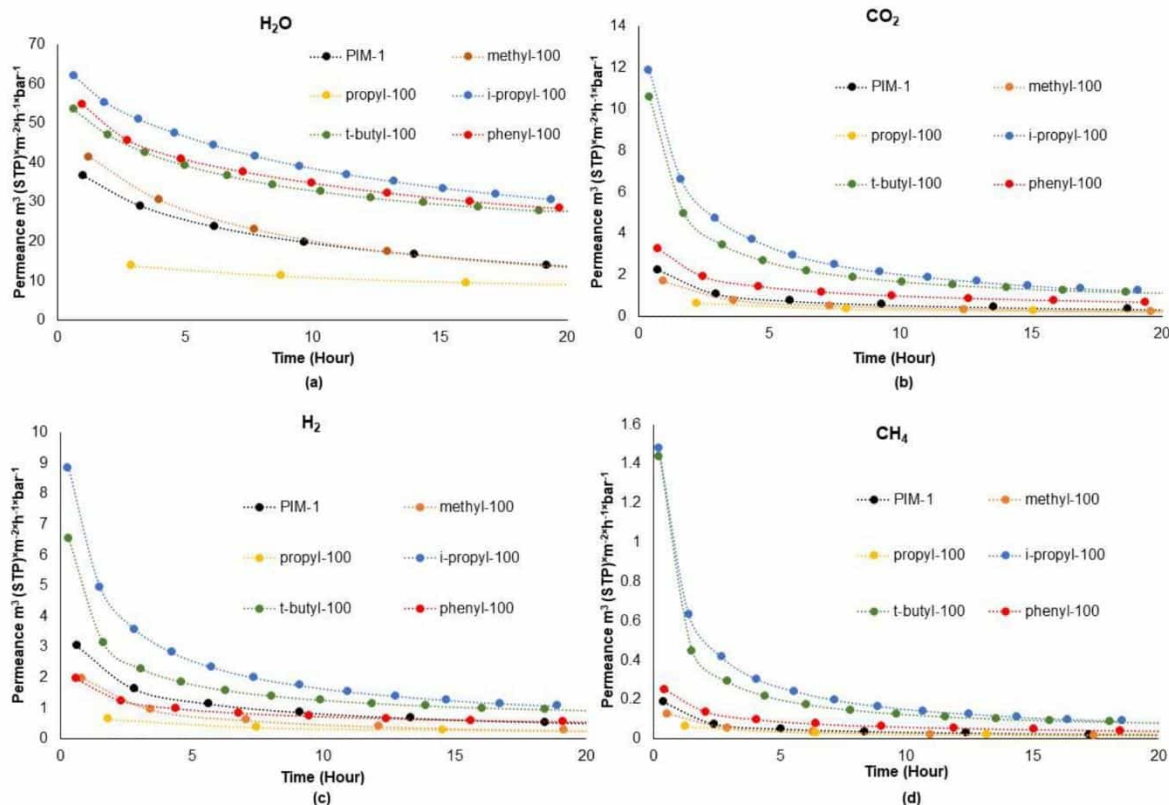


Figure 3. Gas and water vapor permeances of TFC membranes over 20 h. (a) water permeance, (b) carbon dioxide permeance, (c) hydrogen permeance, (d) methane permeance.

Among the studied TFC membranes, those with selective layers of *i*-propyl-100 and *t*-butyl-100 homopolymers exhibited the highest gas permeances. Based on their kinetic diameter, CO₂ and CH₄ are larger molecules while H₂ and H₂O are smaller in size (H₂O: 2.65 Å; H₂: 2.89 Å; CO₂: 3.3 Å; CH₄: 3.8 Å) [31]. If permeance is evaluated according to molecule size, we see that the most permeant homopolymers for CO₂ and CH₄ are *i*-propyl-100 and *t*-butyl-100. This outcome is attributed to the increased free volume created by the incorporation of bulky groups, which in turn enhances the permeance of larger molecules. Previous studies have demonstrated that incorporating bulky groups into polymers enhances their free volume [32,33]. This increase in free volume improves diffusivity, which in turn indirectly boosts gas permeability, as it is a function of diffusivity. Notably, *i*-propyl-100 and *t*-butyl-100 displayed an extremely rapid decline in permeance, which was particularly pronounced within the first two hours of observation. This sharp decrease is likely attributed to the formation of large free-volume elements due to the presence of the bulky side groups in these homopolymers and the impact of the high vacuum applied to the membrane sample during the “pressure increase” causing full degassing of the selective layer and thus enabling easier rearrangement of the free volume within these polymers. Swaidan et al. reported that polymers with bulky and rigid groups are more significantly affected by physical aging. Additionally, it was observed that H₂, with its smaller kinetic size, experiences a smaller reduction in permeance due to physical aging compared to an oxygen molecule which is larger in kinetic diameter [34]. These observations are critical for understanding the behavior of TFC membranes in different applications, particularly under conditions where rapid changes in environmental conditions or gas exposures occur.

When examining the permeance of water vapor, which is the smallest molecule among the studied penetrants, one observes that phenyl-100 is the most permeable homopolymer

after *i*-propyl-100. Due to its chemical nature, water can be considered differently in the permeance mechanism compared to other gasses. Water molecules can form hydrogen bonds with each other, creating unique scenarios during gas transport. These include the formation of clusters of water molecules and plasticization due to the interaction between water molecules and the polymer matrix. Cluster formation is prevalent in hydrophobic environments where water–polymer interaction is weak, whereas plasticization is observed when water–polymer interaction is significant [30,35]. A detailed discussion of water clustering is in the following sections of this paper. Although the homopolymers used in this study are hydrophobic due to their backbone, the phenyl side group in the phenyl-100 homopolymer enhances its affinity for water, as demonstrated by the exceptionally high solubility coefficient of H₂O in this polymer in comparison to that of other substituted homopolymers. The interaction between the aromatic ring functional group in the phenyl-100 and water is likely enhanced by possible OH- π electron interactions, as suggested in other studies [36,37]. This interaction can be expected to increase the affinity of phenyl-100 toward water. Therefore, in addition to the prominent free-volume effect observed in *t*-butyl-100 and *i*-propyl-100, the water vapor permeance of phenyl-100 is evaluated from a distinct perspective.

The variation in polymer order between gas permeances of TFC membranes and permeability coefficients of thick films used in our previous study [20] could arise from the method of TFC membrane sample preparation. Thick films of polymers were prepared by as-slow-as-possible evaporation of the solvent from the polymer solution, while TFC membrane preparation involved rapid evaporation of the organic solvent from the polymer solution layer deposited onto the porous UF membrane. The later method involves significant changes in the polymer solution temperature, while the polymer concentration changes from 1% to 100% by weight in just a few seconds due to the loss of solvent to the ambient; such drastic changes have been previously reported [38]. The change in solution temperature due to intensive evaporation and possible differences in polymer solubility in the organic solvent caused by the presence of different side groups in the polymer can be reasons for the induced difference in polymer packing when a selective layer of TFC membrane is formed.

Regarding permeance decay over time, water exhibited a much slower permeance decay rate compared to the other gasses. This slower decay suggests that either water interacts differently with the polymer matrix or its transport mechanism through the membrane is distinct from that of the other tested gasses. In contrast, CO₂, H₂, and CH₄ showed comparable rates of permeance decay. Accordingly, for the PIM-1 TFC membrane, the permeance loss for CO₂ and CH₄ within 20 h was about 7 and that for H₂ was about 5.9, while that for H₂O was only 3.9.

To further investigate the comparison of water vapor permeance with other gasses, an analysis of relative gas permeance reduction can be made by focusing on PIM-1. Figure 4 shows the decay of the relative permeances of four penetrants measured with the PIM-1 TFC membrane over 60 h. For all gasses, the most drastic permeance decrease occurs in the first 10 h. CH₄, the largest molecule, was the most affected by selective layer aging. It showed a permeance drop of up to 60% in the first two hours of measurement. This was followed by CO₂ and H₂, but H₂O showed a permeance drop of 30% in the first two hours compared to the other gasses. It has been demonstrated in previous studies that thin films are affected by physical aging much more rapidly than dense films [39,40]. In examining the relative permeance decay of gasses through the PIM-1 polymer, as shown in the graph, several key points emerge regarding the interaction between these gasses and the polymer and how these interactions affect their aging and transport properties over time.

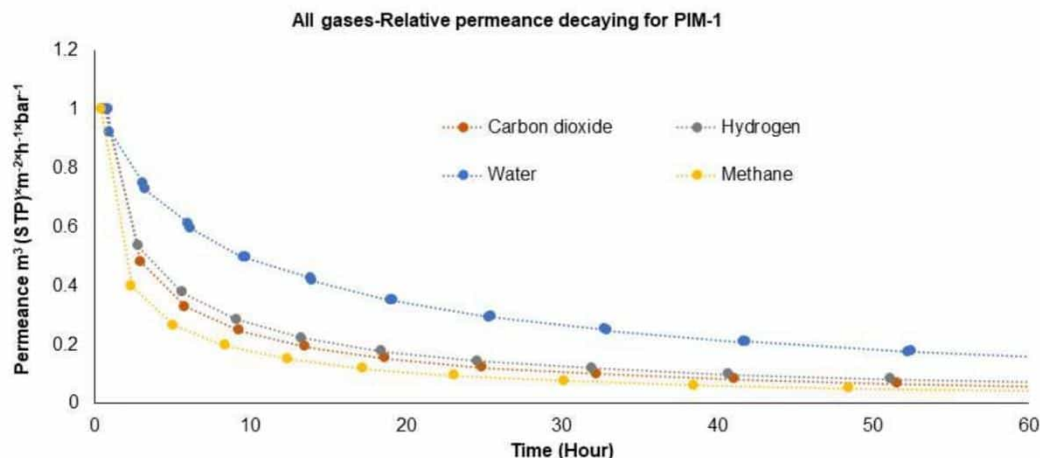


Figure 4. Decay of relative gas and water vapor permeance of PIM-1 TFC membrane.

As can be seen in the graph, water vapor exhibits a notably slower aging process compared to other gasses. This slower decay can be attributed to the highly associated nature of water molecules, which tend to form hydrogen bonds with each other. These bonds likely facilitate a more “organized” movement of water molecules through the selective layer membrane, akin to the anomalous transport behavior observed in carbon nanotubes (CNTs) [41,42], where water moves as a coordinated chain or belt. This property of water significantly impacts its permeance stability over time and can be the only explanation why H_2O molecules do not “feel” changes in the free volume. H_2 , which has a kinetic diameter very similar to that of H_2O , shows much higher permeance decay than H_2O , followed by CO_2 and, finally, CH_4 . These three gasses do not form bonds with the polymer or among themselves, which could contribute to a faster decay in their permeance as they are less able to maintain structured paths through the polymer. Moreover, CO_2 , being the most soluble of the gasses tested, demonstrates a decay pattern that, while faster than water, is slower than hydrogen and methane. The solubility of CO_2 in the polymer likely contributes to its relatively slower decay, as the gas can be absorbed more readily into the polymer matrix, thereby mitigating rapid permeance loss.

Consequently, it is important to bear in mind that the physical properties of the gasses, such as solubility and the ability to form associative interactions, play critical roles in determining how quickly the permeance decays over time through a specific polymer matrix like PIM-1. These insights are crucial for applications where the long-term stability of gas separation and transport properties are of utmost importance.

3.2.2. Vapor Activity

Another aspect that can be examined is water vapor permeance as a function of feed vapor activity. Figure 5 renders a series of plots for different homopolymers and demonstrates that the permeance of all homopolymers, including PIM-1, increases with vapor activity, which is expected as higher vapor activity generally increases the driving force for permeation. Davis et al. reported that at higher vapor activities, water molecule association increased, followed by an enhancement in water permeability [29]. Unfortunately, design limitations of the experimental facility prevent experiments at vapor activity above 90%. But the acquired data demonstrate a clear upward trend in permeance as vapor activity increases. The trend can be fitted by the exponential function with the coefficient of determination above 98%. The use of the exponential function is justified by the consideration of vapor as penetrant due to being close to the condensation, and the equation of the “Free Volume Model” can be applied instead of apparent linear regression [43]. Taking into account no significant swelling of the selective layer by water vapor, clearly indicated by small values of the exponent coefficient, and the fact that the experimental data start at 90%

of vapor activity, one can assume the validity of the applied function to be extended up to 100% activity and thus to prognose vapor permeance at saturation conditions.

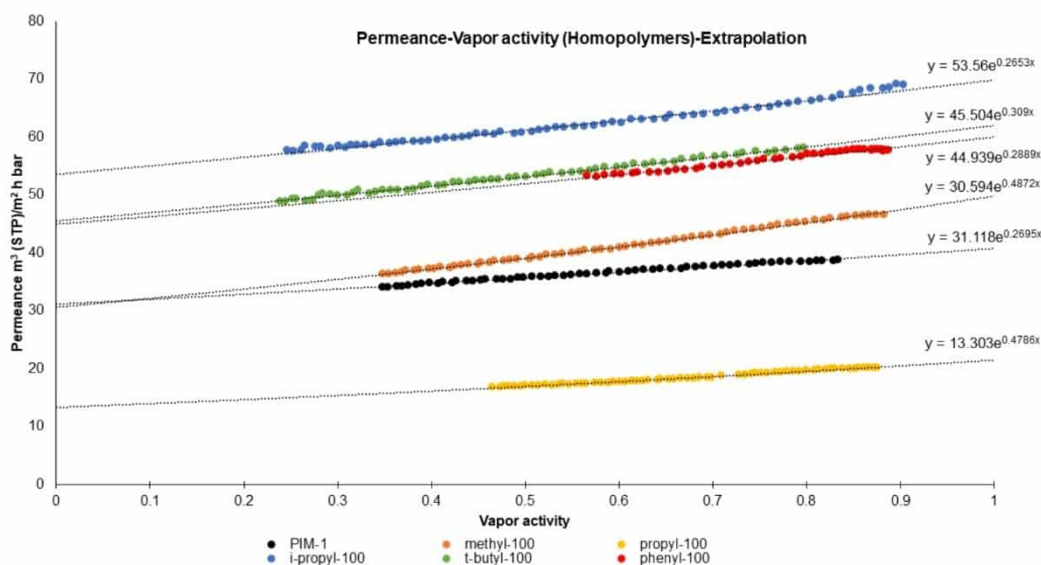


Figure 5. Vapor permeance as function of vapor activity for TFC membranes.

3.2.3. Water Permeance Measurement by Pervaporation Method

In this part, the results of pervaporation experiment will be discussed as the second method employed to investigate water vapor transport in TFC membranes. The results of the pervaporation experiment are essential to understand vapor transport through polymeric membranes at conditions of 100% relative humidity at the feed side interphase and to compare results to that obtained during the “pressure increase” experiment.

Table 1 shows the results of the pervaporation experiment for each TFC membrane. Values for each membrane are the average of 10 separate data points, collected during continuous membrane exposure to liquid H₂O over 2.5 h. The water penetrated through the membrane was collected in the cold trap, the trap was weighted on the balance and the average mass value of penetrant collected over 5 min is presented as “Water flux (g)”. In order to calculate water vapor permeance in the same dimension as in the “pressure increase” experiment, the mass was converted to the volume of vapor in STP conditions; the driving force was assumed as 70 mbar on the feed side and zero pressure on the permeate side. The calculated value is presented as “pervaporation permeance” and can be compared to the “Pressure increase permeance”, the values of which were approximated to the 100% vapor activity using fitting equations from Figure 5.

Table 1. Absolute values of converted water flux obtained by pervaporation.

| TFC Membranes | Water Flux (g) | Pervaporation Permeance m ³ (STP)/m ² × h × bar | “Pressure Increase” Permeance m ³ (STP)/m ² × h × bar |
|----------------------|----------------|--|--|
| PIM-1 | 1.65 | 98.8 | 40.7 |
| methyl-100 | 2.92 | 174.7 | 49.8 |
| propyl-100 | 1.84 | 109.9 | 21.5 |
| <i>i</i> -propyl-100 | 2.40 | 143.5 | 69.8 |
| <i>t</i> -butyl-100 | 1.77 | 105.9 | 61.8 |
| phenyl-100 | 1.98 | 94.9 | 50.0 |

The pervaporation results showed much higher values than those of the “pressure increase” measurements. The substantial difference in results prompted further exploration of the processes occurring within the membrane systems.

The discrepancy of possessing higher water flux in pervaporation than “pressure increase” measurement could be attributed to the abovementioned clustering of water molecules within the free volume of the polymers under investigation, which plays a crucial role. It is most likely that a scenario similar to the transport of water molecules in CNTs [41,42,44] is occurring in our polymer system where we operate the membranes in pervaporation. This particular transport resulting from the formation of water clusters can be explained by the fact that water molecules, owing to their small size and ability to form hydrogen bonds, exhibit a unique “dragging” effect that allows them to pass through bottlenecks between large free-volume elements without having to navigate independently through the polymer cavities [45].

In our pervaporation setup, the initial conditions are such that water molecules are already at saturation point when they encounter the free-volume elements, which differs significantly from conditions in “pressure increase” experiments. This saturation provides conditions for the formation of water molecules aggregates already on the feed/membrane interphase without the need to change the state of molecules and continues within the free-volume elements, a behavior that has been observed in studies of alcohol molecules in perfluorinated polymers, which are known for their extreme hydrophobicity [46]. It can therefore be assumed that the clustering of water molecules plays a substantial role in the transport properties observed in TFC membranes under different experimental conditions. The scope of this study was limited in terms of the availability of quantitative analysis or modeling since our current analysis remains qualitative. Further research focusing on the molecular dynamics might offer valuable insights into designing and optimizing membrane materials for specific applications where water transport efficiency is crucial. This could provide a more comprehensive understanding of the mechanisms driving permeance in thin-film composite membranes.

To understand how the membranes react to aging under two different measurement methods, it would be beneficial to analyze the time-dependent changes observed in the pervaporation experiment results. Figure 6 exhibits the pervaporation measurement results over a span of 2.5 h for each membrane. It can be seen that the curves display a slight scattering trend in water permeance across the membranes. While the trend does show minor fluctuations as in the case of methyl-100, the permeance decay is not as pronounced as that observed in “pressure increase” experiments.

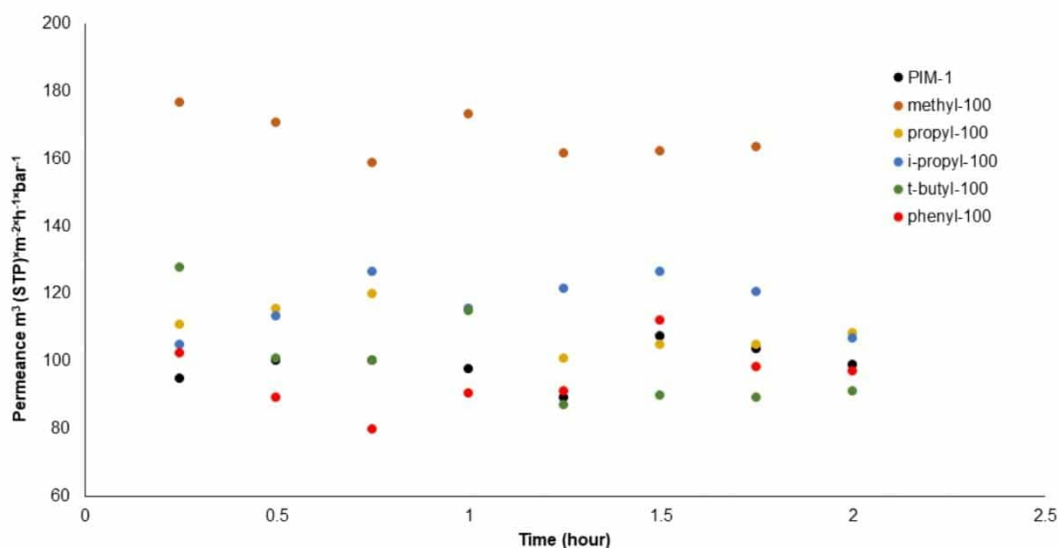


Figure 6. Water flux values from pervaporation over 2.5 h.

This steady water permeance over time can be attributed to the experimental method of pervaporation where the feed side of the membrane is constantly exposed to liquid water,

maintaining an interface between water and the polymer at 100% humidity during the pervaporation process. Such conditions are conducive to the condensation or association of water molecules and, thus, the formation of water clusters already on the feed interphase of the selective layer of the membrane. Consequently, it can be inferred that the presence of these clustered or associated water molecules within the selective layer likely plays a critical role in moderating the decay of the free-volume elements of the membrane. Basically, the void within the polymer matrix is occupied by these clusters, which hinders the rapid decay typically seen in “pressure increase” measurements of hydrogen or carbon dioxide. This effect of water molecule clusters on the stability of the polymer structure supports the concept that the clustered state of water helps preserve the integrity of the polymer, preventing the free volume from collapsing too quickly, a phenomenon corroborated by findings in other studies such as those referenced by Metz et al. [47]. In summary, the pervaporation data suggest that direct exposure to liquid water and the resulting high humidity at the membrane interface play crucial roles in sustaining the polymer structure against rapid degradation, primarily through the stabilizing influence of water molecule clustering within the polymer matrix.

Up to this point in the current study, the water vapor transport of TFC membranes prepared with previously synthesized polymers has been investigated and evaluated in two different applications. In order to extend the scope of this comparison, it would be useful to compare the findings with the “time lag” results from the previous study [20]. With this aim, Figure 7 presents a comparative analysis of three distinct measurement methods: pervaporation, “pressure increase”, and “time lag”. Each data point represents relative values to the performance of methyl-100-based films and TFC membranes. It is crucial to understand that the values indicated are not directly comparable across different methods. For instance, in pervaporation, each membrane value was divided by methyl-100 within its own measurement group. Therefore, all three measurements have the same data on methyl-100 as being equal to 1. The data include relative “pressure increase” values extrapolated to 100% vapor activity to facilitate comparison with pervaporation results. This visualization aims to show the relative changes in properties of different polymers within each method by normalizing the results against the performance of the methyl-100.

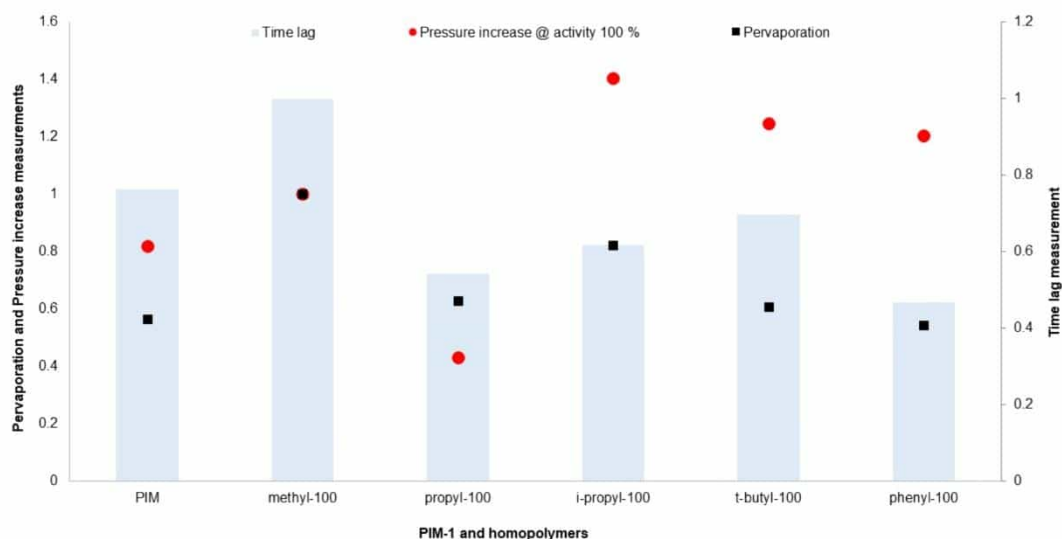


Figure 7. Comparison of relative permeance data of pervaporation, “pressure increase” and relative permeability of “time lag” measurement.

Observations indicate that while the trends in “time lag” and pervaporation measurements appear similar, vapor permeation by pressure increase displays notable differences. This discrepancy can most likely be attributed to the state of the polymer, which varies

significantly between the methods. In time lag measurements, the thick polymer film is as relaxed as possible, allowing for slow evaporation and generally slower aging, which is a phenomenon strongly influenced by film thickness, as discussed in studies such as those by McCaig et al. [48,49]. On the contrary, in TFC membranes which are used in pressure increase measurements, the rapid drying of the polymer solution leads to a thermodynamically unstable state on the surface of the membrane. This instability is compounded by the stress caused by the interface of the polymer, potentially accelerating the degradation of free volume. However, this might be seen as a rearrangement of the polymer structure rather than a mere loss of free volume. Moreover, the influence of the interface to air between the polymer and gas in thick films is minimized compared to that in TFC membranes. According to the observations of this study, it can be assumed that in TFC and thick films, the top layer of the polymer might age similarly, but this does not significantly affect overall performance in thick films. Fundamentally, this graph not only highlights the variations in polymer behavior across different measurement techniques but also underlines the complex interplay of polymer structures, environmental conditions, and measurement methodology in determining polymer performance.

4. Conclusions

This study describes the comparison of gas and water vapor permeances of PIM-derivative TFC membranes obtained under different operating conditions. The different operating conditions include the pervaporation and gas permeation test system “pressure increase” methods. In addition to this, the comparison was also evaluated from the perspective of film thickness by adding “time lag” measurements of thick films obtained from our previous study. Accordingly, TFC membranes were prepared with PIM-1 and homopolymers with different side groups. With these TFC membranes, CO₂, H₂, CH₄ and water vapor permeances were measured with the “pressure increase” measurement. The permeance values were evaluated over a period of 20 h and the aging of the TFC membranes was investigated. In addition to this measurement, the TFC membranes were subjected to pervaporation experiments, water flux was measured and the results were discussed in detail. By comparing the aging behavior and separation performance of thin-film composite membranes against thick films, our work lays the groundwork for future research aimed at optimizing these advanced materials for sustainable and efficient separation processes. The results from the pervaporation experiments are particularly promising, showing much higher water vapor transport rates compared to those observed in pressure increase setups. This suggests that pervaporation could be a viable alternative to traditional porous membrane applications in distillation, especially considering the high permeance values achieved. These findings support the feasibility of using non-porous membranes in applications where high efficiency in water vapor transport is required. However, a critical aspect of implementing such systems involves understanding long-term membrane stability under pervaporation conditions. The current study indicates that while pervaporation offers higher transport rates, the longevity and durability of membranes under continuous operation remain uncertain due to the intensive nature of the required experiments. Such experiments necessitate continuous supervision, primarily because of the need for constant provision of liquid nitrogen, making them labor-intensive and challenging to conduct over extended periods. To fully realize the potential of pervaporation and other non-porous membrane techniques in industrial applications, further research is necessary to assess long-term stability and performance. This would involve designing experiments that can operate safely and effectively over long durations to monitor aging processes and ensuring that the membranes can withstand prolonged operational conditions without significant degradation. In conclusion, while the initial findings are encouraging, confirming the practical viability of non-porous membranes for distillation and similar applications will require more extensive and sustained experimental work. This future research will be crucial in moving from theoretical and initial experimental successes to reliable, scalable industrial applications.

Supplementary Materials: The following supporting information can be downloaded at <https://www.mdpi.com/article/10.3390/polym16202932/s1>. Table S1: Gas and water vapor permeance of PIM-1 at different hours, Figure S1: Gas and vapor permeance decay of homopolymers—complete measurement.

Author Contributions: Conceptualization, E.C. and S.S.; methodology, E.C. and S.S.; investigation, E.C.; writing—original draft preparation, E.C.; writing—review and editing, E.C., S.S. and V.F.; supervision, S.S. and V.F.; project administration, V.F. All authors have read and agreed to the published version of the manuscript.

Funding: We gratefully acknowledge financial support from the Federal Ministry of Education and Research of Germany (BMBF) via the project NAMED (FKZ: 03XP0151A).

Institutional Review Board Statement: Not applicable.

Data Availability Statement: Data are contained within the article and Supplementary Materials.

Acknowledgments: The authors would like to thank Silvio Neumann and Carsten Scholes for their help with the polymerization and pervaporation test, respectively.

Conflicts of Interest: The authors declare no conflicts of interest.

References

- Obringer, R.; Nateghi, R.; Knee, J.; Madani, K.; Kumar, R. Urban water and electricity demand data for understanding climate change impacts on the water-energy nexus. *Sci. Data* **2024**, *11*, 108. [\[CrossRef\]](#) [\[PubMed\]](#)
- He, C.; Liu, Z.; Wu, J.; Pan, X.; Fang, Z.; Li, J.; Bryan, B.A. Future global urban water scarcity and potential solutions. *Nat. Commun.* **2021**, *12*, 4667. [\[CrossRef\]](#) [\[PubMed\]](#)
- Shannon, M.A.; Bohn, P.W.; Elimelech, M.; Georgiadis, J.G.; Marinas, B.J.; Mayes, A.M. Science and technology for water purification in the coming decades. *Nature* **2008**, *452*, 301–310. [\[CrossRef\]](#) [\[PubMed\]](#)
- Shehata, N.; Egirani, D.; Olabi, A.G.; Inayat, A.; Abdelkareem, M.A.; Chae, K.J.; Sayed, E.T. Membrane-based water and wastewater treatment technologies: Issues, current trends, challenges, and role in achieving sustainable development goals, and circular economy. *Chemosphere* **2023**, *320*, 137993. [\[CrossRef\]](#)
- Issaoui, M.; Jellali, S.; Zorpas, A.A.; Dutournie, P. Membrane technology for sustainable water resources management: Challenges and future projections. *Sustain. Chem. Pharm.* **2022**, *25*, 100590. [\[CrossRef\]](#)
- Obotey Ezugbe, E.; Rathilal, S. Membrane Technologies in Wastewater Treatment: A Review. *Membranes* **2020**, *10*, 89. [\[CrossRef\]](#)
- Sayed, E.T.; Olabi, A.G.; Elsaid, K.; Al Radi, M.; Alqadi, R.; Ali Abdelkareem, M. Recent progress in renewable energy based-desalination in the Middle East and North Africa MENA region. *J. Adv. Res.* **2023**, *48*, 125–156. [\[CrossRef\]](#)
- Deshmukh, A.; Boo, C.; Karanikola, V.; Lin, S.; Straub, A.P.; Tong, T.; Warsinger, D.M.; Elimelech, M. Membrane distillation at the water-energy nexus: Limits, opportunities, and challenges. *Energy Environ. Sci.* **2018**, *11*, 1177–1196. [\[CrossRef\]](#)
- Zhang, H.; Xian, H. Review of Hybrid Membrane Distillation Systems. *Membranes* **2024**, *14*, 25. [\[CrossRef\]](#)
- Hussain, A.; Janson, A.; Matar, J.M.; Adham, S. Membrane distillation: Recent technological developments and advancements in membrane materials. *Emergent Mater.* **2021**, *5*, 347–367. [\[CrossRef\]](#)
- Ngo, M.T.T.; Diep, B.Q.; Sano, H.; Nishimura, Y.; Boivin, S.; Kodamatani, H.; Takeuchi, H.; Sakti, S.C.W.; Fujioka, T. Membrane distillation for achieving high water recovery for potable water reuse. *Chemosphere* **2022**, *288*, 132610. [\[CrossRef\]](#) [\[PubMed\]](#)
- Zhang, H.; Zhao, X. Enhanced Anti-Wetting Methods of Hydrophobic Membrane for Membrane Distillation. *Adv. Sci.* **2023**, *10*, e2300598. [\[CrossRef\]](#) [\[PubMed\]](#)
- McKeown, N.B. Polymers of Intrinsic Microporosity (PIMs). *Polymer* **2020**, *202*, 122736. [\[CrossRef\]](#)
- Aloraini, S.; Mathias, M.; Crone, J.; Bryce, K.; Yu, M.; Kirk, R.A.; Ahmad, M.Z.; Asuquo, E.D.; Rico-Martinez, S.; Volkov, A.V.; et al. Crosslinking of Branched PIM-1 and PIM-Py Membranes for Recovery of Toluene from Dimethyl Sulfoxide by Pervaporation. *ACS Appl. Polym. Mater.* **2023**, *5*, 1145–1158. [\[CrossRef\]](#)
- Qiu, B.; Alberto, M.; Mohsenpour, S.; Foster, A.B.; Ding, S.; Guo, Z.; Xu, S.; Holmes, S.M.; Budd, P.M.; Fan, X.; et al. Thin film nanocomposite membranes of PIM-1 and graphene oxide/ZIF-8 nanohybrids for organophilic pervaporation. *Sep. Purif. Technol.* **2022**, *299*, 121693. [\[CrossRef\]](#)
- Butt, T.H.; Tamime, R.; Budd, P.M.; Harrison, W.J.; Shamair, Z.; Khan, A.L. Enhancing the organophilic separations with mixed matrix membranes of PIM-1 and bimetallic Zn/Co-ZIF filler. *Sep. Purif. Technol.* **2022**, *283*, 120216. [\[CrossRef\]](#)
- Kim, H.J.; Kim, D.G.; Lee, K.; Baek, Y.; Yoo, Y.; Kim, Y.S.; Kim, B.G.; Lee, J.C. A Carbonaceous Membrane based on a Polymer of Intrinsic Microporosity (PIM-1) for Water Treatment. *Sci. Rep.* **2016**, *6*, 36078. [\[CrossRef\]](#)
- Jeon, J.W.; Kim, H.J.; Jung, K.H.; Lee, J.; Kim, Y.S.; Kim, B.G.; Lee, J.C. Carbonization of Carboxylate-Functionalized Polymers of Intrinsic Microporosity for Water Treatment. *Macromol. Chem. Phys.* **2020**, *221*, 1900532. [\[CrossRef\]](#)
- Caliskan, E.; Shishatskiy, S.; Abetz, V.; Filiz, V. Pioneering the preparation of porous PIM-1 membranes for enhanced water vapor flow. *RSC Adv.* **2024**, *14*, 9631–9645. [\[CrossRef\]](#)

20. Caliskan, E.; Shishatskiy, S.; Neumann, S.; Abetz, V.; Filiz, V. Investigation of the Side Chain Effect on Gas and Water Vapor Transport Properties of Anthracene-Maleimide Based Polymers of Intrinsic Microporosity. *Polymers* **2021**, *14*, 119. [\[CrossRef\]](#)
21. Kujawska, A.; Knozowska, K.; Kujawa, J.; Kujawski, W. Influence of downstream pressure on pervaporation properties of PDMS and POMS based membranes. *Sep. Purif. Technol.* **2016**, *159*, 68–80. [\[CrossRef\]](#)
22. Silva, R.d.S.; Cavalcanti, C.D.Á.K.; Valle, R.d.C.S.C.; Machado, R.A.F.; Marangoni, C. Understanding the effects of operational conditions on the membrane distillation process applied to the recovery of water from textile effluents. *Process Saf. Environ. Prot.* **2021**, *145*, 285–292. [\[CrossRef\]](#)
23. Du, N.; Song, J.; Robertson, G.P.; Pinnau, I.; Guiver, M.D. Linear High Molecular Weight Ladder Polymer via Fast Polycondensation of 5,5',6,6'-Tetrahydroxy-3,3',3'-tetramethylspirobisindane with 1,4-Dicyanotetrafluorobenzene. *Macromol. Rapid Commun.* **2008**, *29*, 783–788. [\[CrossRef\]](#)
24. Grünauer, J.; Filiz, V.; Shishatskiy, S.; Abetz, C.; Abetz, V. Scalable application of thin film coating techniques for supported liquid membranes for gas separation made from ionic liquids. *J. Membr. Sci.* **2016**, *518*, 178–191. [\[CrossRef\]](#)
25. Jan Roman, P.; Detlev, F.; Thomas, K.; Klaus-Viktor, P. Gas permeation measurement under defined humidity via constant volume/variable pressure method. *J. Membr. Sci.* **2012**, *389*, 343–348. [\[CrossRef\]](#)
26. Lilleepärg, J.; Georgopoulos, P.; Emmeler, T.; Shishatskiy, S. Effect of the reactive amino and glycidyl ether terminated polyethylene oxide additives on the gas transport properties of Pebax® bulk and thin film composite membranes. *RSC Adv.* **2016**, *6*, 11763–11772. [\[CrossRef\]](#)
27. Lilleepärg, J.; Sperling, E.; Blanke, M.; Held, M.; Shishatskiy, S. Multicomponent Network Formation in Selective Layer of Composite Membrane for CO₂ Separation. *Membranes* **2021**, *11*, 174. [\[CrossRef\]](#)
28. Feng, X.; Huang, R.Y.M. Liquid Separation by Membrane Pervaporation: A Review. *Ind. Eng. Chem. Res.* **1997**, *36*, 1048–1066. [\[CrossRef\]](#)
29. Davis, E.M.; Elabd, Y.A. Water clustering in glassy polymers. *J. Phys. Chem. B* **2013**, *117*, 10629–10640. [\[CrossRef\]](#)
30. Barrie, J.A.; Platt, B. The diffusion and clustering of water vapour in polymers. *Polymer* **1963**, *4*, 303–313. [\[CrossRef\]](#)
31. Mehio, N.; Dai, S.; Jiang, D.-e. Quantum Mechanical Basis for Kinetic Diameters of Small Gaseous Molecules. *J. Phys. Chem. A* **2014**, *118*, 1150–1154. [\[CrossRef\]](#) [\[PubMed\]](#)
32. Calle, M.; Lozano, A.E.; de Abajo, J.; de la Campa, J.G.; Álvarez, C. Design of gas separation membranes derived of rigid aromatic polyimides. 1. Polymers from diamines containing di-tert-butyl side groups. *J. Membr. Sci.* **2010**, *365*, 145–153. [\[CrossRef\]](#)
33. Yampolskii, Y.P.; Banerjee, S. Effects of Bulky Substituents on Transport Properties of Membrane Gas Separation Materials. *Pet. Chem.* **2018**, *57*, 1195–1206. [\[CrossRef\]](#)
34. Swaidan, R.; Ghanem, B.; Litwiller, E.; Pinnau, I. Physical Aging, Plasticization and Their Effects on Gas Permeation in “Rigid” Polymers of Intrinsic Microporosity. *Macromolecules* **2015**, *48*, 6553–6561. [\[CrossRef\]](#)
35. Guan, L.; Xu, H.; Huang, D. The investigation on states of water in different hydrophilic polymers by DSC and FTIR. *J. Polym. Res.* **2011**, *18*, 681–689. [\[CrossRef\]](#)
36. Levitt, M.; Perutz, M.F. Aromatic rings act as hydrogen bond acceptors. *J. Mol. Biol.* **1988**, *201*, 751–754. [\[CrossRef\]](#)
37. Vojislavljević, D.Z.; Janjić, G.V.; Ninković, D.B.; Kapor, A.; Zarić, S.D. The influence of water molecule coordination onto the water–aromatic interaction. Strong interactions of water coordinating to a metal ion. *CrystEngComm* **2013**, *15*, 2099–2105. [\[CrossRef\]](#)
38. Rahman, M.M.; Abetz, C.; Shishatskiy, S.; Martin, J.; Muller, A.J.; Abetz, V. CO₂ Selective PolyActive Membrane: Thermal Transitions and Gas Permeance as a Function of Thickness. *ACS Appl. Mater. Interfaces* **2018**, *10*, 26733–26744. [\[CrossRef\]](#)
39. Wang, H.; Chung, T.-S.; Paul, D.R. Physical aging and plasticization of thick and thin films of the thermally rearranged ortho-functional polyimide 6FDA–HAB. *J. Membr. Sci.* **2014**, *458*, 27–35. [\[CrossRef\]](#)
40. Merrick, M.M.; Sujanani, R.; Freeman, B.D. Glassy polymers: Historical findings, membrane applications, and unresolved questions regarding physical aging. *Polymer* **2020**, *211*, 123176. [\[CrossRef\]](#)
41. Hinds, B.J.; Chopra, N.; Rantell, T.; Andrews, R.; Gavalas, V.; Bachas, L.G. Aligned multiwalled carbon nanotube membranes. *Science* **2004**, *303*, 62–65. [\[CrossRef\]](#) [\[PubMed\]](#)
42. Hinds, B. Dramatic transport properties of carbon nanotube membranes for a robust protein channel mimetic platform. *Curr. Opin. Solid State Mater. Sci.* **2012**, *16*, 1–9. [\[CrossRef\]](#)
43. Fang, S.M.; Stern, S.A.; Frisch, H.L. A “free volume” model of permeation of gas and liquid mixtures through polymeric membranes. *Chem. Eng. Sci.* **1975**, *30*, 773–780. [\[CrossRef\]](#)
44. Yu, M.; Funke, H.H.; Falconer, J.L.; Noble, R.D. Gated Ion Transport through Dense Carbon Nanotube Membranes. *J. Am. Chem. Soc.* **2010**, *132*, 8285–8290. [\[CrossRef\]](#)
45. Park, H.B.; Jung, C.H.; Lee, Y.M.; Hill, A.J.; Pas, S.J.; Mudie, S.T.; Van Wagner, E.; Freeman, B.D.; Cookson, D.J. Polymers with cavities tuned for fast selective transport of small molecules and ions. *Science* **2007**, *318*, 254–258. [\[CrossRef\]](#)
46. Jansen, J.C.; Friess, K.; Drioli, E. Organic vapour transport in glassy perfluoropolymer membranes: A simple semi-quantitative approach to analyze clustering phenomena by time lag measurements. *J. Membr. Sci.* **2011**, *367*, 141–151. [\[CrossRef\]](#)
47. Metz, S.; Ven, W.; Mulder, M.; Wessling, M. Mixed gas water vapor/N transport in poly(ethylene oxide) poly(butylene terephthalate) block copolymers. *J. Membr. Sci.* **2005**, *266*, 51–61. [\[CrossRef\]](#)

48. McCaig, M.S.; Paul, D.R. Effect of film thickness on the changes in gas permeability of a glassy polyarylate due to physical agingPart I. Experimental observations. *Polymer* **2000**, *41*, 629–637. [[CrossRef](#)]
49. McCaig, M.S.; Paul, D.R.; Barlow, J.W. Effect of film thickness on the changes in gas permeability of a glassy polyarylate due to physical agingPart II. Mathematical model. *Polymer* **2000**, *41*, 639–648. [[CrossRef](#)]

Disclaimer/Publisher’s Note: The statements, opinions and data contained in all publications are solely those of the individual author(s) and contributor(s) and not of MDPI and/or the editor(s). MDPI and/or the editor(s) disclaim responsibility for any injury to people or property resulting from any ideas, methods, instructions or products referred to in the content.

6. Discussion

In line with the aim of this PhD work, these three studies on the development of PIM-1 and PIM-derived polymer membranes contribute to water separation technologies and their results are discussed profoundly in the articles. This chapter summarizes and highlights the findings of the three studies.

6.1. Summary of findings-Article 1

- Anthracene maleimide based comonomers with various alkyl side chains (-methyl, -ethyl, -propyl, -*i*-propyl, -*t*-butyl, -cyclohexyl, -phenyl) were successfully synthesized via the Diels-Alder reaction and further characterized by ¹H-NMR and TG-FTIR.
- Anthracene maleimide based comonomers were used for homopolymerization using TFTPn and copolymerization by using TFTPn and TTSBI monomer units. ¹H-NMR characterization confirmed a 1:1 molar ratio of TFTPn and TTSBI in copolymers.
- TG-FTIR analysis of comonomers showed that the decomposition temperature of the maleimide unit is lower than that of the anthracene unit in methyl, ethyl, and *t*-butyl comonomers. Retro-Diels Alder reaction has been carried out successfully in order to achieve structure rearrangement of homopolymers.
- TG-FTIR of methyl-100 homopolymer confirmed that retro-Diels Alder reaction occurs before the decomposition of the polymer backbone. Post-thermal treatment of methyl-100 homopolymer demonstrated structural rearrangement, affecting gas transport properties.
- Methyl-50 and *t*-butyl-50 copolymers exhibited higher CO₂ and CH₄ permeability than PIM-1.
- Bulky alkyl side groups (-*t*-butyl and -*i*-propyl) increased fractional free volume of the polymer. This leads an increase on gas permeability as a result of elevated diffusion coefficient of polymers.
- Short alkyl side groups (methyl-100 and ethyl-100) displayed higher water vapor permeability and solubility compared to PIM-1 and other homopolymers. This highlighted

the fact that the shorter side groups allow interaction of maleimide group with the penetrant more than it is the case for the polymers, which have long or bulky alkyl side groups.

- Phenyl-100 homopolymer, which has an aromatic side group, showed high water vapor solubility with a low diffusion coefficient, attributed to water molecule clustering in free volume elements.
- The results highlight the potential of anthracene maleimide-based polymers for water vapor transport studies in water treatment applications.

6.2. Summary of findings-Article 2

- Porous PIM-1 membranes were successfully prepared via the non-solvent induced phase separation (NIPS) method using various solvent/non-solvent combinations.
- NMP/THF was identified as the optimal solvent mixture for casting homogeneous PIM-1 membranes without precipitate formation.
- Four membranes (PM-6, PM-9, PM-11, and PM-13) were prepared using different ratios of NMP/THF/PIM-1. Low molecular weight PIM-1 was used for PM-6, PM-9, and PM-11, while high molecular weight PIM-1 was used for PM-13.
- SEM imaging revealed favorable void formation in PM-6 and PM-9, while PM-13 exhibited large pores, which was attributed to the high molecular weight of PIM-1.
- Liquid entry pressure (LEP) values are consistent with the size of the pores, meaning PM-13 exhibits the lowest LEP value.
- Water contact angle measurements showed that PM-6 and PM-9 demonstrated hydrophobicity sufficient to prevent liquid water while allowing water vapor passes through the membrane.
- Water flux was negligible for PM-6, PM-9, and PM-11 nonetheless high for PM-13, correlating with its large pore size.
- PM-6 and PM-9 exhibited higher water vapor permeance compared to dense PIM-1 TFC membranes, suggesting suitability for membrane distillation.

- PM-6 and PM-9 selectively allowed water vapor transport while preventing liquid water, making them promising candidates for membrane distillation applications.
- Further studies of porous PIM-1 membranes in water separation applications are encouraged due to their favorable properties and ease of handling.

6.3. Summary of findings-Article 3

- Preparation of thin film composite membranes of homopolymers obtained from first study and PIM-1 has been carried out successfully.
- Comparison of gas and water vapor permeability of PIM-derived TFC membranes under different operating conditions has been conducted. “Time lag” measurements of thick films from the first study were included to evaluate the effect of film thickness.
- CO₂, H₂, CH₄ and water vapor permeance were measured by the “pressure increase” method while water flux was evaluated by “pervaporation” experiments.
- In pervaporation experiments, it was observed that the water vapor transport rate of membranes was higher compared to that of pressure increase method. Therefore, it can be interpreted that pervaporation membranes might be viable alternative to conventional porous membranes in distillation. With high water flux values, non-porous membranes were confirmed to be efficient in water vapor transport.
- Permeance values of TFC membranes were monitored for 20 hours and aging behavior was investigated. Long-term stability and durability were identified as important subjects to be studied for pervaporation experiments.
- Further research is needed to evaluate long-term stability and performance for industrial applications. The potential of non-porous membranes in distillation and similar applications is promising, nevertheless more extensive validation with long-term experiments is needed.

7. References

1. Baker, R.W., *Overview of Membrane Science and Technology*, in *Membrane Technology and Applications*. 2004. p. 1-14.
2. Saleh, T.A. and V.K. Gupta, *Chapter 1 - An Overview of Membrane Science and Technology*, in *Nanomaterial and Polymer Membranes*, T.A. Saleh and V.K. Gupta, Editors. 2016, Elsevier. p. 1-23.
3. Li, X. and J. Li, *Fluxes and Driving Forces in Membrane Separation Processes*, in *Encyclopedia of Membranes*, E. Drioli and L. Giorno, Editors. 2015, Springer Berlin Heidelberg: Berlin, Heidelberg. p. 1-3.
4. Onishi, V.C., J.A. Reyes-Labarta, and J.A. Caballero, *Chapter 10 - Membrane Desalination in Shale Gas Industry: Applications and Perspectives*, in *Current Trends and Future Developments on (Bio-) Membranes*, A. Basile, E. Curcio, and Inamuddin, Editors. 2019, Elsevier. p. 243-267.
5. Mulder, M., *Materials and Material Properties*, in *Basic Principles of Membrane Technology*, M. Mulder, Editor. 1996, Springer Netherlands: Dordrecht. p. 22-70.
6. György, V. and S. Zsolt, *Artificial and Natural Membranes*, in *Atomic Force Microscopy Investigations into Biology*, L.F. Christopher, Editor. 2012, IntechOpen: Rijeka. p. Ch. 10.
7. Khulbe, K.C.F., C.Y.; Matsuura, Takeshi, *Synthetic Membranes for Membrane Processes*, in *Synthetic Polymeric Membranes: Characterization by Atomic Force Microscopy*, K.C. Khulbe, C.Y. Feng, and T. Matsuura, Editors. 2008, Springer Berlin Heidelberg: Berlin, Heidelberg. p. 5-18.
8. Sonawane, S., et al., *Chapter 17 - Nanomaterials for membrane synthesis: Introduction, mechanism, and challenges for wastewater treatment*, in *Handbook of Nanomaterials for Wastewater Treatment*, B. Bhanvase, et al., Editors. 2021, Elsevier. p. 537-553.
9. Anis, S.F., R. Hashaiekh, and N. Hilal, *Microfiltration membrane processes: A review of research trends over the past decade*. Journal of Water Process Engineering, 2019. **32**.

10. Kammakakam, I. and Z. Lai, *Next-generation ultrafiltration membranes: A review of material design, properties, recent progress, and challenges*. Chemosphere, 2023. **316**: p. 137669.
11. Yang, Z., et al., *A Review on Reverse Osmosis and Nanofiltration Membranes for Water Purification*. Polymers (Basel), 2019. **11**(8).
12. Bernardo, P., E. Drioli, and G. Golemme, *Membrane Gas Separation: A Review/State of the Art*. Industrial & Engineering Chemistry Research, 2009. **48**(10): p. 4638-4663.
13. Castro-Munoz, R., *Breakthroughs on tailoring pervaporation membranes for water desalination: A review*. Water Res, 2020. **187**: p. 116428.
14. Al-Harby, N.F., M. El Batouti, and M.M. Elewa, *A Comparative Analysis of Pervaporation and Membrane Distillation Techniques for Desalination Utilising the Sweeping Air Methodology with Novel and Economical Pervaporation Membranes*. Polymers (Basel), 2023. **15**(21).
15. Mahenthiran, A.V. and Z.A. Jawad, *A Prospective Concept on the Fabrication of Blend PES/PEG/DMF/NMP Mixed Matrix Membranes with Functionalised Carbon Nanotubes for CO₂/N₂ Separation*. Membranes, 2021. **11**(7): p. 519.
16. Nunes, S.P. and K.-V. Peinemann, *Membrane Preparation*, in *Membrane Technology*. 2006. p. 9-14.
17. Nunes, S.P. and K.-V. Peinemann, *Gas Separation with Membranes*, in *Membrane Technology*. 2006. p. 53-90.
18. Lova, P., G. Manfredi, and D. Comoretto, *Advances in Functional Solution Processed Planar 1D Photonic Crystals*. Advanced Optical Materials, 2018. **6**(24): p. 1800730.
19. Wijmans, J.G. and R.W. Baker, *The solution-diffusion model: a review*. Journal of Membrane Science, 1995. **107**(1): p. 1-21.
20. Baker, R.W., *Gas Separation*, in *Membrane Technology and Applications*. 2004. p. 301-353.
21. Reinecke, S.A. and B.E. Sleep, *Knudsen diffusion, gas permeability, and water content in an unconsolidated porous medium*. Water Resources Research, 2002. **38**(12): p. 16-1-16-15.

22. He, W.L., Weiqiang; Dickerson, James H., *Gas Diffusion Mechanisms and Models*, in *Gas Transport in Solid Oxide Fuel Cells*. 2014, Springer International Publishing: Cham. p. 9-17.
23. Mazumder, A., et al., *Theoretical and Experimental Considerations for Investigating Multicomponent Diffusion in Hydrated, Dense Polymer Membranes*. Membranes (Basel), 2022. **12**(10).
24. Hägg, M.-B., *Gas Permeation: Permeability, Permeance, and Separation Factor*, in *Encyclopedia of Membranes*, E. Drioli and L. Giorno, Editors. 2016, Springer Berlin Heidelberg: Berlin, Heidelberg. p. 1-4.
25. Ghosal, K. and B.D. Freeman, *Gas separation using polymer membranes: an overview*. Polymers for Advanced Technologies, 1994. **5**(11): p. 673-697.
26. Yampolskii, Y., *Polymeric Gas Separation Membranes*. Macromolecules, 2012. **45**(8): p. 3298-3311.
27. Paul, D.R., *Gas Sorption and Transport in Glassy Polymers*. Berichte der Bunsengesellschaft für physikalische Chemie, 1979. **83**(4): p. 294-302.
28. Matteucci, S., et al., *Transport of Gases and Vapors in Glassy and Rubbery Polymers*, in *Materials Science of Membranes for Gas and Vapor Separation*. 2006. p. 1-47.
29. Freeman, B.D., *Basis of Permeability/Selectivity Tradeoff Relations in Polymeric Gas Separation Membranes*. Macromolecules, 1999. **32**(2): p. 375-380.
30. Robeson, L.M., *Correlation of separation factor versus permeability for polymeric membranes*. Journal of Membrane Science, 1991. **62**(2): p. 165-185.
31. Panapitiya, N., et al., *Compatibilized Immiscible Polymer Blends for Gas Separations*. Materials (Basel), 2016. **9**(8).
32. Robeson, L.M., *The upper bound revisited*. Journal of Membrane Science, 2008. **320**(1-2): p. 390-400.
33. Robeson, L.M., et al., *Comparison of transport properties of rubbery and glassy polymers and the relevance to the upper bound relationship*. Journal of Membrane Science, 2015. **476**: p. 421-431.
34. Kober, P.A., *Pervaporation, Perstillation And Percrystallization. I*. Journal of the American Chemical Society, 1917. **39**(5): p. 944-948.

35. Feng, X. and R.Y.M. Huang, *Liquid Separation by Membrane Pervaporation: A Review*. Industrial & Engineering Chemistry Research, 1997. **36**(4): p. 1048-1066.
36. Chapman, P.D., et al., *Membranes for the dehydration of solvents by pervaporation*. Journal of Membrane Science, 2008. **318**(1-2): p. 5-37.
37. Pulyalina, A., et al., *Polyimide Asymmetric Membrane vs. Dense Film for Purification of MTBE Oxygenate by Pervaporation*. Symmetry, 2020. **12**(3).
38. Brüscke, H.E.A., *State-of-the-Art of Pervaporation Processes in the Chemical Industry*, in *Membrane Technology*. 2006. p. 151-202.
39. Liu, G. and W. Jin, *Pervaporation membrane materials: Recent trends and perspectives*. Journal of Membrane Science, 2021. **636**.
40. Figoli, A., et al., *2 - Pervaporation membranes: preparation, characterization, and application*, in *Pervaporation, Vapour Permeation and Membrane Distillation*, A. Basile, A. Figoli, and M. Khayet, Editors. 2015, Woodhead Publishing: Oxford. p. 19-63.
41. Shao, P. and R.Y.M. Huang, *Polymeric membrane pervaporation*. Journal of Membrane Science, 2007. **287**(2): p. 162-179.
42. Lipnizki, F., et al., *Organophilic pervaporation: prospects and performance*. Chemical Engineering Journal, 1999. **73**(2): p. 113-129.
43. Peng, P., et al., *Membranes for bioethanol production by pervaporation*. Biotechnol Biofuels, 2021. **14**(1): p. 10.
44. Ong, Y.K., et al., *Recent membrane development for pervaporation processes*. Progress in Polymer Science, 2016. **57**: p. 1-31.
45. Smitha, B., *Separation of organic-organic mixtures by pervaporation-a review*. Journal of Membrane Science, 2004. **241**(1): p. 1-21.
46. Jiang, L.Y., et al., *Polyimides membranes for pervaporation and biofuels separation*. Progress in Polymer Science, 2009. **34**(11): p. 1135-1160.
47. Koros, W.J. and C. Zhang, *Materials for next-generation molecularly selective synthetic membranes*. Nature Materials, 2017. **16**(3): p. 289-297.
48. Wang, K.Y., T.-S. Chung, and R. Rajagopalan, *Dehydration of tetrafluoropropanol (TFP) by pervaporation via novel PBI/BTDA-TDI/MDI co-polyimide (P84) dual-layer hollow fiber membranes*. Journal of Membrane Science, 2007. **287**(1): p. 60-66.

49. Hussain, A., et al., *Membrane distillation: recent technological developments and advancements in membrane materials*. Emergent Materials, 2021.
50. Karanasiou, A., M. Kostoglou, and A. Karabelas, *An Experimental and Theoretical Study on Separations by Vacuum Membrane Distillation Employing Hollow-Fiber Modules*. Water, 2018. **10**(7).
51. Bindra, S.P. and W. Abosh, *Recent developments in water desalination*. Desalination, 2001. **136**(1): p. 49-56.
52. Alkhudhiri, A., N. Darwish, and N. Hilal, *Membrane distillation: A comprehensive review*. Desalination, 2012. **287**: p. 2-18.
53. Deshmukh, A., et al., *Membrane distillation at the water-energy nexus: limits, opportunities, and challenges*. Energy & Environmental Science, 2018. **11**(5): p. 1177-1196.
54. Khayet, M., et al., *Design of novel direct contact membrane distillation membranes*. Desalination, 2006. **192**(1-3): p. 105-111.
55. Alklaibi, A.M. and N. Lior, *Membrane-distillation desalination: Status and potential*. Desalination, 2005. **171**(2): p. 111-131.
56. Abu-Zeid, M.A.E.-R., et al., *A comprehensive review of vacuum membrane distillation technique*. Desalination, 2015. **356**: p. 1-14.
57. Nthunya, L.N., et al., *A review of nanoparticle-enhanced membrane distillation membranes: membrane synthesis and applications in water treatment*. Journal of Chemical Technology & Biotechnology, 2019. **94**(9): p. 2757-2771.
58. Abdulla AlMarzooqi, F., M. Roil Bilad, and H. Ali Arafat, *Improving Liquid Entry Pressure of Polyvinylidene Fluoride (PVDF) Membranes by Exploiting the Role of Fabrication Parameters in Vapor-Induced Phase Separation VIPS and Non-Solvent-Induced Phase Separation (NIPS) Processes*. Applied Sciences, 2017. **7**(2).
59. Drioli, E., A. Ali, and F. Macedonio, *Membrane distillation: Recent developments and perspectives*. Desalination, 2015. **356**: p. 56-84.
60. Parani, S. and O.S. Oluwafemi, *Membrane Distillation: Recent Configurations, Membrane Surface Engineering, and Applications*. Membranes (Basel), 2021. **11**(12).
61. García-Fernández, L., M. Khayet, and M.C. García-Payo, *11 - Membranes used in membrane distillation: preparation and characterization*, in *Pervaporation, Vapour*

- Permeation and Membrane Distillation*, A. Basile, A. Figoli, and M. Khayet, Editors. 2015, Woodhead Publishing: Oxford. p. 317-359.
62. Khayet, M., *Membranes and theoretical modeling of membrane distillation: a review*. Adv Colloid Interface Sci, 2011. **164**(1-2): p. 56-88.
63. Alessandro, F., F. Macedonio, and E. Drioli, *New Materials and Phenomena in Membrane Distillation*. Chemistry, 2023. **5**(1): p. 65-84.
64. Tai, Z.S., et al., *Membrane innovations to tackle challenges related to flux, energy efficiency and wetting in membrane distillation: A state-of-the-art review*. Sustainable Materials and Technologies, 2024. **39**: p. e00780.
65. Tijting, L.D., et al., *Fouling and its control in membrane distillation—A review*. Journal of Membrane Science, 2015. **475**: p. 215-244.
66. Cheng, D., et al., *Antiwettability and Performance Stability of a Composite Hydrophobic/Hydrophilic Dual-Layer Membrane in Wastewater Treatment by Membrane Distillation*. Industrial & Engineering Chemistry Research, 2018. **57**(28): p. 9313-9322.
67. Peng, P., A.G. Fane, and X. Li, *Desalination by membrane distillation adopting a hydrophilic membrane*. Desalination, 2005. **173**(1): p. 45-54.
68. Zuo, G. and R. Wang, *Novel membrane surface modification to enhance anti-oil fouling property for membrane distillation application*. Journal of Membrane Science, 2013. **447**: p. 26-35.
69. Tan, X. and D. Rodrigue, *A Review on Porous Polymeric Membrane Preparation. Part I: Production Techniques with Polysulfone and Poly (Vinylidene Fluoride)*. Polymers (Basel), 2019. **11**(7).
70. Sidhikku Kandath Valappil, R., N. Ghasem, and M. Al-Marzouqi, *Current and future trends in polymer membrane-based gas separation technology: A comprehensive review*. Journal of Industrial and Engineering Chemistry, 2021. **98**: p. 103-129.
71. Kahrs, C. and J. Schwellenbach, *Membrane formation via non-solvent induced phase separation using sustainable solvents: A comparative study*. Polymer, 2020. **186**.
72. Ma, W., et al., *Membrane formation by thermally induced phase separation: Materials, involved parameters, modeling, current efforts and future directions*. Journal of Membrane Science, 2023. **669**.

73. Pervin, R., P. Ghosh, and M.G. Basavaraj, *Tailoring pore distribution in polymer films via evaporation induced phase separation*. RSC Adv, 2019. **9**(27): p. 15593-15605.
74. Mapossa, A.B., et al., *A review on thermally induced phase separation technology in the fabrication of microporous polymer membrane devices for sustained-repellent delivery: Crystallization and morphological studies*. Journal of Polymer Science, 2024. **n/a**(n/a).
75. Mulder, M., *Preparation of Synthetic Membranes*, in *Basic Principles of Membrane Technology*, M. Mulder, Editor. 1996, Springer Netherlands: Dordrecht. p. 71-156.
76. Li, S., et al., *Recent advances on cellulose-based nanofiltration membranes and their applications in drinking water purification: A review*. Journal of Cleaner Production, 2022. **333**: p. 130171.
77. Yataganbaba, A., B. Ozkahraman, and I. Kurtbas, *Worldwide trends on encapsulation of phase change materials: A bibliometric analysis (1990–2015)*. Applied Energy, 2017. **185**: p. 720-731.
78. Ge, C., et al., *Recent advances of the interfacial polymerization process in gas separation membranes fabrication*. Journal of Membrane Science, 2023. **683**: p. 121854.
79. Song, Y., J.-B. Fan, and S. Wang, *Recent progress in interfacial polymerization*. Materials Chemistry Frontiers, 2017. **1**(6): p. 1028-1040.
80. Dai, Z., L. Ansaloni, and L. Deng, *Recent advances in multi-layer composite polymeric membranes for CO₂ separation: A review*. Green Energy & Environment, 2016. **1**(2): p. 102-128.
81. Ravve, A., *Step-Growth Polymerization and Step-Growth Polymers*, in *Principles of Polymer Chemistry*, A. Ravve, Editor. 2012, Springer New York: New York, NY. p. 403-535.
82. Flory, P.J., *Fundamental Principles of Condensation Polymerization*. Chemical Reviews, 1946. **39**(1): p. 137-197.
83. De Keer, L., et al., *Going Beyond the Carothers, Flory and Stockmayer Equation by Including Cyclization Reactions and Mobility Constraints*. Polymers (Basel), 2021. **13**(15).
84. Choi, K.Y. and K.B. McAuley, *Step-Growth Polymerization*, in *Polymer Reaction Engineering*. 2007. p. 273-314.

85. Abdelghafour, M.M., et al., *The Effect of Molecular Weight on the Solubility Properties of Biocompatible Poly(ethylene succinate) Polyester*. Polymers (Basel), 2021. **13**(16).
86. Budd, P.M., et al., *Polymers of intrinsic microporosity (PIMs): robust, solution-processable, organic nanoporous materials*. Chemical Communications, 2004(2): p. 230-231.
87. McKeown, N.B., et al., *Polymers of intrinsic microporosity (PIMs): bridging the void between microporous and polymeric materials*. Chemistry, 2005. **11**(9): p. 2610-20.
88. Budd, P.M., N.B. McKeown, and D. Fritsch, *Polymers of Intrinsic Microporosity (PIMs): High Free Volume Polymers for Membrane Applications*. Macromolecular Symposia, 2006. **245-246**(1): p. 403-405.
89. Budd, P.M., et al., *Solution-processed, organophilic membrane derived from a polymer of intrinsic microporosity*. Advanced Materials, 2004. **16**(5): p. 456-+.
90. Du, N., et al., *Linear High Molecular Weight Ladder Polymer via Fast Polycondensation of 5,5',6,6'-Tetrahydroxy-3,3',3'-tetramethylspirobisindane with 1,4-Dicyanotetrafluorobenzene*. Macromolecular Rapid Communications, 2008. **29**(10): p. 783-788.
91. Budd, P.M., N.B. McKeown, and D. Fritsch, *Free volume and intrinsic microporosity in polymers*. Journal of Materials Chemistry, 2005. **15**(20).
92. McKeown, N.B. and P.M. Budd, *Polymers of intrinsic microporosity (PIMs): organic materials for membrane separations, heterogeneous catalysis and hydrogen storage*. Chem Soc Rev, 2006. **35**(8): p. 675-83.
93. Yin, H., et al., *Effect of Backbone Rigidity on the Glass Transition of Polymers of Intrinsic Microporosity Probed by Fast Scanning Calorimetry*. ACS Macro Letters, 2019. **8**(8): p. 1022-1028.
94. Budd, P., et al., *Gas separation membranes from polymers of intrinsic microporosity*. Journal of Membrane Science, 2005. **251**(1-2): p. 263-269.
95. Fritsch, D., et al., *Synthesis and Gas Permeation Properties of Spirobischromane-Based Polymers of Intrinsic Microporosity*. Macromolecular Chemistry and Physics, 2011. **212**(11): p. 1137-1146.

96. Ghanem, B., et al., *Synthesis and characterization of novel triptycene dianhydrides and polyimides of intrinsic microporosity based on 3,3'-dimethylnaphthidine*. Polymer, 2016. **101**: p. 225-232.
97. Aliyev, E.M., et al., *Covalently Modified Graphene Oxide and Polymer of Intrinsic Microporosity (PIM-1) in Mixed Matrix Thin-Film Composite Membranes*. Nanoscale Research Letters, 2018. **13**(1): p. 359.
98. Khan, M.M., et al., *Cross-linking of Polymer of Intrinsic Microporosity (PIM-1) via nitrene reaction and its effect on gas transport property*. European Polymer Journal, 2013. **49**(12): p. 4157-4166.
99. Mason, C.R., et al., *Enhancement of CO₂ Affinity in a Polymer of Intrinsic Microporosity by Amine Modification*. Macromolecules, 2014. **47**(3): p. 1021-1029.
100. Starannikova, L., et al., *Effective increase in permeability and free volume of PIM copolymers containing ethanoanthracene unit and comparison between the alternating and random copolymers*. Journal of Membrane Science, 2018. **548**: p. 593-597.
101. Thomas, S., et al., *Pure- and mixed-gas permeation properties of a microporous spirobisindane-based ladder polymer (PIM-1)*. Journal of Membrane Science, 2009. **333**(1-2): p. 125-131.
102. Budd, P.M., et al., *Gas permeation parameters and other physicochemical properties of a polymer of intrinsic microporosity: Polybenzodioxane PIM-1*. Journal of Membrane Science, 2008. **325**(2): p. 851-860.
103. Kirk, R.A., et al., *The potential of polymers of intrinsic microporosity (PIMs) and PIM/graphene composites for pervaporation membranes*. BMC Chemical Engineering, 2019. **1**(1).
104. Ye, H., et al., *Advances in the Application of Polymers of Intrinsic Microporosity in Liquid Separation and Purification: Membrane Separation and Adsorption Separation*. Polymer Reviews, 2021. **61**(2): p. 239-279.
105. Tsarkov, S., et al., *Solvent nanofiltration through high permeability glassy polymers: Effect of polymer and solute nature*. Journal of Membrane Science, 2012. **423-424**: p. 65-72.

106. Gorgojo, P., et al., *Ultrathin Polymer Films with Intrinsic Microporosity: Anomalous Solvent Permeation and High Flux Membranes*. Advanced Functional Materials, 2014. **24**(30): p. 4729-4737.
107. Yang, E., et al., *Intermolecular cross-linked polymer of intrinsic microporosity-I (PIM-I)-based thin-film composite hollow fiber membrane for organic solvent nanofiltration*. Journal of Membrane Science, 2023. **671**: p. 121370.
108. Kuzminova, A., et al., *Novel Mixed Matrix Membranes Based on Polymer of Intrinsic Microporosity PIM-I Modified with Metal-Organic Frameworks for Removal of Heavy Metal Ions and Food Dyes by Nanofiltration*. Membranes (Basel), 2021. **12**(1).
109. Budd, P.M. and N.B. McKeown, *Highly permeable polymers for gas separation membranes*. Polymer Chemistry, 2010. **1**(1).
110. White, R.P. and J.E.G. Lipson, *Polymer Free Volume and Its Connection to the Glass Transition*. Macromolecules, 2016. **49**(11): p. 3987-4007.
111. Merrick, M.M., R. Sujanani, and B.D. Freeman, *Glassy polymers: Historical findings, membrane applications, and unresolved questions regarding physical aging*. Polymer, 2020. **211**: p. 123176.
112. Yampolskii, Y., *Fractional Free Volume (FFV)*, in *Encyclopedia of Membranes*, E. Drioli and L. Giorno, Editors. 2016, Springer Berlin Heidelberg: Berlin, Heidelberg. p. 818-819.
113. White, R.P. and J.E.G. Lipson, *Pressure-Dependent Dynamics of Polymer Melts from Arrhenius to Non-Arrhenius: The Cooperative Free Volume Rate Equation Tested against Simulation Data*. Macromolecules, 2018. **51**(13): p. 4896-4909.
114. Corrado, T. and R. Guo, *Macromolecular design strategies toward tailoring free volume in glassy polymers for high performance gas separation membranes*. Molecular Systems Design & Engineering, 2020. **5**(1): p. 22-48.
115. Low, Z.-X., et al., *Gas Permeation Properties, Physical Aging, and Its Mitigation in High Free Volume Glassy Polymers*. Chemical Reviews, 2018. **118**(12): p. 5871-5911.
116. Perez-De Eulate, N.G. and D. Cangialosi, *The very long-term physical aging of glassy polymers*. Phys Chem Phys, 2018. **20**(18): p. 12356-12361.

117. Mizrahi Rodriguez, K., et al., *Leveraging Free Volume Manipulation to Improve the Membrane Separation Performance of Amine-Functionalized PIM-1*. *Angew Chem Int Ed Engl*, 2021. **60**(12): p. 6593-6599.
118. Li, F.Y. and T.-S. Chung, *Physical aging, high temperature and water vapor permeation studies of UV-rearranged PIM-1 membranes for advanced hydrogen purification and production*. *International Journal of Hydrogen Energy*, 2013. **38**(23): p. 9786-9793.
119. Swaidan, R., et al., *Physical Aging, Plasticization and Their Effects on Gas Permeation in "Rigid" Polymers of Intrinsic Microporosity*. *Macromolecules*, 2015. **48**(18): p. 6553-6561.
120. Ma, X. and I. Pinnau, *Effect of Film Thickness and Physical Aging on "Intrinsic" Gas Permeation Properties of Microporous Ethanoanthracene-Based Polyimides*. *Macromolecules*, 2018. **51**(3): p. 1069-1076.
121. Alberto, M., et al., *Impeded physical aging in PIM-1 membranes containing graphene-like fillers*. *Journal of Membrane Science*, 2018. **563**: p. 513-520.
122. Clarizia, G., F. Tasselli, and P. Bernardo, *Effect of Physical Aging on Gas Transport in Asymmetric Polyimide Hollow Fibers Prepared by Triple-Orifice Spinneret*. *Polymers (Basel)*, 2020. **12**(2).
123. Du, N., et al., *Azide-based cross-linking of polymers of intrinsic microporosity (PIMs) for condensable gas separation*. *Macromol Rapid Commun*, 2011. **32**(8): p. 631-6.
124. Du, N., et al., *High-Performance Carboxylated Polymers of Intrinsic Microporosity (PIMs) with Tunable Gas Transport Properties†*. *Macromolecules*, 2009. **42**(16): p. 6038-6043.
125. Ma, X., et al., *Synthesis and Gas Transport Properties of Hydroxyl-Functionalized Polyimides with Intrinsic Microporosity*. *Macromolecules*, 2012. **45**(9): p. 3841-3849.
126. Du, N., et al., *Polymer nanosieve membranes for CO₂-capture applications*. *Nat Mater*, 2011. **10**(5): p. 372-5.
127. Mason, C.R., et al., *Polymer of Intrinsic Microporosity Incorporating Thioamide Functionality: Preparation and Gas Transport Properties*. *Macromolecules*, 2011. **44**(16): p. 6471-6479.
128. Halder, K., et al., *Polymers of Intrinsic Microporosity Postmodified by Vinyl Groups for Membrane Applications*. *Macromolecules*, 2018. **51**(18): p. 7309-7319.

129. Ahn, J., et al., *Gas transport behavior of mixed-matrix membranes composed of silica nanoparticles in a polymer of intrinsic microporosity (PIM-1)*. Journal of Membrane Science, 2010. **346**(2): p. 280-287.
130. Bushell, A.F., et al., *Gas permeation parameters of mixed matrix membranes based on the polymer of intrinsic microporosity PIM-1 and the zeolitic imidazolate framework ZIF-8*. Journal of Membrane Science, 2013. **427**: p. 48-62.
131. Khan, M.M., et al., *Functionalized carbon nanotubes mixed matrix membranes of polymers of intrinsic microporosity for gas separation*. Nanoscale Research Letters, 2012. **7**(1): p. 504.
132. Halder, K., et al., *Blend membranes of ionic liquid and polymers of intrinsic microporosity with improved gas separation characteristics*. Journal of Membrane Science, 2017. **539**: p. 368-382.
133. Aliyev, E., et al., *Gas Transport Properties of the Metal–Organic Framework (MOF)-Assisted Polymer of Intrinsic Microporosity (PIM-1) Thin-Film Composite Membranes*. ACS Sustainable Chemistry & Engineering, 2020. **9**(2): p. 684-694.
134. Konnertz, N., et al., *Molecular mobility and gas transport properties of nanocomposites based on PIM-1 and polyhedral oligomeric phenethyl-silsesquioxanes (POSS)*. Journal of Membrane Science, 2017. **529**: p. 274-285.
135. Guiver, M.D. and Y.M. Lee, *Polymer Rigidity Improves Microporous Membranes*. Science, 2013. **339**(6117): p. 284-285.
136. Carta, M., et al., *An Efficient Polymer Molecular Sieve for Membrane Gas Separations*. Science, 2013. **339**(6117): p. 303-307.
137. Bezzu, C.G., et al., *A Spirobifluorene-Based Polymer of Intrinsic Microporosity with Improved Performance for Gas Separation*. Advanced Materials, 2012. **24**(44): p. 5930-5933.
138. Rose, I., et al., *Highly Permeable Benzotriptycene-Based Polymer of Intrinsic Microporosity*. ACS Macro Letters, 2015. **4**(9): p. 912-915.
139. Caliskan, E., et al., *Investigation of the Side Chain Effect on Gas and Water Vapor Transport Properties of Anthracene-Maleimide Based Polymers of Intrinsic Microporosity*. Polymers (Basel), 2021. **14**(1).

8. Appendix

8.1. Article 1: Investigation of the side chain effect on gas and water vapor transport properties of anthracene-maleimide based polymers of intrinsic microporosity

8.1.1. Graphical abstract

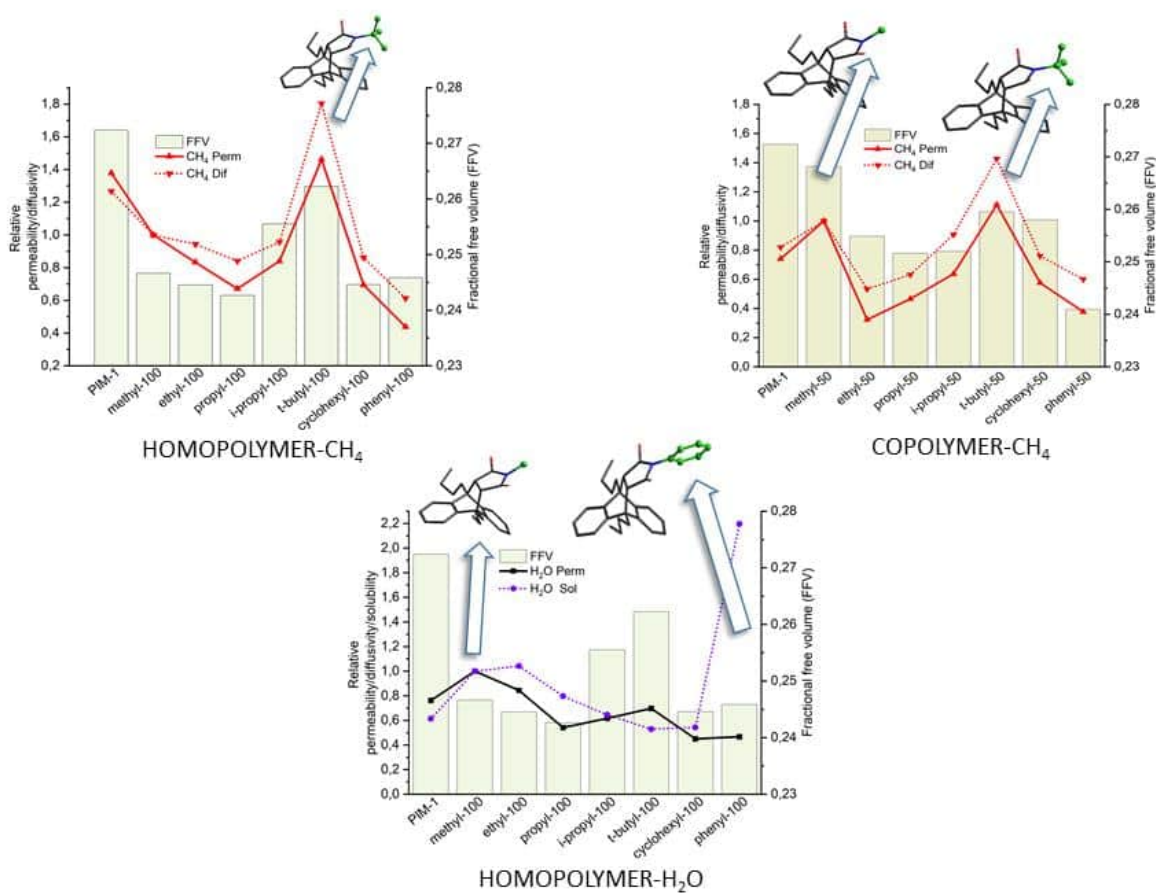


Figure 14: Graphical abstract of article 1.

8.1.2. Supporting information

Supplementary Information

Investigation of the side chain effect on gas and water vapor transport properties of anthracene-maleimide based polymers of intrinsic microporosity

Esra Caliskan¹, Sergey Shishatskiy¹, Silvio Neumann¹, Volker Abetz^{1,2}, Volkan Filiz^{1,*}

¹ Helmholtz-Zentrum Hereon, Institute of Membrane Research, Max-Planck-Str. 1, 21502 Geesthacht, Germany

² University of Hamburg, Institute of Physical Chemistry, Martin-Luther-King-Platz 6, 20146 Hamburg, Germany

* Correspondence: volkan.filiz@hereon.de; Tel.: +49-41-5287-2425

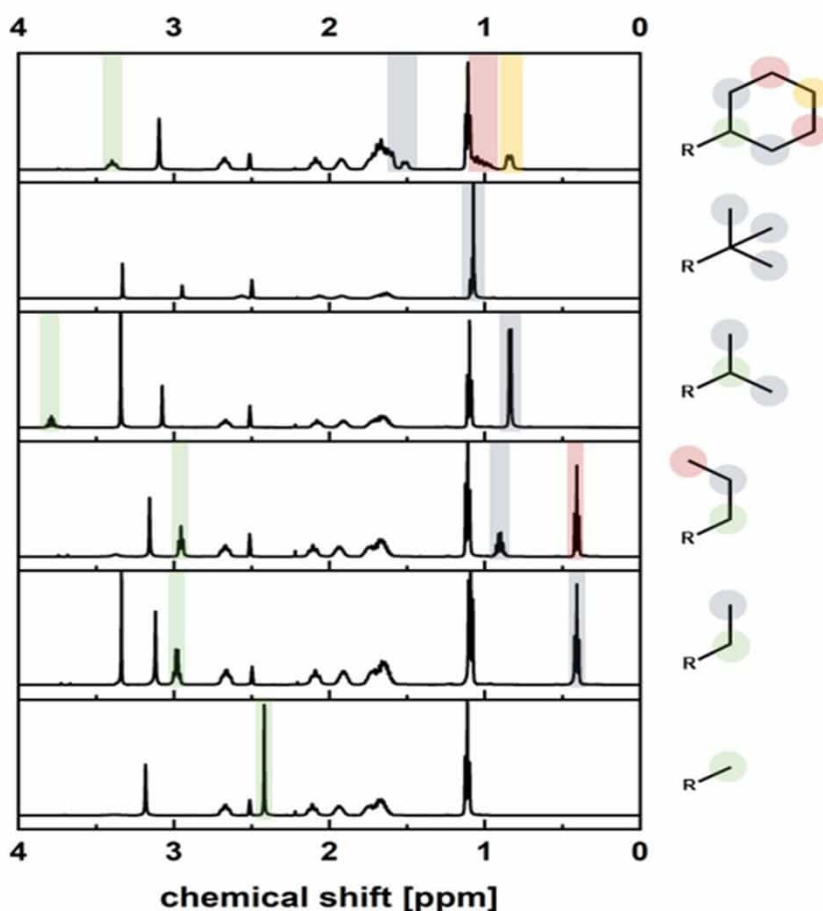


Figure S1. ¹H NMR spectra of all comonomers

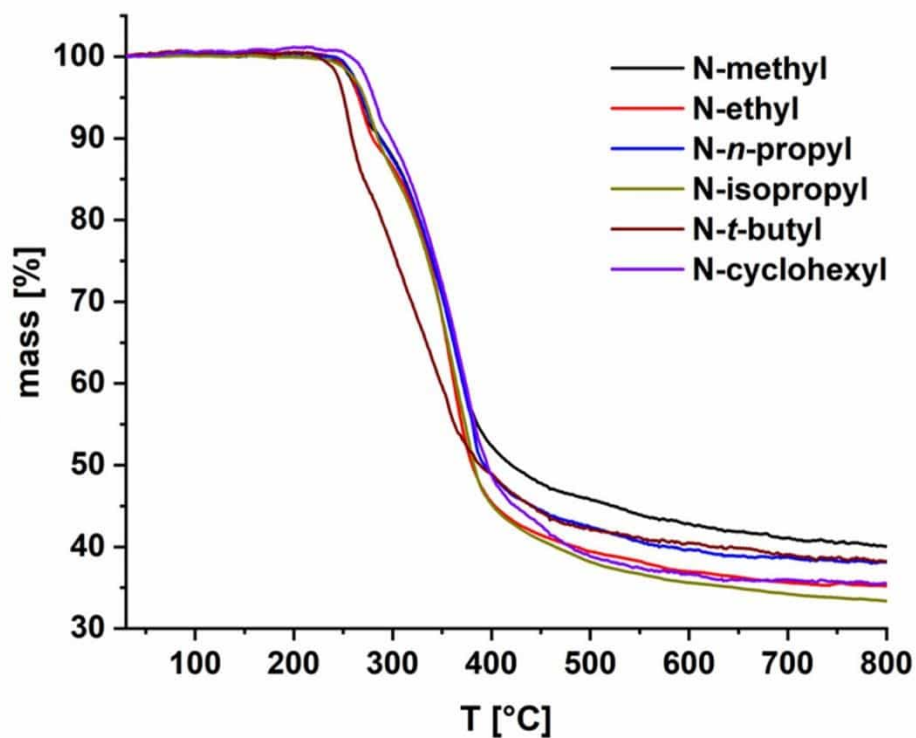


Figure S2. TGA curves of comonomers

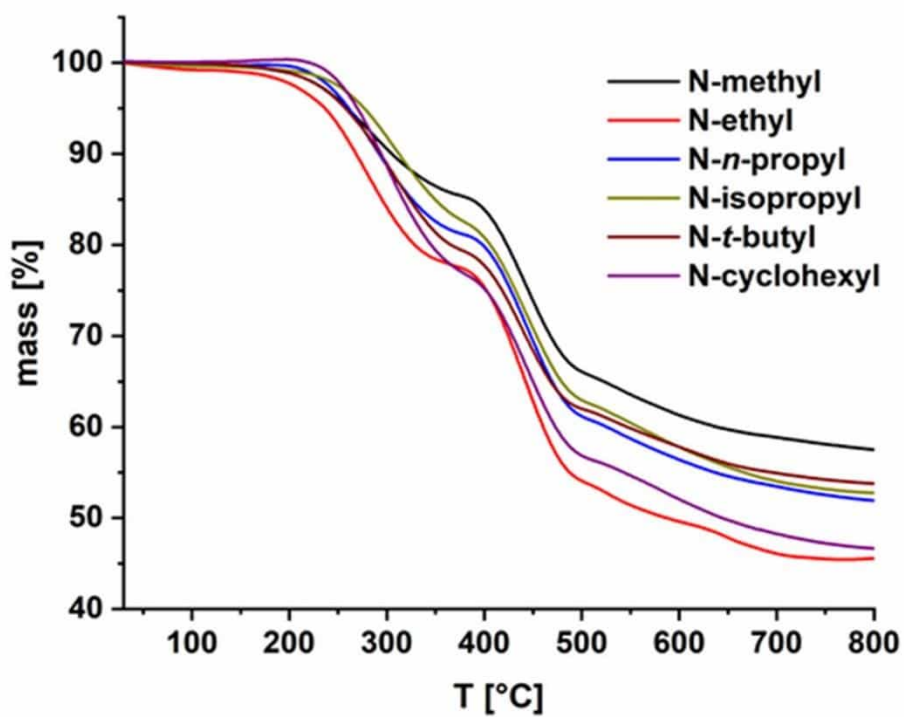


Figure S3. TGA curves of homopolymers

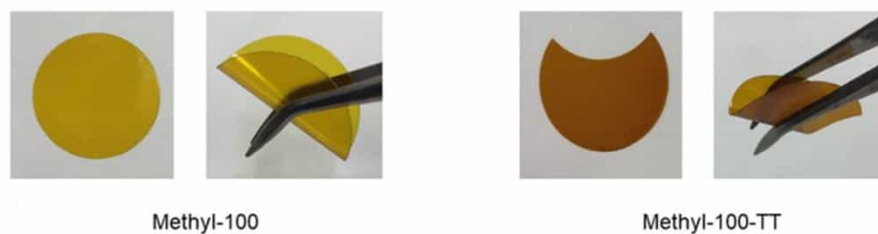


Figure S4. Optical images of methyl-100 before and after thermal treatments

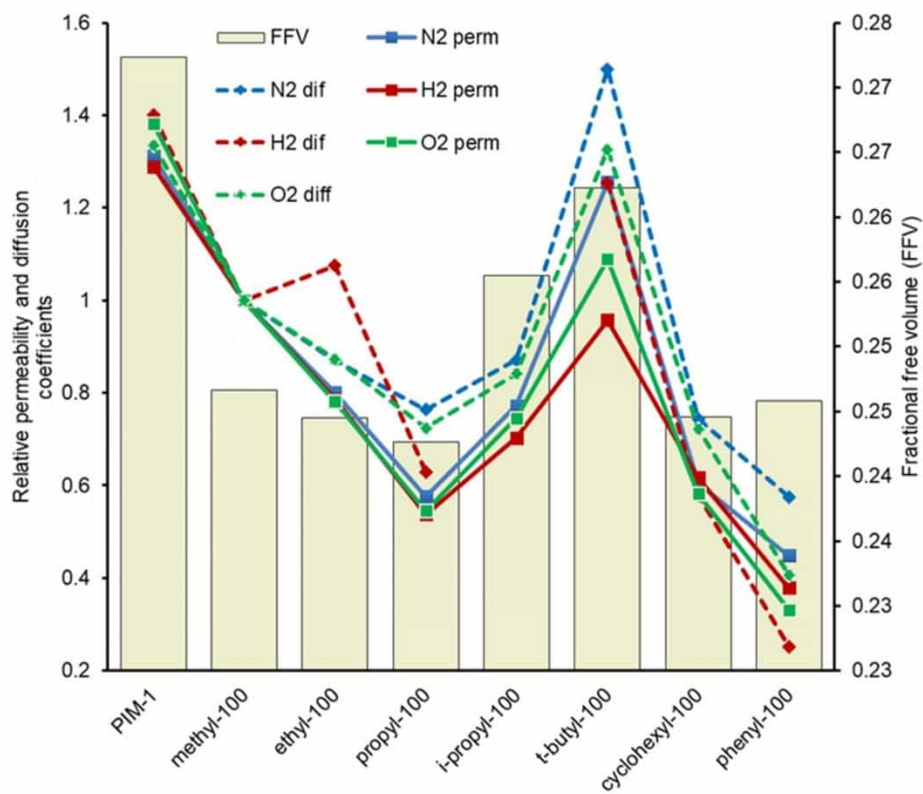


Figure S5. N₂, O₂, H₂ transport properties of homopolymers

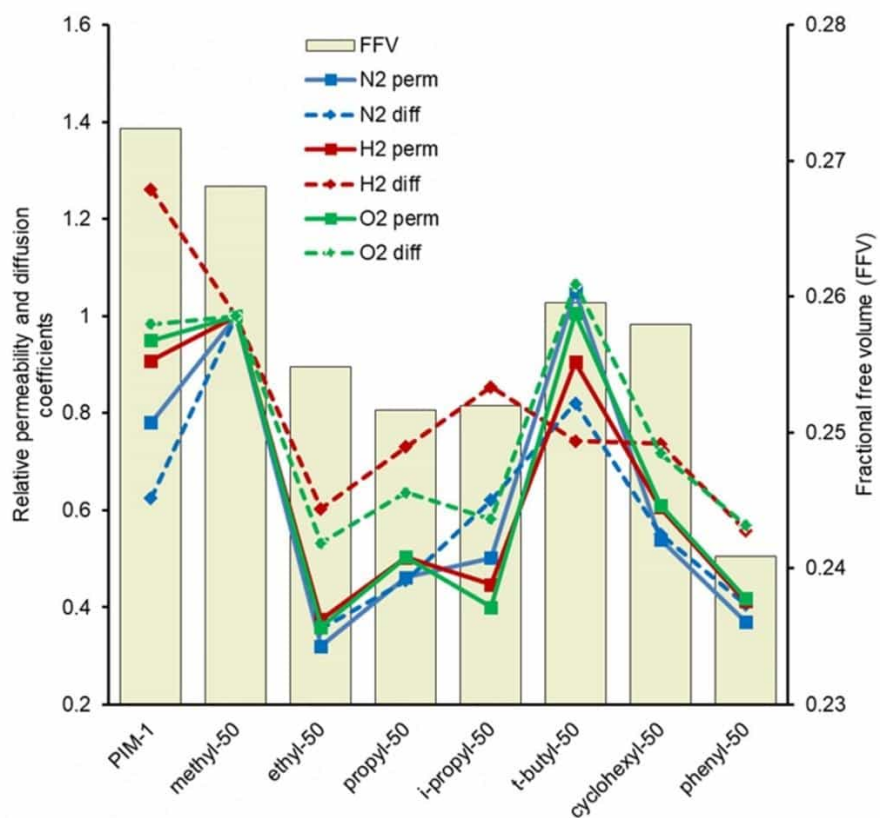


Figure S6. N₂, O₂, H₂ transport properties of copolymers

Table S1. Molecular weight data of polymers by GPC and polymer compositions calculated by ^1H NMR

| | M_w (kg/mol) * | Đ | Comonomer amount (%) ** |
|----------------------|---------------------------------|----------|--------------------------------|
| methyl-100 | 45.9 | 4.35 | - |
| methyl-50 | 85.5 | 4.24 | 49 |
| ethyl-100 | 52.9 | 3.53 | - |
| ethyl-50 | 68.5 | 3.49 | 50 |
| propyl-100 | 38.2 | 3.72 | - |
| propyl-50 | 75.1 | 3.75 | 49 |
| <i>i</i> -propyl-100 | 61.3 | 3.73 | - |
| <i>i</i> -propyl-50 | 98.0 | 4.32 | 48 |
| <i>t</i> -butyl-100 | 78.4 | 3.67 | - |
| <i>t</i> -butyl-50 | 97.1 | 5.27 | 48 |
| cyclohexyl-100 | 45.7 | 3.51 | - |
| cyclohexyl-50 | 63.5 | 3.44 | 48 |
| phenyl-100 | 78.3 | 3.43 | - |
| phenyl-50 | 76.3 | 3.86 | 47 |

Table S2. Permeability coefficients of PIM-1, homo- and copolymers determined at 30°C

| | Permeability (Barrer) | | | | | |
|-----------------------|-----------------------|----------------|----------------|-----------------|-----------------|------------------|
| | H ₂ | N ₂ | O ₂ | CO ₂ | CH ₄ | H ₂ O |
| PIM-1 | 2450 | 300 | 950 | 6120 | 475 | 79300 |
| <i>Homopolymer</i> | | | | | | |
| methyl-100 | 2160 | 300 | 735 | 4990 | 445 | 110000 |
| ethyl-100 | 1500 | 185 | 540 | 3860 | 290 | 87800 |
| propyl-100 | 1020 | 135 | 375 | 2800 | 230 | 56300 |
| <i>i</i> -propyl -100 | 1340 | 180 | 510 | 3680 | 290 | 64100 |
| <i>t</i> -butyl -100 | 1820 | 290 | 750 | 5570 | 505 | 72500 |
| cyclohexyl -100 | 1170 | 140 | 400 | 2860 | 240 | 46800 |
| phenyl-100 | 720 | 105 | 230 | 1640 | 150 | 48600 |
| <i>Copolymer</i> | | | | | | |
| methyl-50 | 2700 | 390 | 995 | 6980 | 640 | 114500 |
| ethyl -50 | 1010 | 125 | 360 | 2720 | 210 | 62700 |
| propyl -50 | 1360 | 180 | 500 | 3610 | 300 | 60100 |
| <i>i</i> -propyl -50 | 1200 | 190 | 400 | 2500 | 300 | 54800 |
| <i>t</i> -butyl -50 | 2440 | 410 | 1010 | 7200 | 710 | 88500 |
| cyclohexyl-50 | 1630 | 210 | 610 | 4280 | 370 | 60600 |
| phenyl-50 | 1110 | 145 | 420 | 3210 | 240 | 56400 |

Table S3. Diffusion coefficients of PIM-1, homo- and copolymers determined at 30°C

| | Diffusion coefficient (*10 ⁷) | | | | | |
|----------------------|---|----------------|----------------|-----------------|-----------------|------------------|
| | H ₂ * | N ₂ | O ₂ | CO ₂ | CH ₄ | H ₂ O |
| PIM-1 | 640 | 7.3 | 21.1 | 8.1 | 2.5 | 8.5 |
| <i>Homopolymer</i> | | | | | | |
| methyl-100 | 460 | 5.7 | 15.8 | 5.4 | 2.0 | 6.8 |
| ethyl-100 | 690 | 4.9 | 13.8 | 4.8 | 1.9 | 5.5 |
| propyl-100 | 290 | 4.3 | 11.4 | 4.2 | 1.7 | 4.6 |
| <i>i</i> -propyl-100 | - | 4.9 | 13.3 | 5.1 | 1.9 | 6.5 |
| <i>t</i> -butyl-100 | 570 | 8.5 | 21.0 | 8.4 | 3.6 | 9.0 |
| cyclohexyl-100 | 270 | 4.2 | 11.4 | 4.3 | 1.7 | 5.7 |
| phenyl-100 | 120 | 3.3 | 6.4 | 2.3 | 1.2 | 1.5 |
| <i>Copolymer</i> | | | | | | |
| methyl-50 | 510 | 11.7 | 21.5 | 7.4 | 3.1 | 5.5 |
| ethyl-50 | 310 | 4.2 | 11.4 | 4.4 | 1.6 | 5.4 |
| propyl-50 | 370 | 5.3 | 13.7 | 5.1 | 1.9 | 6.6 |
| <i>i</i> -propyl-50 | 430 | 7.3 | 12.5 | 3.9 | 2.3 | 2.2 |
| <i>t</i> -butyl-50 | 380 | 9.6 | 22.9 | 9.8 | 4.4 | 5.2 |
| cyclohexyl-50 | 370 | 6.5 | 15.4 | 6.1 | 2.3 | 7.2 |
| phenyl-50 | 283 | 4.8 | 12.2 | 5.1 | 1.8 | 6.6 |

* H₂ diffusion coefficient is given as indication only due to very short time-lag values

Table S4. Solubility coefficient of PIM-1, homo- and copolymers determined at 30°C

| | Solubility coefficient (*10 ³) | | | | | |
|----------------------|--|----------------|----------------|-----------------|-----------------|------------------|
| | H ₂ | N ₂ | O ₂ | CO ₂ | CH ₄ | H ₂ O |
| PIM-1 | 3.9 | 40 | 45 | 760 | 190 | 9350 |
| Homopolymer | | | | | | |
| methyl-100 | 4.2 | 40 | 45 | 900 | 173 | 15250 |
| ethyl-100 | 2.4 | 40 | 40 | 800 | 153 | 15900 |
| propyl-100 | 3.6 | 30 | 33 | 675 | 140 | 12150 |
| <i>i</i> -propyl-100 | - | 35 | 40 | 725 | 150 | 9850 |
| <i>t</i> -butyl-100 | 3.2 | 35 | 35 | 660 | 140 | 8100 |
| cyclohexyl-100 | 4.4 | 33 | 35 | 670 | 140 | 8300 |
| phenyl-100 | 6.3 | 30 | 35 | 715 | 125 | 33500 |
| Copolymer | | | | | | |
| methyl-50 | 5.6 | 40 | 47 | 940 | 210 | 21250 |
| ethyl-50 | 3.3 | 30 | 30 | 625 | 127 | 11350 |
| propyl-50 | 3.7 | 35 | 37 | 705 | 153 | 9150 |
| <i>i</i> -propyl-50 | 3.0 | 25 | 33 | 645 | 130 | 19300 |
| <i>t</i> -butyl-50 | 6.5 | 40 | 45 | 735 | 160 | 17250 |
| cyclohexyl-50 | 4.4 | 33 | 40 | 700 | 160 | 8400 |
| phenyl-50 | 3.9 | 30 | 35 | 630 | 130 | 8500 |

Table S5. Gas transport properties of methyl-100-TT* determined at 30°C

| | H ₂ | N ₂ | O ₂ | CO ₂ | CH ₄ | H ₂ O |
|---|----------------|----------------|----------------|-----------------|-----------------|------------------|
| Permeability (Barrer) | 690 | 105 | 215 | 1410 | 155 | 32000 |
| Diffusion coefficient (10 ⁷) | 127 | 3.5 | 6.6 | 2.2 | 1.2 | 1.0 |
| Solubility coefficient (10 ³) | 5.4 | 30 | 33 | 640 | 125 | 34150 |

*Thermal treatment at 250°C, 2h

8.2. Article 2: Pioneering the preparation of porous PIM-1 membranes for enhanced water vapor flow

8.2.1. Graphical abstract

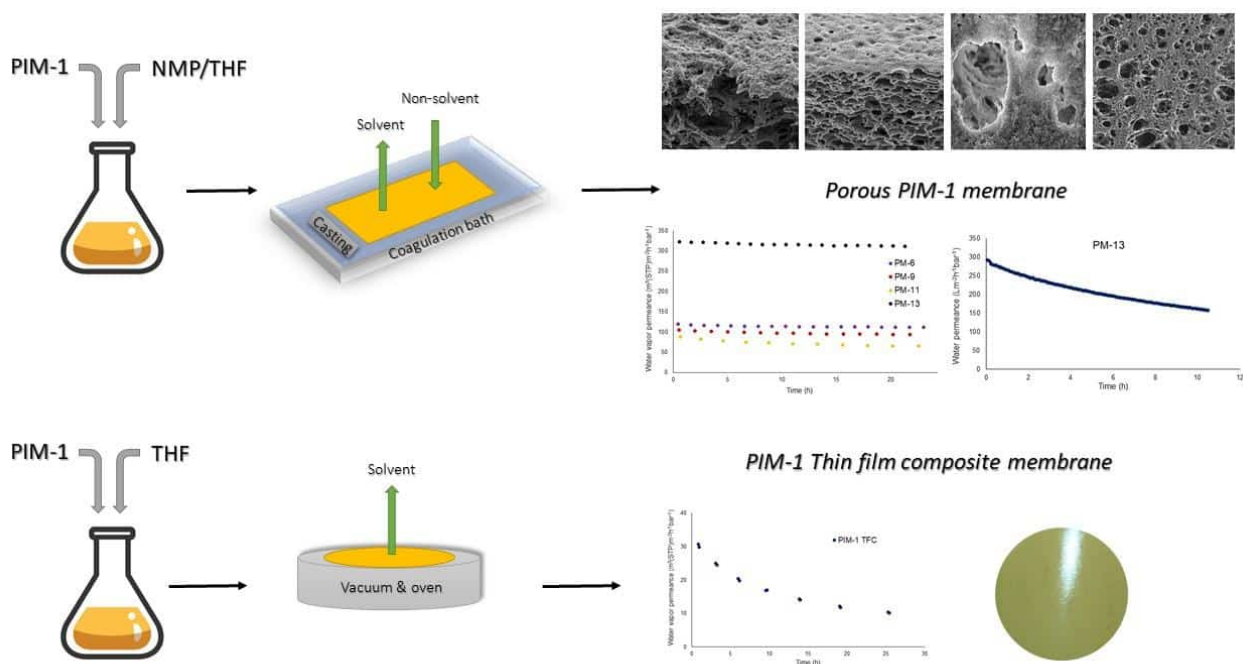


Figure 15: Graphical abstract of article 2.

8.2.2. Supporting information

Pioneering the preparation of porous PIM-1 membranes for enhanced water vapor flow

Esra Caliskan¹, Sergey Shishatskiy¹, Volker Abetz^{1,2}, Volkan Filiz^{1*}

¹ Institute of Membrane Research, Helmholtz-Zentrum Hereon, Max-Planck-Str. 1, 21502 Geesthacht, Germany;

² Institute of Physical Chemistry, University of Hamburg, Martin-Luther-King-Platz 6, 20146 Hamburg, Germany

* Correspondence: volkan.filiz@hereon.de; Tel.: +49-41-5287-242

Supplementary Information

Table S1: Composition of casting solutions and membrane casting parameters

| Name | Composition (%wt.) | Precipitation bath | Batch | Membrane casting thickness | M _w (kDa) |
|------|--|--------------------|----------|--------------------------------|----------------------|
| PM-1 | PIM/THF/DMAc/EtOH: 17.5/67.5/12.75/2.25 | Water | PIM-LT-1 | 200 µm | 76 |
| PM-2 | PIM/THF/DMAc: 17.25/69.5/13.25 | Water | PIM-LT-1 | 150 µm | 76 |
| PM-3 | PIM/NMP/THF: 12.5/69.5/18 | Water | PIM-LT-2 | 150 µm (on glass substrate) | 76 |
| PM-4 | PIM/DCB: 10/90 | MeOH | PIM-LT-2 | 150 µm (on glass substrate) | 76 |

| | | | | | |
|-------|----------------------------------|------------------------|----------|--|-----|
| PM-5 | PIM/DCB: 10/90 | MeOH/BuOH 50:50 | PIM-LT-2 | 150 μm (on glass substrate) | 76 |
| PM-7 | PIM/NMP/THF: 13/80/7 | MeOH | PIM-LT-2 | 150 μm (on glass substrate) | 76 |
| PM-8 | PIM/NMP/THF: 14.5/80.5/5 | Water | PIM-LT-2 | 150 μm | 76 |
| PM-10 | PIM/NMP/THF: 13/79/8 | Water | PIM-LT-1 | 150 μm | 76 |
| PM-12 | PIM/NMP/THF: 11.5/72/16.5 | Water | PIM-HT | 150 μm | 142 |
| PM-14 | PIM/NMP/THF: 13/80/7 | Water | PIM-LT-2 | 150 μm | 76 |

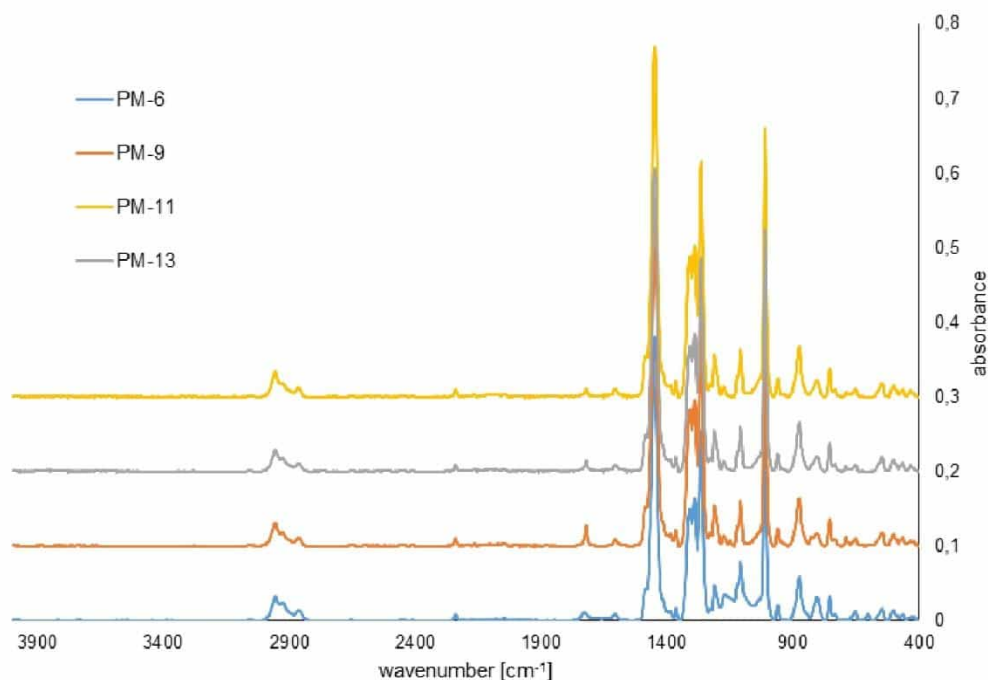


Figure S1: Comparative FTIR spectrum of PM-6, PM-9, PM-11 and PM-13

FTIR analysis was carried out to characterize the porous PIM-1 membranes which are PM-6, PM-9, PM-11 and PM-13. FTIR spectrum show the absorption bands at 2239 cm^{-1} and 1265 cm^{-1} which correspond to nitrile groups ($\text{C}\equiv\text{N}$ stretching). The absorption band between $2800\text{--}2900\text{ cm}^{-1}$ and at 1146 cm^{-1} are associated with CH_2 stretching and bending vibration modes. The spectrum in the region at $1350\text{--}1250\text{ cm}^{-1}$ originates from C-O stretching mode. Characteristic C-N stretching appears at 1009 cm^{-1} and aromatic sp^2 C-H bending is visible at 874 cm^{-1} .

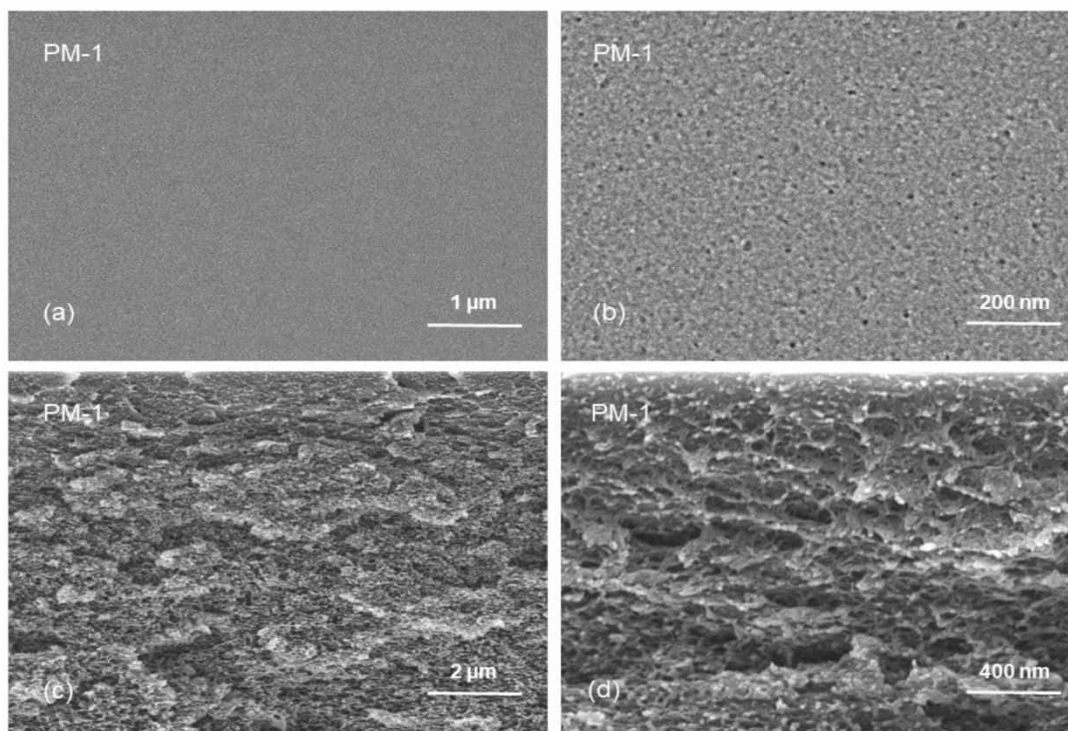


Figure S2: Surface (a, b) and cross-sectional (c, d) morphology of PM-1

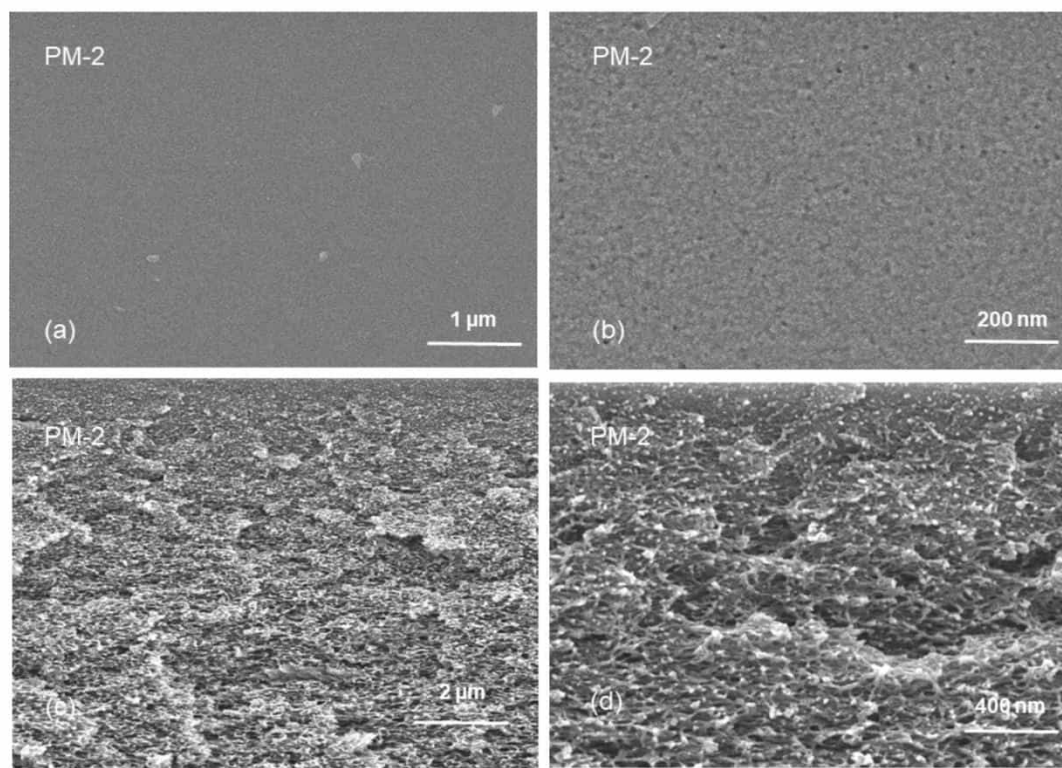


Figure S3: Surface (a, b) and cross-sectional (c, d) morphology of PM-2

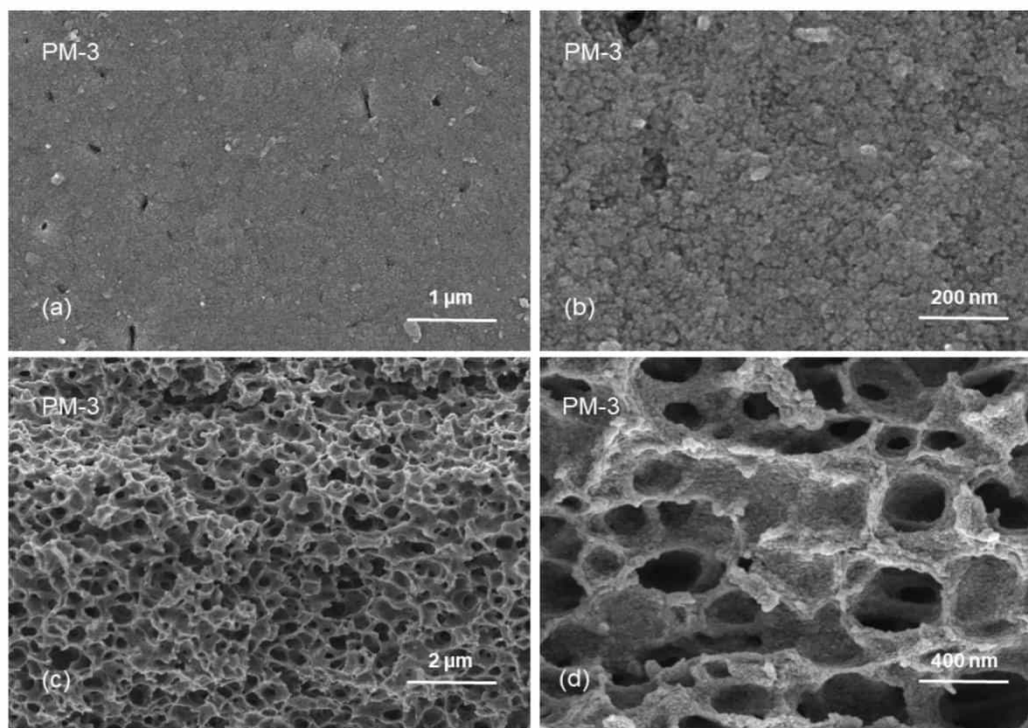


Figure S4: Surface (a, b) and cross-sectional (c, d) morphology of PM-3

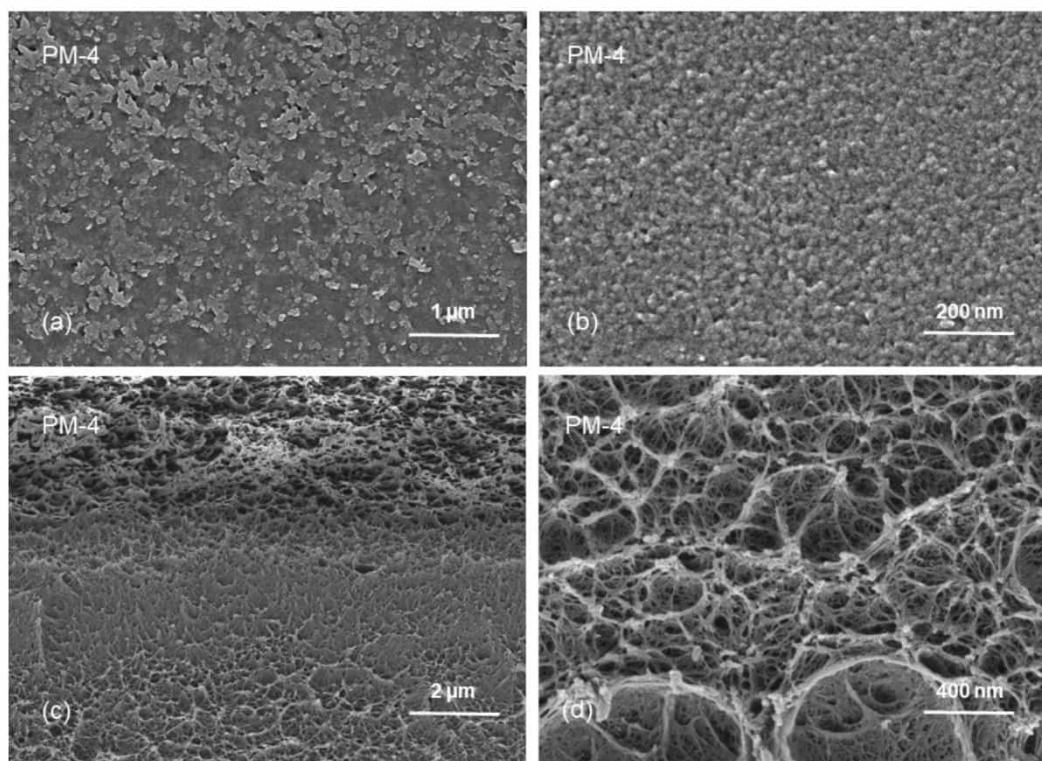


Figure S5: Surface (a, b) and cross-sectional (c, d) morphology of PM-4

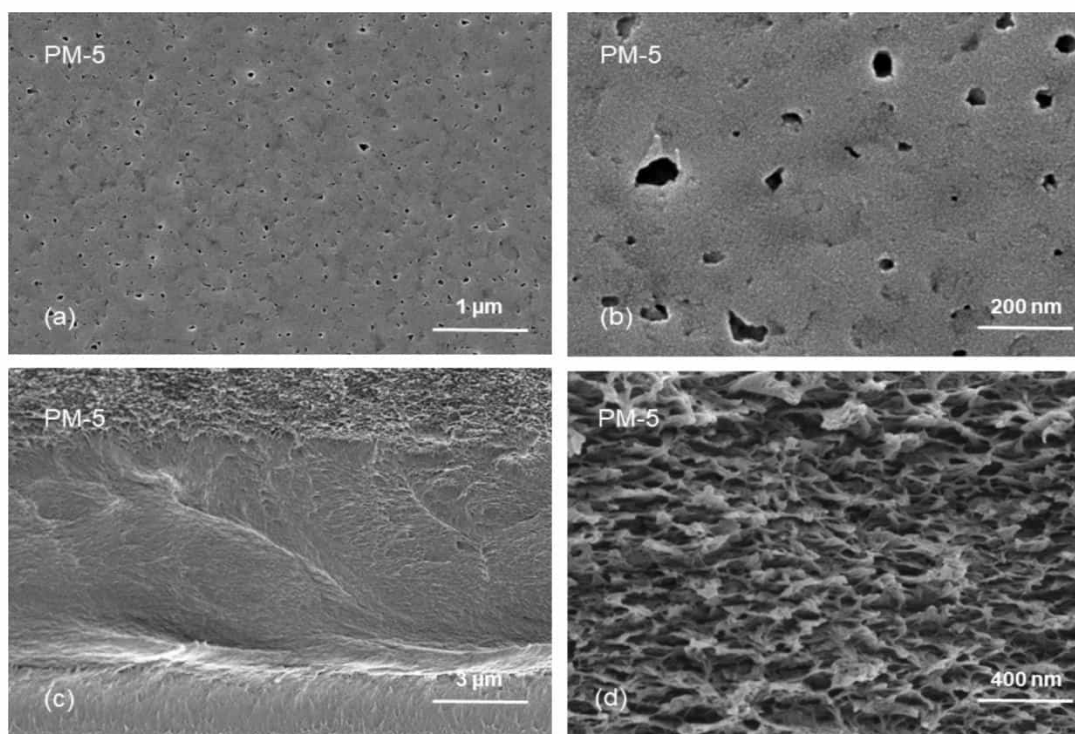


Figure S6: Surface (a, b) and cross-sectional (c, d) morphology of PM-5

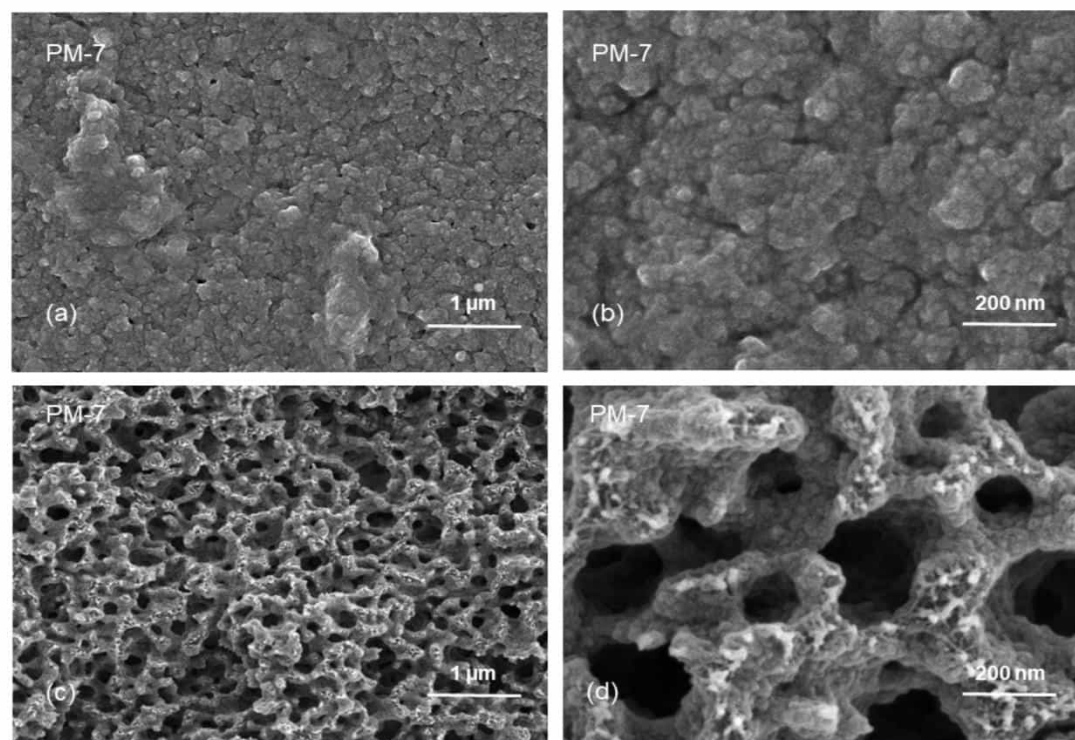


Figure S7: Surface (a, b) and cross-sectional (c, d) morphology of PM-7

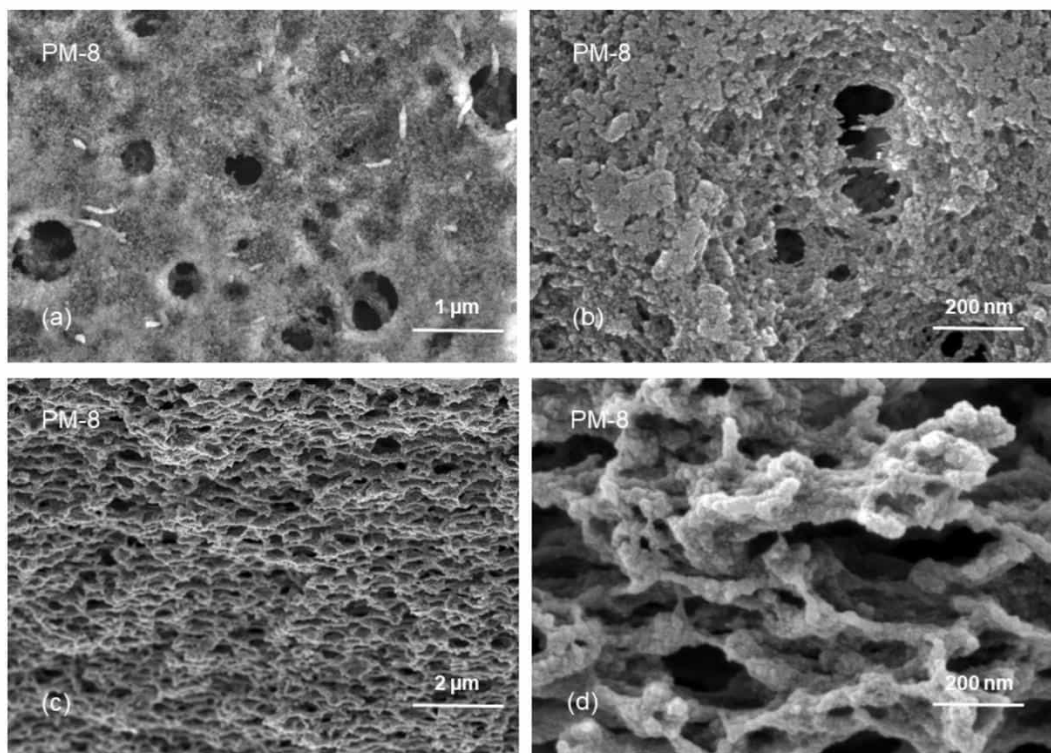


Figure S8: Surface (a, b) and cross-sectional (c, d) morphology of PM-8

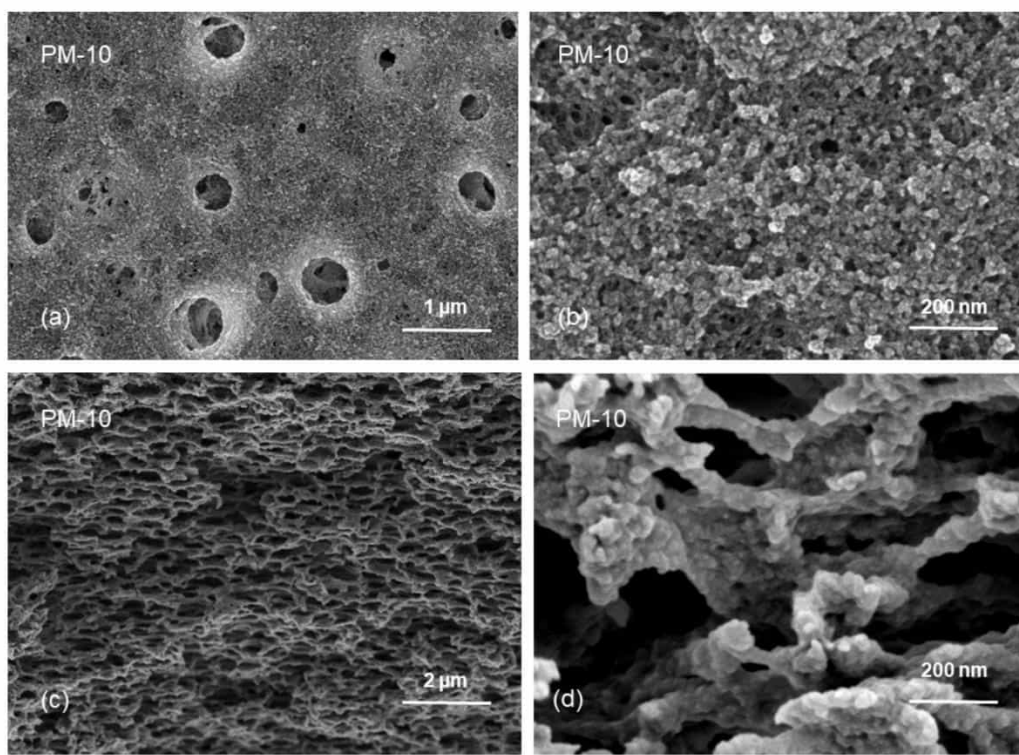


Figure S9: Surface (a, b) and cross-sectional (c, d) morphology of PM-10

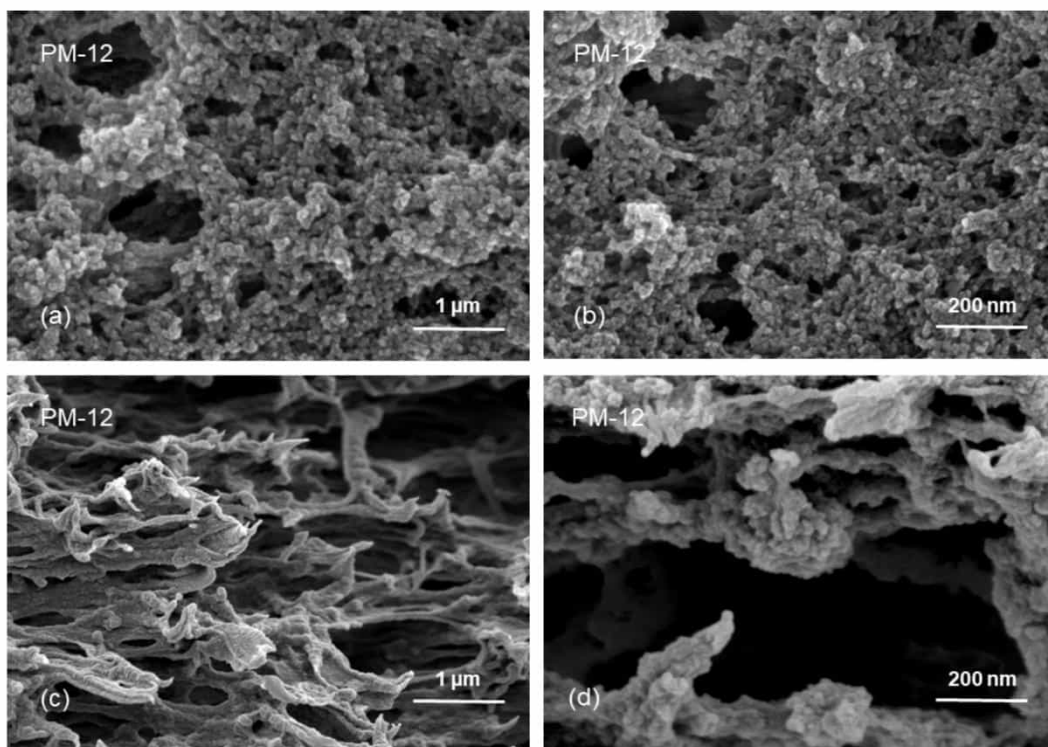


Figure S10: Surface (a, b) and cross-sectional (c, d) morphology of PM-12

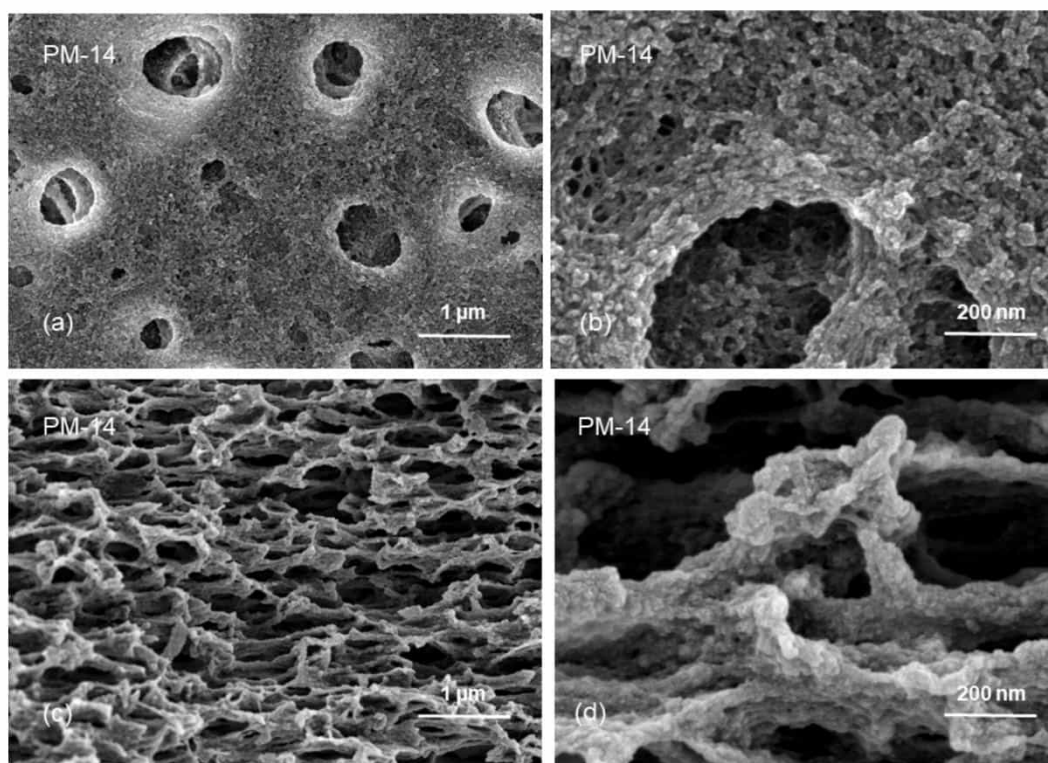


Figure S11: Surface (a, b) and cross-sectional (c, d) morphology of PM-14

Table S2: Water vapor permeance of PIM-1 membranes

| | Water permeance (m ³ (STP)m ⁻² h ⁻¹ bar ⁻¹) | Batch |
|--------------|---|----------|
| PM-1 | 35 | PIM-LT-1 |
| PM-2 | 42 | PIM-LT-1 |
| PM-8 | 124 | PIM-LT-2 |
| PM-10 | 350 | PIM-LT-1 |
| PM-14 | 201 | PIM-LT-2 |

The measurement was performed at 30 °C and first measurement points of each membrane are displayed in **Table-S2**. PM-3, PM-4, PM-5 and PM-7 membranes were casted on a glass substrate. Therefore, water vapor permeance measurement could not be carried out since the membranes were not mechanically stable, it was difficult to handle these samples.

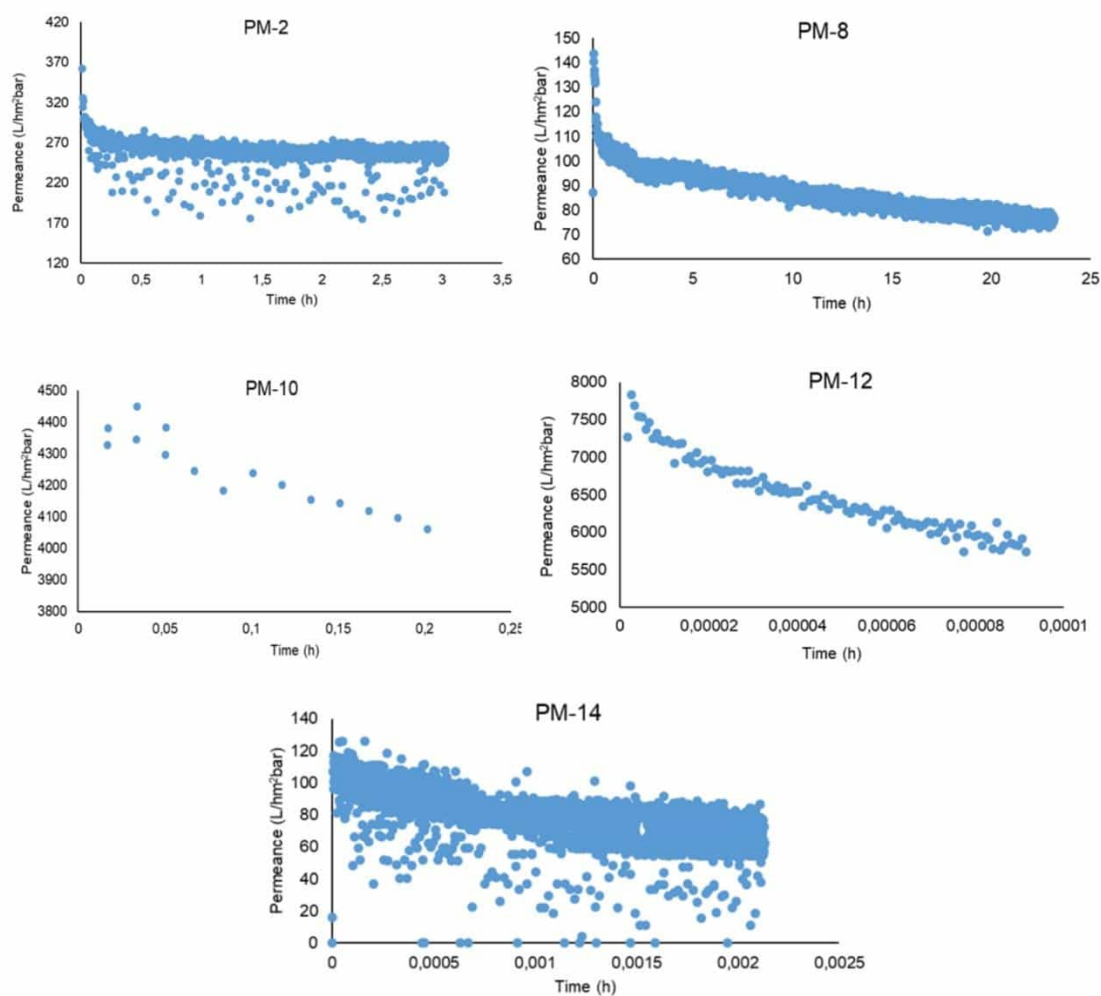


Figure S12: Water flux of membranes

Water flux measurement of PM-1 could not be carried out due to exfoliation of the membrane from the support.

8.3. Article 3: Comparative study of polymer of intrinsic microporosity-derivative polymers in pervaporation and water vapor permeance applications

8.3.1. Graphical abstract

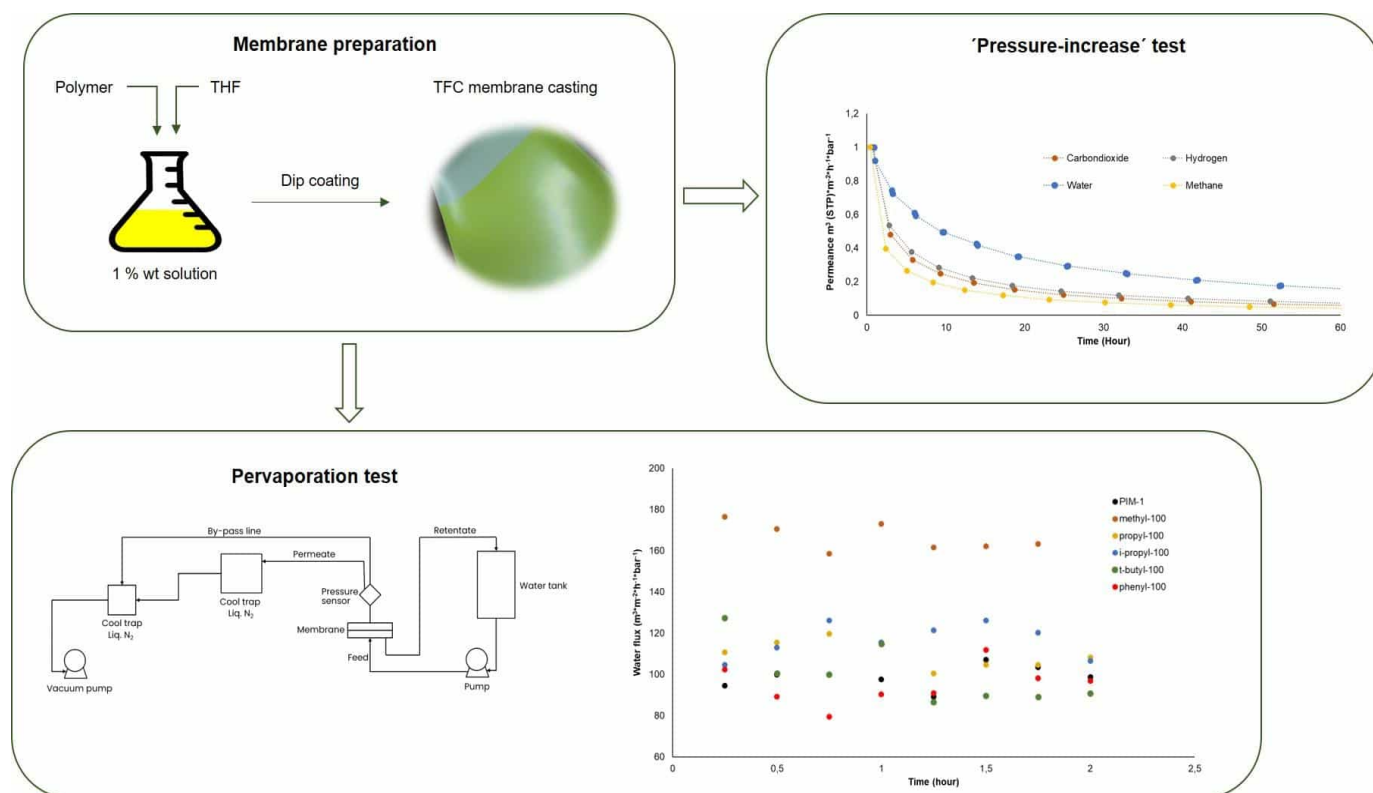


Figure 16: Graphical abstract of article 3.

8.3.2. Supporting information

Supplementary Information

Comparative study of PIM derivative polymers in pervaporation and water vapor permeance applications

Esra Caliskan¹, Sergey Shishatskiy¹, Volkan Filiz¹, *

¹ Helmholtz-Zentrum Hereon, Institute of Membrane Research, Max-Planck-Str. 1, 21502 Geesthacht, Germany

* Correspondence: volkan.filiz@hereon.de; Tel.: +49-41-5287-2425

Table S1. Gas and water vapor permeance of PIM-1 at different hours

| | Gas permeance ($\text{m}^3(\text{STP}) \text{ m}^{-2} \text{ h}^{-1} \text{ bar}^{-1}$) | |
|----------------------------------|---|----------|
| | @hour=1 | @hour=20 |
| CH ₄ | 0.128 | 0.018 |
| CO ₂ | 2.16 | 0.306 |
| H ₂ | 2.830 | 0.482 |
| H ₂ O | 47.8 | 12.3 |
| | Gas selectivity | |
| | @hour=1 | @hour=20 |
| H ₂ /CH ₄ | 22.2 | 26.7 |
| H ₂ /CO ₂ | 1.31 | 1.57 |
| CO ₂ /CH ₄ | 16.9 | 17.0 |
| H ₂ O/CH ₄ | 373.4 | 683.3 |
| H ₂ O/CO ₂ | 22.1 | 40.2 |
| H ₂ O/ H ₂ | 16.9 | 25.5 |

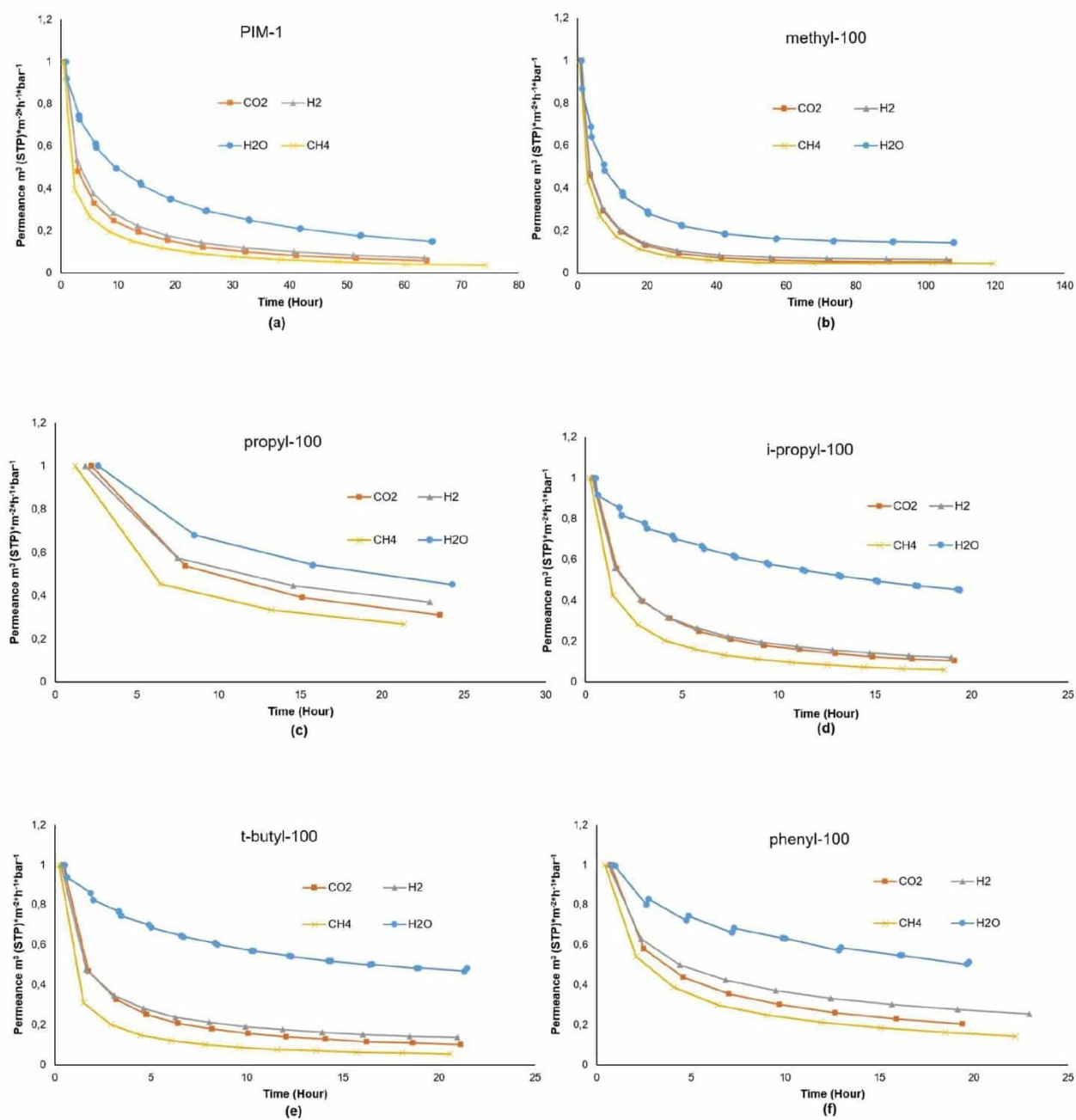


Figure S1: Gas and vapor permeance decay homopolymers-complete measurement

8.4. Safety hazards

| Substance | GHS-Symbol | Hazard statements | Precautionary statements |
|--|---------------------|------------------------------------|--|
| 5,5',6,6'-Tetrahydroxy-3,3,3',3'-tetramethyl-1,1'-spirobisindane | GHS02, GHS07, GHS08 | H301, H315, H319, H335 | P261, P301+ P310, P305+ P351+P338 |
| 2,3,5,6-Tetrafluoro-terephthalonitrile | GHS02, GHS07, GHS08 | H301, HH315, H319, H335 | P261, P301+P310, P305 +P351+P338 |
| Potassium carbonate | GHS02, GHS07, GHS08 | H302, H315, H319, H335 | P261, P301+P310, P305 +P351+P338 |
| Boron tribromide | GHS05, GHS06 | H330, H300, H314 | P260, P264, P280, P284, P301+P310, P305+P351+P338 |
| N-Methyl maleimide | GHS05, GHS07 | H302, H314, H317 | P260, P272, P280 P301 + P312 P303 + P361 + P353 P305 + P351 + P338 |
| N-Ethyl maleimide | GHS05, GHS06 | H300, H31, H314, H317 | P260, P280, P301+P310+P330, P303+P361+P353, P305+P351+P338+P310 |
| N-Propyl maleimide | GHS02, GHS07 | H226, H302, H317 | P210, P280, P301+P312+P330, P302+P352 |
| T-Butyl maleimide | GHS07 | H315, H319, H335 | P261, P264, P271, P280, P302+P352, P305+P351+P338 |
| Cyclohexyl maleimide | GHS06, GHS09 | H301, H315, H317, H319, H335, H410 | P261, P273, P280, P301+P310, P302+P352, P305+P351+P338 |
| Isopropyl amine | GHS02, GHS05, GHS06 | H224, H301+H311+H331, H314, H335 | P210, P233, P280, P303+P361+P353, P304+P340+P310, |


| | | | |
|----------------------|---------------------------|----------------------------------|--|
| | | | P305+P351+P338, P403+P233 |
| Maleic anhydride | GHS05, GHS07, GHS08 | H302, H314, H317, H334, H372 | P260, P280, P301+P312, P303+P361+P353, P304+P340+P310, P305+P351+P338 |
| Acetaldehyde | GHS02, GHS07, GHS08 | H225, H319, H335, H341, H350 | P202, P210, P233, P240, P305+P351+P338, P308+P313 |
| 1,2-Dimethoxybenzene | GHS07 | H302 | P301+P312+P330 |
| Sulphuric acid | GHS05 | H314 | P260, P264, P280, P301+P330+P331, P302+P361+P354, P304+P340, P305+P354+P338, P316, P321, P363, P405, P501 |
| Sodium hydroxide | GHS05 | H314 | P280, P305+P351+P338,P310 |
| Pentanal | GHS02, GHS07 | H225, H317, H319, H332, H335 | P210, P233, P280, P303+P361+P353, P304+P340+P312, P305+P351+P338 |
| Methanol | GHS02, GHS06, GHS08 | H225, H301+H311+H331, H370 | P210, P280, P301+P310+P330, P302+P352+P312, P304+P340+P311 |
| Ethanol | GHS02, GHS07, GHS08 | H225, H302, H371 | P210, P260 |
| I-Propanol | GHS02, GHS07 | H225, H319, H336 | P210, P233, P240, P241, P242, P305+P351+P338 |
| Tetrahydrofuran | GHS02, GHS07 | H225, H319, H351 | P210, P261, P305+P351+P338 |

| | | | |
|-----------------------|-------------------------------------|--|--|
| Acetone | GHS02, GHS07 | H225, H319, H336 | P210, P233, P241, P242, P305 + P351 + P338 |
| Dimethylacetamide | GHS02, GHS07 | H332, H312, H319, H360D | P210, P280, P305+P351+P338, P308+ P313 |
| N,N-Dimethylformamide | GHS02, GHS07, GHS08 | H226, H312+H332, H319, H360D | P201, P280, P305+P351+P338, P308+ P313 |
| Diethyl benzene | GHS02, GHS07, GHS15 | H226, H315, H304, H400, H410 | P273, P301+ P310, P331, P501 |
| Dichloromethane | GHS07, GHS08 | H315, H319, H335, H336, H351, H373 | P261, P281, P305+P351+P338 |
| Acetic acid | GHS02, GHS05 | H226, H314 | P210, P233, P240, P280, P303+P361+P353, P305+P351+P338 |
| Chloroform | GHS02, GHS07, GHS08 | H302, H332, H315, H319, H351, H361d H336, H373 | P261, P281, P305+P351+P338 |
| N-Pentane | GHS02, GHS07, GHS08, GHS09 | H225, H304, H336, H411 | P210, P273, P301+P310+P331 |
| Toluene | GHS02, GHS07, GHS08 | H225, H304, H315, H336, H361d, H373 | P210, P261, P281, P301+P310, P331 |
| Aniline | GHS05, GHS06, GHS08, GHS09 | H301+H311+H331, H317, H318, H341, H351, H372, H410 | P273, P280, P301+P310, P302+P352+P312, P304+P340+P311, P305+P351+P338 |

| | | | |
|------------------------|-------------------------------------|---|--|
| Diethyl ether | GHS02, GHS07 | H224, H302, H336 | P210, P261 |
| 1,4- Dichlorobenzene | GHS07, GHS08, GHS09 | H319, H351, H410 | P202, P264, P273, P280, P305+P351+P338, P308+P313 |
| Cyclohexane | GHS02, GHS07, GHS08, GHS09 | H225, H304, H315, H336, H410 | P210, P233, P273, P301+P310, P303+P361+P353-P331 |
| N-Methyl-2-pyrrolidone | GHS08, GHS07 | H315, H319, H335, H360D | P202, P261, P264, P302 + P352, P305 + P351 + P338, P308 + P313 |
| O-xylene | GHS02, GHS07, GHS08 | H226, H304, H312 + H332, H315, H319, H335, H412 | P210, P273, P280, P301 + P310, P303 + P361 + P353, P331 |

8.5. Copyright permissions

8.5.1. Figure 2



This is a License Agreement between Esra Caliskan ("User") and Copyright Clearance Center, Inc. ("CCC") on behalf of the Rightsholder identified in the order details below. The license consists of the order details, the Marketplace Permissions General Terms and Conditions below, and any Rightsholder Terms and Conditions which are included below. All payments must be made in full to CCC in accordance with the Marketplace Permissions General Terms and Conditions below.

| | | | |
|------------------|-------------|-------------|------------------------------------|
| Order Date | 11-Sep-2024 | Type of Use | Republish in a thesis/dissertation |
| Order License ID | 1525399-1 | Publisher | John Wiley |
| ISSN | 2195-1071 | Portion | Image/photo/illustration |

LICENSED CONTENT

| | | | |
|-------------------|---|------------------|-----------|
| Publication Title | ADVANCE OPTICAL MATERIALS | Publication Type | e-Journal |
| Article Title | Advances in Functional Solution Processed Planar 1D Photonic Crystals | Start Page | 1800730 |
| Date | 01/01/2013 | Issue | 24 |
| Country | United States of America | Volume | 6 |
| Rightsholder | John Wiley & Sons - Books | | |

REQUEST DETAILS

| | | | |
|---|---|-----------------------------|----------------------------------|
| Portion Type | Image/photo/illustration | Distribution | Worldwide |
| Number of Images / Photos / Illustrations | 1 | Translation | Original language of publication |
| Format (select all that apply) | Print, Electronic | Copies for the Disabled? | No |
| Who Will Republish the Content? | Academic institution | Minor Editing Privileges? | No |
| Duration of Use | Life of current and all future editions | Incidental Promotional Use? | No |
| Lifetime Unit Quantity | Up to 14,999 | Currency | EUR |
| Rights Requested | Main product | | |

| NEW WORK DETAILS | | | |
|---|---|--|---|
| Title | Polymers of intrinsic microporosity (thesis name will be defined later) | Institution Name | University of Hamburg |
| Instructor Name | Esra Caliskan | Expected Presentation Date | 2024-12-22 |
| ADDITIONAL DETAILS | | | |
| The Requesting Person / Organization to Appear on the License | Esra Caliskan | | |
| REQUESTED CONTENT DETAILS | | | |
| Title, Description or Numeric Reference of the Portion(s) | Figure 14 | Title of the Article / Chapter the Portion Is From | Advances in Functional Solution Processed Planar 1D Photonic Crystals |
| Editor of Portion(s) | Comoretto, Davide; Lova, Paola; Manfredi, Giovanni | Author of Portion(s) | Comoretto, Davide; Lova, Paola; Manfredi, Giovanni |
| Volume / Edition | 6 | Publication Date of Portion | 2018-12-01 |
| Page or Page Range of Portion | 1800730 | | |

8.5.2. Figure 4

ELSEVIER LICENSE TERMS AND CONDITIONS Dec 07, 2024

This Agreement between Esra Caliskan ("You") and Elsevier ("Elsevier") consists of your license details and the terms and conditions provided by Elsevier and Copyright Clearance Center.

| | |
|--|---|
| License Number | 5866131116705 |
| License date | Sep 11, 2024 |
| Licensed Content Publisher | Elsevier |
| Licensed Content Publication | Journal of Membrane Science |
| Licensed Content Title | Comparison of transport properties of rubbery and glassy polymers and the relevance to the upper bound relationship |
| Licensed Content Author | Lloyd M. Robeson, Qiang Liu, Benny D. Freeman, Donald R. Paul |
| Licensed Content Date | Feb 15, 2015 |
| Licensed Content Volume | 476 |
| Licensed Content Issue | n/a |
| Licensed Content Pages | 11 |
| Start Page | 421 |
| End Page | 431 |
| Type of Use | reuse in a thesis/dissertation |
| Portion | figures/tables/illustrations |
| Number of figures/tables/illustrations | 1 |
| Format | both print and electronic |

| | |
|---|---|
| Are you the author of this Elsevier article? | No |
| Will you be translating? | No |
| Title of new work | Polymers of intrinsic microporosity (thesis name will be defined later) |
| Institution name | University of Hamburg |
| Expected presentation date | Dec 2024 |
| Portions | Figure 14 |
| The Requesting Person / Organization to Appear on the License | Esra Caliskan Helmholtz zentrum hereon Max Planck street |
| Requestor Location | Geesthacht, other Germany |
| Order reference number | 110924 |
| Publisher Tax ID | GB 494 6272 12 |
| Total | 0.00 EUR |
| Terms and Conditions | |

INTRODUCTION

1. The publisher for this copyrighted material is Elsevier. By clicking "accept" in connection with completing this licensing transaction, you agree that the following terms and conditions apply to this transaction (along with the Billing and Payment terms and conditions established by Copyright Clearance Center, Inc. ("CCC"), at the time that you opened your RightsLink account and that are available at any time at <https://myaccount.copyright.com>).

GENERAL TERMS

2. Elsevier hereby grants you permission to reproduce the aforementioned material subject to the terms and conditions indicated.

3. Acknowledgement: If any part of the material to be used (for example, figures) has appeared in our publication with credit or acknowledgement to another source, permission must also be sought from that source. If such permission is not obtained then that material may not be included in your publication/copies. Suitable acknowledgement to the source must be made, either as a footnote or in a reference list at the end of your publication, as follows:

"Reprinted from Publication title, Vol /edition number, Author(s), Title of article / title of chapter, Pages No., Copyright (Year), with permission from Elsevier [OR APPLICABLE SOCIETY COPYRIGHT OWNER]." Also Lancet special credit - "Reprinted from The

Lancet, Vol. number, Author(s), Title of article, Pages No., Copyright (Year), with permission from Elsevier."

4. Reproduction of this material is confined to the purpose and/or media for which permission is hereby given. The material may not be reproduced or used in any other way, including use in combination with an artificial intelligence tool (including to train an algorithm, test, process, analyse, generate output and/or develop any form of artificial intelligence tool), or to create any derivative work and/or service (including resulting from the use of artificial intelligence tools).

5. Altering/Modifying Material: Not Permitted. However figures and illustrations may be altered/adapted minimally to serve your work. Any other abbreviations, additions, deletions and/or any other alterations shall be made only with prior written authorization of Elsevier Ltd. (Please contact Elsevier's permissions helpdesk [here](#)). No modifications can be made to any Lancet figures/tables and they must be reproduced in full.

6. If the permission fee for the requested use of our material is waived in this instance, please be advised that your future requests for Elsevier materials may attract a fee.

7. Reservation of Rights: Publisher reserves all rights not specifically granted in the combination of (i) the license details provided by you and accepted in the course of this licensing transaction, (ii) these terms and conditions and (iii) CCC's Billing and Payment terms and conditions.

8. License Contingent Upon Payment: While you may exercise the rights licensed immediately upon issuance of the license at the end of the licensing process for the transaction, provided that you have disclosed complete and accurate details of your proposed use, no license is finally effective unless and until full payment is received from you (either by publisher or by CCC) as provided in CCC's Billing and Payment terms and conditions. If full payment is not received on a timely basis, then any license preliminarily granted shall be deemed automatically revoked and shall be void as if never granted. Further, in the event that you breach any of these terms and conditions or any of CCC's Billing and Payment terms and conditions, the license is automatically revoked and shall be void as if never granted. Use of materials as described in a revoked license, as well as any use of the materials beyond the scope of an unrevoked license, may constitute copyright infringement and publisher reserves the right to take any and all action to protect its copyright in the materials.

9. Warranties: Publisher makes no representations or warranties with respect to the licensed material.

10. Indemnity: You hereby indemnify and agree to hold harmless publisher and CCC, and their respective officers, directors, employees and agents, from and against any and all claims arising out of your use of the licensed material other than as specifically authorized pursuant to this license.

11. No Transfer of License: This license is personal to you and may not be sublicensed, assigned, or transferred by you to any other person without publisher's written permission.

12. No Amendment Except in Writing: This license may not be amended except in a writing signed by both parties (or, in the case of publisher, by CCC on publisher's behalf).

13. Objection to Contrary Terms: Publisher hereby objects to any terms contained in any purchase order, acknowledgment, check endorsement or other writing prepared by you, which terms are inconsistent with these terms and conditions or CCC's Billing and Payment terms and conditions. These terms and conditions, together with CCC's Billing and Payment terms and conditions (which are incorporated herein), comprise the entire agreement between you and publisher (and CCC) concerning this licensing transaction. In the event of any conflict between your obligations established by these terms and conditions and those established by CCC's Billing and Payment terms and conditions, these terms and conditions shall control.

14. Revocation: Elsevier or Copyright Clearance Center may deny the permissions described in this License at their sole discretion, for any reason or no reason, with a full refund payable to you. Notice of such denial will be made using the contact information provided by you. Failure to receive such notice will not alter or invalidate the denial. In no event will Elsevier or Copyright Clearance Center be responsible or liable for any costs, expenses or damage incurred by you as a result of a denial of your permission request, other than a refund of the amount(s) paid by you to Elsevier and/or Copyright Clearance Center for denied permissions.

LIMITED LICENSE

The following terms and conditions apply only to specific license types:

15. **Translation:** This permission is granted for non-exclusive world **English** rights only unless your license was granted for translation rights. If you licensed translation rights you may only translate this content into the languages you requested. A professional translator must perform all translations and reproduce the content word for word preserving the integrity of the article.

16. **Posting licensed content on any Website:** The following terms and conditions apply as follows: Licensing material from an Elsevier journal: All content posted to the web site must maintain the copyright information line on the bottom of each image; A hyper-text must be included to the Homepage of the journal from which you are licensing at <http://www.sciencedirect.com/science/journal/xxxxx> or the Elsevier homepage for books at <http://www.elsevier.com>; Central Storage: This license does not include permission for a scanned version of the material to be stored in a central repository such as that provided by Heron/XanEdu.

Licensing material from an Elsevier book: A hyper-text link must be included to the Elsevier homepage at <http://www.elsevier.com> . All content posted to the web site must maintain the copyright information line on the bottom of each image.

Posting licensed content on Electronic reserve: In addition to the above the following clauses are applicable: The web site must be password-protected and made available only to bona fide students registered on a relevant course. This permission is granted for 1 year only. You may obtain a new license for future website posting.

17. For journal authors: the following clauses are applicable in addition to the above:

Preprints:

A preprint is an author's own write-up of research results and analysis, it has not been peer-reviewed, nor has it had any other value added to it by a publisher (such as formatting, copyright, technical enhancement etc.).

Authors can share their preprints anywhere at any time. Preprints should not be added to or enhanced in any way in order to appear more like, or to substitute for, the final versions of articles however authors can update their preprints on arXiv or RePEc with their Accepted Author Manuscript (see below).

If accepted for publication, we encourage authors to link from the preprint to their formal publication via its DOI. Millions of researchers have access to the formal publications on ScienceDirect, and so links will help users to find, access, cite and use the best available version. Please note that Cell Press, The Lancet and some society-owned have different preprint policies. Information on these policies is available on the journal homepage.

Accepted Author Manuscripts: An accepted author manuscript is the manuscript of an article that has been accepted for publication and which typically includes author-incorporated changes suggested during submission, peer review and editor-author communications.

Authors can share their accepted author manuscript:

- immediately
 - via their non-commercial person homepage or blog
 - by updating a preprint in arXiv or RePEc with the accepted manuscript
 - via their research institute or institutional repository for internal institutional uses or as part of an invitation-only research collaboration work-group
 - directly by providing copies to their students or to research collaborators for their personal use
 - for private scholarly sharing as part of an invitation-only work group on commercial sites with which Elsevier has an agreement

- After the embargo period
 - via non-commercial hosting platforms such as their institutional repository
 - via commercial sites with which Elsevier has an agreement

In all cases accepted manuscripts should:

- link to the formal publication via its DOI
- bear a CC-BY-NC-ND license - this is easy to do
- if aggregated with other manuscripts, for example in a repository or other site, be shared in alignment with our hosting policy not be added to or enhanced in any way to appear more like, or to substitute for, the published journal article.

Published journal article (JPA): A published journal article (PJA) is the definitive final record of published research that appears or will appear in the journal and embodies all value-adding publishing activities including peer review co-ordination, copy-editing, formatting, (if relevant) pagination and online enrichment.

Policies for sharing publishing journal articles differ for subscription and gold open access articles:

Subscription Articles: If you are an author, please share a link to your article rather than the full-text. Millions of researchers have access to the formal publications on ScienceDirect, and so links will help your users to find, access, cite, and use the best available version.

Theses and dissertations which contain embedded PJAs as part of the formal submission can be posted publicly by the awarding institution with DOI links back to the formal publications on ScienceDirect.

If you are affiliated with a library that subscribes to ScienceDirect you have additional private sharing rights for others' research accessed under that agreement. This includes use for classroom teaching and internal training at the institution (including use in course packs and courseware programs), and inclusion of the article for grant funding purposes.

Gold Open Access Articles: May be shared according to the author-selected end-user license and should contain a [CrossMark logo](#), the end user license, and a DOI link to the formal publication on ScienceDirect.

Please refer to Elsevier's [posting policy](#) for further information.

18. **For book authors** the following clauses are applicable in addition to the above: Authors are permitted to place a brief summary of their work online only. You are not allowed to download and post the published electronic version of your chapter, nor may you scan the printed edition to create an electronic version. **Posting to a**

repository: Authors are permitted to post a summary of their chapter only in their institution's repository.

19. Thesis/Dissertation: If your license is for use in a thesis/dissertation your thesis may be submitted to your institution in either print or electronic form. Should your thesis be published commercially, please reapply for permission. These requirements include permission for the Library and Archives of Canada to supply single copies, on demand, of the complete thesis and include permission for Proquest/UMI to supply single copies, on demand, of the complete thesis. Should your thesis be published commercially, please reapply for permission. Theses and dissertations which contain embedded PJAs as part of the formal submission can be posted publicly by the awarding institution with DOI links back to the formal publications on ScienceDirect.

Elsevier Open Access Terms and Conditions

You can publish open access with Elsevier in hundreds of open access journals or in nearly 2000 established subscription journals that support open access publishing. Permitted third party re-use of these open access articles is defined by the author's choice of Creative Commons user license. See our [open access license policy](#) for more information.

Terms & Conditions applicable to all Open Access articles published with Elsevier:

Any reuse of the article must not represent the author as endorsing the adaptation of the article nor should the article be modified in such a way as to damage the author's honour or reputation. If any changes have been made, such changes must be clearly indicated.

The author(s) must be appropriately credited and we ask that you include the end user license and a DOI link to the formal publication on ScienceDirect.

If any part of the material to be used (for example, figures) has appeared in our publication with credit or acknowledgement to another source it is the responsibility of the user to ensure their reuse complies with the terms and conditions determined by the rights holder.

Additional Terms & Conditions applicable to each Creative Commons user license:

CC BY: The CC-BY license allows users to copy, to create extracts, abstracts and new works from the Article, to alter and revise the Article and to make commercial use of the Article (including reuse and/or resale of the Article by commercial entities), provided the user gives appropriate credit (with a link to the formal publication through the relevant DOI), provides a link to the license, indicates if changes were made and the licensor is not represented as endorsing the use made of the work. The full details of the license are available at <http://creativecommons.org/licenses/by/4.0>.

CC BY NC SA: The CC BY-NC-SA license allows users to copy, to create extracts, abstracts and new works from the Article, to alter and revise the Article, provided this is not done for commercial purposes, and that the user gives appropriate credit (with a link to the formal publication through the relevant DOI), provides a link to the license, indicates if changes were made and the licensor is not represented as endorsing the use made of the work. Further, any new works must be made available on the same conditions. The full details of the license are available at <http://creativecommons.org/licenses/by-nc-sa/4.0>.

CC BY NC ND: The CC BY-NC-ND license allows users to copy and distribute the Article, provided this is not done for commercial purposes and further does not permit distribution of the Article if it is changed or edited in any way, and provided the user gives appropriate credit (with a link to the formal publication through the relevant DOI), provides a link to the license, and that the licensor is not represented as endorsing the use made of the work. The full details of the license are available at <http://creativecommons.org/licenses/by-nc-nd/4.0>. Any commercial reuse of Open Access articles published with a CC BY NC SA or CC BY NC ND license requires permission from Elsevier and will be subject to a fee.

Commercial reuse includes:

- Associating advertising with the full text of the Article
- Charging fees for document delivery or access
- Article aggregation
- Systematic distribution via e-mail lists or share buttons

Posting or linking by commercial companies for use by customers of those companies.

20. Other Conditions:

v1.10

8.5.3. Figure 6

ELSEVIER LICENSE
TERMS AND CONDITIONS
Dec 07, 2024

This Agreement between Esra Caliskan ("You") and Elsevier ("Elsevier") consists of your

license details and the terms and conditions provided by Elsevier and Copyright Clearance Center.

| | |
|---|---|
| License Number | 5872101391353 |
| License date | Sep 18, 2024 |
| Licensed Content Publisher | Elsevier |
| Licensed Content Publication | Journal of Membrane Science |
| Licensed Content Title | Pervaporation membrane materials: Recent trends and perspectives |
| Licensed Content Author | Gongping Liu, Wanqin Jin |
| Licensed Content Date | Oct 15, 2021 |
| Licensed Content Volume | 636 |
| Licensed Content Issue | n/a |
| Licensed Content Pages | 1 |
| Start Page | 119557 |
| End Page | 0 |
| Type of Use | reuse in a thesis/dissertation |
| Portion | figures/tables/illustrations |
| Number of figures/tables/illustrations | 1 |
| Format | both print and electronic |
| Are you the author of this Elsevier article? | No |
| Will you be translating? | No |
| Title of new work | Polymers of intrinsic microporosity (thesis name will be defined later) |
| Institution name | University of Hamburg |
| Expected presentation date | Dec 2024 |
| Portions | Figure 1 |
| The Requesting Person / Organization to Appear on the License | Esra Caliskan Helmholtz zentrum hereon Max Planck street |
| Requestor Location | Geesthacht, other Germany |
| Order reference number | 180924 |
| Publisher Tax ID | GB 494 6272 12 |
| Total | 0.00 EUR |
| Terms and Conditions | |

INTRODUCTION

1. The publisher for this copyrighted material is Elsevier. By clicking "accept" in connection with completing this licensing transaction, you agree that the following terms

and conditions apply to this transaction (along with the Billing and Payment terms and conditions established by Copyright Clearance Center, Inc. ("CCC"), at the time that you opened your RightsLink account and that are available at any time at <https://myaccount.copyright.com>).

GENERAL TERMS

2. Elsevier hereby grants you permission to reproduce the aforementioned material subject to the terms and conditions indicated.

3. Acknowledgement: If any part of the material to be used (for example, figures) has appeared in our publication with credit or acknowledgement to another source, permission must also be sought from that source. If such permission is not obtained then that material may not be included in your publication/copies. Suitable acknowledgement to the source must be made, either as a footnote or in a reference list at the end of your publication, as follows:

"Reprinted from Publication title, Vol /edition number, Author(s), Title of article / title of chapter, Pages No., Copyright (Year), with permission from Elsevier [OR APPLICABLE SOCIETY COPYRIGHT OWNER]." Also Lancet special credit - "Reprinted from The Lancet, Vol. number, Author(s), Title of article, Pages No., Copyright (Year), with permission from Elsevier."

4. Reproduction of this material is confined to the purpose and/or media for which permission is hereby given. The material may not be reproduced or used in any other way, including use in combination with an artificial intelligence tool (including to train an algorithm, test, process, analyse, generate output and/or develop any form of artificial intelligence tool), or to create any derivative work and/or service (including resulting from the use of artificial intelligence tools).

5. Altering/Modifying Material: Not Permitted. However figures and illustrations may be altered/adapted minimally to serve your work. Any other abbreviations, additions, deletions and/or any other alterations shall be made only with prior written authorization of Elsevier Ltd. (Please contact Elsevier's permissions helpdesk [here](#)). No modifications can be made to any Lancet figures/tables and they must be reproduced in full.

6. If the permission fee for the requested use of our material is waived in this instance, please be advised that your future requests for Elsevier materials may attract a fee.

7. Reservation of Rights: Publisher reserves all rights not specifically granted in the combination of (i) the license details provided by you and accepted in the course of this licensing transaction, (ii) these terms and conditions and (iii) CCC's Billing and Payment terms and conditions.

8. License Contingent Upon Payment: While you may exercise the rights licensed immediately upon issuance of the license at the end of the licensing process for the

transaction, provided that you have disclosed complete and accurate details of your proposed use, no license is finally effective unless and until full payment is received from you (either by publisher or by CCC) as provided in CCC's Billing and Payment terms and conditions. If full payment is not received on a timely basis, then any license preliminarily granted shall be deemed automatically revoked and shall be void as if never granted. Further, in the event that you breach any of these terms and conditions or any of CCC's Billing and Payment terms and conditions, the license is automatically revoked and shall be void as if never granted. Use of materials as described in a revoked license, as well as any use of the materials beyond the scope of an unrevoked license, may constitute copyright infringement and publisher reserves the right to take any and all action to protect its copyright in the materials.

9. Warranties: Publisher makes no representations or warranties with respect to the licensed material.

10. Indemnity: You hereby indemnify and agree to hold harmless publisher and CCC, and their respective officers, directors, employees and agents, from and against any and all claims arising out of your use of the licensed material other than as specifically authorized pursuant to this license.

11. No Transfer of License: This license is personal to you and may not be sublicensed, assigned, or transferred by you to any other person without publisher's written permission.

12. No Amendment Except in Writing: This license may not be amended except in a writing signed by both parties (or, in the case of publisher, by CCC on publisher's behalf).

13. Objection to Contrary Terms: Publisher hereby objects to any terms contained in any purchase order, acknowledgment, check endorsement or other writing prepared by you, which terms are inconsistent with these terms and conditions or CCC's Billing and Payment terms and conditions. These terms and conditions, together with CCC's Billing and Payment terms and conditions (which are incorporated herein), comprise the entire agreement between you and publisher (and CCC) concerning this licensing transaction. In the event of any conflict between your obligations established by these terms and conditions and those established by CCC's Billing and Payment terms and conditions, these terms and conditions shall control.

14. Revocation: Elsevier or Copyright Clearance Center may deny the permissions described in this License at their sole discretion, for any reason or no reason, with a full refund payable to you. Notice of such denial will be made using the contact information provided by you. Failure to receive such notice will not alter or invalidate the denial. In no event will Elsevier or Copyright Clearance Center be responsible or liable for any costs, expenses or damage incurred by you as a result of a denial of your permission request, other than a refund of the amount(s) paid by you to Elsevier and/or Copyright Clearance Center for denied permissions.

LIMITED LICENSE

The following terms and conditions apply only to specific license types:

15. Translation: This permission is granted for non-exclusive world **English** rights only unless your license was granted for translation rights. If you licensed translation rights you may only translate this content into the languages you requested. A professional translator must perform all translations and reproduce the content word for word preserving the integrity of the article.

16. Posting licensed content on any Website: The following terms and conditions apply as follows: Licensing material from an Elsevier journal: All content posted to the web site must maintain the copyright information line on the bottom of each image; A hyper-text must be included to the Homepage of the journal from which you are licensing at <http://www.sciencedirect.com/science/journal/xxxxx> or the Elsevier homepage for books at <http://www.elsevier.com>; Central Storage: This license does not include permission for a scanned version of the material to be stored in a central repository such as that provided by Heron/XanEdu.

Licensing material from an Elsevier book: A hyper-text link must be included to the Elsevier homepage at <http://www.elsevier.com> . All content posted to the web site must maintain the copyright information line on the bottom of each image.

Posting licensed content on Electronic reserve: In addition to the above the following clauses are applicable: The web site must be password-protected and made available only to bona fide students registered on a relevant course. This permission is granted for 1 year only. You may obtain a new license for future website posting.

17. For journal authors: the following clauses are applicable in addition to the above:

Preprints:

A preprint is an author's own write-up of research results and analysis, it has not been peer-reviewed, nor has it had any other value added to it by a publisher (such as formatting, copyright, technical enhancement etc.).

Authors can share their preprints anywhere at any time. Preprints should not be added to or enhanced in any way in order to appear more like, or to substitute for, the final versions of articles however authors can update their preprints on arXiv or RePEc with their Accepted Author Manuscript (see below).

If accepted for publication, we encourage authors to link from the preprint to their formal publication via its DOI. Millions of researchers have access to the formal publications on ScienceDirect, and so links will help users to find, access, cite and use the best available

version. Please note that Cell Press, The Lancet and some society-owned have different preprint policies. Information on these policies is available on the journal homepage.

Accepted Author Manuscripts: An accepted author manuscript is the manuscript of an article that has been accepted for publication and which typically includes author-incorporated changes suggested during submission, peer review and editor-author communications.

Authors can share their accepted author manuscript:

- immediately
 - via their non-commercial person homepage or blog
 - by updating a preprint in arXiv or RePEc with the accepted manuscript
 - via their research institute or institutional repository for internal institutional uses or as part of an invitation-only research collaboration work-group
 - directly by providing copies to their students or to research collaborators for their personal use
 - for private scholarly sharing as part of an invitation-only work group on commercial sites with which Elsevier has an agreement
- After the embargo period
 - via non-commercial hosting platforms such as their institutional repository
 - via commercial sites with which Elsevier has an agreement

In all cases accepted manuscripts should:

- link to the formal publication via its DOI
- bear a CC-BY-NC-ND license - this is easy to do
- if aggregated with other manuscripts, for example in a repository or other site, be shared in alignment with our hosting policy not be added to or enhanced in any way to appear more like, or to substitute for, the published journal article.

Published journal article (JPA): A published journal article (PJA) is the definitive final record of published research that appears or will appear in the journal and embodies all value-adding publishing activities including peer review co-ordination, copy-editing, formatting, (if relevant) pagination and online enrichment.

Policies for sharing publishing journal articles differ for subscription and gold open access articles:

Subscription Articles: If you are an author, please share a link to your article rather than the full-text. Millions of researchers have access to the formal publications on ScienceDirect, and so links will help your users to find, access, cite, and use the best available version.

Theses and dissertations which contain embedded PJAs as part of the formal submission can be posted publicly by the awarding institution with DOI links back to the formal publications on ScienceDirect.

If you are affiliated with a library that subscribes to ScienceDirect you have additional private sharing rights for others' research accessed under that agreement. This includes use for classroom teaching and internal training at the institution (including use in course packs and courseware programs), and inclusion of the article for grant funding purposes.

Gold Open Access Articles: May be shared according to the author-selected end-user license and should contain a [CrossMark logo](#), the end user license, and a DOI link to the formal publication on ScienceDirect.

Please refer to Elsevier's [posting policy](#) for further information.

18. For book authors the following clauses are applicable in addition to the above: Authors are permitted to place a brief summary of their work online only. You are not allowed to download and post the published electronic version of your chapter, nor may you scan the printed edition to create an electronic version. **Posting to a repository:** Authors are permitted to post a summary of their chapter only in their institution's repository.

19. Thesis/Dissertation: If your license is for use in a thesis/dissertation your thesis may be submitted to your institution in either print or electronic form. Should your thesis be published commercially, please reapply for permission. These requirements include permission for the Library and Archives of Canada to supply single copies, on demand, of the complete thesis and include permission for Proquest/UMI to supply single copies, on demand, of the complete thesis. Should your thesis be published commercially, please reapply for permission. Theses and dissertations which contain embedded PJAs as part of the formal submission can be posted publicly by the awarding institution with DOI links back to the formal publications on ScienceDirect.

Elsevier Open Access Terms and Conditions

You can publish open access with Elsevier in hundreds of open access journals or in nearly 2000 established subscription journals that support open access publishing. Permitted third party re-use of these open access articles is defined by the author's choice of Creative Commons user license. See our [open access license policy](#) for more information.

Terms & Conditions applicable to all Open Access articles published with Elsevier:

Any reuse of the article must not represent the author as endorsing the adaptation of the article nor should the article be modified in such a way as to damage the author's honour or reputation. If any changes have been made, such changes must be clearly indicated.

The author(s) must be appropriately credited and we ask that you include the end user license and a DOI link to the formal publication on ScienceDirect.

If any part of the material to be used (for example, figures) has appeared in our publication with credit or acknowledgement to another source it is the responsibility of the user to ensure their reuse complies with the terms and conditions determined by the rights holder.

Additional Terms & Conditions applicable to each Creative Commons user license:

CC BY: The CC-BY license allows users to copy, to create extracts, abstracts and new works from the Article, to alter and revise the Article and to make commercial use of the Article (including reuse and/or resale of the Article by commercial entities), provided the user gives appropriate credit (with a link to the formal publication through the relevant DOI), provides a link to the license, indicates if changes were made and the licensor is not represented as endorsing the use made of the work. The full details of the license are available at <http://creativecommons.org/licenses/by/4.0>.

CC BY NC SA: The CC BY-NC-SA license allows users to copy, to create extracts, abstracts and new works from the Article, to alter and revise the Article, provided this is not done for commercial purposes, and that the user gives appropriate credit (with a link to the formal publication through the relevant DOI), provides a link to the license, indicates if changes were made and the licensor is not represented as endorsing the use made of the work. Further, any new works must be made available on the same conditions. The full details of the license are available at <http://creativecommons.org/licenses/by-nc-sa/4.0>.

CC BY NC ND: The CC BY-NC-ND license allows users to copy and distribute the Article, provided this is not done for commercial purposes and further does not permit distribution of the Article if it is changed or edited in any way, and provided the user gives appropriate credit (with a link to the formal publication through the relevant DOI), provides a link to the license, and that the licensor is not represented as endorsing the use made of the work. The full details of the license are available at <http://creativecommons.org/licenses/by-nc-nd/4.0>. Any commercial reuse of Open Access articles published with a CC BY NC SA or CC BY NC ND license requires permission from Elsevier and will be subject to a fee.

Commercial reuse includes:

- Associating advertising with the full text of the Article
- Charging fees for document delivery or access
- Article aggregation
- Systematic distribution via e-mail lists or share buttons

Posting or linking by commercial companies for use by customers of those companies.

20. Other Conditions:

v1.10

8.5.4. Figure 8

JOHN WILEY AND SONS LICENSE
TERMS AND CONDITIONS
Dec 07, 2024

This Agreement between Esra Caliskan ("You") and John Wiley and Sons ("John Wiley and Sons") consists of your license details and the terms and conditions provided by John Wiley and Sons and Copyright Clearance Center.

| | |
|------------------------------|---|
| License Number | 5872130553165 |
| License date | Sep 18, 2024 |
| Licensed Content Publisher | John Wiley and Sons |
| Licensed Content Publication | Journal of Chemical Technology & Biotechnology |
| Licensed Content Title | A review of nanoparticle-enhanced membrane distillation membranes: membrane synthesis and applications in water treatment |
| Licensed Content Author | Sabelo D Mhlana, Bhekie B Mamba, Arne R Verliefde, et al |
| Licensed Content Date | Mar 25, 2019 |
| Licensed Content Volume | 94 |
| Licensed Content Issue | 9 |
| Licensed Content Pages | 15 |
| Type of use | Dissertation/Thesis |
| Requestor type | University/Academic |
| Format | Print and electronic |
| Portion | Figure/table |
| Number of figures/tables | 1 |
| Will you be translating? | No |
| Title of new work | Polymers of intrinsic microporosity (thesis name will be defined later) |

| | |
|---|--|
| Institution name | University of Hamburg |
| Expected presentation date | Dec 2024 |
| Portions | Figure 8 |
| The Requesting Person / Organization to Appear on the License | Esra Caliskan Helmholtz zentrum hereon Max Planck street |
| Requestor Location | Geesthacht, other Germany |
| Order reference number | 180924 |
| Publisher Tax ID | EU826007151 |
| Total | 0.00 EUR |
| Terms and Conditions | |

TERMS AND CONDITIONS

This copyrighted material is owned by or exclusively licensed to John Wiley & Sons, Inc. or one of its group companies (each a "Wiley Company") or handled on behalf of a society with which a Wiley Company has exclusive publishing rights in relation to a particular work (collectively "WILEY"). By clicking "accept" in connection with completing this licensing transaction, you agree that the following terms and conditions apply to this transaction (along with the billing and payment terms and conditions established by the Copyright Clearance Center Inc., ("CCC's Billing and Payment terms and conditions"), at the time that you opened your RightsLink account (these are available at any time at <http://myaccount.copyright.com>).

Terms and Conditions

- The materials you have requested permission to reproduce or reuse (the "Wiley Materials") are protected by copyright.
- You are hereby granted a personal, non-exclusive, non-sub licensable (on a stand-alone basis), non-transferable, worldwide, limited license to reproduce the Wiley Materials for the purpose specified in the licensing process. This license, **and any CONTENT (PDF or image file) purchased as part of your order**, is for a one-time use only and limited to any maximum distribution number specified in the license. The first instance of republication or reuse granted by this license must be completed within two years of the date of the grant of this license (although copies prepared before the end date may be distributed thereafter). The Wiley Materials shall not be used in any other manner or for any other purpose, beyond what is granted in the license. Permission is granted subject to an appropriate acknowledgement given to the author, title of the material/book/journal and the

publisher. You shall also duplicate the copyright notice that appears in the Wiley publication in your use of the Wiley Material. Permission is also granted on the understanding that nowhere in the text is a previously published source acknowledged for all or part of this Wiley Material. Any third party content is expressly excluded from this permission.

- With respect to the Wiley Materials, all rights are reserved. Except as expressly granted by the terms of the license, no part of the Wiley Materials may be copied, modified, adapted (except for minor reformatting required by the new Publication), translated, reproduced, transferred or distributed, in any form or by any means, and no derivative works may be made based on the Wiley Materials without the prior permission of the respective copyright owner. **For STM Signatory Publishers clearing permission under the terms of the [STM Permissions Guidelines](#) only, the terms of the license are extended to include subsequent editions and for editions in other languages, provided such editions are for the work as a whole in situ and does not involve the separate exploitation of the permitted figures or extracts,** You may not alter, remove or suppress in any manner any copyright, trademark or other notices displayed by the Wiley Materials. You may not license, rent, sell, loan, lease, pledge, offer as security, transfer or assign the Wiley Materials on a stand-alone basis, or any of the rights granted to you hereunder to any other person.
- The Wiley Materials and all of the intellectual property rights therein shall at all times remain the exclusive property of John Wiley & Sons Inc, the Wiley Companies, or their respective licensors, and your interest therein is only that of having possession of and the right to reproduce the Wiley Materials pursuant to Section 2 herein during the continuance of this Agreement. You agree that you own no right, title or interest in or to the Wiley Materials or any of the intellectual property rights therein. You shall have no rights hereunder other than the license as provided for above in Section 2. No right, license or interest to any trademark, trade name, service mark or other branding ("Marks") of WILEY or its licensors is granted hereunder, and you agree that you shall not assert any such right, license or interest with respect thereto
- NEITHER WILEY NOR ITS LICENSORS MAKES ANY WARRANTY OR REPRESENTATION OF ANY KIND TO YOU OR ANY THIRD PARTY, EXPRESS, IMPLIED OR STATUTORY, WITH RESPECT TO THE MATERIALS OR THE ACCURACY OF ANY INFORMATION CONTAINED IN THE MATERIALS, INCLUDING, WITHOUT LIMITATION, ANY IMPLIED WARRANTY OF MERCHANTABILITY, ACCURACY, SATISFACTORY QUALITY, FITNESS FOR A PARTICULAR PURPOSE, USABILITY, INTEGRATION OR NON-INFRINGEMENT AND ALL SUCH WARRANTIES ARE HEREBY EXCLUDED BY WILEY AND ITS LICENSORS AND WAIVED BY YOU.

- WILEY shall have the right to terminate this Agreement immediately upon breach of this Agreement by you.
- You shall indemnify, defend and hold harmless WILEY, its Licensors and their respective directors, officers, agents and employees, from and against any actual or threatened claims, demands, causes of action or proceedings arising from any breach of this Agreement by you.
- IN NO EVENT SHALL WILEY OR ITS LICENSORS BE LIABLE TO YOU OR ANY OTHER PARTY OR ANY OTHER PERSON OR ENTITY FOR ANY SPECIAL, CONSEQUENTIAL, INCIDENTAL, INDIRECT, EXEMPLARY OR PUNITIVE DAMAGES, HOWEVER CAUSED, ARISING OUT OF OR IN CONNECTION WITH THE DOWNLOADING, PROVISIONING, VIEWING OR USE OF THE MATERIALS REGARDLESS OF THE FORM OF ACTION, WHETHER FOR BREACH OF CONTRACT, BREACH OF WARRANTY, TORT, NEGLIGENCE, INFRINGEMENT OR OTHERWISE (INCLUDING, WITHOUT LIMITATION, DAMAGES BASED ON LOSS OF PROFITS, DATA, FILES, USE, BUSINESS OPPORTUNITY OR CLAIMS OF THIRD PARTIES), AND WHETHER OR NOT THE PARTY HAS BEEN ADVISED OF THE POSSIBILITY OF SUCH DAMAGES. THIS LIMITATION SHALL APPLY NOTWITHSTANDING ANY FAILURE OF ESSENTIAL PURPOSE OF ANY LIMITED REMEDY PROVIDED HEREIN.
- Should any provision of this Agreement be held by a court of competent jurisdiction to be illegal, invalid, or unenforceable, that provision shall be deemed amended to achieve as nearly as possible the same economic effect as the original provision, and the legality, validity and enforceability of the remaining provisions of this Agreement shall not be affected or impaired thereby.
- The failure of either party to enforce any term or condition of this Agreement shall not constitute a waiver of either party's right to enforce each and every term and condition of this Agreement. No breach under this agreement shall be deemed waived or excused by either party unless such waiver or consent is in writing signed by the party granting such waiver or consent. The waiver by or consent of a party to a breach of any provision of this Agreement shall not operate or be construed as a waiver of or consent to any other or subsequent breach by such other party.
- This Agreement may not be assigned (including by operation of law or otherwise) by you without WILEY's prior written consent.
- Any fee required for this permission shall be non-refundable after thirty (30) days from receipt by the CCC.
- These terms and conditions together with CCC's Billing and Payment terms and conditions (which are incorporated herein) form the entire agreement between you

and WILEY concerning this licensing transaction and (in the absence of fraud) supersedes all prior agreements and representations of the parties, oral or written. This Agreement may not be amended except in writing signed by both parties. This Agreement shall be binding upon and inure to the benefit of the parties' successors, legal representatives, and authorized assigns.

- In the event of any conflict between your obligations established by these terms and conditions and those established by CCC's Billing and Payment terms and conditions, these terms and conditions shall prevail.
- WILEY expressly reserves all rights not specifically granted in the combination of (i) the license details provided by you and accepted in the course of this licensing transaction, (ii) these terms and conditions and (iii) CCC's Billing and Payment terms and conditions.
- This Agreement will be void if the Type of Use, Format, Circulation, or Requestor Type was misrepresented during the licensing process.
- This Agreement shall be governed by and construed in accordance with the laws of the State of New York, USA, without regards to such state's conflict of law rules. Any legal action, suit or proceeding arising out of or relating to these Terms and Conditions or the breach thereof shall be instituted in a court of competent jurisdiction in New York County in the State of New York in the United States of America and each party hereby consents and submits to the personal jurisdiction of such court, waives any objection to venue in such court and consents to service of process by registered or certified mail, return receipt requested, at the last known address of such party.

WILEY OPEN ACCESS TERMS AND CONDITIONS

Wiley Publishes Open Access Articles in fully Open Access Journals and in Subscription journals offering Online Open. Although most of the fully Open Access journals publish open access articles under the terms of the Creative Commons Attribution (CC BY) License only, the subscription journals and a few of the Open Access Journals offer a choice of Creative Commons Licenses. The license type is clearly identified on the article.

The Creative Commons Attribution License

The [Creative Commons Attribution License \(CC-BY\)](#) allows users to copy, distribute and transmit an article, adapt the article and make commercial use of the article. The CC-BY license permits commercial and non-

Creative Commons Attribution Non-Commercial License

The [Creative Commons Attribution Non-Commercial \(CC-BY-NC\)License](#) permits use, distribution and reproduction in any medium, provided the original work is properly cited and is not used for commercial purposes.(see below)

Creative Commons Attribution-Non-Commercial-NoDerivs License

The [Creative Commons Attribution Non-Commercial-NoDerivs License](#) (CC-BY-NC-ND) permits use, distribution and reproduction in any medium, provided the original work is properly cited, is not used for commercial purposes and no modifications or adaptations are made. (see below)

Use by commercial "for-profit" organizations

Use of Wiley Open Access articles for commercial, promotional, or marketing purposes requires further explicit permission from Wiley and will be subject to a fee.

Further details can be found on Wiley Online

Library <http://olabout.wiley.com/WileyCDA/Section/id-410895.html>

Other Terms and Conditions:

v1.10 Last updated September 2015

9. Acknowledgements

First of all, I would like to express my sincere thanks to my PhD advisor, Prof. Dr. Volker Abetz, Director of the Institute for Membrane Research at the Helmholtz-Zentrum Hereon and Group Leader of the Institute of Physical Chemistry at the University of Hamburg, for providing me the opportunity to pursue this PhD under his guidance and for his valuable academic support throughout the process. His expertise in polymer chemistry and his invaluable contributions to the published articles have been pivotal to the success of this research.

I want to sincerely thank to Prof. Dr. Tobias Beck for accepting to be the second assessor of this doctoral thesis.

I would like to express my heartfelt gratitude to Dr. Volkan Filiz, who introduced me to my PhD topic and paved the way for this experience. His invaluable feedback on my work, as well as his consistently positive and understanding approach, has been incredibly meaningful to me.

Dr. Sergey Shishatskiy has been an integral part of my PhD time, providing invaluable contributions and endless support. He never failed to meet my expectations for support and guidance. From him, I learned the ability to analyze and question data within a broader context, which made my doctoral research more stimulating. His unwavering support and motivation were instrumental in the ultimate success of my research goals and my heartfelt thanks to him.

I am deeply grateful to the other senior members Dr. Gisela Bengtson, Dr. Sofia Rangou, Dr. Prokopios Georgopoulos, Dr. Jelena Lillepaerg, Dr. Musfequer Rahman, Dr. Martin Held, Dr. Maryam Radjabian, Kristian Buhr, Clarissa Abetz and Carsten Scholz for their invaluable contributions on scientific discussions throughout my PhD for shaping of the storyline of my articles.

I would like to express my deepest gratitude to my dear colleague Silvio Neumann for his contributions in laboratory work, for broadening my perspective with scientific discussions, and for making this PhD delightful, not only with scientific dialogues but also with pleasant conversations. Along with him, my sincere thanks also to Silke Dargel, Petra Merten, Barbara

Bajer, Ivonne Ternes, Dr. Erik S. Schneider, Dr. Evgeni Sperling, and Anke-Lisa Höhme for their support in carrying out the characterizations and for the valuable conversations we had in interpreting the results.

Throughout the time of completing my PhD, I had the privilege of spending enjoyable moments with my fellow young scientists. I would like to extend my heartfelt thanks to Dr. Michael Appold, with whom I shared my office, for the wonderful days we spent together. Beyond his academic support, I am deeply grateful for the countless fun and creative activities we engaged in, which made those times even more memorable. In addition, the scientific exchanges, and great social activities I shared with Dr. Fynn Weigelt, Dr. Sarah Glass and Dr. Aniket Atul Raje were also among the unforgettable highlights of this journey. I am also thankful to my other fellows Dr. Elvin Aliyev, Dr. Zhenzen Zhang, Dr. Mahboubeh Kargar, Florian Brennecke, Nicolas Cevallos Cueva for their valuable companionship, which enriched my PhD experience.

During the time of completing my PhD, life outside the institute brought many experiences, both joyful and challenging. It was a long road, marked by losses and lessons. Beyond my professional life, I am deeply grateful to the individuals whose invaluable support and presence cannot be expressed in words.

I would like to first extend my heartfelt thanks to my dear cousin, and in many ways like a sibling, Irem Düzgünoglu. From the very first day of my PhD, when I left my home behind, until the very last, she was always there for me, offering unwavering emotional support at any hour and in any situation. Her place in my life is beyond description, and she has been a safe harbor—one that anyone would wish to have in their life.

I am deeply grateful to my beloved friend Cansu Ferda Gül, who has been a constant source of support and understanding throughout this journey. As a fellow PhD candidate, her empathy and encouragement have been invaluable. Our long-standing friendship has been further strengthened during this period, as we shared similar experiences and supported each other through the challenges of this process. Her presence has been an indescribable source of comfort and reassurance.

And to my family... I am deeply grateful to my mother, Nazan Güldür, whose eternal love has always been a constant in my life and whose support made the distance more bearable. I also want to acknowledge those who are no longer with me, yet whose warmth and cherished memories have continued to be a source of strength. To my father, İrfan, my grandfather, Cavit, my aunt, Nilüfer, and my uncle, Basri, I extend my deepest gratitude for their everlasting belief in me and the pride I know they always carried in their hearts.

Finally, I would like to express my heartfelt gratefulness to my partner, Umut Can Kaya, who will witness the next chapter of my life and with whom I have vowed to share our lives. His presence, unconditional support, and the sense of comfort he brings have been a source of hope and strength for me in overcoming all the challenges I have faced.

10. Declaration of oath

I solemnly swear that I have written this dissertation on my own and have not used any sources other than approved sources and assistance. Furthermore, this work has not been previously published elsewhere. I declare that I have not previously applied for or obtained a PhD. I concede that this thesis is a cumulative dissertation and that parts of it have been published in scientific journals. Thus, resemblances to these publications do exist, but they have been cited wherever necessary in the dissertation. I recognize that any infringement of this oath may result in penalties for disciplinary action.

Münster, 07.04.2025